Identification and characterization of notch3 as a new asymmetric factor during heart looping

Tobias Holm Bønnelykke

Sorbonne Université

Complexité du Vivant

Institut Imagine, Institut Pasteur : Heart Morphogenesis Unit

Identification et caractérisation de *Notch3*, un nouveau facteur asymétrique au cours de la boucle cardiaque

Identification and Characterization of Notch3 as a Novel Asymmetric Factor in Heart Looping

Par Tobias Holm BØNNELYKKE

Thèse de doctorat de Biologie cellulaire

Dirigée par Sigolène MEILHAC et Audrey DESGRANGE

Présentée et soutenue publiquement le 21/10/2022

Devant un jury composé de :

Silvia FRE Directrice de recherche, Institut Curie	*Présidente*
Natasza KURPIOS Associate professor, Cornell University	*Rapporteure*
Robert KELLY Directeur de recherche, Aix Marseille University	*Rapporteur*
Richard TYSER Principle Investigator, University of Cambridge	*Examinateur*
Sigolène MEILHAC Directrice de recherche, INSERM, Paris	*Directrice de thèse*
Audrey DESGRANGE Post-doctoral researcher, Institut Imagine, Paris	Co-*directrice de thèse*

Table of Content

Abbreviations

A: anterior

AVN: Atrioventricular node

AVC: atrioventricular canal

Ao: aorta

AT: atria

Ca: Caudal

CC: cardiac crescent

Cr: Cranial

CHD: congenital heart defects

DA: dorsal aorta

DM: dorsal mensentery

Ec: endocardium

FD: foregut diverticulum

FP: floor plate

HT: heart tube

ISH: in situ hybridization

JCF: juxta-cardiac field

L: left

LA: left atrium

LHF: late head fold

LHT: late heart tube

LV: left ventricle

No: node

n.s.: not significant

OF: outflow tract

OFT: outflow tract

P: posterior

PhA: pharyngeal arch

Pt: Pulmonary trunk

R: right

RA: right atrium

RV: right ventricle.

SHF: second heart field

So: somites

SV: sinus venosus.

TAD: transcriptional activation domain

VSD: ventricular septal defect

YS: yolk sac

List of Figures

Introduction

Results

Figure 1. Size of the second heart field of progenitors

Figure 2. RNA sequencing of left-right differential expression in the heart field

Figure S1 related to Fig. 2. Development of protocols for single cell RNA sequencing of heart progenitor patterning

Figure 3. Left-sided enrichment of *Notch3* expression at E8.5

Figure S2 related to Fig. 3. Additional transcriptomic analyses

Figure 4. Decreased *Notch3* asymmetric expression in *Nodal* mutants

Figure S3 related to Fig. 4. *Nodal* expression in *Notch3* mutants

Figure 5. Heart looping defects in *Notch3*$^{-/-}$ mutants

Figure 6. Notch receptor gene expression profile in control and *Notch3* mutants

Figure S4 related to Fig. 6. Additional profiling of Notch paralogues

Figure 7. Expression of Notch ligand *Jag1* and Notch canonical target *Hey1*

Figure 8. Bioinformatic predictions of potential Notch targets in cardiac cells

Figure 9. Phenotype of *Notch3 ; Nodal* double heterozygotes

Figure S5 related to Fig. 9. Additional profiling of Notch3 heterozygote

Figure 10. Establishing a sub-phenotypic dosage of gamma-secretase inhibition in embryo culture

Discussion

Figure 1. Summary of asymmetric signal during heart looping

Acknowledgements

Although media might present us otherwise, modern scientific work is seldomly a solitary affaire, and the work presented in this thesis is no exception. On the contrary, I think that all the best work in this thesis came from collaborations, or it was born from ideas that had been shaped through discussions with supervisors, colleagues, friends and students.

The biggest thank you goes to Sigolène Meilhac and Audrey Desgrange, who supervised the thesis. I am grateful for you selecting me almost 5 years ago to be your candidate for the PPU PhD application. Even if the PhD journey has sometimes been a bumpy road[1], you were always very dedicated to my supervision – both on a professional level to strengthen the project, but also on a personal level in my training as a scientist. Sometimes our meetings were tough (tougher than my soft Danish *skin* was used to), and we had many of them, but they were often enjoyable, and we always managed to find solutions to our problems.

Sigolène, I admire how you have been able to promote a culture in our team of strong scientific thinking, logical decision making, outreach and teamwork. I have enjoyed working with you in particular because your passion for science and for how the scientific method can benefit our society is contagious. I know it was not always easy to have in your lab a Danish capoeira player who prefers to-do lists over Google calendars, but I think in the end we managed. At least we often laughed!

Audrey, thank you for always taking me seriously. I learned from you how to get the most from the least amount of work, to ask for help and to design experiments so we could always draw conclusions. We were very different when I started, but we found a way to work together to complement each other. Finally, it has been a pleasure to see your professional progress the past years. When I started, you were a great developmental biologist – now you are *unspeakably* amazing, and I hope you will accomplish whatever you set your sights on.

Many senior researchers have contributed to the project. I would like to thank Laure Bally-Cuif, Raphaelle Grifone, Stéphane Zaffran and Heather Marlow for participating in my thesis

[1] In particular les gilets jaunes, covid and the *Notch3* mutant mouse

advisory committee. Your advice helped shaping the project, and your comments helped me focus on what was important for the project. Additionally, I would like to thank Silvia Fre, Natasza Kurpios, Robert Kelly and Richard Tyser for accepting to be members of my jury. The research you guys have done has been an inspiration for the thesis, and I am looking forward to the day of the defense, so that I can discuss my work with you. Furthermore, I would like to thank Francesca Rochais for *Isl1*^{MerCreMer}*; R26*^{tdTomato} embryos, José Luis de la Pompa for the *CBF:H2B-Venus* embryos and Kenzo Ivanovitch for the *BRE:H2B-Turquoise* embryos (the latter unfortunately didn't make it into the thesis).

I would also like to extend my thanks to all the researchers at Institut Imagine and at the Department of Stem Cell and Developmental Biology at Institut Pasteur, who always had great suggestions and questions when I presented my project. Finally, I would like to thank Palle Serup and (especially) Philip Seymour from the Notch group at ReNEW (Univ. of Copenhagen), who contributed with advice and protocols related to the Notch project.

Many researchers also played a more active part of the project. Audrey Desgrange, who beyond just *teaching me the ropes*, helped perform experiments. Without you the project would not be where it is – there would especially be no embryo culture. The ever reliant and eternally patient Laurent Guillemot, who directly contributed to the project through PCR and qPCR experiments (along with his students). Vanessa Benhamo laughed at my poor jokes in French and contributed with *in situ* hybridizations and HREM imaging. Emeline Perthame suffered through endless questions and contributed with bioinformatical- and statistical analysis of both single cell RNA seq data as well as for the left-right heartfield bulk RNA seq screening (and you helped me make pretty visualization! #pimpmygraph).

From the Genomics platform at Institut Imagine, I would like to thank Christine Bole, Mélanie Parisot and Mohammed Zarhrate for their help with designing the left-right bulk sequencing screen, performing the RNA library kit test and performing the bulk RNA sequencing. From the bioinformatics team, I would like to thank Cécile Masson and Nicolas Cagnard for advices for experimental design, kit test and their bioinformatical analysis. Similarly, I would like to thank Hugo Varet from the Bioinformatic Hub at Institut Pasteur for his help with bioformatical analysis.

Finally, I would like to thank my students, Vera Nikovics, Cypriane Tazi, Zoé Tiprez and Marie-Amandine Chabry. Vera contributed to qPCR experiments, is an amazing poster presenter and

a close friend, Cypriane helped with making beautiful pSmad1/5 stainings and asked the greatest questions, Zoé contributed with the N1ICD wholemount stainings and was the best with the pipette and finally Marie-Amandine, who helped with *Hey1* stainings during her M1 internship and with the *Nodal; Notch3* genetic interaction project during her M2 internship. Marie-Amandine also performed all experiments during the two months where I was recovering from injury. She's also very stubborn, has a kind spirit and it has been amazing to see her grow the past year as a scientist. Dear students, you all did very well (much beyond the good grades you all got), and I am both honored and proud to have been your supervisor.

A PhD is a journey, and I have met many people along the way, who all helped to make life in Paris something more than just research. In the lab I would like to send my thanks to current and previous colleagues (that haven't been mentioned earlier): Ségolène, Daniel, Adrien, Sami, Clara, Mathilde, Manon, Marta, Clémire, Jules, Jean-François, Paul, Amaia, Rhizlane, Aurélian, Zoé and Heloïse. In particular it was great to do my PhD together with first Ségolène and later Amaia, who are both extremely talented researchers as well as great people. Additionally Daniel has become a great friend, who I am very thankful for. Imagine would have been very lonely without you.

Sometimes it was hard being a developmental biologist working at a hospital. However the DSCB was never far away, and I was grateful that they were always welcoming. A special thank you goes to the *Germans* (Anna and Miri) and the *Italians* (Paolo and Pierre).

Furthermore, the PPU made us never feel alone because they often arranged events for us. People I met through the PPU programme became friends that I experienced a lot of my Parisian life with. In particular, there are two people to mention: Adriana, although we neither shared the beginning nor the end of the journey, a beautiful chunk in the middle belonged to you. Thank you for the happy times and thank you for the many lessons and for always trying. Lukas, thank you for everything (besides the hangovers). You are a true friend.

Beyond research, I spent lots of time with my two sets of sport families. I owe a big thank you to *Mestre Chicote* and the other members of *Capoeira de Ouro* (Paris) for welcoming me into your family. Many of my fondest moments here were spent with you guys in the different salle de sport in Paris. Additionally, I would like to thank the members of the *Imagine Sports Association*, who survived having me as president for two years, and allowed me to connect with great people of the institute beyond my own lab.

There are many people back home, who also helped a lot the past four years. You will be thanked in person. However, a special *shout out* goes to Banden (the “gang”) consisting of my six earliest school friends, who have been my friends for over 25 years. I am very grateful for you guys, in particular for your support after my Mom’s passing.

The final thank you goes to the family, in particular my mother. Without her I would not be a quarter of the person I am, and I miss her every day.

Research is expensive, and it could not be possible without benefactors allowing us to do our work. In my case I would like to thank PPU, Institut Pasteur, FRM and REVIVE for funding.

Résumé de la thèse en français

Mots clés

Asymetrie droite-gauche ; Morphogenèse du cœur ; Champ cardiaque ; Signalisation notch ; Genetique de la souris ; Transcriptomique

Résumé

L'asymétrie droite-gauche du cœur est essentielle à l'établissement de la double circulation sanguine : des anomalies dans l'information de position droite-gauche dans l'embryon entraînent des malformations cardiaques congénitales dans le syndrome d'hétérotaxie. Alors que le cœur se forme initialement comme un tube droit, il acquiert une forme hélicoïdale asymétrique au cours du processus de la boucle cardiaque. Il s'agit d'une étape clé de la morphogenèse cardiaque, au cours de laquelle les cavités cardiaques sont alignées, condition préalable à la canalisation de la circulation sanguine.

Bien que le déterminant gauche NODAL soit un régulateur important de la boucle cardiaque, des travaux antérieurs en laboratoire ont montré qu'il n'est pas le seul facteur d'asymétrie : NODAL oriente et amplifie des asymétries préexistantes. Pourtant, les asymétries autres que la signalisation NODAL sont restées floues. Afin d'étudier l'information de position droite-gauche des précurseurs cardiaques, nous avons conçu une approche transcriptomique pour mettre en évidence l'expression différentielle des gènes dans les champs cardiaques droit et gauche de l'embryon de souris. Le crible transcriptionnel a été réalisé sur des embryons individuels, à sept stades séquentiels de la boucle cardiaque, fournissant une ressource de centaines de gènes marquant l'asymétrie du champ cardiaque.

À partir d'un crible pilote initial, nous avons identifié Notch3 comme un nouveau gène asymétrique et l'avons sélectionné pour validation. La cartographie spatio-temporelle de pointe, quantitative et en 3D, de l'expression de *Notch3* a révélé une expression transitoire dans le mésoderme de la plaque latérale gauche, y compris le deuxième champ cardiaque, précédent la formation de la boucle cardiaque. Nous avons montré que *Notch3* était co-exprimé avec *Nodal* au sein de cette population et que l'asymétrie de *Notch3* était amplifiée

par la signalisation NODAL, fournissant la première preuve moléculaire que NODAL agit comme un amplificateur d'asymétrie.

Étant donné que la souris possède quatre récepteurs Notch paralogues, nous avons étudié la redondance potentielle entre eux. À partir de données publiées de séquençage d'ARN en cellules uniques et de nouvelles cartographies quantitatives, nous avons observé des profils d'expression spécifiques : l'expression de *Notch4* est négligeable, celle de *Notch1* est limitée à l'endocarde et à l'aorte dorsale, tandis que *Notch2* est exprimé dans les progéniteurs cardiaques et enrichi dans le champ juxta-cardiaque, où le niveau de *Notch3* est bas. Nous n'avons pas détecté d'asymétrie évidente de Notch autre que Notch3. Dans les champs cardiaques des mutants *Notch3*, *Notch1* et *Notch2* ont été trouvés surexprimés, indiquant ainsi une compensation potentielle.

Pour élucider la contribution de *Notch3* à la boucle cardiaque, nous avons adopté trois approches. L'analyse des cœurs mutants pour *Notch3* indique que *Notch3* est haploinsuffisant. *Notch3* est partiellement requis pour la boucle cardiaque embryonnaire et à la naissance, pour la septation, la croissance du ventricule droit et pour l'artère coronaire septale. Faisant suite à l'observation que *Notch3* est en aval de *Nodal*, nous avons généré des double mutants. La perte d'un allèle de *Nodal* n'a pas exacerbé le phénotype des hétérozygotes pour *Notch3*, indiquant l'absence d'interaction génétique dans le mésoderme de la plaque latéral entre ces deux gènes asymétriques. Compte tenu de la pénétrance partielle des phénotypes mutants pour *Notch3*, nous voulons surmonter la compensation potentielle par d'autres paralogues de Notch : nous traiterons les mutants pour *Notch3* avec une dose sub-phénotypique d'inhibiteurs de la gamma-sécrétase et évaluerons si cela aggrave les anomalies de la boucle cardiaque. Ces expériences fonctionnelles sont en cours de réalisation.

Durant ce projet, nous avons développé de nouveaux outils pour cribler et quantifier l'expression asymétrique des gènes dans les précurseurs cardiaques. Nous discuterons de la découverte de *Notch3* dans le contexte de l'asymétrie droite-gauche et du développement cardiaque. Par analogie avec le rôle de *Notch3* dans d'autres tissus, nous aborderons les

mécanismes cellulaires régulés par *Notch3*. Dans l'ensemble, ce travail fournit un nouvel éclairage sur les mécanismes de l'organogenèse asymétrique droite-gauche.

Summary of the Thesis in English

Keywords

Left-right asymmetry; Heart morphogenesis; Heart field; Notch pathway; Mouse Genetics; Transcriptomics

Summary

Left-right asymmetry of the heart is essential for establishing the double blood circulation : abnormal left-right patterning of the embryo leads to congenital heart defects in the heterotaxy syndrome. Whereas the heart initially forms as a straight tube, it acquires an asymmetric helical shape during the process of heart looping. This is a key step of heart morphogenesis, during which cardiac chambers are aligned, as a prerequisite for the correct plumbing of the blood circulation.

Although the left determinant NODAL is an important regulator of heart looping, previous work in the lab has shown that it is not the only asymmetry factor : NODAL plays a key role in orienting and amplifying pre-existing asymmetries. Yet, asymmetries other than NODAL signaling have remained unclear. In order to investigate the left-right patterning of cardiac precursors, we designed a transcriptomic approach to screen for differential gene expression in the left and right heart fields of the mouse embryo. The transcriptional screen has been performed in individual embryos, at seven sequential stages of heart looping, providing a resource of hundreds of candidate genes patterning heart field asymmetry.

From an initial pilot screen, we have identified *Notch3* as a novel asymmetric gene and selected it for validation. State-of-the-art 3D spatio-temporal quantitative mapping of *Notch3* expression revealed that it was transiently expressed in the left lateral plate mesoderm including the second heart field, before heart looping. We found that *Notch3* was co-expressed with *Nodal* within this population and that *Notch3* asymmetry was amplified by NODAL signaling, providing the first molecular evidence that NODAL acts as an amplifier of asymmetry.

Given that the mouse has four paralogue Notch receptors, we have investigated potential redundancy between them. From published single cell RNA sequencing and new quantitative mapping, we observed specific expression patterns : *Notch4* expression was negligible, *Notch1* was restricted to the endocardium and dorsal aortae, whereas *Notch2* was expressed in heart progenitors and enriched in the juxta-cardiac field, where *Notch3* is low. We have not detected any obvious asymmetry of *Notch* other than *Notch3*. In *Notch3* mutant heart fields, *Notch1* and *Notch2* were found upregulated, thus indicating potential compensation.

To elucidate the contribution of *Notch3* to heart looping, we have adopted three approaches. Analysis of *Notch3* mutant hearts indicate that *Notch3* is haploinsufficient. *Notch3* is partially required for embryonic heart looping and, at birth, for septation, right ventricular growth and the septal coronary artery. Following the observation that *Notch3* lies downstream of *Nodal*, we have generated double mutants. Loss of one allele of *Nodal* did not exacerbate the phenotype of *Notch3* heterozygotes, indicating no genetic interaction in the lateral plate mesoderm between these two asymmetric genes. Given the partial penetrance of *Notch3* mutant phenotypes, we aim to overcome potential compensation by other *Notch* paralogues : we will treat *Notch3* mutants with a sub-phenotypic dose of gamma-secretase inhibitors and assess whether it worsens heart looping defects. These functional experiments are ongoing.

During this project, we have developed novel tools to screen and quantify asymmetric gene expression in cardiac precursors. We discuss the discovery of *Notch3* in the context of left-right asymmetry and heart development. By analogy with the role of *Notch3* in other tissues, we discuss cellular mechanisms regulated by *Notch3*. Altogether, this work provides novel insight into the mechanisms of left-right asymmetric organogenesis.

Introduction

Left-right asymmetry

On the physiological relevance of left-right patterning

When seeing an organism with a bilateral body plan from the outside, be it human, beluga whale or butterfly, most of them at a glance look to be left-right symmetric. However, this is not the case, as many of our internal organs are not mirror images between their left and right sides or not positioned symmetrically along the midline. For instance in humans, the lungs have different number of lobes on each side, the apex of the heart points towards the left, the liver is located on the right, the stomach and spleen on the left. Even the embryonic gut tube rotates counter-clockwise (Fig 1A).

The left-right asymmetry of organs is an advantage, because it allows a diversification of functions and, consequently, a greater complexity (Belo et al., 2017). One example is the brain, where the centers responsible for controlling language or hand motor coordination are usually restricted to one hemisphere. This is thought to save space, as the alternative would be that each side encompass one of each center, thereby leading to duplications and thus redundancy. Another example is the heart, where the right side is responsible for pumping deoxygenated blood to the lungs, and the left side is responsible for receiving the newly oxygenated blood and pumping it to the body (Fig 1B). The heart is thus a double pump, where the separation and diversification on function between left and right are key for its proper function.

Organs are usually positioned as in Fig. 1A, a condition referred to as *situs solitus*. A rare part of the population has their visceral organs positioned in a mirror image, which is referred to as *situs inversus* (Fig 2A). An American epidemiology study spanning ten years and including examinations of more than 4.6 million individuals calculated that 3:100,000 births have *situs inversus* (Lin et al., 2014).

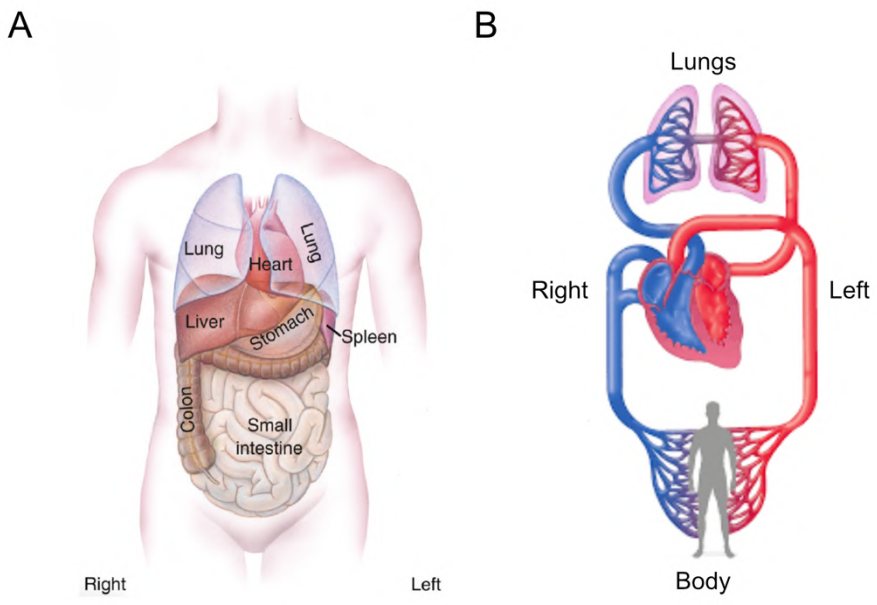

Fig 1. Internal organs can be left-right asymmetric. (A) The visceral organs display left-right asymmetry in shape or position, which is important for their proper function. Schematics from (Blum & Ott, 2018) **(B)** Schematic of the circulatory system, in which the heart serves as a double pump for the blood. deoxygenated blood (blue) is pumped to the lungs, where it oxygenated (red). Afterwards it is transferred to the left side of the heart and pumped into the body. Adapted from Pearson[2]

Heterotaxia can be described as the situation in which organ shape or position is abnormal and neither *situs solitus* nor *situs inversus*. This syndrome is associated with failures in either establishment or maintenance of left-right patterning during development. the prevalence is around 1:10,000 and in general occurrs around twice as often as *situs inversus* (Khoshnood et al., 2012; Lin et al., 2014 ; Guimier, 2015 ; Szenker-Ravi, 2021).

Heterotaxia syndrome is associated with a wide range of abnormalities, including defects in positioning and shaping of organs. The most severe defects are congenital heart diseases (Fig 2A lower panel) and cases of right- or left-sided isomerisms that will impact the vital prognosis of patients. Cases of isomerism are reported when abdominal organs have predominantly either a right- or left-sided identity on both sides, which can lead to a range of defects in these organs (Fig 2A upper panel).

Congenital heart defects are the most common form of congenital defects, and up to 3% of congenital heart defects have been reported to be related to heterotaxia (Zhu et al., 2006).

[2] https://www.pearsonhighered.com/assets/samplechapter/0/1/3/4/0134760611.pdf

Furthermore, up to 90% of all patients with heterotaxia syndrome have a congenital heart defect (with more than nine out of ten of these being severe) (Gabriel & Lo, 2020 ; Lin 2014). Two of these defects are schematized in Fig 2B. Atrioventricular septal defects are defined by holes in the septum between the left- and right sides of the heart, which cause a mixing of oxygenated and deoxygenated bloods. Another defect is transposition of the great arteries, where the two blood circulatory systems are running in parallel, because the pulmonary artery and aorta have switched position. This leads to that oxygen-poor blood flows through the right side of the heart and back to the body without passing through the lungs. Concomitantly, the oxygen-rich blood flows through the left side of the heart and directly back into the lungs without being pumped to the rest of the body. These, along with other congenital heart defects associated with heterotaxia, can arise both alone and in combination, and they can be lethal if not surgically repaired (Desgrange et al., 2018).

As mentioned above, heterotaxia is caused by failure in establishing and/or maintaining the left- and right sided identity of tissues. During development, the embryo is initially left-right symmetric. How this symmetry is broken and laterality is established in the developing embryo has been investigated in great detail during the past 25 years and will be described below (see *Introduction - The breaking of asymmetry and the Nodal pathway*). Our understanding of how organs develop asymmetrically is currently undergoing a paradigm shift.

In the clinics, cases of heterotaxia syndrome were categorized into either right- or left-isomerism. This idea is also seen in the schematics of Fig 2A (upper panel), where the cases of heterotaxia are displayed with the two isomerisms. This grouping of heterotaxia patients associates different defects with each other, and the overall *situs* of the organs is determined from looking at a few dominant criteria. For instance, it has been argued that isomerism can be defined based on the morphology of the atrial appendages (Tremblay et al., 2017).

This is however challenged by case reports such as (de Bellaing et al., 2021), where the authors report a patient, whose organ pattern does not fit into these discrete categories of left- and right isomerism according to the atrial appendages. In fact, when this has been studied systematically, it is found that for more than 20% of heterotaxia cases, these classical patterns are breached (Yim et al., 2018). Instead, it would be more proper if each organ laterality is assessed independently, as heterotaxy encompasses a broad range of defects.

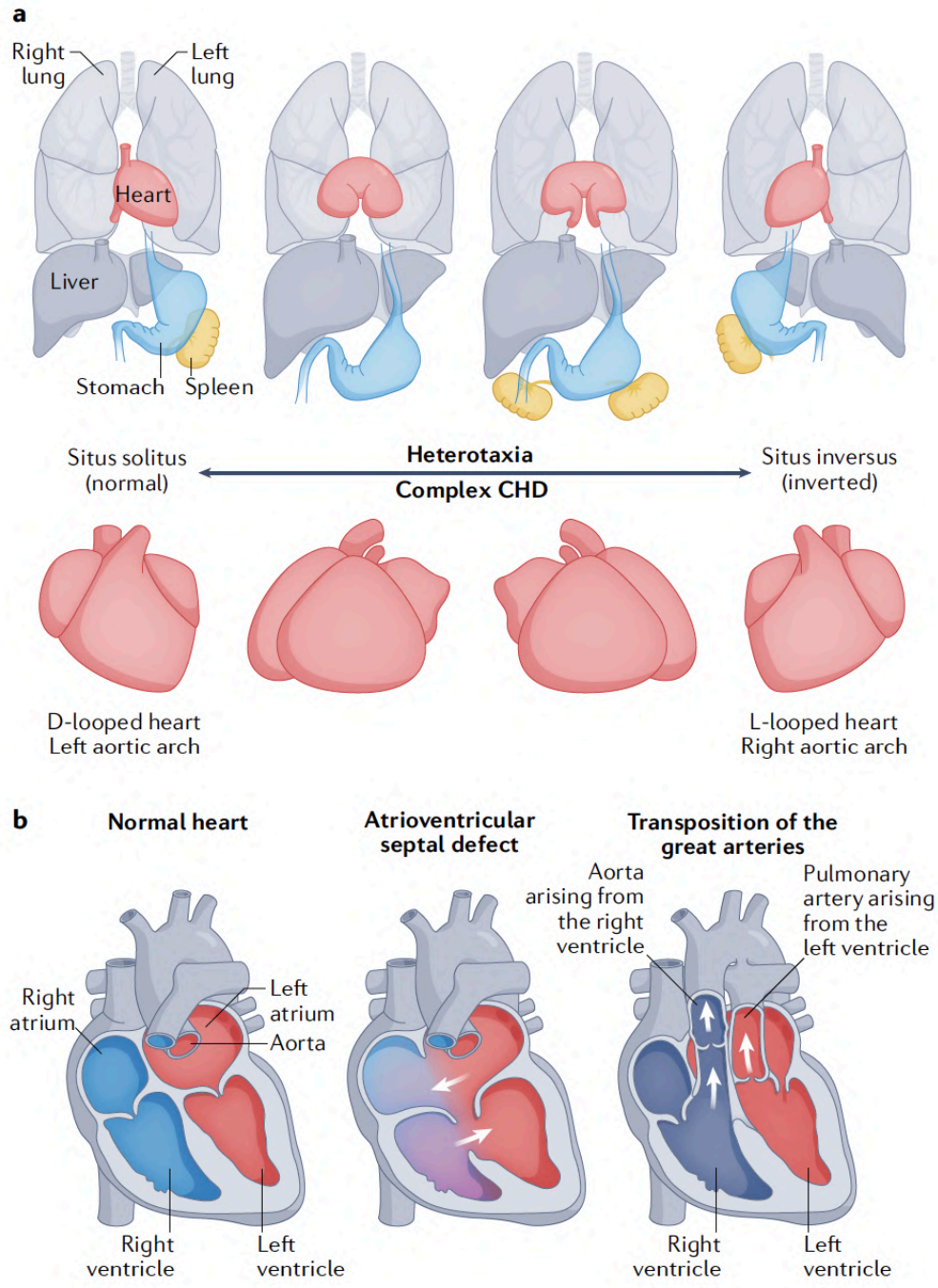

Fig 2. Heterotaxia syndrome can lead to congenital heart diseases (A) Schemes showing normal positioning (*situs solitus*) of the visceral organs (left) and the *situs inversus* (right), in which organs are positioned in mirror images. In-between these two situses are the heterotaxia cases, where improper laterality in the organs can lead to a spectrum of defects including congenital heart defects (CHD). **(B)** Left: Scheme of a normal heart with proper separation between the left- and right sides and proper connection of cardiac segments. Middle: Scheme of a heart suffering from atrioventricular septal defects causes a mixing of blood (purple). Right: Scheme of a heart with transposition of the great arteries, where the oxygenated (red) and deoxygenated (blue) blood are separated in two independent circuits, and thus the systemic blood will not get oxygenated. From (Djenoune et al., 2022)

This emerging assessment of organ laterality fits with how some developmental biologists view the process of left-right asymmetry establishment. A main hypothesis is that each organ independently develops its asymmetries, and that there is a biasing signal coordinating laterality across the organism. This idea was proposed already in 1990 by the phenomenal biologists Nigel A. Brown and Lewis Wolpert (Brown & Wolpert, 1990). They suggested a three-step model, which can be reduced to a two-step process (Fig 3).

As taught in general chemistry classes, molecules can have a chirality. This is relevant in biology, where for instance only the L-stereoisomer of amino acids are used to construct proteins in nature. The first step is thus to convert this molecular asymmetry into a cellular- or tissue asymmetry, which will give a left-right bias. The next step is the interpretation of this bias. Organs (according to the model) have random generators of asymmetry that in the absence of signal bias will form random deformations (such as generating the same number of lung lobes on each side). However, during normal development, the signal bias will provide a reference axis that is used by several organs to orient their laterality consistently.

As will be described below, our understanding of how left-right symmetry is broken and the signals that govern the left-right bias has grown tremendously the past 25 years. However, as the example regarding heterotaxy and congenital cardiac malformations described above shows, there are still many open questions on how symmetry breaking and left-right bias is translated into organ shape. Regarding this, the two most explored organs are the heart and the gut (le Garrec et al., 2017; Savin et al., 2011), where there has been a research focus on exploring which genes are asymmetrically expressed, and how these asymmetrically expressed genes can drive organ asymmetry. In the work of this thesis, we have screened for novel genes and pathways asymmetrically expressed in the cells driving asymmetric heart morphogenesis, and we have characterized the role of one of these (Notch signaling) in regarding to this. But before we can explore how organs can become asymmetric, we first have to review how left-right asymmetry is initially established in the embryo.

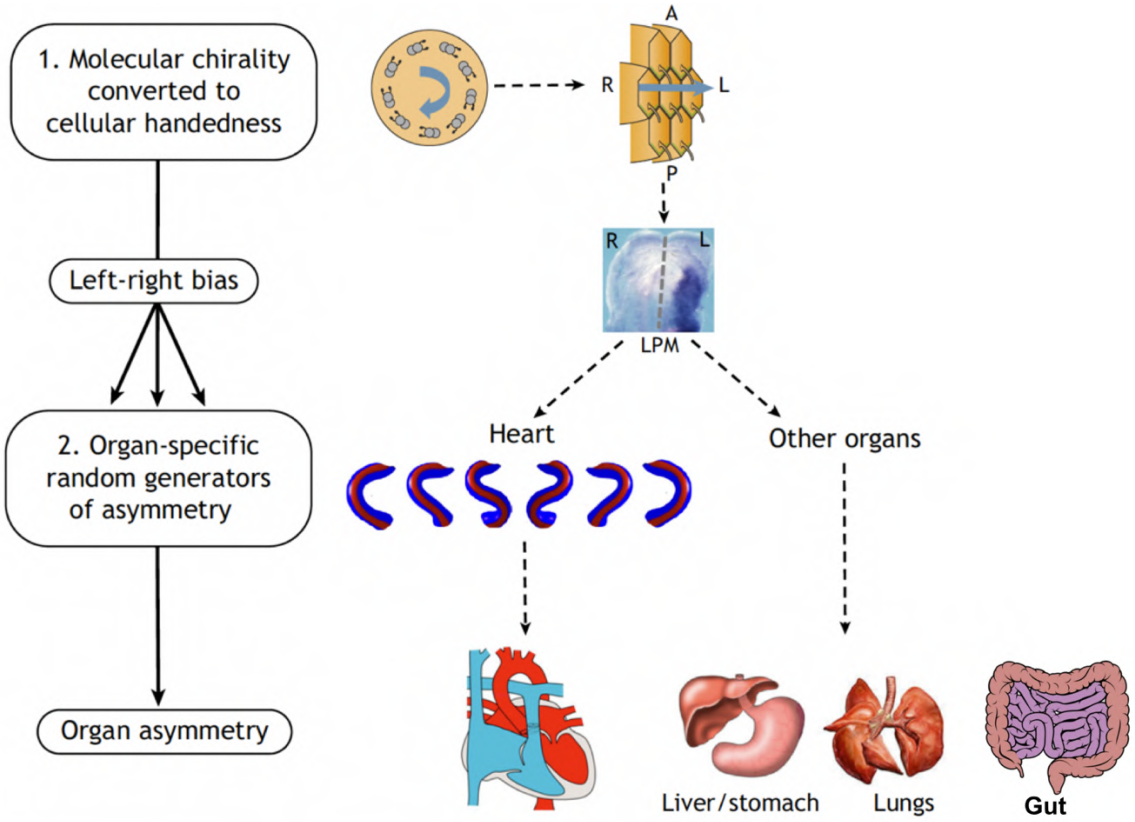

Fig 3. Brown-Wolpert model of asymmetry generation. Molecular chirality stemming from protein structures is converted into a cellular handedness/direction, thus forming a left-right bias. This bias functions as a reference axis for organs that each contain specific generators of asymmetry (such as looping in the heart and the gut), thus generating the final shape. A, anterior; L, left; LPM, lateral plate mesoderm; P, posterior; R, right. From (Desgrange et al., 2018)

The breaking of symmetry and the *Nodal* pathway

The Brown-Wolpert model of symmetry breaking was confirmed experimentally in the following decades, in which researchers both investigated how asymmetry is initially established as well as the signaling pathways involved in propagating left-right asymmetry. In short, most of the higher animals studied so far (from zebrafish to mice) use a transient organ generally referred to as the left-right organizer, which induces the Nodal pathway on the left side of the embryo[3] (Fig 4). Molecular asymmetry between the left and the right sides of the embryo can be detected at the time when the first somite pairs forms (Nonaka et al., 2002;

[3] There are exceptions to this. For instance, in *Drosophila*, where the two asymmetric organs, the sperm duct and gut tube, are rotating dextrally due cell rotations caused by myosin genes (Spéder et al., 2006). Myosins are powerful regulators of rotations. If overexpressed in not rotating tissues, they can induce rotation. Furthermore, the direction can change depending on the myosin sub-type (Lebreton et al., 2018).

Vincent et al., 2004), which in the mouse is around E8.0. The core of the Nodal pathway consists of the TGF-β superfamily member Nodal, a secreted factor which induces (among others) itself, *Lefty1/2* and *Pitx2*. *Lefty1/2* are both repressors of *Nodal* expression, and thus serve as feedback inhibition mechanism. The left-sided Nodal pathway serves as the a left determinant and will be described in detail later.

Although left-sided Nodal pathway expression is well conserved among deuterostomes, the inductive mechanism is not always the same (Coutelis et al., 2014). This diversity is also reflected in their naming, for instance the left-right organizer in the mouse is named the node, in zebrafish Kupffer's vesicle, in chicken Hensen's Node and gastrocoel roof plate in *Xenopus*. The mouse node and the zebrafish Kuppfer's vesicle are the two most studied left-right organizers. They are both small transient structures positioned on the ventral side of the embryo, where they form a mono-layered cup (mouse) or sac (zebrafish) consisting of epithelial-like cells that are mono-ciliated (Jurand, 1974; Lee & Anderson, 2008).

Some of the cilia in the left-right organizer are motile and generate a flow, which is necessary for proper left-right patterning. If the cilia are missing (Nonaka et al., 1998), shorter (Lopes et al., 2010), immotile (McGrath et al., 2003) or if the fluid flow is compromised by e.g. increasing the viscosity of the fluid (Nonaka et al., 2002) it all leads to randomization of lateralization. That fluid flow is the inducer of lateralization has been shown by that creating artificial flow in mutants with immotile cilia, which can rescue laterality defects. Similarly, if fluid flow is reversed, it can induce an opposite pattern of lateralization (Nonaka et al., 2002).

Not all left-right organizers are dependent on motile cilia. For instance, Hensen's node in the chicken uses an alternative strategy for symmetry breaking that relies on a counter-clockwise cell displacement leading to left-sided *Nodal* pathway expression (Cui et al., 2009; Gros et al., 2009). Upstream of the asymmetric cell displacement are asymmetric Fgf- and Shh signaling as well as ion differences caused by H^+/K^+-ATPases. What is upstream of those is still unknown.

From an evolutionary developmental biology perspective, it is surprising (and thereby interesting) that the process of symmetry breaking is mechanistically not well conserved, and several publications in the recent years have looked into symmetry breaking in non-model organisms and found diversity (Kajikawa et al., 2020; Onuma et al., 2020; X. Zhu et al., 2020). As reviewed in (Coutelis et al., 2014), there are both common and divergent principles of left-right formation, which might be related to how organisms ensure that their symmetry

breaking is robust. It goes beyond the scope of this introduction to cover this diversity, and therefore the focus will be on cilia-driven flow models of symmetry breaking (as seen in e.g. mouse and zebrafish), as this is believed to be the mechanism in humans. Although not experimentally proven or directly observed, as left-right organization occurs around embryonic day 20 (Carnagie stage 9) in human embryos (O'Rahilly & Müller, 2003) (thereby after the gastrulation/14-day limit set for human experimentation), human symmetry breaking is believed to be dependent on cilia driven flow because mutations in cilia genes cause heterotaxy syndrome (Guimier et al., 2015; Szenker-Ravi et al., 2022).

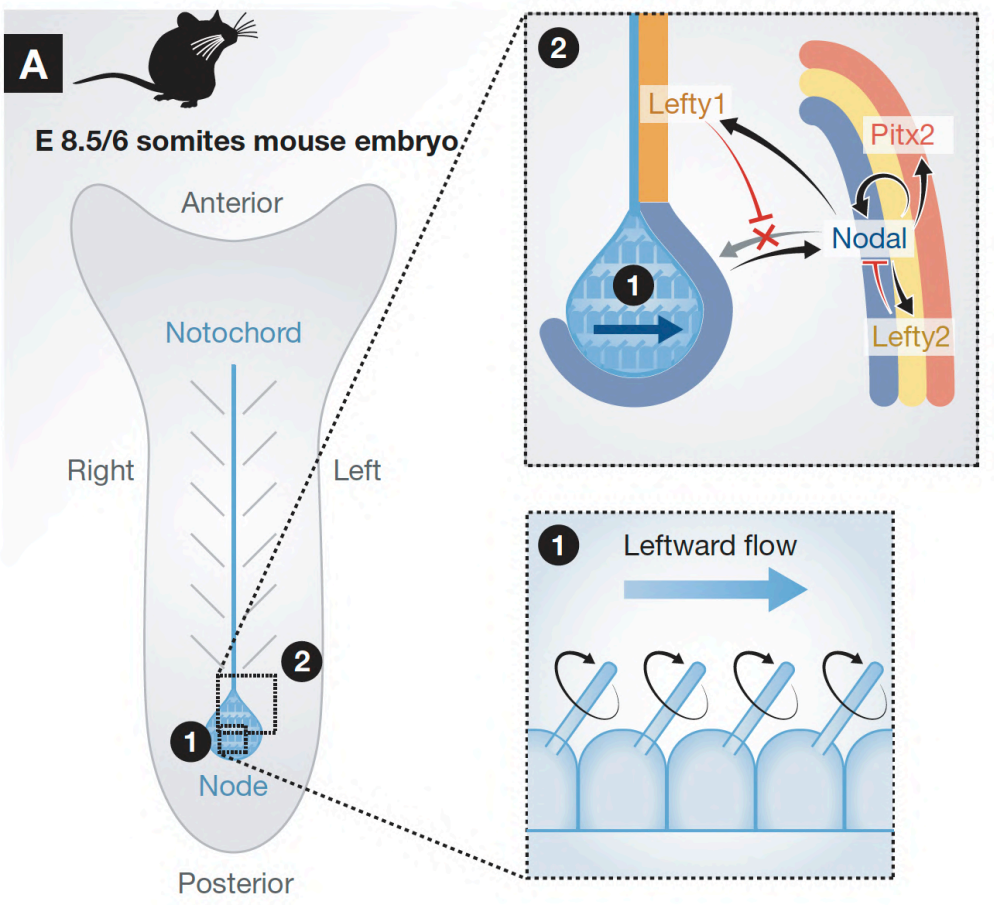

Fig 4. Symmetry breaking in the mouse. At the posterior end of the notochord is a transient organ named the node, which acts as the left-right organizer in the mouse. The node is a pit, consisting of mono-ciliated cells. cilia generate a leftward flow (1), which restricts expression of *Nodal* on the left side of the node (1) and of the Nodal pathway genes on the left side of the embryo (2). The Nodal pathway consists of the *Nodal* gene and its direct targets *Lefty1/2* and *Pitx2*. The *Lefty* genes encode antagonists of *Nodal* and thus provide a negative feedback loop. From (Coutelis et al., 2014)

Careful work by Sulik *et al.* using scanning electronic microscopy and dye-injection cell labelling has described the origin and development of the mouse node (Sulik et al., 1994). Cells that during the mid-late streak phase (E7.0-E7.5) are located near the anterior end of the primitive streak, will at the zero bud (0B) stage form a plateau of mono-ciliated cells with a small apical surface (Fig 5A-B). These will be surrounded by cells with a larger apical surface. One stage later, at the early headfold stage (EHF) (E7.5-E7.75), the node has formed a concave shape (Fig 5C-D), where the cells with the small apical surface are within the pit of the concave (and are referred to as pit cells), while the cells with the larger apical surfaces are on the edge of the pit. These cells are referred to as crown cells.

Both pit- and crown cells have a single cilium, however studies have shown that the cilia located on the pit cells contain the dynein protein Dnah11 making them motile, while the cilia of the crown cells are immotile and are instead responsible for sensing the flow (Fig 5E) (McGrath et al., 2003).

A leftward flow is necessary and sufficient for proper lateralization (Nonaka et al., 2002), and the leftward flow is generated by the posterior tilt of cilia. The latter is due to the positioning of the basal body within the cell (which anchors the cilium), downstream of PCP signaling (Nonaka et al., 2005 ; Minegishi et al., 2017). As the cilia rotates clockwise, this will lead to the leftward flow. This clockwise rotation is due to the structure of the microtubules in the cilia (J. Lin & Nicastro, 2018), and it is an example of how molecular chirality is converted to a cellular handedness as described in the Brown-Wolpert model (Fig 3).

When immotile cilia sense the flow, a molecular cascade is induced that ends with the *Nodal* pathway being expressed on the left side. There have been two main hypotheses on how the immotile cilia could initiate molecular events leading to asymmetric gene expression; *chemosensing*, where small molecules or vesicles are transported predominantly to one side and thus inducing changes, and *mechanosensing*, where the immotile cilia of the crown cells senses the directed flow. No secreted small molecule or vesicle has been identified so far in the node, with functional impact on left-right patterning. Recent work by Katoh et al. in the mouse rather supports the mechanosensing model, because they show that manipulating single cilia on crown cells, using atomic force microscopy, is enough to generate asymmetric gene expression (Katoh et al., 2022). Further work is required to exclude the possibility that asymmetric chemical signal exists concomitantly.

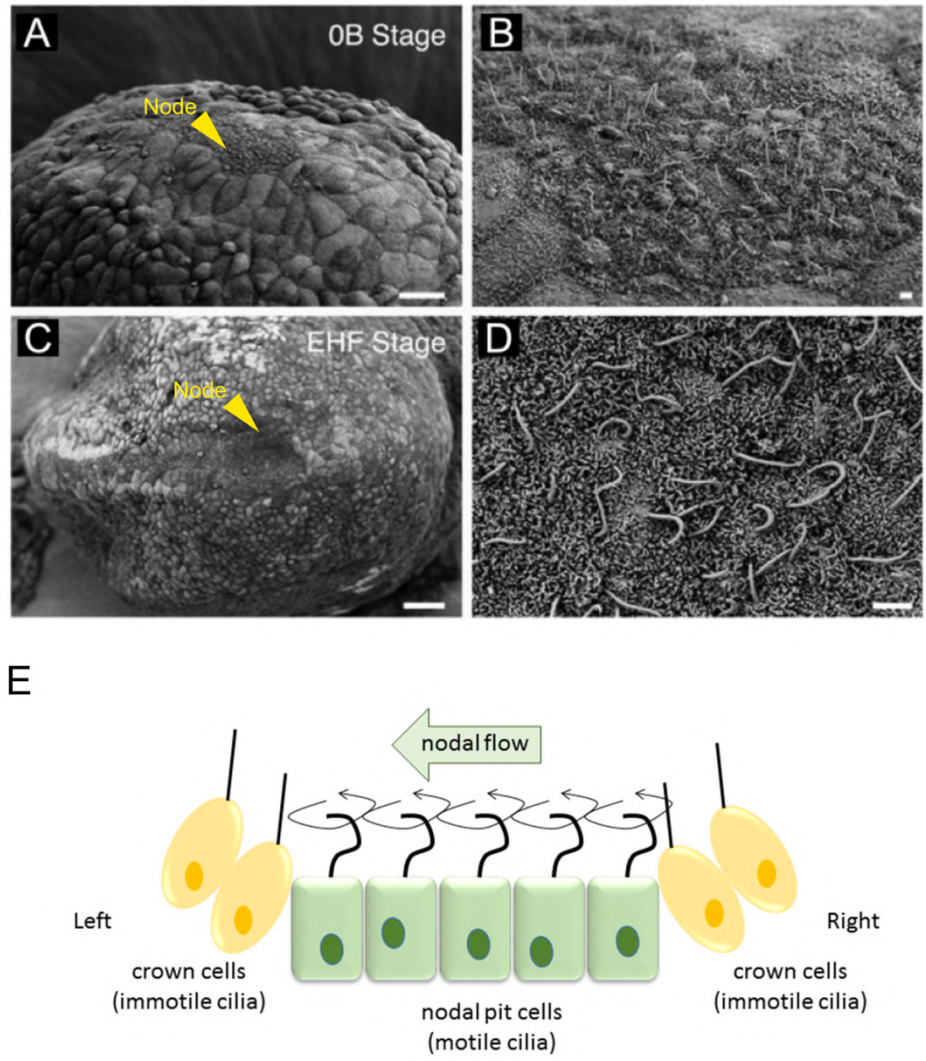

Fig 5. **The formation of the node and the leftwards flow within the pit.** Scanning microscopy images of the node cells at the zero bud (0B) **(A-B)** and the early headfold stage (EHF) **(C-D)**. At the 0B stage, node cells are ciliated however the concave has not yet formed. One stage later, the node has the shape of a pit. Size bars: A,C = 20 μM; B,D = 2 μM. From (Lee & Anderson, 2008) **(E)** Model of the node pit. Motile cilia located on the pit cells will induce a leftwards flow. This directional flow will be sensed by immotile cilia on the crown cells. From (Vingerhoets et al., 2021)

In 1996, two papers were published back-to-back reporting the expression of two genes asymmetrically expressed in the lateral plate mesoderm of the mouse around early somite stages (Collignon et al., 1996; Meno et al., 1996). These were *Nodal* and *Lefty*, who are two of the three core-members of the left-sided Nodal pathway, which is now known to regulate organ laterality (see Fig 4) (Actually, the *Lefty* probe detects two genes, *Lefty1* and *Lefty2*, which are both involved in left-right patterning). The last member, *Pitx2*, was found a few

years later to be left-sided in the same regions (Ryan et al., 1998). It was later shown that the isoform *Pitx2c* is the main asymmetric isoform (Kitamura et al., 1999), however work in the host lab demonstrated that the other isoforms, Pitx2a and Pitx2b, also play role in asymmetric heart development (Desgrange et al., 2020). For all three members it was shown that their asymmetry is dependent on a functional left-right organizer, and that they regulate each other to control organ laterality.

Nodal expression begins in the crown cells of the node around the early headfold stage (Fig 6A) (Collignon et al., 1996; Kitajima et al., 2013). It is initially expressed symmetrically in the crown cells, but then around the 2-3 somite stage becomes predominantly left-sided (Kawasumi et al., 2011; Kitajima et al., 2013), and it has been studied in great detail how the node flow leads to left-sided expression of *Nodal*.

Dand5 (also known as *Cerl2*) encodes an inhibitor of Nodal signaling important for restricting Nodal activity on the left side of the node crown cells. *Dand5* is expressed asymmetrically in the node prior to *Nodal* with higher levels on the right, and if *Dand5* is absent it leads to symmetric *Nodal* expression (Marques et al., 2004; Oki et al., 2009). Dand5 is a potent inhibitor of *Nodal* expression, as right-sided *Dand5* will lead to asymmetric Nodal signaling (measured by its downstream effector pSmad2) even if *Nodal* is symmetric (Fig 6B) (H. Hamada, 2020).

Mechanical activation of cilia in crown cells is enough to bias *Dand5* expression on the right (Katoh et al., 2022), and right-sided Dand5 localization has been shown to be dependent on mRNA degradation (Maerker et al., 2021; Minegishi et al., 2021). It has also been proposed that *Wnt3* is an upstream regulator of *Dand5*, as *Wnt3* is expressed asymmetrically prior to *Dand5*, and inhibition of Wnt signaling leads to symmetric *Dand5* (Kitajima et al., 2013). On top of this, asymmetric Ca^{2+} in the left-right organizer (on both an intracellular and extracellular level) has been shown to play a role in left-right asymmetry breaking at a level downstream of flow-sensing, but upstream of *Dand5* and *Nodal* asymmetric expression, and inhibition of this leads to laterality defects (McGrath et al., 2003; Raya et al., 2004; Takao et al., 2013). So far, a complete model integrating all these observations has not been proposed, as we for instance do not mechanistically understand how vibration of cilia leads to gene expression. Additionally, we do not understand how every asymmetrically identified gene is related to each other, and if there are other asymmetrically expressed genes in the node (for instance during the work of this thesis, we identified a new gene

asymmetrically expressed in the node crown cells). Further work (likely involving very careful manipulations of the left-right organizer as well as careful screenings) is necessary to completely understand symmetry breaking in the mouse node.

Altogether these data have demonstrated the importance of *Nodal* to be asymmetrically expressed in crown cells. As the cells of the node do not contribute to other organs (Lee & Anderson, 2008), the next step is then to relay this information from the crown cells of the node into organ precursors to further establish a left identity during organ formation.

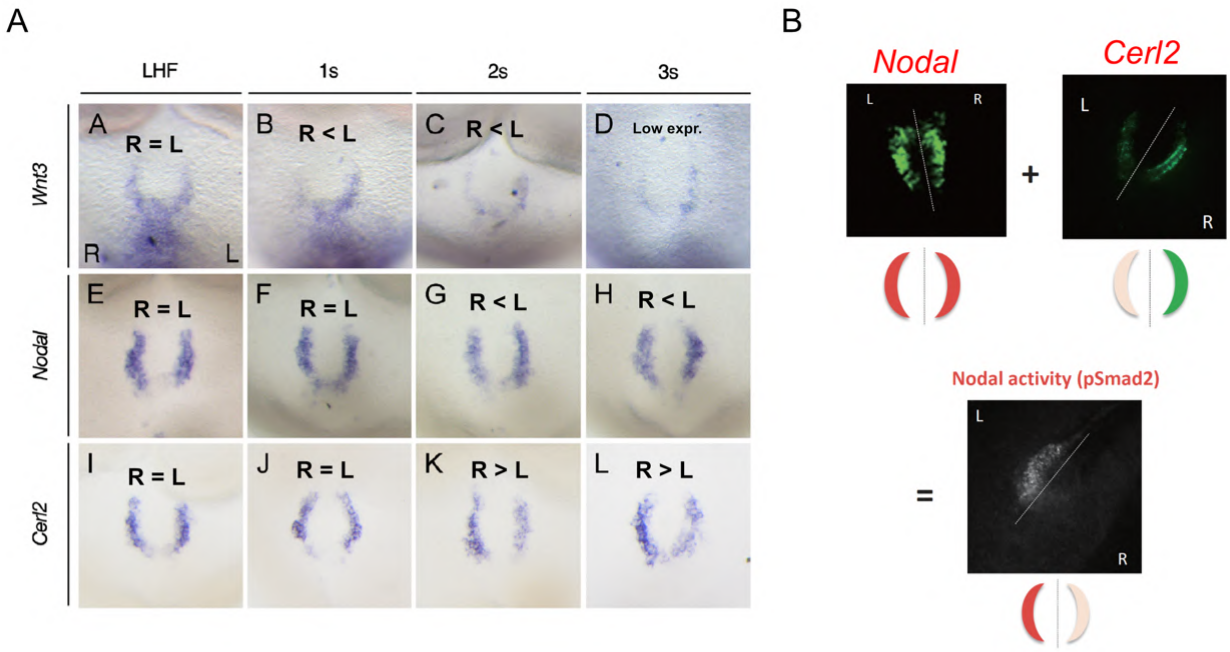

Fig 6. Gene expression patterns within the node. **(A)** In situ hybridization of *Wnt3*, *Nodal* and *Cerl2* expression in the node show their relative kinetics. At the late headfold stage (LHF), they are all left-right symmetrically expressed. One stage later, *Wnt3* is higher on the left, followed by *Cerl2* on the right at the next stage and *Nodal* on the left. Adapted from (Kitajima et al., 2013). **(B)** *Cerl2* is a potent inhibitor of Nodal signaling, as symmetric expression of *Nodal* combined with asymmetric expression of *Cerl2* leads to asymmetric Nodal activity (measured by pSmad2). Adapted from (H. Hamada, 2020). L = Left; R = Right

Beyond the left-right organizer

Nodal signaling in the lateral plate mesoderm is a determinant of organ laterality, and depends on prior asymmetric expression of *Nodal* in crown cells (Brennan et al., 2002). The mechanism by which *Nodal* is relayed from the crown cells to the lateral plate mesoderm (which is several cells away) without activating *Nodal* expression in the pre-somitic mesoderm in-between is

not well understood, however it has been demonstrated that proper Nodal propagation is dependent on sulfated glucosaminoglycans (Oki et al., 2007) as well as the *Nodal* co-ligand *Gdf1* (C. Tanaka et al., 2007). Similarly, how Nodal is relayed from one cell to another in the lateral plate mesoderm is also not clarified. There is evidence suggesting a relay mechanism, where *Nodal* expression in one cell induces *Nodal* expression in the next one (L. Liu et al., 2021). This also explains how the Nodal pathway propagates through the left lateral plate mesoderm, where it is initially expressed laterally to the node and then propagates anterior and posteriorly.

In the context of left-right asymmetry, the *Nodal* gene has two relevant enhancer elements. The node-specific enhancer (NDE), which controls *Nodal* expression in the left-right organizer, and the left-side specific enhancer (ASE, stemming from *asymmetric expression*), which is required for left-sided expression of *Nodal* in the lateral plate mesoderm (Adachi et al., 1999; Brennan et al., 2002; Norris et al., 2002; Norris & Robertson, 1999; Saijoh et al., 1999). *Nodal* signals through P-Smad2 and the transcription factor Foxh1, which activate transcription through the ASE genetic element (Norris et al., 2002), which explains why *Nodal* induces itself in the lateral plate mesoderm. The other Nodal pathway genes, *Lefty2* and *Pitx2*, also have ASE elements (Shiratori et al., 2001). Beyond these known asymmetrically expressed genes, Desgrange et al. has shown that *Nodal* regulates a range of cardiomyocyte differentiation- and extracellular matrix genes, and 50% and 40% of these (respectively) have an ASE element in their viscinity (Desgrange et al., 2020).

What is the role of Nodal pathway members? As seen above, *Nodal* itself serves as a left determinant, which is important for inducing asymmetric gene expression. *Lefty2* is a direct inhibitor of *Nodal*, which is important for restricting *Nodal* expression in time and space (Meno et al., 2001). *Nodal* also induces another *Lefty* gene, *Lefty1*, which is expressed at the midline and servers as a barrier, ensuring that Nodal is not inducing its own expression on the right (Meno et al., 1996). Like the Nodal protein, Lefty1 and Lefty2 belong to the TGF-β superfamily and they inhibit *Nodal* through receptor binding and thus out-competing Nodal binding to its receptor (Cheng et al., 2004). Beyond signal restriction in time and space, the *Lefty* genes are also responsible for dampening *Nodal* signal, which increases the robustness of the system (Montague et al., 2018; Rogers et al., 2017). Altogether this feedback inhibition leads to a

short time window of *Nodal* and *Lefty2* expression in the left lateral plate mesoderm, between the 3 and 6 somite stages (Desgrange et al., 2020; Vincent et al., 2004) (Fig 7A).

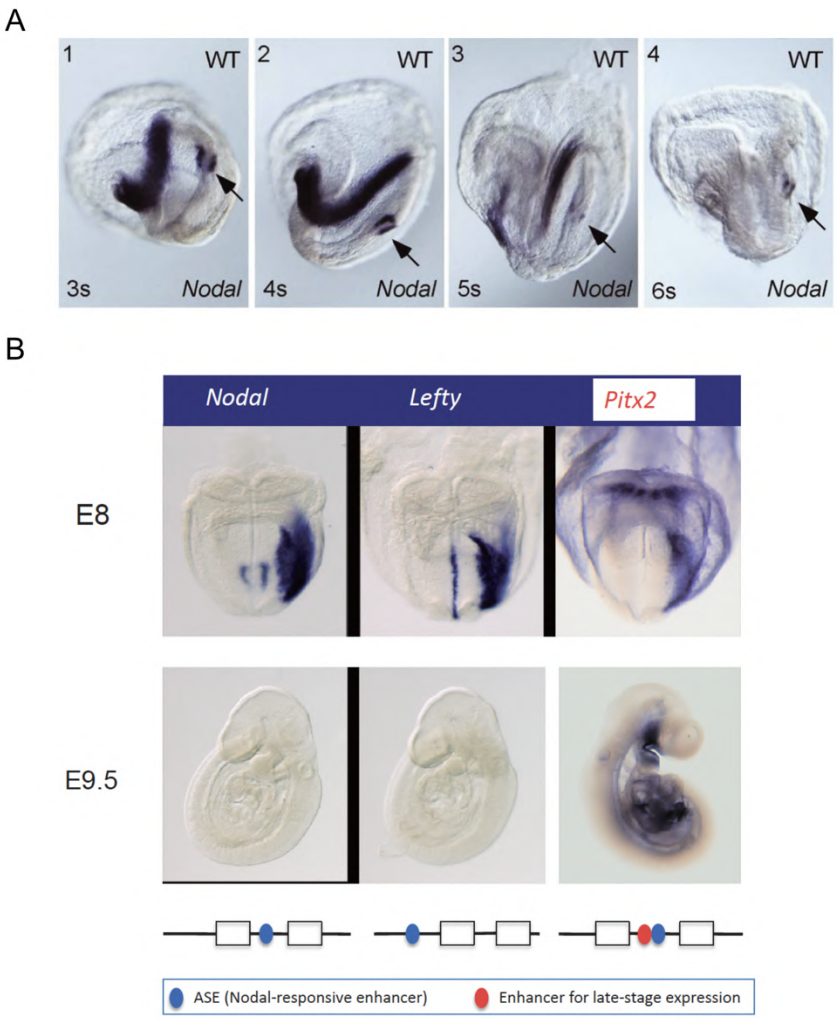

Fig 7. Expression pattern and kinetics of the Nodal pathway. (A) Brightfield images of the left side of embryos at the 3-6 somite stage after *in situ* hybridization of *Nodal*. The kinetics of *Nodal* expression is rapid as *Nodal* expression is almost gone by the 6 somite stage. Arrow points to the node. From (Vincent et al., 2004). **(B)** At the E80-E8.5 stage, *Nodal, Lefty1/2* and *Pitx2* are asymmetrically expressed in the left lateral mesoderm, however at E9.5 only *Pitx2* expression persists. This is because *Pitx2* has another enhancer element responsible for continued expression and alternative induction. From (H. Hamada, 2020)

Pitx2 is also asymmetrically expressed in the left lateral plate mesoderm, but compared to *Nodal* and *Lefty2*, its asymmetry persists longer (Fig 7B). This is because *Pitx2* has another element than the ASE, which ensures longer expression (Shiratori et al., 2001). Furthermore, *Pitx2* has been shown to be downstream of the heart progenitor markers *Tbx1* and *Nkx2-5*,

demonstrating that Pitx2 is also regulated by genes which are anterior-posterior regionalized within the lateral plate mesoderm (Nowotschin et al., 2006). Because *Pitx2* mutants harbor laterality defects, it has been said that *Pitx2* is the effector of the Nodal pathway and is responsible for providing cells a left-sided identity controlling further asymmetric morphogenesis of visceral organs (Piedra et al., 1998; Ryan et al., 1998). On a cellular level, experiments in the zebrafish have shown that *pitx2* is able to regulate asymmetric properties of extracellular matrix proteins, cell migration and the planar cell polarity pathway (Collins et al., 2018)

Although *Pitx2* is very important, new research shows that *Nodal* dependent, *Pitx2* independent laterality defects exist. This is for instance seen by the different heart laterality defects observed in *Nodal* conditional mutants and *Pitx2* mutants, where *Nodal* mutants can lead to leftwards or rightwards rotation, while *Pitx2* mutants always rotate rightwards. However, the *Pitx2* mutants display anomalies of ventricle position, and as such regulates some aspects of *Nodal* signaling. Oppositely, *Pitx2* mutants also display defects in the heart not observed in *Nodal* mutants, showcasing that *Pitx2* has roles beyond *Nodal* (Desgrange et al., 2020).

On a molecular scale, several miRNAs have been shown to be regulated by *Nodal* in a *Pitx2* independent manner (Rago et al., 2019) as well as cardiac differentiation- and extracellular matrix genes (Desgrange et al., 2020).

This opens up new lines of research aiming understand how organs develop asymmetrically. Two of the most studied organs are the heart and the gut, who both become asymmetric during a looping process. However, even though both organs loop, they are very different in form, function and timing of development, which is also reflected in how differently they become lateralized. Asymmetric development of the heart is the focus of this thesis work, and thus heart development (along with how it acquires its asymmetric shape) will be described in details in the following chapter, while gut looping will be described below.

How molecular signaling can drive asymmetric organogenesis is now being analysed with increased spatiotemporal and molecular resolution (le Garrec et al., 2017; Sivakumar et al., 2018). As stated in the Brown-Wolpert model (Fig 3), each organ should have a random asymmetry generator that should sense the Nodal pathway (or potential other left-right

asymmetric signaling). A proof of such random generators is seen in the heart, where a buckling mechanism drives proper formation of the asymmetric heart (see *Heart looping – when the heart becomes asymmetric*). In the gut, which loops counter-clockwise, proper rotation is dependent on a leftwards tilt in the dorsal mesentery, the structure which connects the embryonic gut tube to the body wall (Davis et al., 2008). This tilt occurs around E10.5 (Fig 8A-B).

The research on gut looping has primarily been performed in first the lab of Cliff J. Tabin and later in the lab of Natasza Kurpios. They initially showed that gut looping is dependent on Pitx2, as *Pitx2* mutants are left-right symmetric in terms of gut tilting (Davis et al., 2008), meaning that *Pitx2* is the effector of left-right asymmetry in the gut (Fig 8C). As will be described later (see *Heart looping – how the heart becomes asymmetric*), this is not the case in the heart. They found that extracellular matrix genes and cell adhesion genes were regulated by Pitx2, which were important for proper gut looping (Kurpios et al., 2007).

It was recognized that there is dynamic left-right asymmetric gene patterning occurring within the dorsal mesentery, so a transcriptomics screen was at performed on the left- and right dorsal mesentery at different stages of gut looping (Mahadevan et al., 2014; Welsh et al., 2013). This screen lead to the discovery of novel mechanisms in left-right asymmetric organogenesis and in the role of *Pitx2*. For instance, it was found that Pitx2 acts through Wnt signaling via the Wnt effector *Daam2* (Welsh et al., 2013). Furthermore it was shown that arteries are only formed in the left side of the dorsal mesentery, which is important for proper vascularization of the gut (Mahadevan et al., 2014). It also revealed a key process to how the gut tube becomes asymmetric. It was realized early that the right-sided dorsal mesentery expanded, which is important for the leftwards tilt (Fig 8B) (Kurpios et al., 2007). This right-sided expansion was shown to be due to covalent modification of hyaluronan, an extracellular matrix component, through the enzyme Tsg6 (Sivakumar et al., 2018). Connected this work shows that multiple genes, pathways and processes are important for proper organ asymmetry.

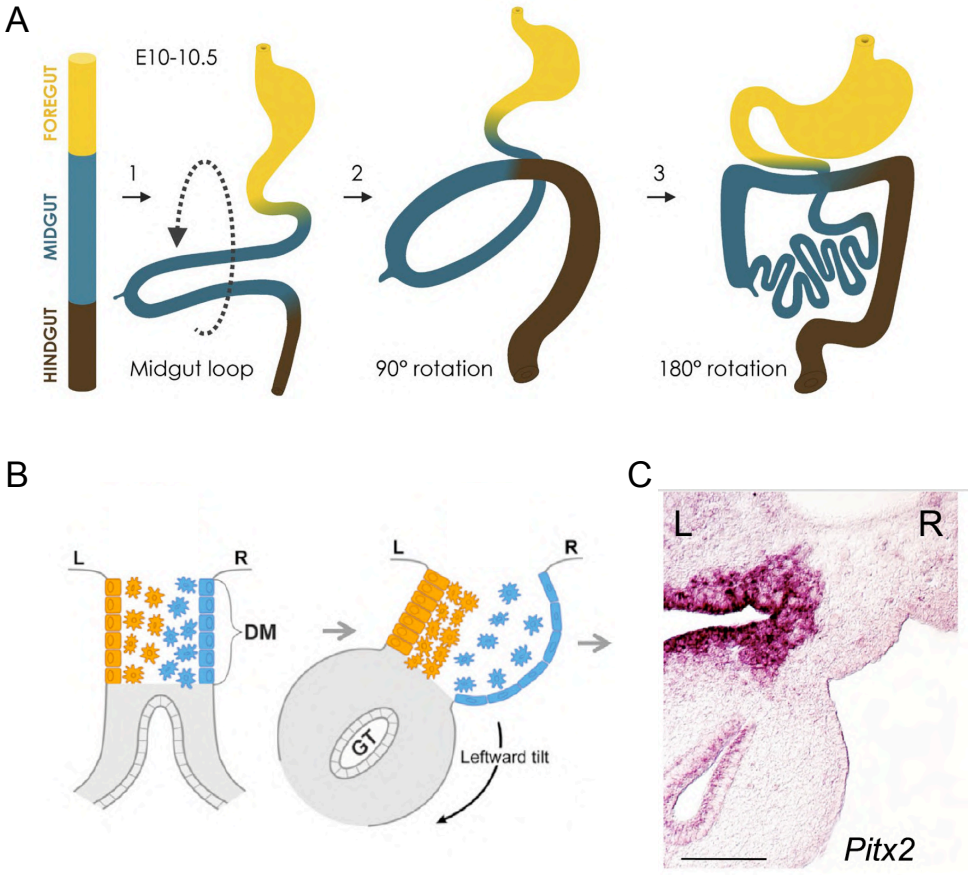

Fig 8. Looping in the gut. (A) The counter-clockwise looping of the gut tube (GT) occurs around E10.5 in the mouse. From (Sivakumar & Kurpios, 2018). **(B)** This rotation is driven by a leftwards tilt in the dorsal mesentery (DM), which is caused by among other expansion of the extracellular matrix. **(C)** *Pitx2* is expressed only on the left side of the dorsal mesentery. In the absence of *Pitx2*, there is no tilt. B+C from (Mahadevan et al., 2014).

The research on how the gut loops have described novel genes that play roles in left-right asymmetric organ development and shows the complexity of how organs become lateralized. Similar work has also been performed in regard to the heart, but sometimes there have been conflicting reports. In 2013 it was for instance claimed that early stages of heart asymmetry were independent of *spaw* signaling (*Nodal* paralogue) in the zebrafish (Noël et al., 2013). However, it was later pointed out that this was not the case, as Crispr mutants of *spaw* affected heart looping (Montague et al., 2018). Montague et al., has argued that the *sfw* mutant used by Emily et al., is not a true null-allele. Moreover, a right-handed pathway (consisting of Bmp signaling and driver of epithelial to mesenchymal transition prrx1) regulating asymmetric heart morphogenesis was reported in (Ocaña et al., 2017), but later

work connected this right-handed pathway to Nodal signaling through miRNA regulation (Rago et al., 2019). Both examples show that developmental biologists have to work carefully to answer questions of left-right asymmetric organogenesis and the relationship between new asymmetric genes and the Nodal pathway.

In the course of this PhD project, we have aimed to understand how the heart becomes asymmetric in greater details. In order to tackle the challenges associated with this (and inspired by among other the work in the gut) we decided on a transcriptomics approach. As will be described in the next chapter, recent work in the lab has made it clear that there are more pathways involved in left-right asymmetry beyond the Nodal pathway, and that these asymmetries are occurring rapidly (Desgrange et al., 2020). To explain the reasoning for how we designed our transcriptomics strategy to explore the kinetics of left-right asymmetry in the heart, it will be necessary first to review the heart and its development.

Development of the Heart

Anatomy and Development of the Heart

The heart is a muscular organ whose main role is to pump blood, containing nutrients and oxygen, through the vessels of the body. Inside the heart, the blood will be either oxygenated or deoxygenated, and the heart must ensure that deoxygenated blood is pumped to the lungs, while oxygenated blood is propelled to the body. The mixing of oxygenated and deoxygenated blood is prevented by the segregation of the heart into two halves, where the blood will pass through each half per circuit. Because of this separation the heart is referred to as a double-circuit system.

Deoxygenated blood from the body reaches the heart though the caval veins and right atrium (Fig 9A). Here it flows through one of the atrioventricular valves, the triscupid valve, before reaching the right ventricle. When the heart contracts, the right ventricle pumps the blood towards the lungs via the pulmonary arteries. After oxygenation, the blood returns to the heart via the pulmonary veins and left atrium. After flowing through the other atrioventricular valve (the mitral valve), the blood reaches the left ventricle, whereupon it is pumped to the body through the aorta (Depicted in *Introduction - Fig 1B*).

The two ventricles are positioned next to each other, and they are separated by the inter-ventricular septum. An electrical pulse from the sinoatrial node orchestrates heart contraction. It propagates through the atria and the atrioventricular node, which (after a delay) will relay the pulse into the ventricles, leading to heartbeat.

There are three main layers of the heart; (1) the outer layer of epicardium, important for protecting the heart and involved in cardiac repair, (2) the inner layer of myocardium underlying the contraction of the heart and (3) the inner layer of endocardium, which among other is required for making sure the blood flows smoothly inside the heart. Between the epi- and myocardium runs the coronary arteries, which are important for supplying energy to cardiomyocytes.

As seen above, the shape of the heart reflects its function as a pump driving a double circuit system, and thus the formation of the heart during development must ensure that such a shape is generated properly. Like human, the mouse has four cardiac chambers (2 ventricles

and 2 atria) and is widely used as a model organism for cardiac related research (for instance in the work of this thesis), and will in this chapter be used as an example of heart development (Harvey, 2002).

The earliest cardiomyocyte cells arise at the headfold stage in the mouse around E7.5-8.0, forming a crescent below the headfolds, referred to as the cardiac crescent (Fig 9B). Already at this stage, cardiomyocytes are beating (Tyser et al., 2016). When they differentiate, cardiomyocytes detach from the endoderm (Ivanovitch, 2017). By E8.5, cardiomyocytes have bulged out and formed a tube consisting of cells that will give rise to the future left ventricle (Zaffran, 2004). The tube is open dorsally, connected to the dorsal pericardial wall via the dorsal mesocardium. The tube is initially straight. However, as the tube continues to grow, it loops and form a rightward helix – a process referred to as heart looping. During this process, the dorsal mesocardium breaks down, thereby freeing the tube from its dorsal attachment. The tube grows by two mechanisms; by division of differentiated cardiomyocytes (Thompson, 1990) and by addition of new cells from a reservoir outside the tube ((Viragh and Challice, 1973 ; de la Cruz et al., 1989 ; Kelly et al., 2001). After the dorsal mesocardium has broken down, newly differentiated cardiomyocytes integrate into the heart tube through its two poles.

Concomitantly with looping, cells of the right ventricle and atria is added to the tube. Initially, they are all connected, as there is no separation between them. As the tube completes its looping, the chambers will be positioned relatively to each other in a manner corresponding to their future positions. The inter-ventricular septum, which will separate the left- and right side of the heart, starts forming around E10.5 and the tube has been shaped into a form reminiscent of the adult heart. Septation is completed in the fetal heart.

Remodeling of a tube into a functioning heart is an intricate 3D process, and one can easily imagine that defective growth, septation or positioning of chambers will lead to congenital heart defects. Congenital heart defects represent 1/3 of major congenital abnormalities, and in Europe 1% of children are born with a congenital heart defect (Dolk et al., 2011 ; Khoshnood 2012).

Thus, it is clear that the development of the heart is directly relevant to cardiac diseases, and that understanding the molecular mechanisms driving heart morphogenesis will give a better framework to understand these malformations. In this chapter, the focus will be first

directed on heart progenitor cells, and later on how left-right asymmetric morphogenesis leads to an asymmetric heart shape.

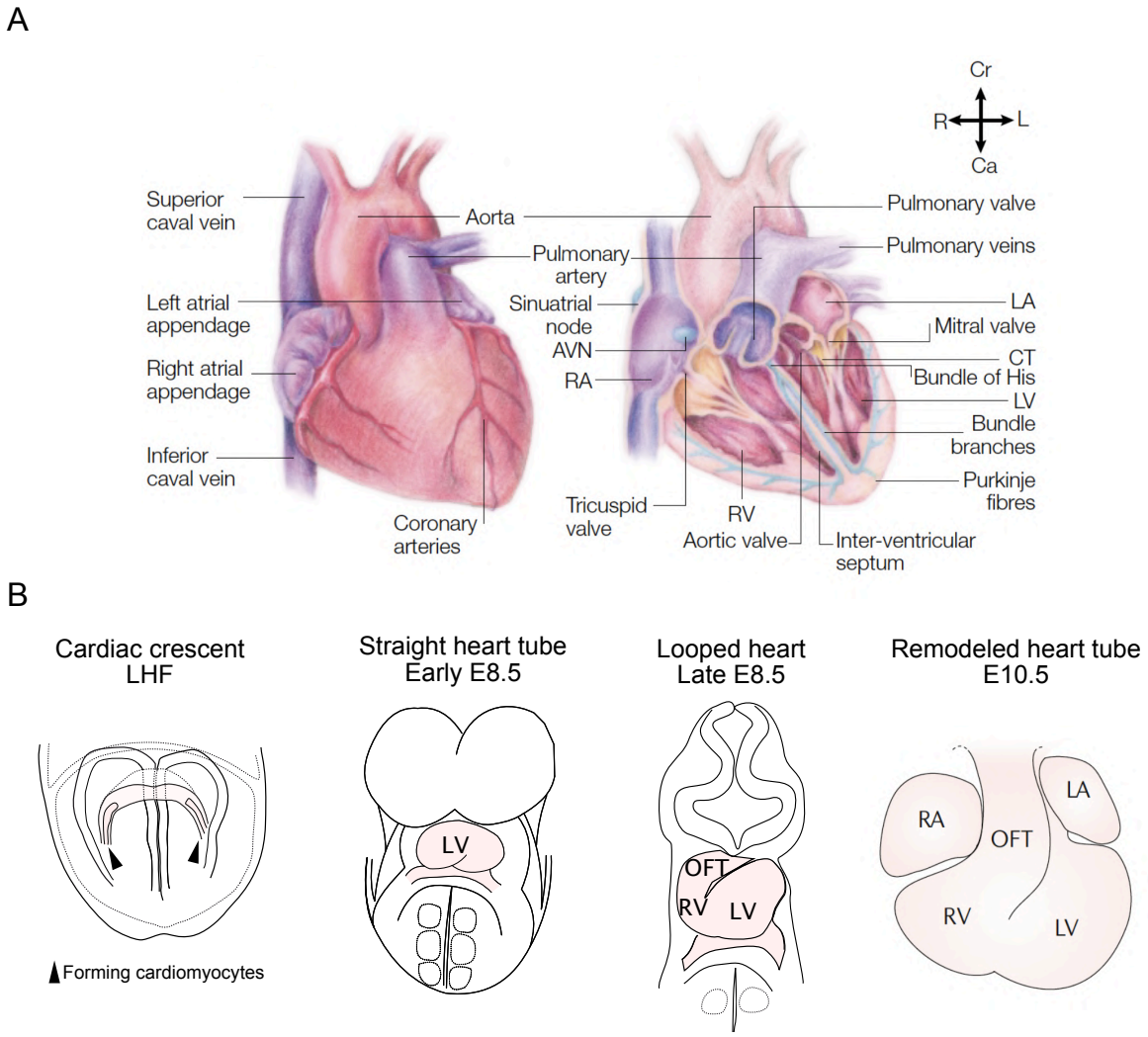

Fig 9. The adult and embryonic heart. (A) Illustrations of an adult mammalian (Human) heart in external view (left side) and in section (right side). Description of the heart is found in the text. From (Harvey, 2002). **(B)** Steps of the early cardiac heart. Initially a cardiac crescent forms, where differentiating cardiomyocyte progenitors from the left- and right side fuses and form a tube. This tube grows and loop, positioning the future left and right ventricles next to each other. Afterwards the heart tube undergoes remodeling, and a shape reminiscent of the adult heart is seen around E10.5. Images adapted from (Buckingham et al., 2005; Desgrange et al., 2018). AVN: Atrioventricular node; Ca: Caudal; Cr: Cranial; L: Left; LA: Left atrium; LV: Left ventricle; OFT: Outflow tract; R: Right; RA: Right atrium; RV: Right ventricle

The Origin and Early Development of the Embryonic Heart

Dye injection and fate mapping studies in first avian- and later mouse embryos have shaped our understanding of how the heart arises during development. At the epiblast stage, precursor cells of the heart are not yet committed to the cardiac lineage, as they can also

differentiate into other tissues such as the endoderm, paraxial mesoderm and extra-embryonic mesoderm (Buckingham, M., Biben, C. & Lawson 1997 ; Tzouanacou et al., 2009; reviewed in Meilhac & Buckingham, 2018). During gastrulation, these cells migrates through the primitive streak from the mid-streak stage (Fig 10) (Kinder et al., 1999). After ingression, the cells moves anteriorly along the two sides of the lateral plate mesoderm towards just below the headfold. Along this process, they will differentiate into cardiomyocytes and fuse at the midline, thus giving rise to the cardiac crescent (Ivanovitch et al., 2017; Kaufman & Navaratnam, 1981).

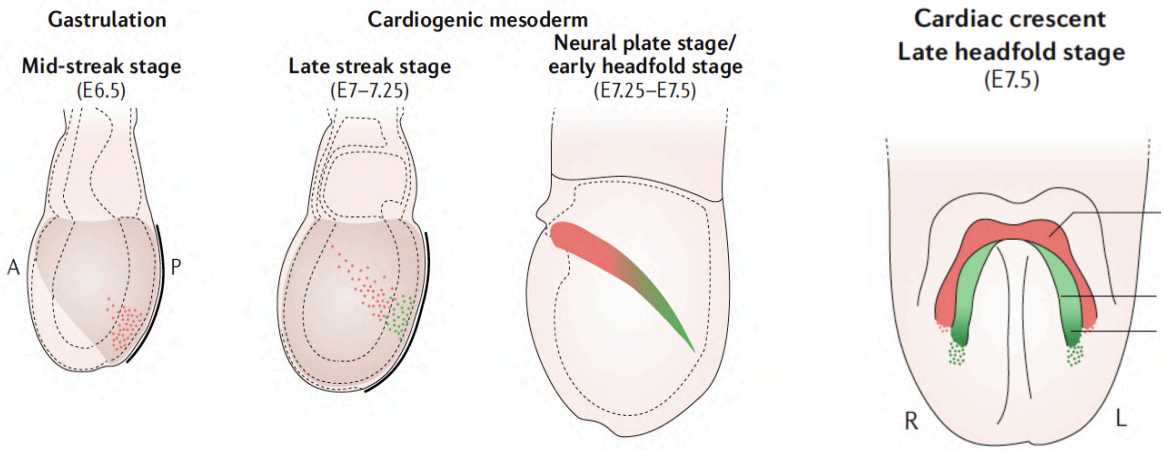

Fig 10. Cells migrate from the primitive streak anteriorly to form the heart. At the mid-streak stage, cells that form the heart migrate through the primitive streak and migrate anteriorly. Here they differentiate into cardiomyocytes and form the cardiac crescent (red). From (Meilhac & Buckingham, 2018)

Depending on when cells migrate through the primitive streak, they will contribute to different compartments within the heart (Lescroart et al., 2014). Retrospective clonal analysis had found that there are distinct clonal lineages of heart progenitors. Indeed, one group of clones gives rise at E8.5 to the left ventricle and contributed to other compartments besides the outflow tract. Alternatively, the second group of clones gives rise to the myocardium of the outflow tract, the atria, the right ventricle and to a subset of pharyngeal skeletal muscles (Meilhac et al., 2004 ; Lescroart 2010). These clonal lineages are termed the first- and second lineage respectively, based on the earlier appearance of the first lineage (Meilhac et al., 2004). Fitting with this, Lescroart et al., demonstrated that the cells of the first lineage turn on their cardiogenic transcriptional program earlier than the second lineage, and they migrate earlier (Lescroart et al., 2014). The two lineages segregate from early common progenitors, as it has

been possible to find mega-clones (samples with many labelled cells due to early labelling/recombination) where both the first- and second lineage derivatives are marked (Meilhac et al., 2004).

The formation of the early heart tube has also been imaged live (Tyser et al., 2016 ; Ivanovitch et al., 2017). These showed that myocardial differentiation occurs in two phases; the first begins at the early headfold stage and results in the cardiac crescent. There is then a break of 5-7 hours before cardiomyocyte differentiation commences again, providing cells elongating the straight tube that then undergoes looping. These live video observations are in agreement with that there are two lineages that migrate at two different times and form different compartments of the heart.

Besides heart progenitors arising from the first and second lineages, other cell types also contribute to the growing heart. This is the case of neural crest cells, a particular cell type that is derived from the neuroectoderm (in contrast to the other cell types contributing to the heart, which are derived from the mesoderm). Cardiac neural crest cells are important for outflow tract development and proper septation of the great arteries, however they are first present in the heart after E9.5, i.e. after the heart has completed looping (George et al., 2020; Jiang et al., 2000).

As written above, the heart tube grows from proliferation of differentiated cardiomyocytes, but also from integration of new cells into the tube. After ingression into the primitive streak, the heart progenitors migrates to different regions before forming and entering the heart tube. The regions of undifferentiated heart precursors are referred to as the heart fields. Two were initially defined, and they were named first and second heart field (Buckingham et al., 2005). At the cardiac crescent stage the first and second heart fields are adjacent, with the second heart field lying medially to the first heart field. It is the cells in the first heart field which then form the structure known as the cardiac crescent (Buckingham et al., 2005). (Fig 11A). The cells of the first heart field will deplete itself while forming the cardiac crescent, and thus it gives rise mainly to the left ventricle (Zaffran et al., 2004). The cells of the second heart field extend anteriorly at the border with the pharyngeal mesoderm, to the dorsal mesocardium and posteriorly into the splanchnic mesoderm of the lateral plate mesoderm (Cai et al., 2003); they will give rise to the right ventricle and atria (with overlapping

contributions from the first heart field) and to the outflow tract[4]. The cells of the second heart field can be further sub-divided into an anterior- and posterior region, with distinct transcriptional programmes, who have both overlapping and specific contributions (Kelly et al., 2001, 2014; Meilhac & Buckingham, 2018). Fate mapping studies have also been used to show the contributions of the second heart field to the heart. Through these it was found that cranial and caudal posterior second heart field have different, but overlapping contributions, and that cells until the 2nd somite pair can contribute to the heart (Domínguez et al., 2012).

The juxta-cardiac field, which contributes both to the cardiomyocytes and to the epicardium, is a new field that has been identified through single cell RNA sequencing (Fig 11B) (Tyser et al., 2021). At the cardiac crescent stage, the juxta-cardiac field is positioned anteriorly and ventrally to the cardiomyocytes in a continuous layer that folds over them (Fig 11C). The juxta-cardiac field extends into the extra-embryonic mesoderm, which is likely why it was only discovered recently (as it was thought the extra-embryonic mesoderm would not contribute to the heart). Inference of lineage trajectories from transcriptomic profiling indicates that the juxta-cardiac field is a reservoir of undifferentiated precursors for the first heart field, which rather contains intermediate differentiating cells. Thus single cell transcriptomic analyses coupled to spatio-temporal gene mapping have refined our understanding of cardiac lineages. It further supports the double segregation of myocardial lineages and the anterior/posterior regionalization of the second heart field, while providing precise mapping and molecular profiling of the different cell populations.

From the single cell RNA sequencing, it was possible to define several clusters, and as this data have been used also in the work of this PhD thesis, these will be described explicitly. The Me7 cluster represents the second heart field, while the Me5 cluster represents the juxta-cardiac field. Upon differentiation to cardiomyocytes, they will cluster either at Me4 or Me6, which represent two different clusters of differentiating cells, which are localized in different regions (See Fig 11C). Upon differentiation, the cells will form the cardiomyocytes and cluster as Me3. During this trajectory, they will express cardiomyocyte markers such as *Actc1* or *Acta2*.

[4] As seen, there are great similarities between the contributions of the first lineage and the first heart field and between the contributions of the second lineage and the second heart field, and as such these terms have been used sometimes interchangeably. This is imprecise, as they are not referring to the same thing, and as such great care should be implemented to avoid confusing the two concepts. Lineages refer to clonally related cells with specific migration times, while the heart field refers to regions containing heart progenitor cells in the developing embryo.

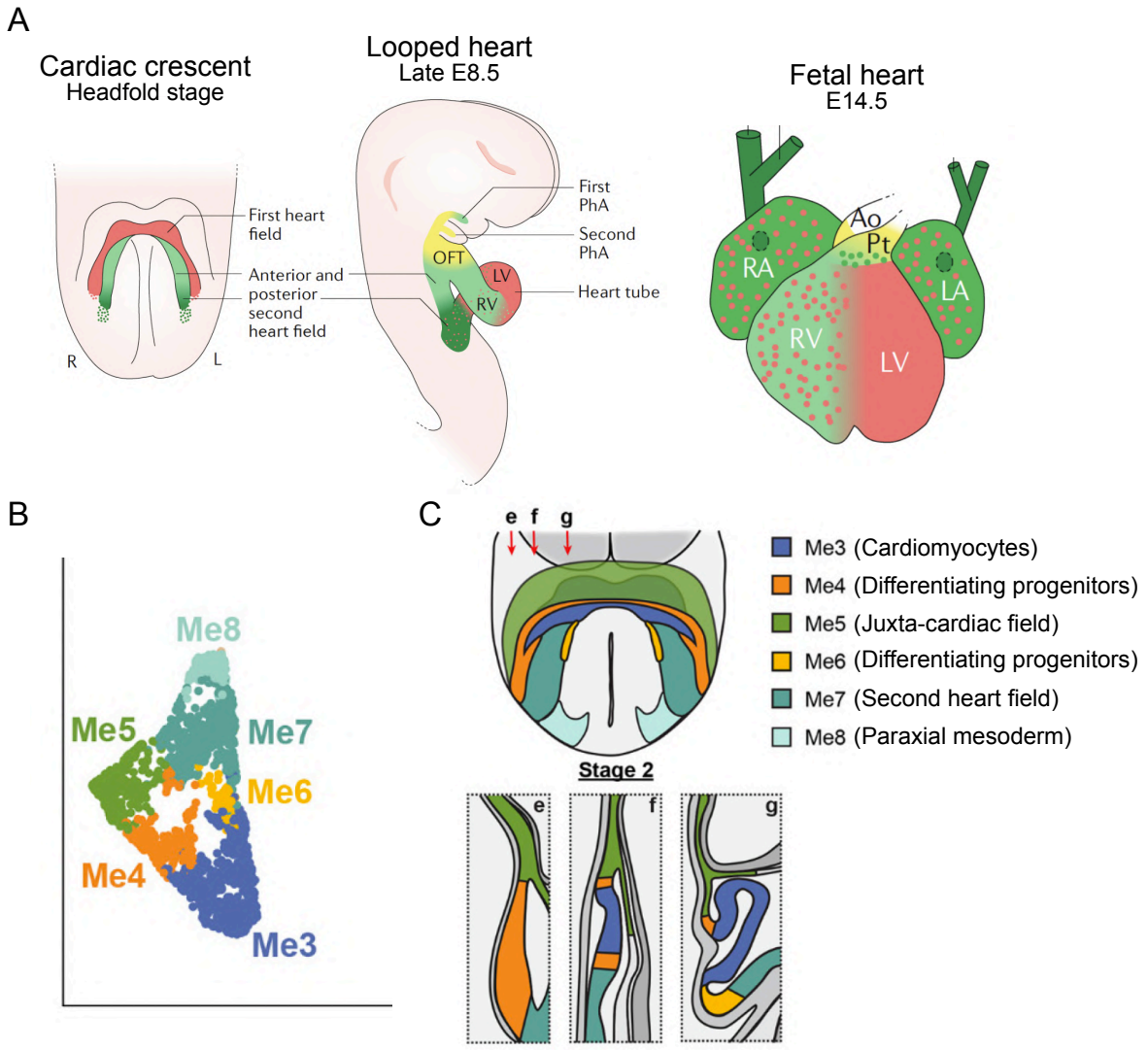

Fig 11. The heart progenitors are localized in into different heart fields. (A) Structure of the first (red) and second heart field (green and yellow) at the headfold and heart looping stages. The first lineage forms the left ventricle and contribute to the right ventricle and atria. The second heart field can be segregated into an anterior (yellow) and posterior region (green), who also has specific contributions to the chambers of the fetal heart. LA: Left atrium; LV: Left ventricle; OFT: outflow tract; PhA: pharyngeal arch; Pt: Pulmonary trunk; RA: Right atrium; RV: Right ventricle. Adapted from (Meilhac & Buckingham, 2018). **(B)** 2D UMAP projection of single cell RNA sequencing of cardiogenic cells at early stages of heart development. These can be clustered into different populations (labelled Me2-8). **(C)** Location of the newly discovered juxta-cardiac heart field (Me5/green), which is located at the cardiac crescent ventrally and anteriorly to the cardiomyocytes. The other clusters from B are also indicated. Left image: front view; (a) and (b) are sections at the level indicated in the left image. CC: Cardiac crescent; Endo: Endoderm; HF: Head fold; JCF: Juxta-cardiac field. B-C adapted from (Tyser et al., 2021).

Concomitantly with researchers exploring the heart lineages and -fields, genes marking these populations were also identified. One of the earliest markers of cardiac cells is *Mesp1*, which encodes a basic helix-loop-helix transcription factor that is active in the nascent mesoderm (Saga et al., 1999). *Mesp1* genetic tracing labels both cells of the first-, second and juxta-cardiac field as well as several other mesoderm-derived tissues (Saga et al., 1999; R. C. V. Tyser et al., 2021). However, it has been found that only 70% of the adult heart is derived from cells that have expressed *Mesp1* (Ragni et al., 2017). Fitting with this, *Mesp1*$^{-/-}$ mouse mutants still develop some cardiomyocytes (Saga et al., 1999). An interesting marker, which challenges the view of first- and second lineage, is *Foxa2*. *Foxa2* lineage tracing reveals that cells derived from Foxa2-expressing cells give rise mainly to the ventricle, and contribute very little to the atria (Bardot et al., 2017). These cells like represent a group of very early heart progenitors.

Identifying markers of the first heart field is particularly complicated, as the field is transient due to the rapid cell differentiation into cardiomyocytes and because markers of cardiomyocyte differentiation are not specific to the first lineage. As a consequence, many of the used markers also label other populations, in particular overall early cardiomyocytes. One useful marker is *Hcn4*, which encodes a subunit of a potassium channel. Hcn4 labels from E7.5 the first heart field (Liang et al., 2013).

The most common marker of the second heart field is the gene *Isl1*, which encodes a transcription factor. *Isl1* is expressed in the full second heart field (Fig 12), however it is not restricted to only mesodermal cells, as e.g. endodermal cells of the cardiogenic region are also *Isl1*-positive (Cai et al., 2003). Fitting with *Isl1* being a marker of the second heart field, *Isl1*$^{-/-}$ mutants die at E10.5 and only develop a single ventricle. However, there are reports challenging that Isl1 is only a marker of the second heart field. For instance it has been shown that Isl1 protein (but not mRNA) is expressed in the first heart field (Prall et al., 2007).

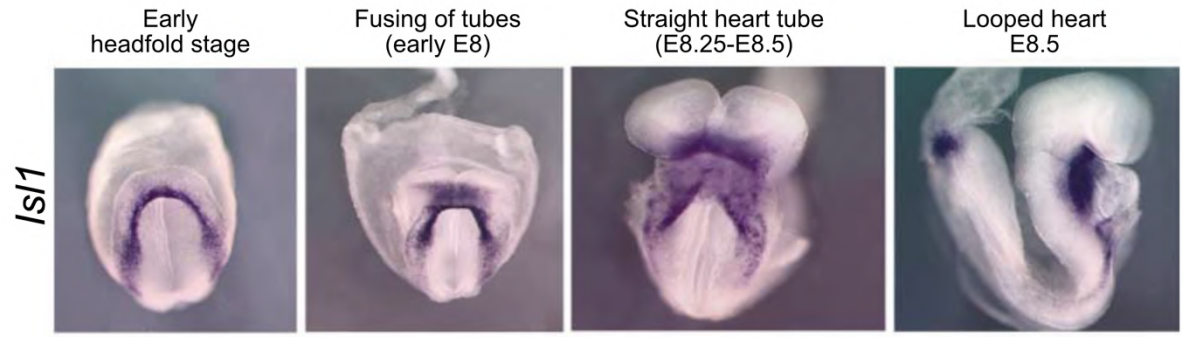

Fig 12. **Expression of Isl1 in the heart progenitors**. In situ hybridization labelling of *Isl1* expression at different stages of heart development shows that dorsally located cells extending from around the headfold to posteriorly below the heart express *Isl1*. This region has been shown to contribute to the heart, and *Isl1* expression is considered a marker of the second heart field. However, *Isl1* marks a wider population than heart progenitors. Adapted from (Cai et al., 2003)

As mentioned, the second heart field can also be patterned into an anterior- and posterior region, and markers and regulators have been found for each. For instance, it has been shown that *Tbx1* labels the anterior second heart field, while *Tbx5* labels the posterior second heart field – however, they are not mutually exclusive, as *Tbx1*; *Tbx5* double positive cells are found at the anterior-posterior border between the two regions (de Bono et al., 2018). Furthermore this is also stage dependent as *Tbx1* labels the full second heart field at early stages.

Another classical marker of the anterior heart field is an enhancer element from the cardiomyocyte differentiation gene *Mef2c*, which is termed *Mef2c-AHF* (Dodou et al., 2004; Verzi et al., 2005). This enhancer element has been used for several genetic tracing studies that explored the contributions of the anterior second heart field.

Several markers of the posterior heart field have been identified, however some of them are not exclusive for this region, as for instance *Sfrp5* and *Tbx5* also label the first heart field (Reviewed in Meilhac & Buckingham, 2018). Other markers, such as *Hoxb1*, are specific to the posterior second heart field, however they label other tissues of the posterior embryo (Bertrand et al., 2011).

The newly identified juxta-cardiac field was discovered through single cell RNA sequencing. In particular, *Mab21l2* appears as a specific marker for this population at early stages (Tyser et al., 2021).

There is an abundance of literature on the markers of heart progenitors, and it is clear that their relationships are complex and that the different domains of the heart field are dynamic. Thus, it is also a question that has been tackled through single cell RNA sequencing, and in addition the work published by Tyser et al., several other single cell RNA sequencing papers have been published the last years (de Soysa et al., 2019; Jia et al., 2018; Q. Zhang et al., 2021). Through analysis of these, new markers can be discovered, and questions of overlapping expression can be tackled. Of course, these findings must be validated using classical lineage tracing approaches. Furthermore, single cell RNA sequencing analysis is complex and will have to be revisited several times. For instance, Zhang et al., has proposed that the juxta-cardiac field can be segregated into two regions, one more differentiated than the other (Q. Zhang et al., 2021).

The mechanisms of cardiac specification described above explains the formation and elongation of the heart tube from different heart field sources and differentiation trajectories, however they cannot explain how the heart develops its asymmetric shape. For this, left-right patterning of the heart field is involved.

Heart looping – When the Heart Becomes Asymmetric

At the straight heart tube stage, the embryo looks left-right symmetric from the outside, and as such heart looping is the first morphological sign of asymmetry. Heart looping is defined as the process when the straight tube transforms into a rightward helix. because it is the first sign of asymmetry in the embryo, it was often used as a the first readout of left-right asymmetry establishment and has sparked the interest of researchers for a long time. In fact, this year marks the 100 year anniversary of one of the first description of this process (Patten, 1922). Bradley M. Patten investigated a range of chick embryos, matched them by somite number and developmental stage and observed how the tube changed from being straight to looped (Fig 13). These observations sparked a fundamental developmental biology question: which mechanisms control the formation of a rightward helix?

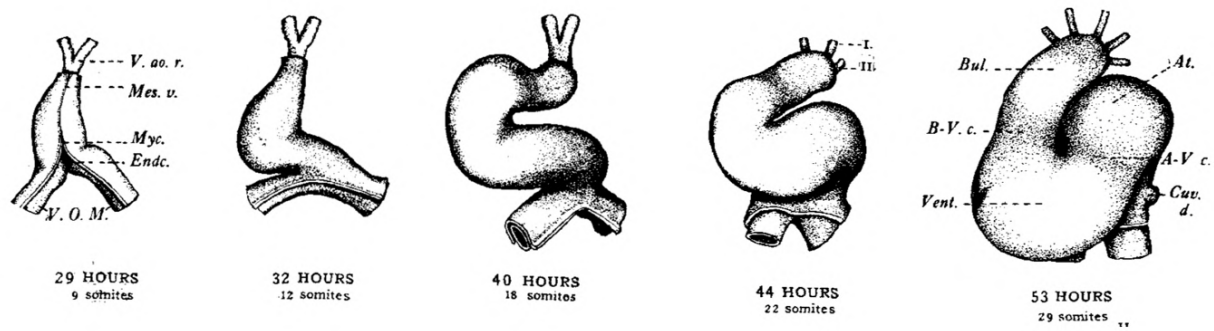

Fig 13. **Heart looping in the chicken.** First detailed description of heart looping in the chick shows how the tube develop from a straight tube to a rightward helix. Schemes are ventral views. Adapted from (Patten, 1922).

Computer simulations have shown that heart looping depends on a buckling mechanism (Le Garrec et al., 2017). Buckling is a mechanical instability, deforming a tube when it grows while its poles are fixed (Fig 14). In the context of the developing heart, the two fixed poles are the anterior arterial pole and the posterior venous pole, and when the tube grows between these, a curved shape appears (Patten, 1922 ; Männer, 2004). However, buckling is random and alone cannot explain how a rightward helix is formed. For this, asymmetries are required, such that the tube is steered or biased, e.g. through rotations or differential cell ingression (le Garrec et al., 2017; Männer, 2004).

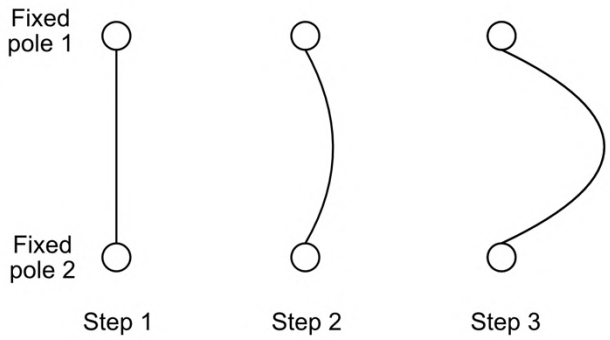

Fig 14. The Buckling mechanism. Buckling mechanism, where a tube will start bending as it grows between two fixed poles, has been proposed as a mechanism of heart looping. However, a simple buckling mechanism cannot explain the formation of a rightward helix

Work in the host lab has studied heart looping in the mouse. At E8, a litter of embryos displays a spectrum of heart shapes ranging from cardiac crescent to a complete looped heart. This shows that heart looping is a very rapid process.

Staging criteria like Theiler stages are not resolutive enough to account for these kinetics, thus a more precise staging grid was designed (Fig 15A). This grid, containing nine stages ranging from E8.5b-j, uses morphological criteria of the heart to segregate embryos into discrete groups, and illustrate how the cardiac crescent transforms into a looped helix. It was initially described in (le Garrec et al., 2017) and further precised in (Desgrange et al., 2018) with the inclusion of an earlier stage. Beyond the morphological criteria, the staging grid was also established using morphometric analysis of 3D imaged hearts. From these analysis it was also found that somite numbers were not correlated with heart shape, and as such it is necessary to stage the heart depending on the shape of the heart. Furthermore, heart looping is a rapid process, and the mouse somite clock is around 2 hours (Cinquin, 2007),

There are other staging grids that also describe early heart morphogenesis and heart tube formation. For instance, Tyser et al., have proposed another nomenclature using stage numbers (from -1 to 3 with an additional stage defined as late heart tube) (Fig 15B) (R. C. V. Tyser et al., 2021; R. C. V. Tyser & Srinivas, 2020), while Esteban et al., have proposed a continuous staging tool, based on quantitative measures of either length of inner and outer curvatures of the heart tube or (more easily measured) the height and width of the early heart tube (Fig 15C) (Esteban et al., 2022). For the sake of clarifications and for making it easier for people outside the field, a goal of the heart development research community should be to agree on a staging grid with clearly defined criteria.

Fig 15. **Mouse staging grids related to the heart**. **(A)** Heart looping staging grid from (le Garrec et al., 2017). Detailed description of each stage can be found in the text, however note that at stage E8.5f the arterial pole undergoes a rightwards rotation, while at the stage after, E8.5g, the venous pole will be displaced towards the left. These opposite asymmetries are important for right ventricle re-positioning from cranial to the right side of the left ventricle at stage E8.5j (the end of heart looping). Bright pink annotates region of cardiomyocytes/ developing heart tube. LHF: Late headfold stage; LV: Left ventricle; OFT: Outflow tract; RV: Right ventricle. Adapted from (Desgrange et al., 2018; le Garrec et al., 2017). **(B)** Staging grid of early heart development from (R. C. V. Tyser et al., 2021; R. C. V. Tyser & Srinivas, 2020). This staging grid has very fine separation at early stages, however it does not describe stages until the end of heart looping. CC, cardiac crescent; FD, foregut diverticulum; HT, heart tube; LHT, late heart tube **(C)** Staging grid based on morphometric analysis from (Esteban et al., 2022).

A

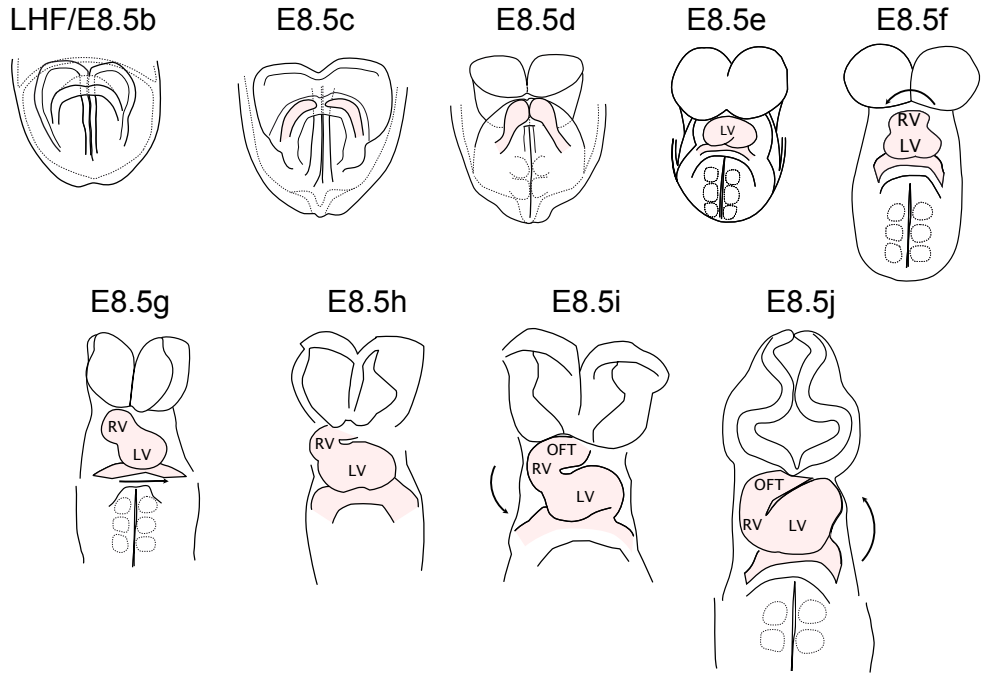

B

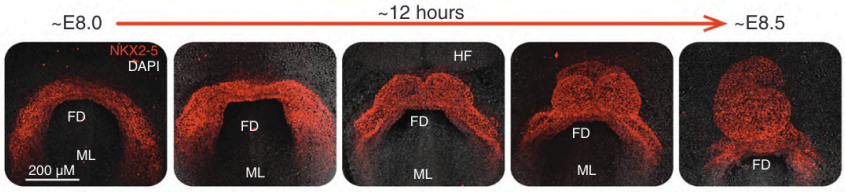

	Stage 0	Stage 1	Stage 2	Stage 3	LHT
Embryonic day	7.75–8.0	8.0–8.25	8.0–8.5	8.25–8.5	8.25–8.5
Somites	0–2	1–3	2–4	3–6	5+
Thelier stage	12	12	12	12	13

C

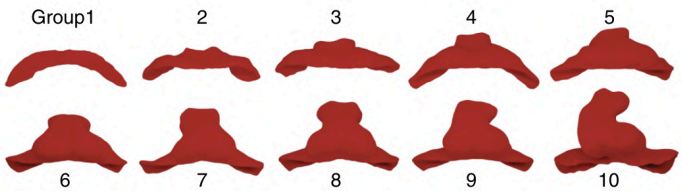

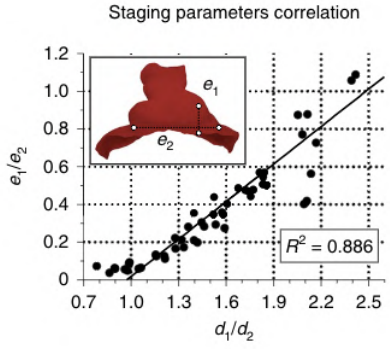

The E8.5b stage is equivalent to the late headfold stage of (Downs & Davies, 1993). When the cardiomyocytes start forming a cardiac crescent, it marks the beginning of the E8.5c stage (c for cardiac crescent). Following this, the left and right cardiac populations starts bulging, and the E8.5d stage is defined by that the two bulbs are in close proximity but not yet fused.

The fusion of the bulbs marks the E8.5e stage. Initially shaped like a round bulb after bulging out the heart will form a straight tube. At this stage, the embryo looks symmetric, however careful 3D reconstructions of early heart morphogenesis have shown that already at this stage, the angle of the left- and right inflow relative to the midline differs between the two sides (Esteban et al., 2022). The right inflow angle tends to be more perpendicular compared to the left one. Interestingly, this asymmetry is dependent on *Nodal*.

Following this, the future right ventricle forms anteriorly of the future left ventricle (Zaffran et al., 2004). At this stage, Le Garrec et al. 2017 has shown, using 3D analyses, that the anterior arterial pole undergoes a rightwards rotation of around 25^{o} degrees. This rotation marks the E8.5f stage, and it was seen in all wild-type embryos investigated at this stage. Sequentially after this, with similar strategy they have identified a venous pole displacement towards the left side, which defines the E8.5g stage, together with the rightward tilting of the RV. On a cellular aspect, using DiI injections, they have identified that this step is associated with asymmetric cell ingression at the venous posterior pole. The two asymmetries occurring at E8.5f and -g take place at the arterial and venous pole respectively, and through 3D modelling it has been shown that they are important to generate a rightwards helix in combination with the buckling mechanism (le Garrec et al., 2017).

The next stage (E8.5h) is marked by a growing outflow tract. Following this, the dorsal mesocardium starts breaking down at the arterial pole, freeing the future right ventricle. An intermediate step is referred to as E8.5i, and when the right ventricle has reached its final position on the right side of the left ventricle, it marks the E8.5j stage and the end of heart looping. Overall the heart looping process takes around 12-15hours (based on observations in embryo cultures in the lab).

As described in the paragraph above, we are now starting to have a good understanding of the physical processes necessary to generate a rightward helix from a straight tube. The next question is then to understand what are the molecular pathways and cellular mechanisms that control this.

As described in the first introduction section on left-right asymmetry, the Nodal pathway has been shown to regulate heart looping (as well as other laterally asymmetric organs). This was initially reduced to a question of direction, i.e. if looping was rightwards, leftwards or the tube was straight (Brennan et al., 2002). This view of laterality is connected to how heterotaxia syndrome has been described clinically as either right or left isomerism (see *Introduction - Left-right asymmetry*). Sometimes, particularly in zebrafish, heart looping is still reduced to a question of rightwards- or leftwards looping (Rago et al., 2019).

Work in the host lab has demonstrated the role of *Nodal* during heart looping leading to a different view. In conditional mutants, where *Nodal* is genetically ablated in the lateral plate mesoderm, the heart does not receive left-sided Nodal signaling anymore. Surprisingly the heart still undergoes some looping, however the shape is incorrect (Fig 16) (Desgrange et al., 2020). This means that *Nodal* is not required to initiate heart looping, instead *Nodal* is required for orienting the random asymmetry generator of the heart, i.e. the buckling mechanism, thus acting as a bias in the sense of Brown and Wolpert (See Fig. 3). It was shown in Le Garrec et al., 2017 that the poles undergo opposite asymmetries (See Fig 15A). Fitting with these two separate events, *Nodal* mutants fall into four classes of heart looping, which arise at equal frequency (Desgrange et al., 2020). Furthermore, it was shown that the amplitude of the asymmetries (such as arterial pole rotation) is smaller in *Nodal* mutants (independently on if the rotation is to the correct- or incorrect direction). This shows that Nodal is both required for orienting and amplifying asymmetries. The existence of the classes was shown by 3D quantitative morphometric analysis and principal component analysis. It has been possible to simulate the mechanism leading to the four classes, based on normal buckling and defective asymmetries at the two poles (Desgrange et al., 2020).

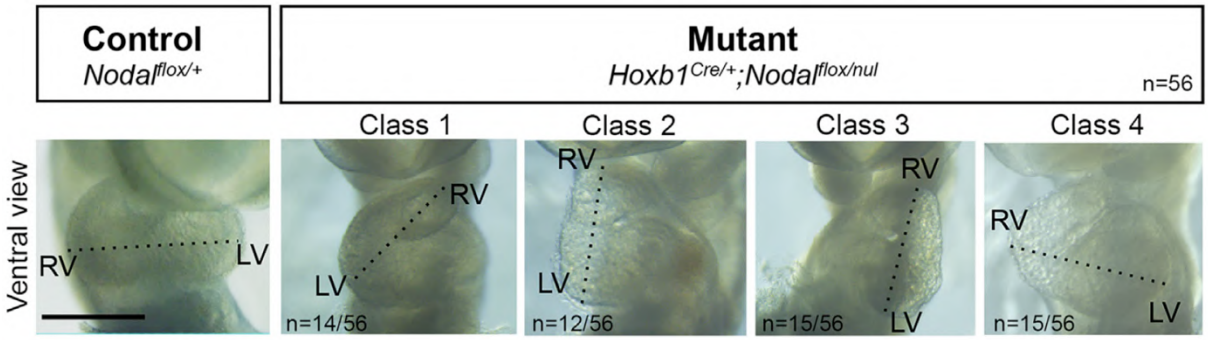

Fig 16. Nodal and heart looping. *Nodal* mutants group into four classes of heart shapes that arise at equal frequency. These classes arise from the randomized orientation of two opposite asymmetries at E8.5 being also reduced, thus showing that *Nodal* is both required for orienting and amplifying asymmetries. From (Desgrange et al., 2020)

There are still many open questions on how *Nodal* orients and coordinates the heart looping process. It is clear that orientation of heart looping is independent of *Pitx2*, as *Pitx2* mutants loop to the correct side (M.-F. Lu et al., 1999) and they do not phenocopy the whole spectrum of *Nodal* mutants. This is in contrast to gut looping, where *Pitx2* mutants are symmetric (see *Introduction – Beyond the left-right organizer*) (Davis et al., 2008), thus showing that different organs rely to a different degree on *Pitx2* signaling to become asymmetric. Concomitantly, this also means that different organs rely on the different components of the Nodal pathway to different degrees, showcasing that organ lateralization is different from organ to organ.

But *Pitx2* is an important effector of the Nodal pathway, and it seems that *Pitx2* is important for some aspects of cardiac left-right asymmetry, as 25% of *Pitx2abc* null mutants (for all isoforms) show a shape like Nodal class 2, which is indicative of improper left-right orientation at the venous pole (Desgrange et al., 2020). In addition, Pitx2 is required for the left/right identity of atria (Galli, 2008; Desgrange 2020). This means that *Pitx2* governs some aspect, but not all, of left-right asymmetric heart morphogenesis.

Thus, since *Pitx2* mutants do not phenocopy *Nodal* mutants in the context of the heart, it means that *Nodal* must regulate something beyond the classic Nodal pathway. Furthermore, as the heart tube still becomes asymmetric in the absence of Nodal, some of these signals (important for generating the asymmetric heart shape), must be expressed also in *Nodal* mutants. As described above, the role of Nodal is instead to orient and amplify these properly. This leads to two questions: (1) which signals does *Nodal* orient and amplify and (2) where and when does *Nodal* do it?

Nodal is expressed in the left lateral plate mesoderm (containing the second heart field) at a narrow time window between the 3-6 somite stage, which translates to E8.5c-e, i.e. prior to heart looping (Desgrange et al., 2020; Vincent et al., 2004). Genetic tracing using a *Nodal-ASE-LacZ* transgene has shown contribution of cells that have expressed Nodal to the tube poles further supporting the role of Nodal in pole asymmetry.

That Nodal is expressed within the heart progenitors (and not within the heart tube) suggest that the left-right asymmetric signal occurs there. Furthermore, since the time window of the Nodal pathway is short, and that heart looping is directed by dynamic sequential asymmetries, these left-right asymmetries with the heart progenitors must be rapid. Furthermore, since both *Nodal*- and *Pitx2* mutants become asymmetric, there must be other pathways involved beyond the classic Nodal pathway.

Some roles of *Nodal* within the heart progenitors have already been described. Rago et al., has pointed towards Nodal controlling miRNA upstream of Bmp signaling (with Bmp signaling being more active on the right), while Desgrange et al., has shown that Nodal regulates cell proliferation, differentiation and extracellular matrix proteins (Desgrange et al., 2020; Rago et al., 2019). Extracellular matrix proteins have also been found to important for looping in the gut (Kurpios et al., 2007; Sivakumar et al., 2018), and one can speculate that the arterial pole rotation and the venous pole displacement both require a changing in the surround extracellular matrix.

Fitting with this, it has been shown that when the dorsal mesocardium is not degraded, the heart tube cannot undergo looping (le Garrec et al., 2017). This breakdown is dependent on both sonic hedgehog signaling and matrix metalloproteases (le Garrec et al., 2017; Linask et al., 2005), and the matrix metalloprotease *Mmp9* has been shown to be asymmetrically expressed in left heart progenitors during heart looping and to be regulated by *Nodal* (Desgrange et al., 2020). Furthermore, genes like *Ablim1* (Stevens et al., 2010) and *Six2* (Zhou et al., 2017) have been reported as being asymmetric within the heart progenitors, but their role in heart looping is not characterized.

Apart from this, left-right asymmetries within the heart progenitors beyond the Nodal pathway is not well explored, and in particular little is known about their kinetics in relation to heart looping. As such, this became the fundamental question driving this thesis.

During the PhD I have explored left-right patterning kinetics of heart progenitors through a transcriptional screening approach with the aim of identifying novel genes involved in heart looping beyond *Nodal* (see *Objectives*). We selected a transcriptomics approach targeting heart progenitors for two reasons:

(1) RNA sequencing is able to quantify gene expression levels without knowing the target sequences *a priori* (compared to e.g. microarray), which makes RNA sequencing suitable for detecting novel asymmetric genes and quantifying their expression levels.

(2) We expect the kinetics of left-right asymmetric gene expression in heart progenitors to be very rapid. By performing the RNA sequencing on morphologically staged embryos (according to our staging grid, see Fig 15A) we can explore the kinetics of asymmetric gene expression in relation to their heart looping stage. As described elsewhere in the introduction, a similar approach has been utilized in the gut, which lead to several discoveries regarding which genes and processes regulate gut looping (Welsh et al., 2013, 2015).

From the screens performed during this thesis, several novel candidates of left-right asymmetric heart formation were discovered. We focused on characterizing one of these, as we found the Notch pathway, with particularly the Notch receptor *Notch3*, to be a novel left-sided asymmetric signal.

Notch signaling have been shown to regulate left-right asymmetry before. However, this was on the level of the left-right organizer and not as an asymmetric signal, which could potentially regulate asymmetric organogenesis. In the final chapter of the introduction, Notch signaling will be introduced with a focus on its role in left-right asymmetry and heart formation.

Notch Signaling Pathway

The Notch pathway is a highly evolutionary conserved signaling pathway which has been shown to regulate biological processes ranging from tissue patterning, cell fate choices and patterning during development, to homeostasis in adult tissues and cancer (Hori et al., 2013). The study of Notch began more than a hundred years ago, where work by legendary geneticists such as John. S. Dexter and Thomas H. Morgan described a mutation in *Drosophila*, where females displayed a notch, i.e. a small nick, in their wings and a thickening of their arteries (Dexter, 1914; Morgan, 1917). The notch in the wing gave the name to the gene locus.

The Notch pathway is a juxtacrine signaling pathway, whose basic *modus operandi* at a glance is quite simple. A transmembrane ligand on one cell will bind a transmembrane receptor on another cell, leading to a series of proteolytic cleavages of the Notch receptor, which free its intracellular domain. The Notch intracellular domain (usually referred to as NICD) translocates into the nucleus, where it functions as a co-transcriptional regulator of the transcription factor Rpbj, within a broader Notch transcriptional complex (Fig 17) (Bray, 2016).

That the Notch pathway is relatively simple in design is somehow surprising given the number of different biological processes that the pathway regulates. One way that pathway diversity can be explained is through different combinations of receptors and ligands. For instance, *Drosophila* has a single *notch* receptor gene and two ligands, while in mammals there are four different Notch receptor paralogues, *Notch1-4*, and 5 different Notch ligands, *Jag1/2* and *Dll1/3/4*. Notch receptors have been shown during development to have both overlapping and specific functions (Andersson et al., 2011; Meester et al., 2019): they can work either as activator (Domenga et al., 2004) or repressor (Alunni et al., 2013; Kitamoto & Hanaoka, 2010), of cell differentiation, or as a regulator of cell fate choices by lateral inhibition (Coumailleau et al., 2009). Even if there are multiple receptors and ligands, this cannot explain the diversity of the Notch pathway outcome: extensive research has shown that the pathway is regulated on many levels. These regulations are thought to be important for explaining why Notch signaling is dependent on the cellular context.

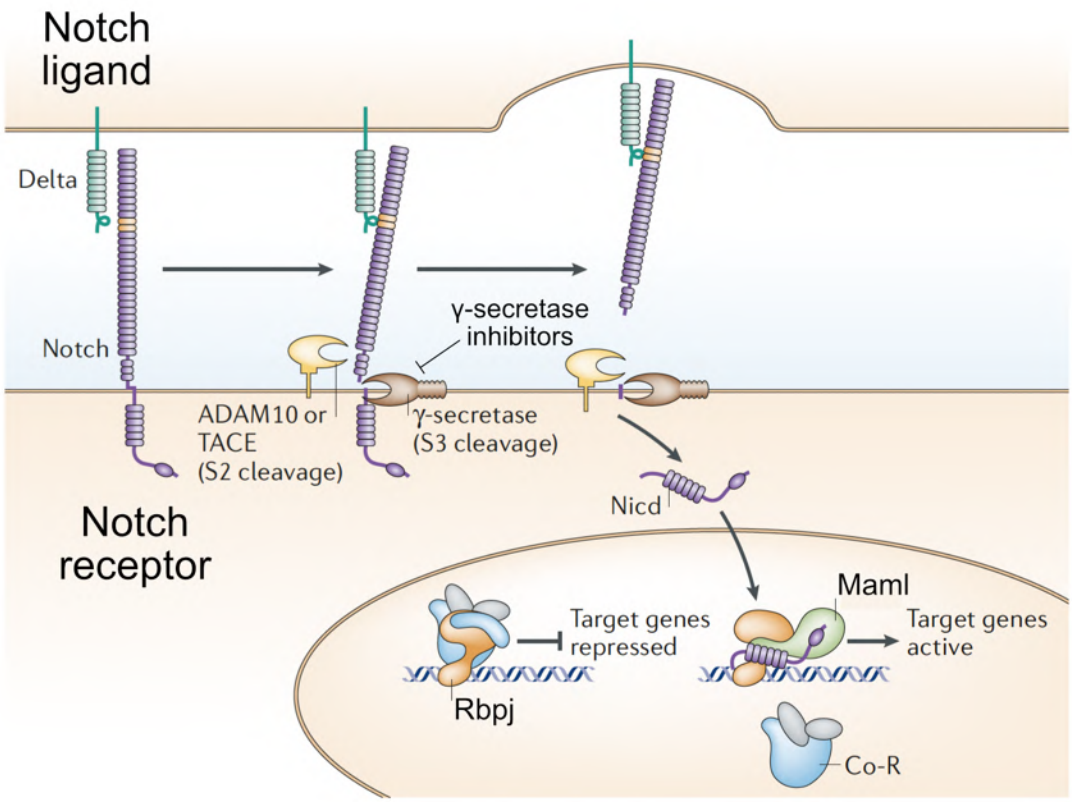

Fig 17. Notch signaling pathway. The transmembrane Notch ligand, located on the signal sending cell, bind a transmembrane Notch receptor on the signal receiving cell. This leads to a series of proteolytic cleavages that ends with the release of the Notch intracellular domain (NICD). Following cleavage, the intracellular domain then translocates to the nucleus, where it binds other factors (Such as Rbpj or Maml) and form the Notch transcriptional complex, which will lead to expression or repression of target genes. Drugs inhibiting the gamma secretases, involved in the third proteolytic cleavage (S3), are used in therapy and experiments to inhibit the Notch pathway. Figure from (Bray, 2006)

The canonical ligands belong to two families, delta (*Dll1/3/4*) and serrate (*Jag1/2*), and experimental evidence suggests that any of the Notch canonical ligands can interact with any of the receptors (Shimizu et al., 1999, 2000). However, binding strength and interaction may vary depending on the combination of receptors and ligands, and for instance binding strength is thought to regulate the pathway outcome, which has been shown to lead to different cell fate choices in the haemogenic endothelium (Gama-Norton et al., 2015).

The Notch ligands can also be regulated via the process of endocytosis, where ligands are removed from the surface of the cell (Hori et al., 2013). Ligand endocytosis and proper interactions between Notch ligand and receptor have been shown to be regulated by

ubiquitination. In particular, the E3 ubiquitin ligase *Mib1* has been found to be essential for all Notch signalling (Motoyuki et al., 2003 ; Koo, 2007) : *Mib1*$^{-/-}$ mouse mutants are embryonic lethal at E10.5, and they show multiple defects related to failure in Notch signaling, for instance a shortened tail, vascularization defects and a straight heart tube (Barsi et al., 2005).

Beyond the ligands belonging to the Serrate and Delta families, it has also been found that other non-canonical ligands can also activate Notch receptors. These ligands are thought to induce Notch signaling in a manner different from what is shown in Fig 17 (for instance through β-catenin or through NF-κB in a *Rbpj*-independent manner) (Andersen et al., 2012; M. Katoh & Katoh, 2007). How canonical or non-canonical Notch signaling relates to heart development is not well understood, however cell culture experiments points towards the fact that *Rbpj*-independent Notch signaling might play a role during early heart development (Miyamoto et al., 2021).

The four *Notch* paralogues in mammals are not equivalent, as they differ in both length and domains (the structure of the four Notch receptors are shown in figure 18). Most of the extracellular N-terminal end consists of epidermal growth factor (EGF)-like tandem repeats. *Notch4*, the shortest, have 29 repeats, while *Notch3* has 34 and *Notch1* and *Notch2* both have 36 repeats (Hori et al., 2013). From studies of the single *Notch* gene in Drosophila (Rebay et al., 1991), and from studies of human *NOTCH1* expressed in bacterial systems (Whiteman et al., 2013), EGF-like repeat 11 and 12 have been shown to be necessary for ligand interaction. In particular, the study by Rebay et al. is interesting, as they generated 32 different deletions of regions of the EGF repeats and found that any construct without the EGF 11-12 repeats could not bind the ligand, while a construct consisting only of EGF repeats 1,12 and 13 (i.e. missing the other 33 repeats) can.

At the intracellular C-terminal end, the RAM and Ankyryn sites are essential for Rbpj binding in the nucleus after receptor cleavage (Hori et al., 2013). Only *Notch1* and *Notch2* have the transcriptional activation domain (TAD), however it is not well understood how missing this domain affects *Notch3* and *Notch4*, as without the TAD, Notch3 and Notch4 can still form transcriptional complexes with Rbpj. Overexpression of the different Notch intracellular domains (an often used method to induce Notch signaling) has been shown in cases to activate the same target genes (Q. Wang et al., 2012). This is in part attributed to the fact that overexpression leads to very high, non-physiological levels, which might cause a promiscuous

binding to targets. Also, when these tissues have been studied in greater detail, it has been possible to find both overlapping- and specific functions for the different NICD (see *Notch3 as a promoter of differentiation*) (Baeten & Lilly, 2015).

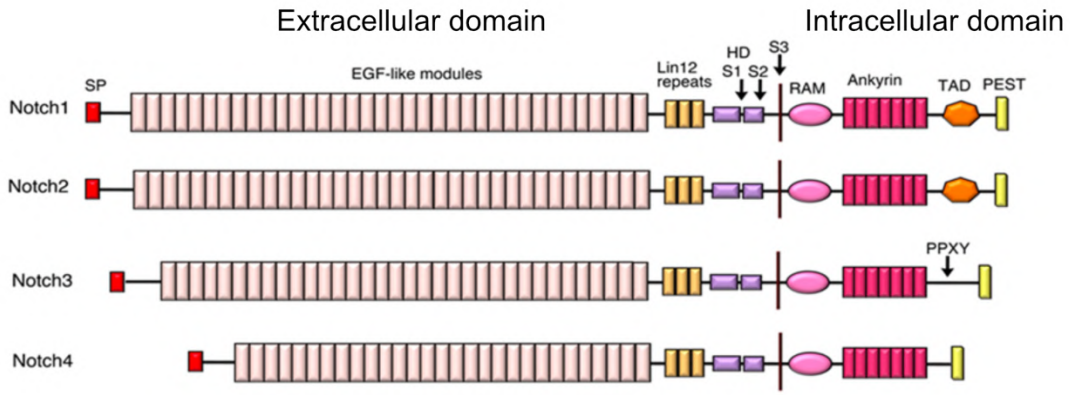

Fig 18. **Structure of the mammalian Notch receptors.** The extracellular regions consist mostly of EGF-like repeats, which differ in numbers depending on the paralogue. All receptors have the RAM and Ankyrin domains in their intracellular domains, which are required for interactions with the transcription factor Rbpj. Notch3 and Notch4 both lack the transcriptional activation domain (TAD). From (Hosseini-Alghaderi & Baron, 2020)

Like the Notch ligands, the Notch receptors are also regulated at a post-translational level. After translation, the Notch receptor undergoes a series of modification. For instance, in the Golgi apparatus, the extracellular domain is proteolytically cleaved into two peptides, which are then bound together through non-covalent interactions (Hori et al., 2013). This is termed the S1 cleavage, and it is necessary for the two cleavages (termed S2 and S3) occurring when the Notch ligand- and receptor binds. The presence of proteases for the S1-S3 cleavages, in particular gamma-secretases involved in the S3 cleavage, is key for Notch signaling, and many cancer drugs targeting the Notch pathway are gamma secretase inhibitors (Shih & Wang, 2007).

Furthermore, the Notch receptors are glycosylated, for instance by the glucosaminyltransferase Lfng. Lfng has been shown in *Drosophila* to regulate the function of Notch signaling, where it can change the affinity between a ligand and Notch receptor depending on the context (Panin et al., 1997). Furthermore, the reason why EGF-like repeats 11-12 are necessary and sufficient for ligand interactions has also been linked to these being

glycosylation sites (Rebay et al., 1991). These repeats are also important to mention, as several of the *Notch* mutants were designed to target these sites (Krebs, Xue, et al., 2003).

The Notch transcriptional complex consists of the Notch intracellular domain along with other factors, the most known being the transcription factor Rbpj (also known as *CSL* or *su(H)*). Depending on the other co-factors, the Notch transcriptional complex alters its output. It does so through changing which genes the complex will bind to or through being either a repressor or activator of transcription (Sakano et al., 2010). Another important co-factor is encoded by the *Maml* gene, which has been coupled to activation of transcription. Furthermore, a dominant negative form of Maml has been made, which inhibits activity of the Notch transcriptional complex and has been a useful tool for studying the role of Notch (for instance in the heart as will be described later) (Kitagawa et al., 2001).

Classical direct targets of the Notch transcriptional complex are the *Hes* and *Hey* genes, which encode basic helix-loop-helix transcriptional regulators (Fischer & Gessler, 2007). The Hes- and Hey proteins will form homo- and heterodimers with itself or other basic helix-loop-helix proteins. For instance, it has been shown in cell culture that Hey1 inhibits myogenic differentiation, because it forms a heterodimer with MyoD, which represses MyoD and muscle differentiation (Buas et al., 2010). There are a multitude of different ways in which Hes and Hey proteins can regulate transcription beyond binding to other basic helix-loop-helix proteins, in which some of them involves DNA binding and others do not (Fischer & Gessler, 2007). Relevant to this, mutations in *Hey* genes (as well as other members of the Notch signaling pathway) can lead to congenital heart defects.

Although the *Hes* and *Hey* genes are the most known targets of Notch signaling, there are also others. Some (as for instance *Atp1a1*, which is explored in this thesis) have been found through RNA sequencing of developing Notch mutant embryos (Than-Trong et al., 2018), while others (e.g. *Erbb2*) have been discovered through studying Notch signaling in the context of cancer (Pradeep et al., 2012). On this note it is important to mention that it has not been possible to find specific targets related to specific Notch receptors, despite the fact that the receptors have different structures in their intracellular domain (see Fig 18). Similar to this, the transgenic Notch signaling reporter lines (such as the *CBF:H2B-Venus* line or the Notch Activity Sensor line), which have been generated to study the activity of Notch, are not specific for single Notch receptors (Nowotschin et al., 2013; Souilhol, Cormier, Monet, et al., 2006).

Concomitantly, the different reporter lines do not report all Notch activity, and thus it is necessary to perform additional experiments in order to decipher which receptor is inducing Notch activity at a given site.

During the work of this thesis, the Notch receptor *Notch3* was found to be left-sided asymmetric in heart progenitors, and as such we investigated its role during asymmetric heart morphogenesis. As described with a few examples above, Notch signaling has been shown to play roles in the formation of the heart. However, this is not the only site where Notch signaling can influence asymmetric heart morphogenesis, as Notch signaling has also been shown to be important for left-right symmetry breaking.

Notch Signaling is Involved in the Establishment of Left-right Asymmetry

A role for Notch signaling in left-right asymmetry was shown in 2000, when it was reported that specific cells on the left side of *C. elegans* experience more Notch signaling, and this is essential for proper gut rotation in the worm (Hermann et al., 2000). The left-sided Notch asymmetry is due to higher levels of the canonical ligand Lag-2. This led researchers to question if similar processes occurs in mammals.

In 2003, it was published that Notch signaling is required for proper formation of left-right asymmetry at the level of the left-right organizer. mouse mutants removing global Notch signaling (*Rbpj*$^{-/-}$) display heart looping- and other laterality defects (Raya et al., 2003). This is evolutionary conserved, as *Notch* mutants in zebrafish (Raya et al., 2003) and *Notch* morpholino treatment in the frog (Sakano et al., 2010) lead to similar phenotypes. From here, there has been two lines of research questions: 1) which are the components of the Notch signaling pathway present in the left-right organizer? and 2) what kind of cellular effects does Notch signaling play?

Patterning of the left-right organizer by Notch signaling

Around the left-right organizer, multiple Notch ligands and receptors are present with specific regionalization. For instance, *Notch2* is located in pit cells, while *Notch1* is expressed in the posterior mesoderm cells. *Jag1* is expressed in the anterior adjacent mesoderm , while *Dll1* and *Dll3* are expressed in the posterior adjacent mesoderm (Przemeck et al., 2003; Raya et al., 2004). To our knowledge, the patterns of the remaining Notch receptors, Notch3 and Notch4,

have not been examined in the context of the node. Through various mutant studies across multiple species, the role of some of these components have been explored (Fig 19A).

Similar to the *Rbpj* mutants, mutants for the Notch canonical ligand *Dll1* display heart looping- and laterality defects (Fig 19B), indicating that it is the main Notch ligand in the left-right organizer (Krebs et al., 2003; Przemeck et al., 2003; A. Raya et al., 2003). Comparatively, *Jag1* mutants have normal left-right asymmetry establishment (Przemeck et al., 2003).

In the mouse, neither *Notch1* or *Notch2* single mutants display laterality defects (Hamada et al., 1996; Krebs et al., 2003), however *Notch1/2* double mutants do, showing that there is redundancy among the Notch receptors (it has to be mentioned that the N*otch2* mutant allele used in (Krebs et al., 2003) is a strong hypomorph and not a true null, indicating that there is a genetic dosage component as well). This redundancy is not evolutionary conserved, as *notch1a*$^{-/-}$ mutants in zebrafish (Lopes et al., 2010) and *notch1* knockdown through morpholinos in *Xenopus* (Sakano et al., 2010) develop laterality defects.

Thus, Notch pathway components are present in- and around the node. In the next chapter, it will be described which functions that Notch signaling has been shown to be involved in.

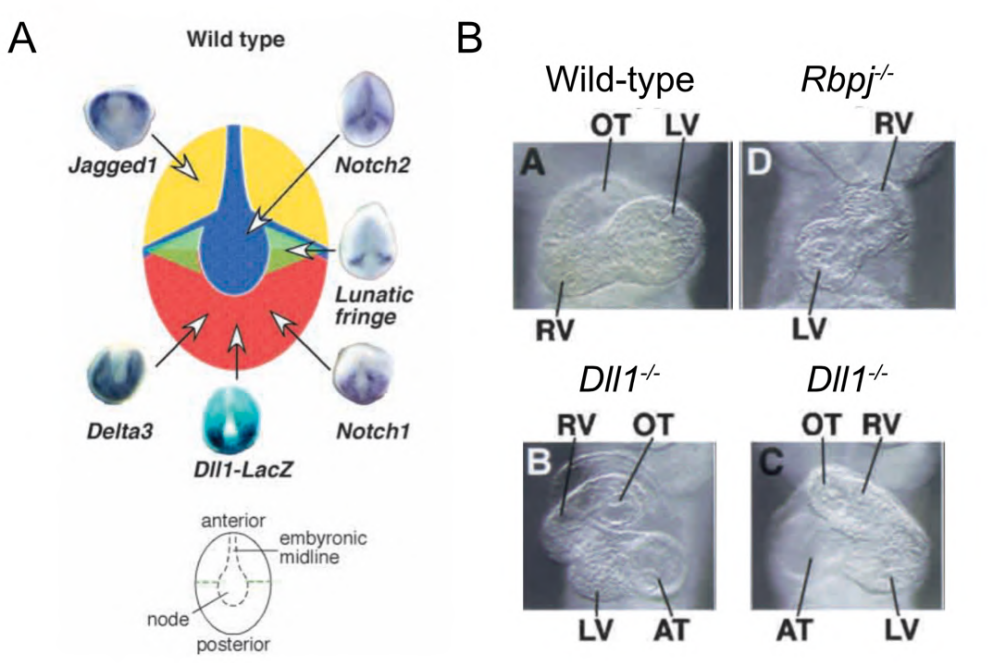

Fig 19. Notch signaling is involved in the formation of the left-right organizer. (A) Patterning of Notch genes in and around the left-right organizer. *Notch2* is expressed within the pit, while other *Notch* genes are expressed in the adjacent mesoderm in different patterns. From (Przemeck et al., 2003). **(B)** Heart looping defects in *Rbpj*$^{-/-}$ and *Dll1*$^{-/-}$ mutants secondary to defects in the left-right organizer. AT: atria; LV: left ventricle; OT: outflow tract; RV: right ventricle. From Raya et al., 2003

Cellular mechanisms involved in left-right asymmetry establishment regulated by Notch signaling

Complementary studies have demonstrated that Notch signaling is involved in at least three different processes in the left-right organizer.

First, it has been reported that Notch signaling is important for regulating the formation of the node, as *Rbpj*$^{-/-}$; *Dll1*$^{-/-}$ and *Smarcd3*$^{-/-}$ mutants show deformed nodes (Przemeck et al., 2003; Takeuchi et al., 2007). *Smarcd3* encodes a protein named Baf60c, which is involved in chromatin remodeling. Baf60c has also been shown to enhance interactions between Notch intracellular domain and Rbpj, thus promoting the activity of the Notch transcriptional complex. *Smarcd3*$^{-/-}$ mutants also display heart looping defects (Takeuchi et al., 2007).

Secondly, Notch signaling is required for the regulation of cilia length and motility. In the context of zebrafish, it has first been shown that the length of cilia in the Kupffer's vesicle (left-right organizer of the fish) is regulated by Notch. *deltaD*$^{-/-}$ embryos display shorter cilia, while *deltaD* or NICD overexpression leads to longer cilia (Lopes et al., 2010). It has also been shown that the ratio of motile- versus immotile cilia is dependent on Notch signaling. As mentioned previously, motile cilia are present mostly in the pit and are important for generating flow, while immotile cilia are present on crown cells and they are associated with the sensing of flow in the mouse (McGrath et al., 2003). *Notch* mutants in *Xenopus* (Boskovski et al., 2013) and *deltaD*$^{-/-}$ mutants in zebrafish (Sampaio et al., 2014) have a higher ratio of motile cilia, while overexpression of NICD or of the Notch canonical target *her-12* (a zebrafish paralogue of *Hes5*) leads to a higher ratio of immotile cilia (Tavares et al., 2017). These regulations of cilia specification occurs already in the dorsal forerunner cells, which are precursors of the Kupffer's vesicle (Melby et al., 1996).

Although cilia are affected, the flow of the left-right organizer has been shown to be still present: reports from mouse studies indicate regular flow in *Rbpj*$^{-/-}$ and *Dll1*$^{-/-}$ Notch pathway mutants (Krebs et al., 2003; Takeuchi et al., 2007), while data from zebrafish show a reduced flow, which leads to a reduced expression of asymmetric genes such as *charon* (Lopes et al., 2010). A reduction of the flow in the node is delicate to measure; thus it is possible that Notch mutant mouse embryos display a reduced flow in the left-right organizer, and a re-examination of this using state-of-the-art methods would be required to drive further

conclusions. Furthermore, it is not clear if the regulation by the Notch pathway of cilia length and the ratio of motile versus immotile cilia are related.

Finally, the third level of Notch involvement in the left-right organizer is through regulation of *Nodal* gene expression. As mentioned previously, the *Nodal* gene has two important regulatory elements associated with its asymmetric expression; the node-specific enhancer (NDE) and the asymmetric enhancer (ASE) (Adachi et al., 1999; Norris & Robertson, 1999). Of the two, only the node-specific enhancer (NDE) has been shown to be regulated by Notch signaling, as it includes two Rbpj binding sites, which are required for its function (Krebs, Iwai, et al., 2003; Raya et al., 2003). If these sites are mutated, it leads to defective expression of *Nodal* in the left-right organizer, thus demonstrating that Notch signaling is upstream of *Nodal* in this region.

That Notch signaling is required for *Nodal* asymmetry does not automatically infer that Notch is responsible for asymmetric expression of *Nodal* in the left-right organizer, as multiple pathways are involved in this. For instance, it has been shown that *Wnt3*, which is expressed higher on the left side of crown cells at a stage prior to *Nodal* (as well as regulate *Nodal* asymmetry), also has Rbpj binding sites in its enhancer (Kitajima et al., 2013). If these Rbpj sites are mutated (thus preventing Rbpj to bind), it leads to a reduction of *Wnt3* expression in the crown cells, but it also leads to ectopic expression of *Wnt3* in the pit cells. This repression of *Wnt3* in the pit cells is argued to be Rbpj-dependent, in a manner where the Notch transcriptional complex does not contain a Notch Intracellular domain and is therefore Notch-independent, and as such it is the output of a cell not experiencing Notch signaling. it highlights a role for Notch signaling in the patterning of the left-right organizer.

Finally, it has been reported that Notch signaling in the left-right organizer in the chicken (the Hensen's node) is asymmetric and could thus directly drive asymmetric *Nodal* expression. (Raya et al., 2004) showed that *Dll1* and *Lfng* are left-sided asymmetrically expressed in the left-right organizer of the chick during development (while for instance *Notch1* and *Jag1* are not) (Fig 20). *Dll1* and *Lfng* have previously been reported to be downstream of Notch signaling, and Raya et al., demonstrated that if Notch signaling is blocked using a gamma-secretase inhibitor, *Dll1* and *Lfng* lose their asymmetric expression. Furthermore, there is a higher left-sided concentration of Ca^{2+} in the left-right organizer (McGrath et al., 2003; Raya et al., 2004). This ion difference is driven by H^+/K^+-ATPases, and if this is repressed, it leads to

a randomization of Nodal pathway expression, loss of *Dll1* and *Lfng* asymmetry and morphological laterality defects. From experiments in the sea urchin, it is shown that Ca^{2+} asymmetry is upstream of Notch signaling prior to the S3 cleavage. It is hypothesized that the ion differences can affect the extracellular domain of Notch receptors due to their non-covalent bonds following S1 cleavage (Bessodes et al., 2012). However, it is not clear if mechanisms also applies in the mouse. As described elsewhere in the introduction (See *The breaking of symmetry and the Nodal pathway*) the Hensen's node cells of the chicken undergo a counter-clockwise cell movement. This cell displacement can also explain the pattern observed in Fig 20.

There are still uncertainties, as it has so far not been demonstrated whether or not classical direct targets of Notch signaling (such as the *Hes*/*Hey* genes) are asymmetric in the left-right organizer, or if there is a higher activity of Notch signaling in left crown cells. For instance, Notch1 is necessary for left-right asymmetry in *Xenopus* and zebrafish, making it a candidate for asymmetric Notch signaling in the left-right organizer. Immunofluorescent labelling and measurements of left-right asymmetry of Notch1 intracellular domain (which is a direct readout of Notch1 activity) in the left-right organizer at different stages of development would help to answer this question.

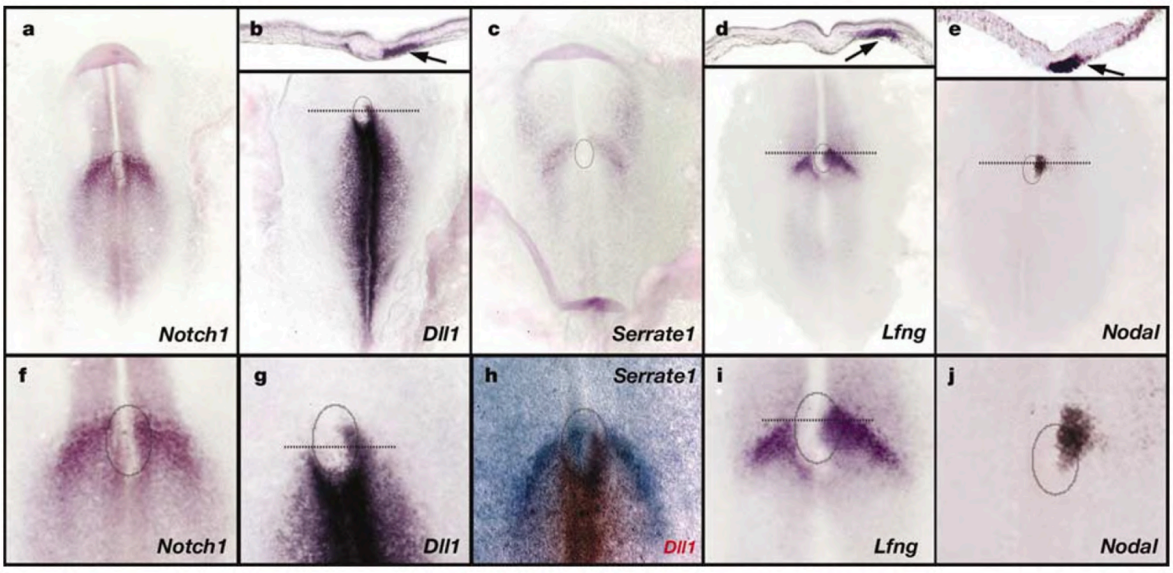

Fig 20. Some Notch pathway components are asymmetric in the Hensen's node. *In situ* hybridization images of Notch pathway genes in the left-right organizer of the chick. Most genes are symmetrically expressed, however *Dll1* and *Lfng* have been reported to be left-sided asymmetrically expressed. From Raya et al., Nature 2004

Beyond the left-right organizer, phenomenal work by (Sakano et al., 2010) has also shown that Notch signaling can have a role in left-right asymmetry establishment outside the left-right organizer.

Among the first reports of Notch signaling's role in Nodal pathway asymmetry, there were some discrepancies in the results of the Notch signaling mutants. (Przemeck et al., 2003) reported that expression of *Nodal*, *Lefty2* and *Pitx2* were randomized in the lateral plate mesoderm, while (Krebs, Iwai, et al., 2003; Raya et al., 2003) reported that neither *Nodal* nor *Lefty2* were expressed in the lateral plate mesoderm, but that *Pitx2* expression was randomized. Finally, (Takeuchi et al., 2007) detected neither *Nodal*, *Lefty2* nor *Pitx2*. These discrepancies were initially attributed to differences in mouse strains and *in situ* hybridization protocols (in particular, *Nodal* is lowly and transiently expressed and can be challenging to detect), however (Sakano et al., 2010) has challenged this by showing that Notch signaling has a *Nodal* independent role in the lateral plate mesoderm, where it regulates *Pitx2* expression.

Sakano *et al*. observed initially that *notch1* knockdown followed by NICD overexpression only rescued *xnr1* (*Nodal Xenopus* paralogue) but not *pitx2* expression. This made them hypothesize a *Nodal* independent role of Notch signaling in regulating *pitx2*. The authors also observed that knockdown of *bcl6* and *bcor* leads to a similar pattern. Bcl6 and BCoR are co-factors and transcriptional repressors in the Notch pathway. Mutations in *BCOR* has been associated with heterotaxia syndrome in humans (Hilton et al., 2007), and knockdown of either *bcl6* or *bcor* leads to laterality defects in *Xenopus*. Sakano et al. demonstrated that when Bcl6 or Bcor are present, they bind the Notch transcriptional complex and out-competes Maml1 (Fig 21). By changing co-factors, the Notch transcriptional complex change binding sites, and the BCoR-Bcl6-NICD-Rbpj complex binds and represses the expression of genes such as *esr1* (paralogue to *Hes5*). In follow-up work they have demonstrated that Esr1 can bind the asymmetric enhancer site (ASE) of the *pitx2* gene, and if doing so, can block the activity of the *Nodal*-induced Foxh1 transcriptional complex through inhibition of p300 recruitment, thus showing that if Bcl6 and BCoR are not present, Notch signaling (through Esr1/Hes5) will downregulate *pitx2* in the lateral plate mesoderm and induce laterality defects (K. Tanaka et al., 2014). The work presented by Sanako and Tanaka *et al*., is particularly solid, because it explores direct binding targets. How much these processes are evolutionary conserved in the mouse remains unknown.

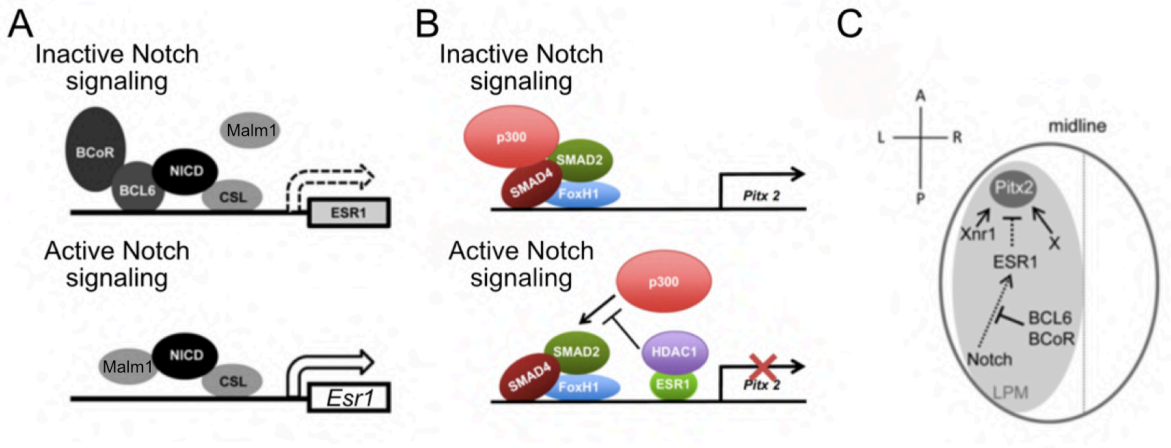

Fig 21. **Proposed role of Notch signaling regulating *Pitx2* expression in the lateral plate mesoderm**. **(A-B)** When Notch signaling is active, it leads to the expression of *Esr1*, which is a direct inhibitor of Pitx2 expression. If Bcl6 and BCoR are present, they will outcompete Mam1 from the Notch transcriptional complex, which instead leads to the repression of Esr1m and thus no repression of *Pitx2*. **(C)** Model of Notch signaling, *Nodal* paralogue Xnr1 and other genes regulating *Pitx2* expression in the left lateral plate mesoderm. A+C from (Sakano et al., 2010), B from (K. Tanaka et al., 2014).

Notch Signaling in the Context of Heart Development

The effect of Notch signaling on heart morphogenesis goes beyond the left-right organizer and establishment of left-right asymmetry. Already in the early 1990s, Notch signaling components were found to be expressed in the heart (Franco Del Amo et al., 1992). Around the same time, mutations of Notch pathway components were identified to cause cardiovascular diseases in humans, such as JAG1 and NOTCH2 in Alagille syndrome (L. Li et al., 1997; Mcdaniell et al., 2006), NOTCH3 in CADASIL (Cerebral Autosomal Dominant Arteriopathy with Subcordical Infarcts and leukoencephalopathy) (Joutel et al., 1996) and NOTCH1 in aortic valve disease (Garg et al., 2005). These findings prompted researchers to unravel the role of Notch during the formation of the heart.

Early work in the frog (using inducible activation and inhibition of Notch signaling during gastrulation) showed Notch to be a repressor of cardiomyocyte specification while heart field related genes were not affected (Rones et al., 2000). These findings were supported by *in vitro* studies using mouse embryonic stem cells, where *Rbpj*- or *Notch1* mutants would promote cardiomyocyte formation, while Notch1 overexpression would demote cardiomyocyte formation and instead favor neurogenesis (Schroeder et al., 2003; Nemir et al., 2006). This

work shows how Notch can regulate cardiomyocyte cell fate, however the developing heart is a complex tissue. Therefore, there has been a research focus on understanding exactly when and where Notch signaling is required in the heart and for which processes.

As described earlier in the introduction, Notch signaling is involved in left-right asymmetry breaking, and therefore global *Notch* mutants display heart looping defects. Abnormal left-right patterning is not necessarily lethal, as patients are born with heterotaxia syndrome. However, due to that Notch signaling is involved in multiple processes during development, embryos die early. For instance, Notch pathway mutants, such as the *Mib1*$^{-/-}$ (Barsi et al., 2005) and the *Rbpj*$^{-/-}$ (Oka, Nakano, Wakeham, Luis de la Pompa, et al., 1995; Souilhol, Cormier, Tanigaki, et al., 2006), have a straight heart tube. They also display a short tail at E9.5 due to failure in somitogenesis as well as defects in vascularization (Fig 22A). Likely due to the vascularization defects, the embryos die around E10.5-11.5, which hinders further analysis. Thus, researchers have been forced to either look at other Notch pathway components or use conditional genetic ablation to further investigate the role of the Notch pathway specifically in the heart and heart field.

Interestingly, *Notch1* and *Notch2* single mutants also die at similar stages, while they don't display laterality defects (Hamada et al., 1996; Krebs et al., 2003). In stark contrast to this, *Notch3* and *Notch4* mutants are viable and fertile, and were initially reported to have no obvious defects (Krebs et al., 2000; Krebs, Xue, et al., 2003). This prompted research to focus more on *Notch1/2* compared to *Notch3/4*. The *Notch3* receptor is the main focus of this PhD thesis and will be discussed in details separately in a chapter below.

To investigate how different cardiac populations are dependent on Notch signaling, experiments have been performed using Cre-drivers. Overall, there have been three types of Cre-drivers used for studying the heart; drivers targeting the heart progenitor population, drivers targeting the endothelial (including the endocardial) population and finally drivers targeting the myocardium.

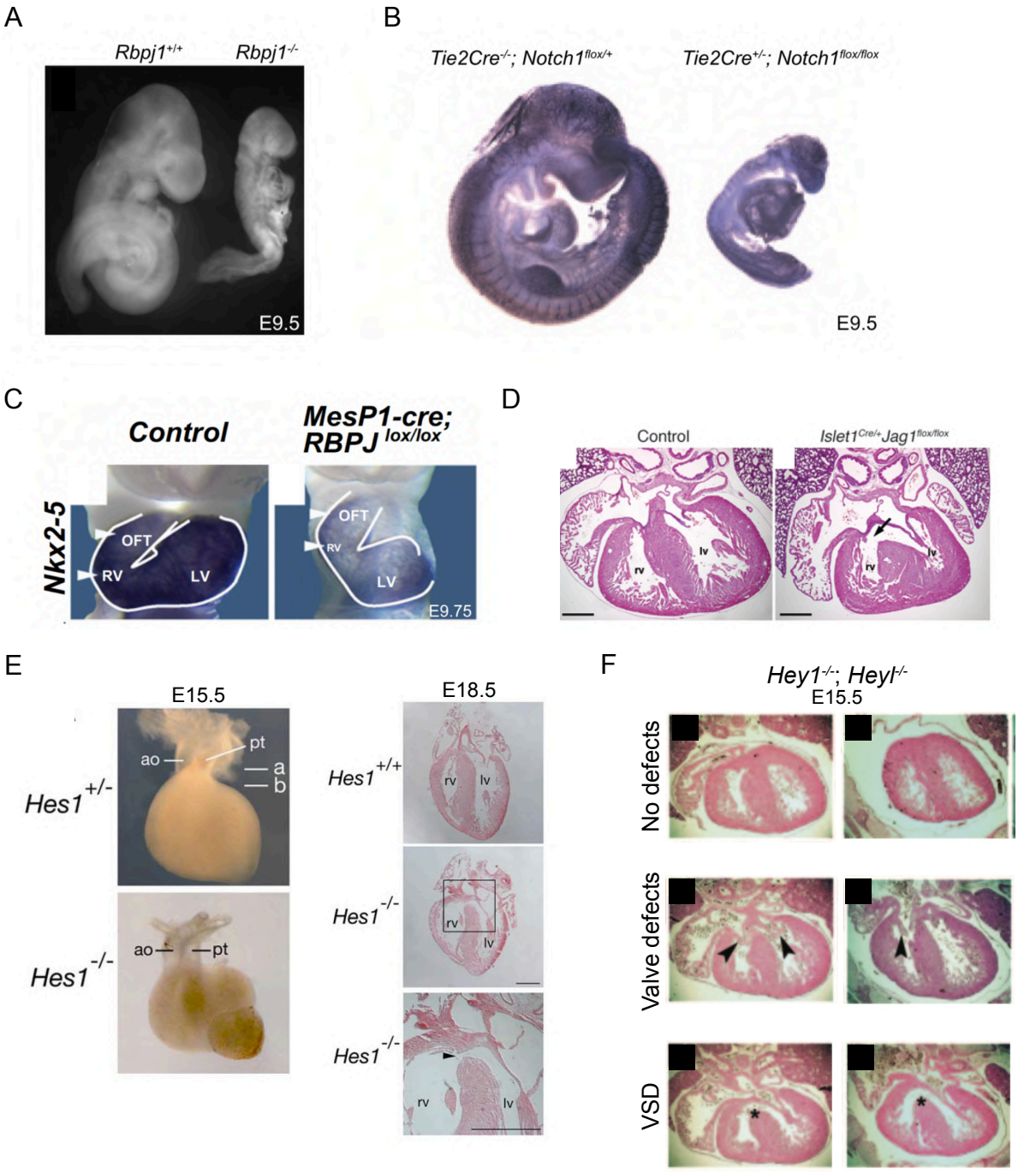

Fig 22. **Images of Notch pathway mutants. (A)** The global Notch signaling mutant (Rbpj-/-) displays severe phenotypes, such as a shortened tail, vascularization and randomized heart looping direction. From (Souilhol, Cormier, Tanigaki, et al., 2006) **(B)** Knockout of *Notch1* in the endothelial lineage does not cause randomized heart looping, however the embryos are grossly underdeveloped, showing that Notch1 in the endothelium is important for early embryonic development. From (Limbourg et al., 2005) **(C)** Removal of Notch signaling in the mesodermal population leads to lesser overall defects, however they display heart looping defects due to shortening of outflow tract and right ventricle. From (Klaus et al., 2012). **(E)** *Hes1* mutants display dextraposed aorta (left) and ventricular septal defects (right, arrowhead) with partial penetrance. From (Rochais et al., 2009). **(F)** While *Hey1*$^{-/-}$ and *Heyl*$^{-/-}$ do not show developmental defects, *Hey1*; *Heyl* double mutants do. For instance in the heart there are both observed valve defects (arrowhead) and ventricular septel defects (VSD) (asterisk). From (Fischer et al., 2007)

Notch signaling in the endothelial population is likely the most important in early embryonic development, as ablation of *Rbpj* or *Notch1* in the endothelium (Tie2-Cre) phenocopies constitutive *Notch1* knock-out (Fig 22B) (Limbourg et al., 2005; Grego-Bessa et al., 2007). Similar results have been reported for the overexpression of N1ICD in the endothelial population (Luna-Zurita et al., 2010). This has sometimes been attributed to effects in the endocardial population (see e.g., the review Luxán et al., 2016).

However, it is surprising that the endocardial phenotypes (driven by Tie2-Cre) have been reported to be so strong, as is more severe than the genetic ablation- (High et al., 2009; Klaus et al., 2012) or activation (Watanabe et al., 2006) of Notch signaling in heart progenitor cells including endocardial precursors (Fig 22C). Embryos where Notch signaling has been genetically ablated in either mesodermal cells (via Mesp1-Cre) or in heart progenitor cells (Isl1-Cre) instead display shorter outflow tract and smaller right ventricle at E9.5, while they also have severe congenital defects at birth leading to neonatal lethality. That these have a less severe phenotype than global Notch signaling mutants or endothelial-cell specific mutants can be hard to gauge from the images in Fig 22, however global Notch signaling mutants or endothelial-cell specific mutants die around E10.5, while conditional ablation of Notch signaling in heart progenitors leads to death at late gestational stages (while displaying several cardiac malformations) (High et al., 2009).

The Cre-driver mainly used for studying the endothelium, the *Tie2-Cre* (Kisanuki et al., 2001), has effects beyond the endocardial population, as it targets the full endothelial population. It remains to be clarified if affecting Notch signaling in the endothelial population is causing the severe phenotype due to effects in the endocardial population of the heart or if it is due to a systemic reaction in the embryo caused by disruption of Notch signaling throughout the endothelial tissue.

This confusion likely stems from that Notch signaling, in particular Notch1, has been shown to be important for the endocardium. *Notch1* has been shown to be expressed in the endocardial population (Timmerman et al., 2004), where it induces, among others, *Hey1* and has been reported to be important for the patterning of the cushions (Watanabe et al., 2006).

Knockout of *Notch1* in heart progenitors and cardiomyocytes leads to a smaller right ventricle and higher proliferation in cardiac progenitors (Kwon et al., 2009), while ectopic activation of Notch1 signaling throughout the heart and heart progenitors also leads to a reduction of right ventricle size (Watanabe et al., 2006). Furthermore, in this context of

overexpression, cardiomyocytes are formed but they are not able to form proper sarcomere structures, indicating that Notch signaling inhibits proper maturation of cardiomyocytes. The fact that both knockout and overexpression lead to similar phenotypes suggests that the role of Notch signaling in the heart is complex and it is likely dependent on tissue, timing and genetic dosage of the Notch pathway components. Additionally, it has to be noted that in several studies using Cre-drivers targeting heart progenitors, it was stated that the effect of the genetic ablation or -overexpression was due to biological processes occurring within the progenitors. Nevertheless, heart progenitors form both the myocardial- and endocardial populations, and these conclusions cannot be drawn without supplementary experiments.

Ablation of Notch signaling in the myocardium displays the least severe phenotype. Indeed, it has been found that conditional ablation of Notch signaling or *Notch1* in the myocardium leads to defective trabeculations of the left ventricle (cTnT-Cre in Luxán et al., 2013), abnormal patterning of the atrioventricular canal causing issues with the conduction (Mlc2v-Cre in Rentschler et al., 2011) or no phenotype (Tnnt2-Cre in Salguero-Jiménez et al., 2018) depending on the cre-driver used.

The key role of Notch signaling in the endocardium has also been investigated through studies of the Notch ligands. During heart development, the main ligands are Dll4, Jag1 and Jag2. Dll4 is restricted to the endocardium, while Jag1 is localized in a wide population containing endocardium, heart progenitors and to a lesser degree myocardium (Luxán et al., 2016; R. C. V. Tyser et al., 2021). *Jag2* is upregulated around E10.5 and primarily in the myocardium (D'Amato et al., 2016; R. C. V. Tyser et al., 2021).

Early interactions between Notch1 and Dll4 in the endocardium have been shown to induce ventricular trabeculation, while later interactions between Notch1 in the endocardium and Jag1/2 in the myocardium is important for ventricular maturation and compaction (D'Amato et al., 2016).

Constitutive *Jag1* and *Dll4* mutants share some similarities with *Notch1* mutants (vascular defects, no obvious heart looping phenotype and embryonic lethality at E10.5-11.5), which again point towards the role of Notch signaling in the vascular tissue (Duarte et al., 2004; Xue et al., 1999). To explore the role of Jag1 and Dll4 in cardiac tissue beyond the endothelium, gene knockout using cre-drivers has also been utilized. When either *Jag1* or *Dll4* are knocked-

out using cre-drivers of the second heart field (e.g. Isl1-Cre), this leads to congenital heart defects such as ventricular septal defects or double outlet right ventricle (Fig 22D). These defects, at least in the case of *Dll4*, could be related to a reduced size of the right ventricle and length of the outflow tract (de Zoysa et al., 2020; High et al., 2009). Altogether, this shows that the Notch ligands have roles beyond the endocardium, however it remains to be understood if they are needed in the heart progenitors or in the cardiomyocytes.

It has also been shown that the classical Notch targets, the *Hes* and *Hey* genes, are involved in cardiogenesis. For instance, mutant mice of *Hes1* and *Hey2* die at late gestational stages with defects in multiple organs, among others the heart (Gessler et al., 2002; Ishibashi et al., 1995).

Hey2$^{-/-}$ mutants are the most severe, as they display a wide range of congenital heart defects such as hypertrophy, ventricular septal defects and tetralogy of Fallot (Donovan et al., 2002; Kokubo et al., 2004). *Hes1*$^{-/-}$ mutants display defects with partial penetrance, the most common being dextraposed aorta and ventricular septal defects (Fig 22E) (Rochais et al., 2009). The role of *Hes1* has been linked to the second heart field, as heart progenitors of *Hes1*$^{-/-}$ mutants proliferate less at E8.5, which leads to a shorter outflow tract at E10.5.

Hey1 and *Heyl* single mutants are viable, and they don't display evident defects. However, this is probably due to functional redundancy with other bHLH factors, as *Hey1*$^{-/-}$; *Heyl*$^{-/-}$ and *Hey1*$^{-/-}$; *Hey2*$^{-/-}$ leads to neonatal- and embryonic death, respectively. *Hey1*$^{-/-}$; *Hey2*$^{-/-}$ mutants die at E10.5-11.0, where they have vascular defects and only form a single ventricle with a left (-ventricle) identity (Kokubo et al., 2005). On the other hand, *Hey1*$^{-/-}$; *Heyl*$^{-/-}$ mutants develop ventricular septal defects (Fig 22F) (Fischer et al., 2007).

Compared to Hes1, the functions of Hey1/Hey2/Heyl have been associated to processes occurring within the heart tube, where they have been coupled to chamber identity (among other by Bmp2 inhibition) and in epithelial-to-mesenchymal transition important for forming the cushions in the atrioventricular canal (MacGrogan et al., 2018). Whether the *Hey* genes (like *Hes1*) also play a role in the heart progenitors remains unsolved.

All this shows that Notch signaling plays a role in the formation of the heart. Some Notch mutants display defects in several organs leading to embryonic lethality, which complicates studying the specific contributions of Notch pathway components during development. From investigating conditional mutants and classical Notch target, it is clear that they develop

cardiac defects, usually related to the outflow tract, the valves or septal defects. Furthermore, there is redundancy within the heart, as some of these mutants do not display defects (e.g. *Hey1*$^{-/-}$ or *Heyl*$^{-/-}$), while others only show partial penetrance (e.g. *Hes1*$^{-/-}$). There are still many questions regarding the role of Notch within the heart. Next will be described the Notch receptor *Notch3*, which has previously not been linked to asymmetric heart morphogenesis.

Notch3

During the thesis work, *Notch3* has been identified as a novel candidate factor in asymmetric heart morphogenesis. Although *Notch3* was the first specific Notch receptor to be related to a disease (CADASIL, (Joutel et al., 1996)), its specific role has been less studied compared to *Notch1* and *Notch2*. *Notch3*$^{-/-}$ were initially reported as viable and fertile with no obvious defects (Krebs, Xue, et al., 2003). However, Notch3 has been shown to play roles in e.g. smooth muscle cell differentiation (Domenga et al., 2004), progenitor maintenance (Lafkas et al., 2013) and injury response (Sahu et al., 2021).

Similarly to the other Notch receptors, the role of *Notch3* in development is not very clear, as it can promote both stemness and differentiation depending on the context. Coherently with this, NOTCH3 has been shown to be both a tumor suppressor- and an oncogene in cancer (Aburjania et al., 2018), and below the research investigating the role of Notch3 in stemness and in differentiation is described.

There have been developed several mouse lines to explore the function of *Notch3*; ranging from full knockout mutants (Dickinson et al., 2016; Kitamoto et al., 2005; Krebs et al., 2003) to inducible overexpression of Notch3 activity (Lafkas et al., 2013). Of the three reported *Notch3* null alleles, the *Notch3*^{tm1Grid} generated by Krebs et al. is the most used with more than 35 publications using it. There are 33 exons of *Notch3* (see *Results – Fig S4F*), and there are no report on isoforms of *Notch3* (www.ncbi.nlm.nih.gov/gene/18131).

In the *Notch3*^{tm1Grid} mouse mutant (Krebs et al., 2003), exon 6-8 are removed (See *Results – Fig S4F*), which among other encodes EGF-like repeats 11+12 that have been reported to be necessary for the function of Notch receptors (Rebay et al., 1991). Beyond the *Notch3*^{tm1Grid} mouse mutant, there are two other null alleles, the *Notch3*^{tm1Khan} (Kitamoto et al., 2005) and the *Notch3*$^{tm1.1(KOMP)Vlcg}$ (Dickinson et al., 2016). The *Notch3*^{tm1Khan} has a neomycin cassette inserted in exon 4, while the *Notch3*$^{tm1.1(KOMP)Vlcg}$ is reported as a complete removal of all 33

exons. All three *Notch3* mutants report that they mice are viable and fertile, and these mutant lines have been useful to understand the role of *Notch3* in quiescence, stemness and differentiation.

Notch3 as a Promoter of Stemness and Quiescence

The role of *Notch3* has been associated with quiescence induction (i.e. non-proliferative, non-differentiating) in multiple tissues such as muscle satellite cells (Kitamoto & Hanaoka, 2010), neuronal stem cells in zebrafish (Alunni et al., 2013) and mice (Kawai et al., 2017) as well as in mammary gland luminal cells (Lafkas et al., 2013). All these cell types have to continuously balance between replenishing lost cells and maintaining the progenitor pool. In these cells, Notch3 induces a quiescent progenitor stage, as overexpression of Notch3 intracellular domain leads to loss of both proliferation- and differentiation markers. Similarly for muscle satellite cells and for neuronal progenitors, where quiescence has been studied in the greatest details, acute loss of *Notch3* leads to a higher number of activated, proliferating progenitors as well as differentiated cells (Alunni et al., 2013; Kawai et al., 2017). This can lead to specific phenotypes; for instance if *Notch3*$^{-/-}$ mutant mice are subjected to multiple rounds of muscle injury, hyperplasia of muscle tissue is induced (Kitamoto & Hanaoka, 2010).

In this process of progenitor pool maintenance, *Notch1* has also been shown to play a role. *Notch3* is higher expressed in the quiescent progenitors, while *Notch1* is typically expressed in activated progenitors prior to differentiation (Kawai et al., 2017; Kitamoto & Hanaoka, 2010) (Fig 23). Careful work in the zebrafish has shown that while *notch1b* only regulates stemness of the progenitor cells, *notch3* regulates both quiescence and stemness, potentially through two different transcriptional programs (Than-Trong et al., 2018). This is for instance the case in *Notch1* mutants, in which the number of quiescent progenitors is comparable to controls, however the number of active progenitors is lower due to precocious differentiation. Similar to this, absence of *Notch3* in retina injury models will lead to a lower threshold of differentiation, i.e. that more cells will commit to regeneration following injury (Sahu et al., 2021).

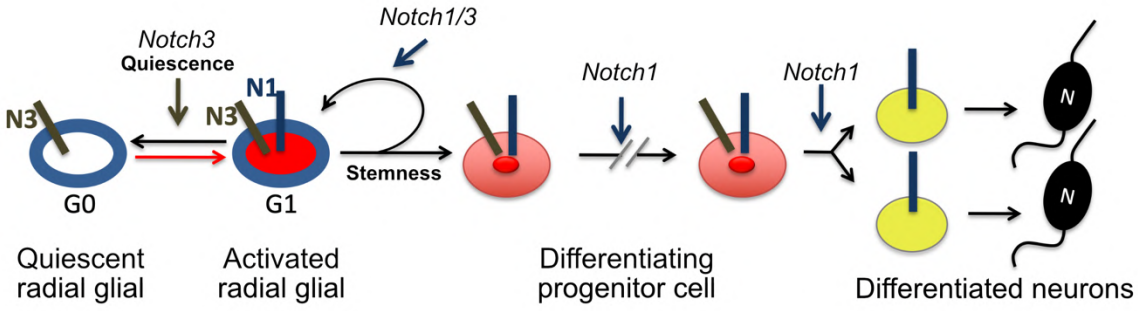

Fig 23. **Model of Notch signaling involvement in the regulation of the neuronal cell progenitor pool.** Radial glial cells can replenish lost neurons, and they exist as two states: a quiescent stage, where the cells are in G0, and an activated stage, where the cells are dividing. *Notch3* has been shown to promote the quiescent cell state as well as regulating the stemness of activated cells. *Notch1* is important for stemness in the activated radial glial cells and important for early steps of differentiation. This is also an example of *Notch* receptors having both overlapping and specific functions. Figure adapted from Bally-Cuif lab (Institut Pasteur)

Altogether, it is clear that Notch3 promotes stemness and quiescence across multiple cell types and organisms, which is important for progenitor pool maintenance, however it is not well understood if the mechanism upon which *Notch3* ensures this function is conserved. Some evidence points towards this: for instance *Notch1* is associated with an activated state prior to differentiation. Furthermore, some Notch classical targets are regulated by Notch3 in the different systems. *hey1* is induced by Notch3 in both neuronal stem cells and in retina upon injury, and *Hey1* has been shown to be important for the function of *Notch3* (Sahu et al., 2021; Than-Trong et al., 2018). Although formally not shown for *Notch3*, *Hey1* is induced by Notch signaling myogenic cells (Castel et al., 2013) and *Hey1* has been shown to be a repressor of myogenesis (Buas et al., 2010). Further work is needed to elucidate if these mechanisms are conserved in the mouse. In particular it is important to understand what is the specific role of Hey1 in relationship to Notch3, and to determine which other targets are regulated by Notch3 (in the context of stemness and quiescence).

Notch3 as a Promoter of Differentiation

That *Notch3*$^{-/-}$ mice are viable and do not die prematurely initially came as a surprise, since mutations in NOTCH3 were linked already in 1996 to CADASIL, the most common form of late onset hereditary stroke disorder (Joutel et al., 1996). Since CADASIL is related to the vessels, it prompted researchers to look into the vessels of adult mice, where it was found that the

arteries are thinner due to improper differentiation of smooth muscle cells, which ultimately affects the blood flow (Domenga et al., 2004).

Further studies have shown that *Notch3* is expressed in mural cells, a heterogenous cell type that surrounds vessels and is important for regulating and maintaining vascular function and -structure (A. Lin et al., 2021). From cell co-culture experiments it was discovered that Jag1, localized in endothelial cells, induces the expression of *Notch3* in mural cells, where Notch3 through a positive feedback loop auto-regulates itself, which finally leads to activation of smooth muscle gene expression (H. Liu et al., 2009). This process has also been studied *in vivo*, for instance in renal vasculature (H. Liu et al., 2010) and in coronary arteries within the heart (Volz et al., 2015).

Volz *et al*. demonstrated that a sub-type of the mural cells, the pericytes, develop into coronary artery smooth muscle cells in the mouse heart during development, and Notch3 is required for this process. They also demonstrated that Jag1 is localized only on endothelial cells close to blood flow, and that similarly to the co-culture system of Liu *et al.*, Jag1 is important for inducing *Notch3* in the pericytes. In the absence of *Notch3*, the differentiating pericytes will not mature into proper smooth muscle cells (Volz et al., 2015). These data links blood flow, development and vascular remodeling and shows that *Notch3* is an important factor in this. Notch3 has also been found to promote differentiation in other cell types, for instance in the airway basal cells (Bodas et al., 2021).

Notch2 has been shown to have a role in vascularization, so that *Notch2/3* double mutants develop vascular defects that are more severe than single mutants (Q. Wang et al., 2012). However, careful studies in cell culture have shown that the functions of *Notch2* and *Notch3* in vascular smooth muscle cells are not completely overlapping, as they are regulated by different genes and can induce different targets leading to different outcomes (Baeten & Lilly, 2015). Notch2 promotes proliferation, while Notch3 promotes differentiation and protection against apoptosis. That Notch2 and Notch3 have overlapping and specific functions has also been shown in airway basal cell culture differentiation experiments. Work by Carrora et al. has shown that it will lead to different distribution of differentiated cell types depending on if *Notch2* or *Notch3* is inhibited (Carraro et al., 2020). These findings demonstrate that *Notch3* signaling is involved in differentiation and has overlapping and specific roles with other Notch receptors.

However, *Notch3* is not always found as a promoter of differentiation, as in mouse models of pulmonary arterial hypertension, *Notch3* has been found to be a promoter of proliferation and inhibitor of differentiation through the activation of *Hes5*, which leads to the repression of smooth muscle genes such as *Myh11* (X. Li et al., 2009). This discrepancy can come from the fact that *Notch3* can have different functions in different tissues, but it can also come from the fact that many of these studies were conducted with overexpression of Notch3 intracellular domains. When expressed at high levels, these are suspected to lose their specific targets (Than-Trong et al., 2018; Z. Wang et al., 2009). Further studies in different cell types with emphasis on targets and cellular mechanisms are necessary to elucidate the role of Notch3.

Thus, *Notch3* can promote quiescence, stemness and differentiation, and it can do so across different tissues and species. Although evidence suggests that some components are conserved (e.g. *Notch3*-*Hey1* in stemness), how *Notch3* is regulating these processes is not well understood. In this thesis, *Notch3* was identified as a novel asymmetric gene, whose asymmetry is amplified by Nodal and plays a role in proper heart morphogenesis. This links *Notch3* to asymmetric organogenesis. As described in the next chapter (*Objectives*) *Notch3* was identified through a screen aiming to find novel asymmetrically expressed genes.

Objectives

As described in the introduction, recent experiments in the lab have pinpointed that *Nodal* functions by biasing and amplifying pre-existing asymmetries, and therefore there must be asymmetrically expressed genes beyond the Nodal pathway. Additionally, the fact that *Nodal* is expressed within the second heart field (and not within the heart), in combination with the observation that the two sequential events biasing heart looping occurs at the poles of the tube, where newly differentiated cardiomyocytes are entering the heart, made us hypothesize that there must be several aspects of left-right patterning within heart progenitors. This led to the formulation of the main question driving the work of this PhD thesis:

Are there genes other than that of the Nodal pathway, which are left-right asymmetrically expressed in heart progenitors ?

To answer this question, we selected a transcriptomics approach, as this would allow an genome-wide screening. Initially we explored both single cell- and bulk RNA sequencing approaches. In particular we reasoned that a more resolutive segregation of samples in time (see *Introduction - Fig 15*) was important, as the kinetics of Nodal asymmetry had been shown to be transient (Desgrange et al., 2020), and the heart acquires sequential asymmetric changes (le Garrec et al., 2017).

To prepare for sequencing, we first characterized the second heart field population at different stages of heart looping (Figure 1). As we initially planned for a FACS based single cell RNA sequencing approach, we estimated the total number of cells in the second heart field and we compared the proportion of labelled cells with different markers.

During the PhD, several great reports of single cell RNA sequences in heart progenitors were published. In particular (1) a data set of full mouse embryos at stage E6.5-E8.5 (Pijuan-Sala et al., 2019) and (2) a data set focused on microdissected cardiac regions at different stages of early heart development (R. C. V. Tyser et al., 2021). Considering that patterning is more difficult to detect in single cells, due to lower gene coverage and cell loss upon FACS sorting, we decided to concentrate efforts on the bulk approach. We used the published scRNA sequencing data sets whenever relevant. Figure 2 describes how we initially performed a pilot

screen at two stages. Although we were able to detect novel left-right asymmetrically expressed genes using the pilot screen, we were not satisfied with the overall data quality (e.g. number of duplicated reads), so we optimized conditions to then performed a wider screen at seven stages of heart looping.

Among the novel asymmetric genes detected in the pilot screen, Notch signaling was the most striking. It caught our surprise, as we had not expected Notch to be asymmetric in the heart field. Thus, I have identified Notch3, as a novel left-sided gene. To validate this candidate from the screen, I have been exploring the following questions:

What is the spatio-temporal pattern of *Notch3* during heart looping?

Is *Notch3* the only asymmetric Notch receptor?

Can other Notch receptors compensate when *Notch3* is absent?

What is the relationship between *Notch3* and Nodal signaling?

Is Notch3 required for asymmetric heart morphogenesis?

Material and Methods

EXPERIMENTAL MODEL AND SUBJECT DETAILS

C56Bl6J mice were used as wild-type embryos. *Notch3*$^{tm1Grid/\ tm1Grid}$ mutants (abbreviated *Notch3*$^{-/-}$) were kept in a C56Bl6J background (Krebs et al., 2003). *Nodal*$^{null/+}$*; Hoxb1*$^{Cre/+}$ males were maintained in a mixed genetic background and crossed to *Nodal*$^{flox/flox}$ females (C. C. Lu & Robertson, 2004) to generate *Nodal* conditional mutants. *Notch3*$^{-/-}$ were crossed to *Nodal*$^{flox/flox}$ to generate *Notch3*$^{-/-}$; *Nodal*$^{flox/flox}$ females. Tg *CBF:H2B-Venus* embryos (Nowotschin et al., 2013) were produced in a mixed genetic background. *Rosa26*^{mTmG} mice (Muzumdar et al., 2007) were kept in a mixed genetic background. *Mesp1*^{Cre} (Saga et al., 2000), *Hoxb1*^{Cre}; *Mef2c-AHFCre* (Bertrand et al., 2011; Verzi et al., 2005) and *Isl1*^{MerCreMer} (Sun et al., 2007) were kept in C57Bl6J background. For RNA sequencing experiments, only male embryos were used to reduce variability in a small cohort. For all other experiments, both male and female embryos were collected and used randomly. Embryonic day (E) 0.5 was defined as noon on the day of vaginal plug detection. Embryonic stages were determined according to the staging grid established in Le Garrec et al., 2017 and Desgrange et al, 2020. Somite numbers were evaluated from brightfield images, and samples with somite pair numbers < 18 were deemed too young for E9.5 analysis and thus excluded. All embryos were genotyped by PCR. Genotyping of *Notch3* alleles was simplified by using three primers together to amplify the wild-type (752b) and deleted (380b) alleles. Animals were housed in the Laboratory of Animal Experimentation and Transgenesis of the SFR Necker, Imagine Campus, Paris. Animal procedures were approved by the ethical committees of the Institut Pasteur and Paris Descartes and the French Ministry of Research.

METHOD DETAILS

RNA sequencing

Left and right paired heart fields of morphologically staged single embryos were micro-dissected and the tissue flash frozen in liquid nitrogen. The heart tube and back were removed, the anterior boundary was set below the headfolds and the posterior boundary at the level of the second somite, in agreement with fate maps (Dominguez et al., 2012). For the full screen, the head was included at early stages (E8.5b-d). The yolk sac was used for sex determination by PCR. All samples were collected within 1 hour of sacrificing the mother. RNA was extracted in TRIzol-Chloroform and purified using the RNeasy micro kit (QIAGEN) including DNAse treatment. RNA quality and quantity were measured on Fragment Analyzer (Agilent). All RQN were higher than 9.7.

For the pilot screen, libraries were established using the Nugen Universal Plus mRNA-Seq kit, using 15ng of total RNA per sample. The oriented cDNAs produced from the poly-A+ fraction were PCR amplified (15-18 cycles). An equimolar pool of the final indexed RNA-Seq libraries was sequenced on an Illumina NovaSeq6000, with paired-end reads of 130 bases and a mean sequencing depth of 37,15 million reads per sample. Quality check of samples for the microdissection is shown in Fig. S2B-C. The RNA-seq data will be available in the NCBI Gene Expression Omnibus (GEO) database upon publication.

For the library kit test, libraries were established using either the Nugen Universal Plus mRNA-Seq kit, the NuGEN Trio RNA sequencing kit or the NEBnext Single Cell/Low Input RNA Library Prep Kit, using between 0.5-15 ng of total RNA per sample. Each condition was performed in duplicates, and to each sample was added ERCC spike-in RNA. The oriented cDNAs produced from the poly-A+ fraction were PCR amplified (17 cycles). An equimolar pool of the final indexed RNA-Seq libraries was sequenced on an Illumina NovaSeq6000 with a mean sequencing depth of ∼40 million reads per sample.

For the full left-right screen, libraries were established using the NuGEN Trio RNA sequencing kit, and using 2.5ng RNA per sample at stage E8.5b and 5ng per sample for the remaining stages. To each sample there was added ERCC spike-in RNA. Each condition was performed in duplicates, and to each sample was added ERCC spike-in RNA. The oriented cDNAs produced from the poly-A+ fraction were PCR amplified (17 cycles). After a final purification, all the individual libraries were first controlled by fluorimetry Qbit Double Strand DNA and capillary

electrophoresis double strand DNA on the Fragment Analyzer. An equimolar pool of all the 59 libraries was prepared according to these 2 first measurements. The concentration of this pool was measured by qPCR (KAPA Library Quantification kit, Roche) and then this pool was sequenced on the iSeq100 (Illumina) to get the percentage of reads obtained for each of the 59 libraries. A second corrected pool of libraries was prepared to correct in-balances and was then sequenced on the NovaSeq6000, Illumina (S2 FlowCells, paired-end 100+100 bases, with the target of ~50 millions of reads/clusters per library). One outlier was excluded from stage E8.5e, as Ward's hierarchical clustering grouped this sample independently.

Embryo dissection

Embryos were dissected in 1xDPBS (Gibco) and fixed in 4% paraformaldehyde either 6 hours at room temperature or 24 hours at 4°C. Yolk sac or tail pieces were collected for genotyping. For embryos dissected at E9.5, hearts were arrested in diastole by treatment with cold 250mM KCl for 5 minutes. Fixed embryos were gradually dehydrated into methanol and stored at -20°C.

Genotyping

Tissue samples were lysed either using proteinase K in lysis buffer (200 mM NaCl; 100 mM Tris pH 7.8; 5 mM EDTA; 0.2% SDS) or using the Smart Extract DNA kit (Eurogentec). Primers and PCR programs used are listed below. Expected sizes: Sex determination PCR = Y-chromosome 280bp, X-chromosome 660bp and 480bp; *Notch3* alleles = wild-type allele 758 bp, deleted allele 380bp; *Hoxb1* alleles = wild-type allele 301 bp, cre allele 1300bp; *Nodal* alleles = wild-type allele 540bp, flox allele 590bp, null allele 1050bp.

Sex determination PCR

Gene Target	Primer	Sequence
Sly (intron 8) / *Xlr* (intron 6)	SX_F	5'-GATGATTTGAGTGGAAATGTGAGGTA-3'
Sly (intron 8) / *Xlr* (intron 6)	SX_R	5'-CTTATGTTTATAGGCATGCACCATGTA-3'

From (McFarlane et al., 2013)

Temperature	Length	Cycles
94°C	2 min	x 1
94°C	30 sec	x 33
60°C	30 sec	

72°C	30 sec	
72°C	10 min	x 1

Notch3 PCR

Gene Target	Primer	Sequence
Notch3 (exon 7)	N3WT3 (Forward)	5'-CCATGAGGATGCTATCTGTGAC-3'
Neomycin	HoxNeo2 (Forward)	5'-TCGCCTTCTATCGCCTTCTTG-3'
Notch3 (intron 8-9)	N3MTR (Reverse)	5'- GGTACTGAGAACCAAACTCAG-3'

Temperature	Length	Cycles
94°C	2 min	x 1
94°C	30 sec	x 32
61°C	30 sec	
72°C	30 sec	
72°C	10 min	x 1

Hoxb1-Cre PCR

Gene Target	Primer	Sequence
Hoxb1	Hoxb1F (Forward)	5'-ACGCAGGTGAAGATCTGGTT-3'
Hoxb1	Hoxb1R (Reverse)	5'-CTGGGCAGCTCTAAACTGGT-3'
Cre	CRE1 (Forward)	5'-TGATGGACATGTTCAGGGATC-3'

Temperature	Length	Cycles
94°C	2 min	x 1
94°C	30 sec	x 35
60°C	30 sec	
72°C	30 sec	
72°C	10 min	x 1

Nodal-Flox-Null PCR

Gene Target	Primer	Sequence
Nodal (exon 3)	Nodal1 (Forward)	5'-ATTCCAGCAGTTGAGGCAGA-3'
Nodal (intron 3)	Nodal2c (Reverse)	5'-CCTGACTCAAAACCCAAGGC-3'
Nodal (intron 1)	Nodal3e (Forward)	5'-CCACCCAATTTCTAGCCCAG -3'

Temperature	Length	Cycles
94°C	2 min	x 1
94°C	30 sec	x 7
60°C (Decreasing 0.5°C per cycle)	30 sec	
72°C	30 sec	
94°C	30 sec	X25
57°C	30 sec	
72°C	30 sec	
72°C	10 min	x 1

RNA *in situ* hybridization

Wholemount RNAscope ISH was performed using the Mutliplex Fluorescent v2 Assay (Advanced Cell Diagnostic, cat. no.323110) as described in Desgrange et al, 2020. Probes used are listed in the table below, Hoechst (1:1000) was used as a nuclear counterstain. Amplification steps were performed using the TSA cyanine5 and cyanine3 amplification kits (Akoya Bioscence). Samples were then cleared in R2 CUBIC reagents and embedded in R2 reagent containing agarose (Susaki et al., 2015). Multi-channel 16-bit images were acquired with a Z.1 lightsheet microscope (Zeiss) and a 20X/1.0 objective.

Probe	Channel	Catalogue number
Notch3	1	425171
Notch3	3	425171-C3
Nodal	1	436328
Notch1	2	404641-C2
Notch2	3	425161-C3
Mab21l2	1	456901
Hey1	3	319021-C3

Wholemount immunofluorescence

Wholemount immunofluorescent staining was performed on embryos using a CUBIC clearing protocol as described in Bernheim et al. Antibodies are listed in the table below. For antigen retrieval before N1ICD staining, embryos were boiled for 1h in 10mM NaCitrate (adjusted to pH6) in screw cap tubes. Samples were then blocked for at least 2h in TNB Blocking buffer (Perking Elmer) and then incubated for 48h with the primary antibody in TNB Blocking, followed by overnight incubation with secondary antibodies and nuclear counterstain. For Jag1 staining, TSA amplification (Perkin Elmer) was used. Multi-channel 16-bit images were acquired with a Z.1 lightsheet microscope (Zeiss) and a 20X/1.0 objective.

Primary antibody

Name	Concentrations	Provider	Reference
Rabbit α N1ICD	1:300	Cell Signaling	ab4147
Goat α Jag1	1:300	R&D Systems	AF599

Secondary antibody and nuclear counterstain

Name	Ratio	Provider	Reference
Alexa Flour 647 Goat α Rabbit	1:500	Molecular Probes	A21244
Cy3 Affinipure Donkey α Goat	1:500	Jackson Immunoresearch	705-145-167
Hoechst 33342	1:1000	Sigma Aldrich	14533
Draq5	1:500	Invitrogen	65-0880-92

RT-qPCR

The second heart field was micro-dissected in DPBS 1X (Gibco) by cutting embryos below the headfolds and above the second somite pair. The myocardium and neural tube were removed to enrich for cardiac progenitors, and the tissue was flash frozen in liquid nitrogen. RNA was extracted using TRIzol-Chloroform and purified using the RNeasy micro kit (QIAGEN). Reverse transcription was performed using the Reverse Transcription kit (Quantitect). Quantitative PCR was carried out using the ViiA7 real-time PCR system (Applied Biosystems). The mRNA expression levels were measured relatively to *Polr2b* and normalized with a reference cDNA sample (pool of 7 embryos at stage E8.5c-g), using the standard $\Delta\Delta$Ct method. Primers used are listed in the table below.

Gene	Direction	Sequence (5' to 3')	Reference	Comment
Notch3 (ex10-11)	Fwd	AGGCCATGGTCTTCCCCTAT	This paper	Outside the deleted region in the *Notch3*^{tm1Grid} allele
	Rev	AGCCGGTTGTCAATCTCCAG		
Notch3 (ex8-9)	Fwd	CGTGTCTTGACCGAATTGGC	This paper	Inside the deleted region in the *Notch3*^{tm1Grid} allele
	Rev	GTGCAGCTGAAGCCATTGAC		
Notch3 (ex25-26)	Fwd	AGGCCATGGTCTTCCCCTAT	This paper	Outside the deleted region in the *Notch3*^{tm1Grid} allele
	Rev	AGCCGGTTGTCAATCTCCAG		
Notch1	Fwd	GCCGCAAGAGGCTTGAGAT	(Bone et al., 2014)	Exon 1-3
	Rev	GGAGTCCTGGCATCGTTGG		
Notch2	Fwd	CAGGAGGTGATAGGCTCTAAG	(R. Zhang et al., 2019)	Exon 26-28
	Rev	GAAGCACTGGTCTGAATCTTG		
Hey1	Fwd	TGAGCTGAGAAGGCTGGTAC	(Fischer et al., 2004a)	Exon 3-5
	Rev	ACCCCAAACTCCGATAGTCC		
Hey2	Fwd	AAAGGCGTCGGGATCGAATAA	This paper	Exon 7
	Rev	GGCATCAAAGTAGCCTTTACCC		

Hes1	Fwd	ACACCGGACAAACCAAAGAC	This paper	Exon1-2
	Rev	AATGCCGGGAGCTATCTTTCT		
Erbb2	Fwd	TTGTGGTCATCCAGAACGAGG	This paper	Exon 8
	Rev	GGGGAGAAGAATCCCTGCTG		
Atp1a1	Fwd	GTATGAGCCTGCCGCTGTAT	This paper	Exon 1
	Rev	GCAGGTGTTAATCCTCGGCT		
Pitx2c	Fwd	GAGGTGCATACAATCTCCGATA	(Desgrange et al., 2020)	
	Rev	TGCCGCTTCTTCTTGGAC		
Emilin1	Fwd	TGTTCCCGAAGTATCATGTACCG	This paper	Exon 2-3
	Rev	CTGTCTTGTAAGCCACCCGA		
Bcar3	Fwd	GAGAGGATCCTGGCAGATTTCC	This paper	Exon 8-9
	Rev	CCCTTGCTGCCCCATAACA		
Pald1	Fwd	GATGCCTTTGTCAGCGTTCTTCG	Sequence from Origene	
	Rev	GTTGGTTCTGCCTACACCTGAC		
Crip2	Fwd	TGCAACAAGAGAGTGTACTTCG	This paper	Exon 4-7
	Rev	GCACCAGTATTCACTCCTTTGG		
Cap2	Fwd	ACCTGAGCTCTACAGCAGAATG	This paper	Exon 1-2
	Rev	CCTCTGGGAGGTCCGTCTAA		
Dok4	Fwd	CACTGTCCGTGGAATGTCTG	(Bourane et al., 2007)	
	Rev	GGTAAAGCGCGTAGCATCTC		
Nebl	Fwd	CCTGGCCAGTGATTGGGAAT	This paper	Targets only splice variant NM_001362722.1
	Rev	GGAGGGTGGCGTTTCCTTTA		
Nexn	Fwd	GAAGCGAGACGACGCTTAGA	This paper	Exon 8-9
	Rev	TCCTCCTCATTTACCATGTGCC		
Acta2	Fwd	CACCATTGGAAACGAACGCT	This paper	Exon 7-8
	Rev	CCGCTGACTCCATCCCAATG		
Actc1	Fwd	AGCCCTCTTTCATTGGTATGG	(Williams et al., 2020)	
	Rev	CCTCCAGATAGGACATTGTTGG		
Tbx1	Fwd	AAGGCAGGCAGACGAATGTT	This paper	Exon 4-6
	Rev	TAGTGTACTCGGCCAGGTGTA		
Rfx4	Fwd	GGAGGAACCCGACATGGATT	This paper	Exon 1-4
	Rev	TCTCATAGTTTTCCTCCAGCCATT		
Six2	Fwd	CGCAAGTCAGCAACTGGTTC	This paper	
	Rev	GAACTGCCTAGCACCGACTT		
Isl1	Fwd	CAGTCCCAGAGTCATCCGAGT		
	Rev	CCTGTCATCCCCTGGATATTAGTT		
Nodal	Fwd	AGCCAAGAAGAGGATCTGGTATGG	(Desgrange et al., 2020)	
	Rev	GACCTGAGAAGGAATGACGGTGAA		
Lefty2	Fwd	ATCGACTCTAGGCTCGTGTCCATTC	(Desgrange et al., 2020)	
	Rev	CACAATTGCCTTGAGCTCCGTAGTC		
En1	Fwd	TCCTACTCATGGGTTCGGCTA	This paper	
	Rev	GGTGCGTGGACCAGAGGAC		
Hoxb4	Fwd	AGCACGGTAAACCCCAATTACG	This paper	
	Rev	TGTAGTGAAACTCCTTCTCCAACT		

Egr2	Fwd	TGCTAGCCCTTTCCGTTGA	This paper	
	Rev	TCTTTTCCGCTGCTGTCCTCGAT		

High Resolution Episcopic Microscopy

E9.5 embryos or heart from P0 pups were subjected to HREM imaging by first embedding them in methacrylate resin (JB4) containing eosin and acridine orange as contrast agents (Desgrange et al., 2020). Two channel images of the surface of the resin block were acquired using the optical high-resolution episcopic microscope (Indigo Scientific) and a 1X Apo objective repeatedly after removal of 1.75-1.76 μm thick sections : the tissue architecture was imaged with a GFP filter and the staining of enzymatic precipitates with an RFP filter. The datasets comprise 855-1150 images of 0.90-1.45 μm resolution in x and y depending on the stage. Icy (de Chaumont et al., 2012) and Fiji (ImageJ) softwares were used to crop or scale the datasets. 3D reconstructions and analysis were performed in Imaris (Bitplane).

Embryo culture

For identifying a sub-phenotypic dosage of gamma-secretase inhibitor drug treatment, wildtype E8.5 embryos were collected in Hank's solution. DAPT, LY411575 or an equivalent volume of the adjuvant (DMSO) were added to the 75% rat serum, 25% T6 medium, supplemented with 1X Penicillin/Streptomycin. Embryos were cultured with 5% CO2, 5%O2 until E8.5g in rolling bottles in a precision incubator (BTC Engineering, Milton, Cambridge, UK) At the end of the treatment, embryos were rinsed in T6 medium and further culture in embryo culture medium in 5% CO2, 20%O2. At the end of the culture embryos were rinced in PBS and fixed in paraformaldehyde (PFA) 4%. Brightfield images were acquired at the end of the culture with a Zeiss AxioCamICc5 Camera and a Zeiss StereoDiscovery V20 stereomicroscope with a Plan Apo 1.0X objective.

QUANTIFICATION AND STATISTICAL ANALYSIS

Bioinformatics Analyses of bulk RNA Sequences

FASTQ files were mapped to the ENSEMBL Mouse GRCm38/mm10 reference using Hisat2 and counted by featureCounts from the Subread R package. Read count normalizations and group comparisons were performed using DESeq2 statistical method: DESeq2. For the pilot screen,

duplicates were excluded due to a high number of duplicates (89%, see Fig 2B). Flags were computed from counts normalized to the mean coverage. All normalized counts < 20 were considered as background (flag 0) and ≥ 20 as signal (flag = 1). P50 lists used for the statistical analysis gather genes showing flag=1 for at least half of the samples. P50 lists used for the statistical analysis gather genes showing flag=1 for at least half of the samples. Clustering of samples by stage and side was controlled by hierarchical clustering using the Spearman correlation similarity measure and ward linkage algorithm.

Differential gene expression analysis was performed using the Limma R package v3.40.6 (Wu and Smyth, 2012) for the pilot screen and the DESeq2 R package v1.24.0 (Love et al., 2014) for the full screen.

Ingenuity Pathway Analysis

The ingenuity pathway analysis (QIAGEN IPA) performed on the E8.5f left-right RNA bulk sequencing data from the pilot experiment (Fig. 3) was performed by taking the group comparisons obtained through three independent methods (DESeq2, edgeR and LimmaVoom) and running the analysis using the fold change and p-value of differentially expressed genes from the three methods using standard parameters.

Quantification of Immunofluorescence and RNAscope ISH Signal

Immunofluorescent or RNAscope labelled lightsheet imaged samples were analyzed using Imaris (Bitplane).

For quantification of left-right asymmetry in the second heart field, we manually segmented out the second heart field using headfold and the second somite pair as cranial and caudal boundaries, respectively (based on dye labelling from (Domínguez et al., 2012)), and separated the object into left and right. Both Hoechst and target signal were extracted. To account for imaging differences between left and right, the spot detector function was used on Hoechst signaling to make a normalization score between the two sides by measuring at which threshold 50% of spots were covered at each side, respectively. To calculate left-right ratio, number of spots were measured on the left- and right side (using the Hoechst normalization score to decide threshold) and normalized to the volume.

For progenitor characterization, the heart fields were segmented as described above, and the signal was extracted in these channels. For quantifications of number of Isl1

immunofluorescent positive cells and for the number *R26*^{Tomato}-positive cells (in *Isl1*^{MerCreMer} cross), the cells were counted manually. To count the number of Hoechst-positive and to count the number of Hoechst-positive cells within mGFP-positive cells, the Hoechst signal was extracted within the segmented heart field and from with this field, Hoechst signal within mGFP-positive cells were extracted. To count the two numbers of Hoechst-positive cells, three regions were set up in the heart field of two different embryos of 100 μm x 100 μm x 40 μm. Within these areas, the cells were counted manually, and the best parameters for automatic cell counting that counted similar numbers were used.

Bioinformatics Analyses of published single cell RNA sequences

scRNA seq data from Tyser et al., 2021 was downloaded from https://marionilab.cruk.cam.ac.uk/heartAtlas/ and analysed using scran (Lun et al., 2016) and visualized using Seurat v3.1.2 (Stuart et al., 2019). Co-expression analysis to find genes associated with *Notch1/2/3* was performed in several steps. First, the data set was reduced to appropriate clusters (different combinations of Me2-Me7). Secondly, using the findMarkers function (scran), cells were divided into a positive (normalized counts > 0) and negative (normalized counts = 0) group. The non-parametric test of Mann Whitney Wilcoxon was used, with the development stage added as a blocking factor, and both directions of expression were allowed (direction = 'any'). Finally, in order to find genes with normalized counts significantly correlated with the selected target, a correlation analysis was performed. Each candidate gene of the dataset was selected for correlation analysis whether it was expressed together with the target gene in at least 100 cells: the pairwise Spearman correlation coefficient between normalized read counts was computed and its significance tested using an asymptotic t approximation. Corresponding p-values were adjusted for multiple testing using Benjamini-Hochberg correction (Benjamini and Hochberg, 1995).

Quantification of the geometry of the heart tube at E9.5

Using HREM images, the different compartments of the heart tube were segmented using Imaris (Bitplane). Using this, eight landmarks along the tube were extracted and used for calculations of geometry similarly to what has been described in (Desgrange et al., 2020).

Heart shapes were aligned in 3D using an in-house MATLAB code so that the Z-axis corresponds to the notochord axis and the x-axis corresponds to a perpendicular dorso-ventral

axis (Described in Desgrange et al., 2020) The length of the tube and the angle of left- and right ventricle were measured as done in (le Garrec et al., 2017).

Statistical analyses

Statistical tests as well as p-values are described in figure legends. In general, wilcoxon tests were predominantly used to compare two groups, as sample numbers were low and thus it was not possible to test for normal distribution. For E9.5 heart shape analysis, student two tailed t-tests were used. All statistical tests were performed in R except for the chi^2-test, which was performed using excel. All sample numbers (n) indicated in the text refer to biological replicates, i.e. different embryos. One pair of left-right heart field was excluded at stage E8.5e in the full left-right bulk sequencing screen, as it was shown to be an outlier. Samples with severe injuries in the segmented area were also excluded for 3D lightsheet quantification.

Results

Characterization of the second heart field during heart looping

In order to identify novel left-right asymmetric genes that can play a role in heart looping, we selected a transcriptomics approach. We first aimed to estimate the number of cells in the second heart field, and secondly, we aimed to identify which marker would label the most cells in this tissue. Heart looping is a very rapid process, and therefore we did this characterization across multiple stages to see if there are changes in the second heart field. As we initially explored both single cell and bulk RNA sequencing approaches, counting cell number gives an estimate for the number of cells collected per sample (scRNA) and how much RNA we could expect to collect per sample (bulk RNA).

Regarding our single cell RNA sequencing approach, we planned to use MARS-seq (Jaitin et al., 2014), as it allows to enrich for cells of interest using fluorescence-activated single cell sorting (FACS). Thus, we needed a marker compatible with FACS, that would label as many cells as possible in the second heart field.

Isl1 is a classical marker of the second heart field. *Isl1* is expressed in the second heart field as well as in the endoderm close to the heart at E8.5 (Cai et al., 2003). Previous work in the lab (Nji Asong, Audrey Desgrange) had found that *Isl1*$^{tm1(cre)Tmj}$ (Srinivas et al., 2001) crossed with a fluorescent Cre reporter line *Rosa26*^{mTmG} (Muzumdar et al., 2007) labelled very few cells in the heart field (< 5 %) at E8.5. We decided to test an alternative tool for *Isl1* genetic tracing, the inducible *Isl1*^{MerCreMer} line (Sun et al., 2007), as we observed in published work that it might label more cells– a difference likely originating from the design of the genetic construct.

We received from our collaborator F. Rochais (Marseille) embryos from crosses with the reporter line *Rosa26*^{tdTomato} (Madisen et al., 2010) along with tamoxifen injection at E6.5 (Fig 1A). Some cells are labelled within the heart tube, while only few labelled cells were detected in the second heart field (Fig 1a2). The labelled cells are located in the SHF dorsal to the heart tube and not in the posterior region (Fig 1a3). Although the ratio of labelled cells was higher than for the *Isl1*^{Cre} line (data not shown), very few cells in the heart field were labelled compared to wholemount immunofluorescent labelling of Isl1 (Fig 1B), where Isl1 is strongly localized in the heart field and endoderm dorsal to the heart (Fig 1b2). At more posterior

levels, Isl1 is still detected in the SHF, but less so (Fig 1b3). The low ratio of labelled cells in the *Isl1*^{Cre} and the *Isl1*^{MerCreMer} lines compared to Isl1 immunofluorescent labelling likely comes from the delay between Isl1 promoter expression and recombination and reporter expression in the Cre-lox system, which usually takes 12-36 hours. Thus, *Cre* expression under the control of the *Isl1* promoter is too late to mark all SHF cells at E8.5.

To obtain a higher ratio of labelled cells, we combined two transgenic lines. We used the *Mef2c-AHF-Cre* line (Verzi et al., 2005) which labels the anterior second heart field, and crossed it with *Hoxb1*$^{Cre/+}$ (Bertrand et al., 2011) that is expressed at gastrulation and labels a wide population of mesodermal cells, including the posterior second heart field. We generated *Mef2c-AHF-Cre*; *Hoxb1*$^{Cre/+}$ studs and crossed them with *Rosa26*^{mTmG} to generate *Mef2c-AHF-Cre*; *Hoxb1*$^{Cre/+}$; *Rosa26*$^{mTmG/+}$ embryos that were then imaged (Fig 1C). The *Rosa26*^{mTmG} is a double reporter line, where Cre- cells will be labelled with mTomato, while Cre+ cells will be labelled with mGFP. In these embryos, the posterior heart field was well covered (Fig 1c3), however, labelling of the anterior region was patchy (Fig 1c2). Quantification shows that overall ~76% of second heart field cells are labelled (Fig 1G). The patchiness may depend on the Mef2cAHF transgene driving restricted *Cre* expression (Verzi et al., 2005) and thus the double *Mef2c-AHF-Cre*; *Hoxb1*$^{Cre/+}$ is unsuitable for marking the full heart field at E8.5. From this it is clear that early expression of *Cre* is necessary for sufficient fluorescent labelling of the second heart field at E8.5.

Mesp1 is expressed transiently at E6.0 in the nascent mesoderm and is one of the earliest markers of cardiogenesis (Saga et al., 2000). *Mesp1* marks both early and late migrating heart progenitors of the first and second lineages (Lescroart et al., 2014). We generated and imaged *Mesp1*$^{Cre+/-}$; *Rosa26*$^{mTmG/+}$ embryos at E8.5 (Fig 1D). Almost all cells (96%) within the second heart field are labelled, both in the anterior (Fig 1d2) and posterior regions (Fig 1d3). Furthermore, cells within the second heart field were mTomato-negative in *Mesp1*$^{Cre+/-}$; *Rosa26*$^{mTmG/+}$ embryos, which is not the case for cells of the both the anterior and posterior regions of the second heart field of *Mef2c-AHF-Cre*; *Hoxb1*$^{Cre/+}$; *Rosa26*$^{mTmG/+}$ embryos, where cells express both mGFP and mTomato. This indicated that the recombination occurred earlier or more efficiently in the *Mesp1*^{Cre} line.

To quantify volume, cell number and ratio of labelled cells, we manually segmented out the second heart field. The headfolds and second somite pair were used as cranial and caudal boundaries respectively, as dye-injection tracing experiments has shown that cells within this

region contribute to the heart (Domínguez et al., 2012). We found that the volume (Fig 1E) and cell numbers (Fig 1F) were stable between stage E8.5d and E8.5i with around 3000-4000 Hoechst-positive cells. This shows that although the embryo is growing in overall size between these stages, the volume and cell number of the second heart field is rather constant.

The stable size of the second heart field means that E8.5 stages are equally suitable for RNA sequencing. Furthermore, *Mesp1*^{Cre} is the most appropriate marker for cell sorting prior to sequencing, as it labels almost all cells within the second heart field (Fig 1G).

Figure 1. Size of the second heart field of progenitors

(A) Whole-mount imaging of an *Isl1*$^{MerCreMer/+}$*; R26*$^{tdTomato/+}$ embryo at E8.5f, injected with tamoxifen at E6.5. a1: front view, a2-a3: transverse sections at levels indicated in a1. **(B)** Isl1 whole-mount immunofluorescent staining in a wild-type embryo at E8.5f. b1: front view, b2-b3: transverse sections at levels indicated in b1. **(C)** Whole-mount imaging of a *Hoxb1*$^{Cre/+}$*; Mef2c-AHFCre; R26*$^{mTmG/+}$ embryo at E8.5f. c1: front view, c2-c3: transverse sections at levels indicated in c1 **(D)** Whole-mount imaging of a *Mesp1*$^{Cre/+}$*; R26*$^{mTmG/+}$ embryo at E8.5f. d1: front view, d2-d3: transverse sections at levels indicated in d1. **(E-F)** Volume (E) and cell count (F) of the segmented second heart field at different stages of heart looping (n = 1 for E8.5d, 3 for E8.5e, 3 for E8.5f, 3 for E8.5g; 4 for E8.5h; 2 for E8.5i). **(G)** Ratio of cells in the second heart field labelled by different modalities. (n = 4 for *Isl1*$^{MerCreMer/+}$*; R26*$^{tdTomato/+}$, 3 for Isl1 immunofluorescence, 5 for *Hoxb1*$^{Cre/+}$*; Mef2c-AHFCre; R26*$^{mTmG/+}$, 4 for *Mesp1*$^{Cre/+}$*; R26*$^{mTmG/+}$). Means and standard deviations are shown; HT, heart tube (pink dotted outline); L, left; R, right. SHF, second heart field (cyan dotted outline). The midline is marked by a yellow dotted line.

Figure 1

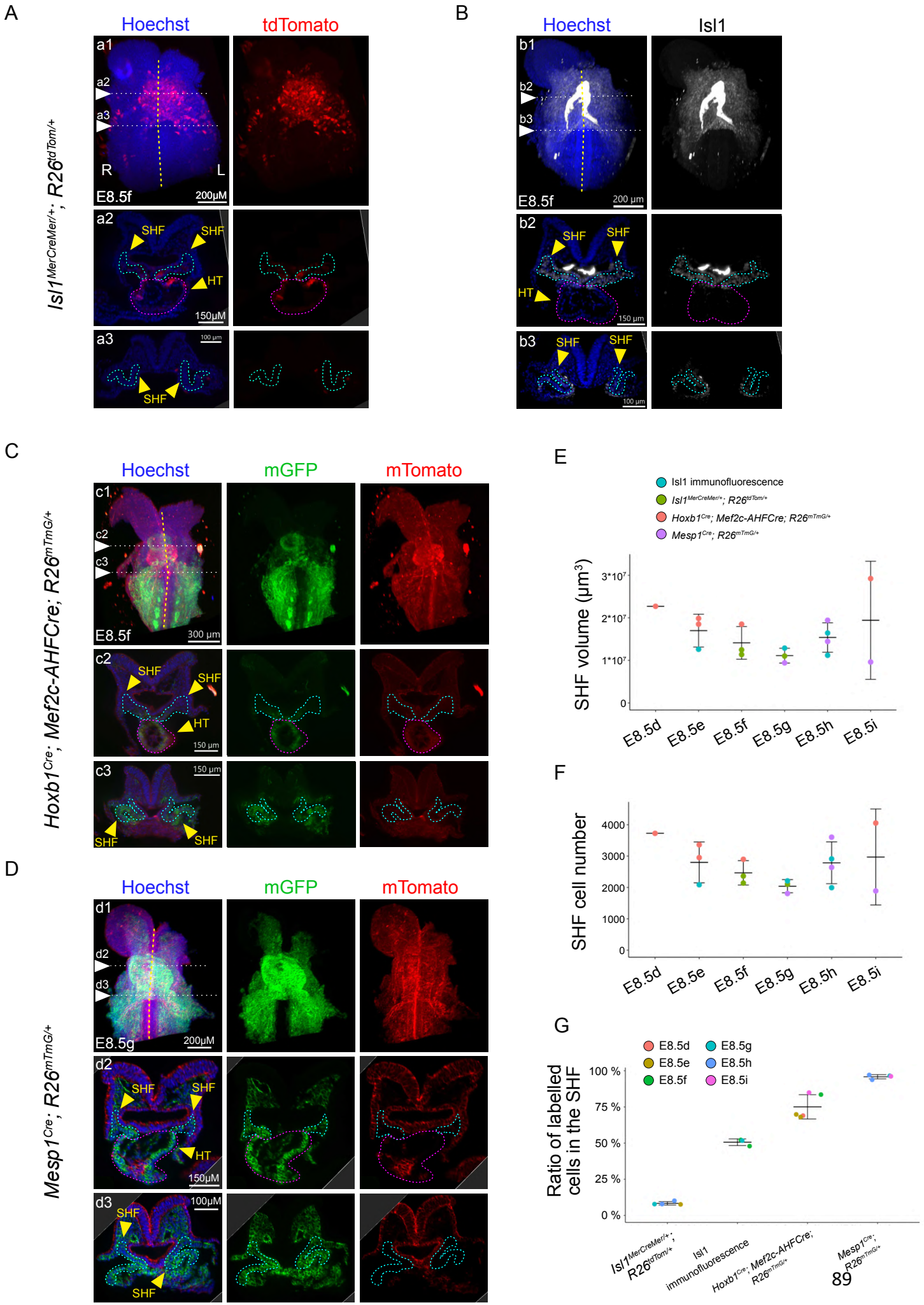
A
Hoechst
tdTomato
Isl1MerCreMer/+; R26tdTom/+
a1
a2
a3
R
L
E8.5f
200μM
SHF
HT
150μM
100 μm
B
Hoechst
Isl1
b1
b2
b3
E8.5f
200 μm
150 μm
100 μm
C
Hoechst
mGFP
mTomato
Hoxb1Cre; Mef2c-AHFCre; R26mTmG/+
c1
c2
c3
E8.5f
300 μm
150 μm
D
Hoechst
mGFP
mTomato
Mesp1Cre; R26mTmG/+
d1
d2
d3
E8.5g
200μM
150μM
100μM
E
Isl1 immunofluorescence
Isl1MerCreMer/+; R26tdTom/+
Hoxb1Cre; Mef2c-AHFCre; R26mTmG/+
Mesp1Cre; R26mTmG/+
SHF volume (μm3)
3*10^7
2*10^7
1*10^7
0
E8.5d
E8.5e
E8.5f
E8.5g
E8.5h
E8.5i
F
SHF cell number
4000
3000
2000
1000
0
G
E8.5d
E8.5e
E8.5f
E8.5g
E8.5h
E8.5i
Ratio of labelled cells in the SHF
100 %
75 %
50 %
25 %
0 %
Isl1MerCreMer/+; R26tdTom/+
Isl1 immunofluorescence
Hoxb1Cre; Mef2c-AHFCre; R26mTmG/+
Mesp1Cre; R26mTmG/+
89

Development of a protocol of single cell RNA sequencing of heart progenitors

To profile gene expression in the heart progenitors and explore heterogeneity within these populations, we tested protocols of cell dissociation and sorting as a pre-requisite to single cell RNA sequencing. An outline of the experiment is shown in Fig S1A. From our characterization of the second heart field, we had identified *Mesp1*^{Cre} as a suitable marker. We initially decided not to micro-dissect out the left- and right heart field, as we aimed to first assess how many cells could be collected from the heart field of a single embryo.

After testing several conditions for cell dissociation and filtration, we found that enzymatic digestion by Liberase (Roche) in combination with dispase followed by filtration using FlowMi cell strainer (Bel-Art) worked well in dissociating cells without killing them. Liberase is a collection of different proteases (primarily collagenases) used in previous publications (Sebé-Pedrós et al., 2018). Dispase, which has a high affinity towards Fn1, was added because in a previous RNA bulk sequencing of the lab (Desgrange et al., 2020), we found *Fn1* to be the most expressed extracellular matrix gene in the cardiogenic region of wildtype embryos (Fig S1B).

After cell sorting, we decided to control both cell survival as well as the number of collected cells per embryo. Cell survival was measured by adding the dead cell marker DRAQ7 (Biostatus). Cell survival was correlated with the duration of embryo dissection. Almost all cells (98.5%) were alive when FACS was performed on tissues within 1h15 after euthanizing the mother (Fig S1C). At 1h40 this dropped to 87% and dropped further to 76% after 2h10, showing that working quickly is important for collecting live cells for RNA sequencing. The number of cells collected per embryo (reported in Fig S1D) ranges from 2651-4251 depending on the experiment, which is accordance with the number of cells we quantified in the second heart field (Fig 1F).

From the profiling of *Nodal* pathway gene expression, we had identified the E8.5d stage as particularly interesting. At E8.5d, *Lefty2* (a direct target of Nodal) expression peaks, and thus we expect other genes directly regulated by *Nodal* to be asymmetrically expressed at this stage. For this reason, our aim was to perform scRNAseq on E8.5d embryos, and we therefore assessed how many cells could be collected from a single embryo. From an experiment micro-dissecting the cardiogenic region in a single embryo, we collected 4251 mGFP^{+} cells (Fig S1E), which is more than sufficient for cell collection prior to scRNAseq. Thus, we found that our protocol is suitable for this purpose.

The aim was to perform scRNAseq using the MARSeq approach (Jaitin et al., 2014) on heart fields of embryos at stage E8.5d, however as described in Objectives, we decided to concentrate our efforts on the bulk RNA sequencing approach.

Development of a protocol for bulk sequencing of the left and right heart field

To profile asymmetric gene expression in the heart field at different stages of heart looping, we performed micro-dissections to separate left- and right heart field tissue (Fig S1F). As the kinetics of heart looping is fast, we decided against pooling embryos, as this would lower resolution. We instead reasoned that it would be stronger to compare left- and right heart field tissue of the same embryo to eliminate stage biases.

In order to confirm our micro-dissections, we performed RT-qPCR experiments using known markers of the heart field, of the left lateral plate mesoderm and of dissected out surrounding tissue (anterior head: *En1*, posterior tail: *Hoxb4* and dorsal neural tube: *Egr2*). Expression of these markers showed that our micro-dissections were of sufficient quality to isolate heart progenitor tissue and to separate left and right (summarized in Fig S1G). At later stages (from E8.5f) we did not detect any marker of outside tissue, while at early stages we detected expression of the head- and neural tube markers. This is due to the fact that at early stages, the head- and neural tube are close to the heart progenitor tissue and can therefore not be completely removed by microdissection.

From these RT-qPCR validations, we also profiled the kinetics of the Nodal pathway. These results are published in (Desgrange et al., 2020) – See *Annex 1* Figure 2A and Figure S4. We find that *Nodal* peaks at stage E8.5c, while its direct target *Lefty2* peaks one stage later at E8.5d. As a consequence of *Lefty2* expression, the expression of *Nodal* is downregulated from E8.5d and is not detectable from E8.5f. *Pitx2c* becomes expressed at E8.5c, but compared to *Nodal* and *Lefty2*, its expression gets stronger and persists across all E8.5 stages.

Having shown that isolated left- and right sides of heart fields of single embryos are sufficient for RNA detection and gene profiling, we then aimed to perform bulk RNA sequencing of these tissues. Our measures estimate that the number of cells in a half heart field is around 1500-2000 cells (Fig 1F), which is expected to provide a low amount of RNA. Therefore, we started by performing a pilot RNA sequencing experiment at E8.5e and E8.5f (dissections outlined in Fig 2A) using the standard RNA library building kit NuGEN Universal Plus and a sequencing depth of on average 50 millions reads per sample. To avoid gender effects, we selected only

male samples. After sequencing ~35 million polyA+ transcript reads were uniquely assigned per sample. However, due to the small amount of input RNA available, the number of duplicates was 89.2% (+/- 2.5%) per sample (Fig 2B). After removal of duplicated reads along with additional quality control, there was on average ~1,9 million reads per sample. Even with this relatively low number of reads, we were able to detect 129 significantly differentially expressed genes (DEGs) at E8.5e (Fig 2C) and 44 at E8.5f (Fig 2D), among which control genes involved in Nodal signaling, such as *Pitx2* and *Lefty2* (Saijoh et al., 2003), both in the left heart field. Among the DEGs there were also new genes that had previously not been associated with left-right asymmetry. One of these will be further analysed from Figure 3 and onwards.

Albeit able to detects DEGs at both stages, the low number of useable reads reflects a low sensitivity. To obtain higher data quality, we decided to test alternative RNA library building kits suited for low input material: the NuGEN Trio RNA sequencing kit and the NEBnext Single Cell/Low Input RNA Library Prep Kit. As the total amount of RNA collected from one side of micro-dissected heart fields was in the range of 5-50ng, we also tested the sensitivity of kits to a range of input materials from 500pg to 15ng (Fig 2E). To obtain homogeneous mix of RNA for the kit test, we pooled the left- and right heart fields of four micro-dissected female embryos at stage E8.5d. We performed each measurement in duplicates, and added ERCC spike-in RNA (Thermo Fischer), which contains a known amount of RNA and is suitable to eliminate biases in sample preparation. Additionally, we adjusted the sequencing depth to 40 million reads per sample to avoid generating too many duplicates. Both low-input RNA sequencing kits performed better than the NuGEN Universal plus kit: the rate of duplicates were 19.8 % (+/- 0.52%) and 24.3% (+/- 1.93%) (Fig 2F) and the proportion of uniquely[5] assigned reads was above 33.7% (+/- 0.87%) and 40.2% (2.98%) for the NuGEN Trio RNA sequencing kit and the NEBnext Single Cell/Low Input RNA Library Prep Kit , respectively (Fig 2G) (compared to 73.9% rate of duplicates and 5.9% uniquely assigned reads with the NuGEN Universal plus kit). Between the two kits, NuGEN Trio RNA sequencing kit performed slightly better on rate of duplicates, and it was also more reproducible at low amount of input RNA (not shown). Thus, the Nugen Trio RNA sequencing kit is suitable for performing RNA sequencing of heart field tissue and expected to generate up to 6.5 times more useable reads

[5] Uniquely assigned read refers to how many of the total reads can be assigned to the genome and are at the same time not duplicated (i.e. two identical assigned reads would count for one uniquely assigned read).

than the NuGEN Universal plus kit. We therefore selected this kit for our full screen of left-right asymmetrically expressed genes across heart looping stages.

Bulk sequencing of paired left- and right heart fields at different stages of heart looping

We collected left- and right heart field tissues for seven different stages of heart looping. The earliest stage selected is the late headfold stage, because this is prior to *Nodal* expression in the heart field and we therefore expect to find no difference between left- and right (Desgrange et al., 2020). From E8.5c-g there is molecular- and from E8.5f morphological asymmetry occurring, thus all these stages were selected for profiling. E8.5j marks the end of heart looping and was thus selected as a final point.

RNA sequencing was performed using the NuGEN Trio RNA sequencing kit (Fig 2H-N). At the late headfold (LHF) stage, prior to the expression of *Nodal* in the lateral plate mesoderm, no significant left-right asymmetry in gene expression can be detected (Fig 2H). We found *Nodal* asymmetrically expressed in the left heart field at E8.5c and d, in keeping with the short time window of *Nodal* expression in the lateral plate mesoderm that we have previously identified by RT-qPCR (Desgrange et al., 2020) (Fig 2O). The Nodal targets *Pitx2* and *Lefty2* were also found asymmetrically expressed on the left at most stages of heart looping. New asymmetric genes were found either in the right or left heart field. Interestingly, we found that at the first stage of asymmetry, stage E8.5c, 30 out of 36 DEGs are enriched on the left side. Additionally, E8.5d was the stage with the most DEGs, with 132 of 211 DEGs being higher expressed on the right.

To conclude, we have established conditions to screen for new asymmetrically expressed genes during heart looping, and our screen identifies new asymmetrically expressed genes. The overall analysis of asymmetric genes is a long-term project that is ongoing in the laboratory. Within the time-window of my PhD, I decided to focus on one new asymmetric gene, discovered in the pilot screen (NuGEN Universal Plus kit).

Figure 2

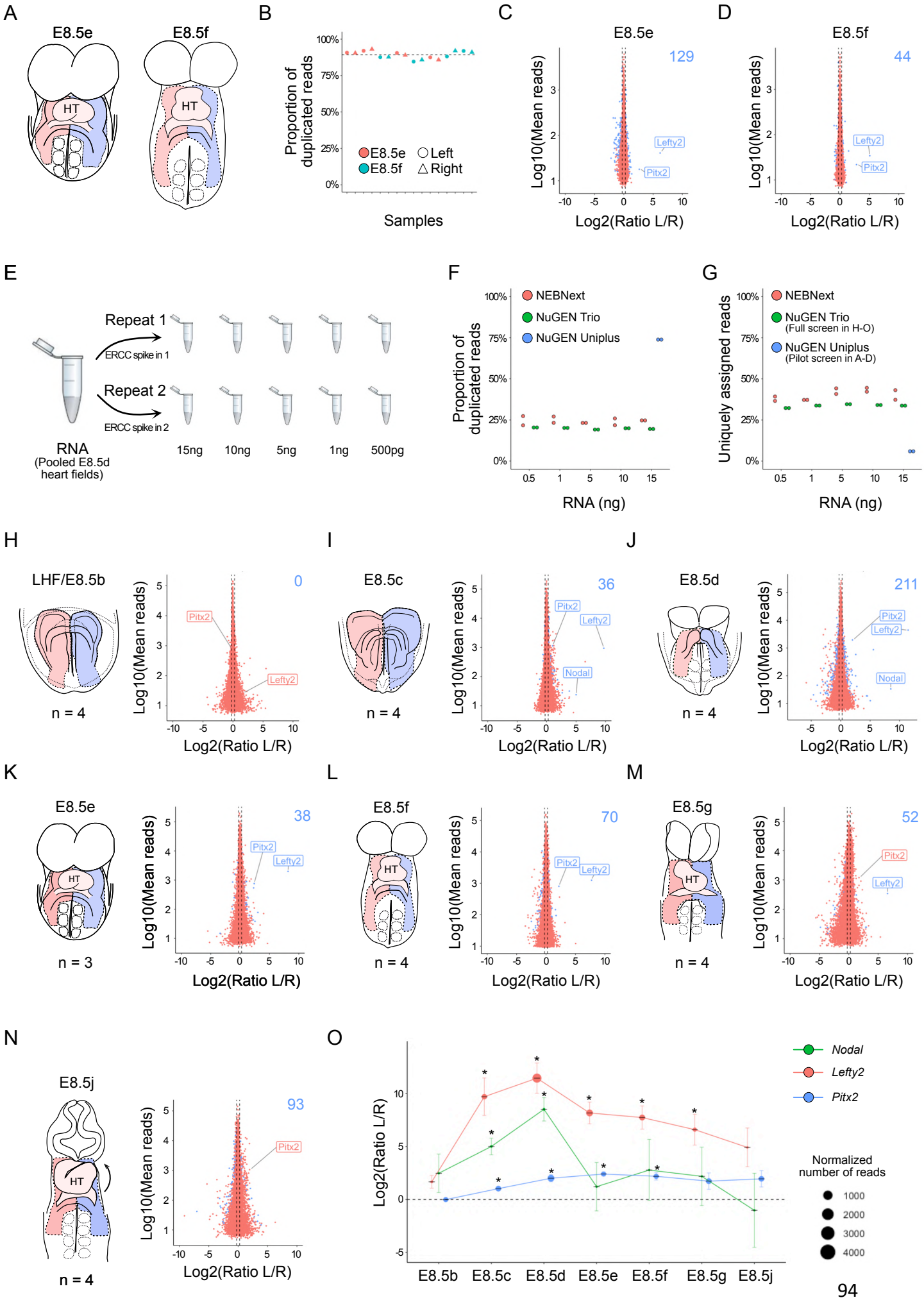
A
E8.5e
E8.5f
HT
B
Proportion of duplicated reads
100%
75%
50%
25%
0%
E8.5e
E8.5f
Left
Right
Samples
C
E8.5e
129
Log10(Mean reads)
Lefty2
Pitx2
Log2(Ratio L/R)
D
E8.5f
44
E
Repeat 1
ERCC spike in 1
Repeat 2
ERCC spike in 2
RNA
(Pooled E8.5d heart fields)
15ng
10ng
5ng
1ng
500pg
F
NEBNext
NuGEN Trio
NuGEN Uniplus
RNA (ng)
G
Uniquely assigned reads
NuGEN Trio
(Full screen in H-O)
NuGEN Uniplus
(Pilot screen in A-D)
H
LHF/E8.5b
n = 4
0
I
E8.5c
36
Nodal
J
E8.5d
211
K
E8.5e
n = 3
38
L
E8.5f
70
M
E8.5g
52
N
E8.5j
93
O
Log2(Ratio L/R)
Nodal
Lefty2
Pitx2
Normalized number of reads
1000
2000
3000
4000
E8.5b
E8.5c
E8.5d
E8.5e
E8.5f
E8.5g
E8.5j

Supplementary figure 1 (related to figure 2)

A

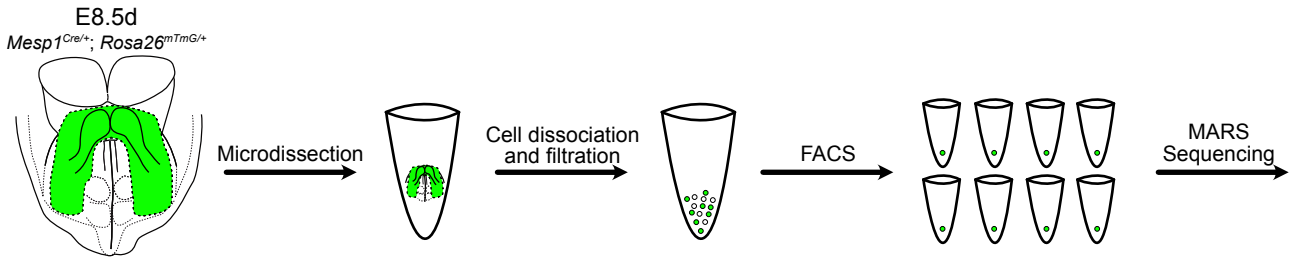

B

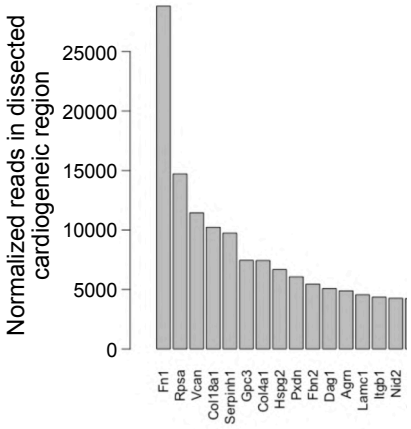

C

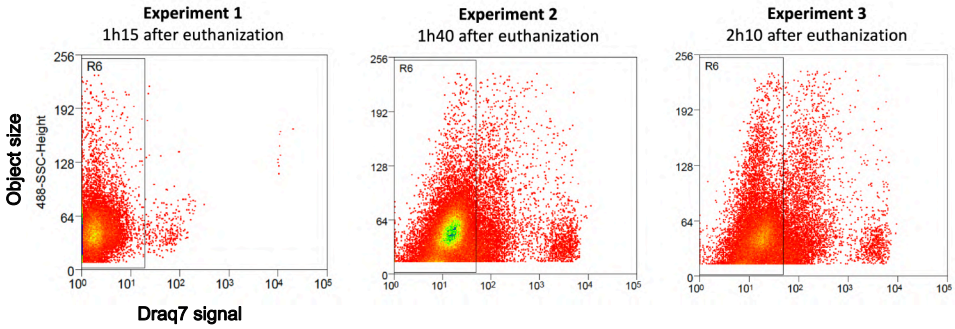

D

Experiment	Embryo stages	Number of cells per embryo	Survival rate	Time FACS was performed after euthanization of mother
1	E8.5f, f, g	2651	98.5%	1h15
2	E8.5c, c, d	2649	87%	1h40
3	E8.5d	4251	76%	2h10

E

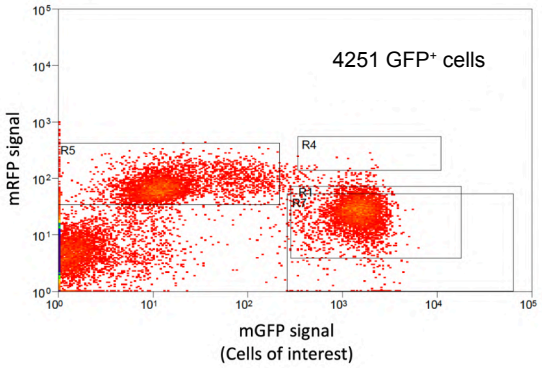

F

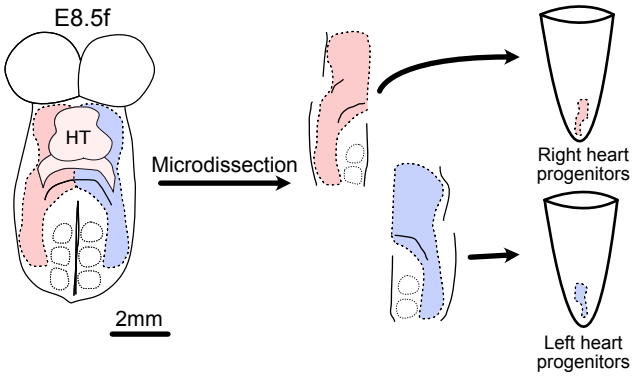

G

					Left markers									
		SHF genes			Nodal		Lefty2		Pitx2		Outside markers		
Stage	Numbers	Six2	Isl1	Tbx1	L	R	L	R	L	R	En1	Hoxb4	Egr2
E8.5c	3												
E8.5d	6												
E8.5e	3												
E8.5f	3												
E8.5g	3												
E8.5h	3												
E8.5i	3												
E8.5j	1												
Sum	25												

Upregulated
Lowly expressed
Very lowly expressed
Not detected

Figure 2. RNA sequencing of left-right differential expression in the heart field

(A) Outline of the left (light blue) and right (light red) heart field micro-dissected in mouse embryos for bulk RNA-sequencing at the indicated stages in a pilot screen. **(B-C)** MA plots representing relative gene expression between paired left and right heart fields at E8.5e (B) and E8.5f (C). Non-significant differential expression is represented in red, differential expression in blue (Benjamini-Hochberg corrected p-value < 0.05, Voom, n = 4). Coloured number represent the number of DEGs at each stage. **(D)** Rate of duplication per sample in the pilot screen (mean = 89,2%). **(E)** Structure of experiment for testing novel RNA library kits suited for low amount of input RNA. **(F)** Duplication rates at different amount of input RNA in the kit test. **(G)** Assigned reads at different amount of input RNA in the kit test. **(H-N)** Full screen using the NEBnext Single Cell/low Input RNA kit. Dissection schema (left panel) and MA plot (right panel) representing relative gene expression between paired left (light blue) and right (light red) heart fields at stages LHF/E8.5b (H), E8.5c (I), E8.5d (J), E8.5e (K), E8.5f (L), E8.5g (M) and E8.5j (N). Non-significant differential expression is represented in red, differential expression in blue (Benjamini-Hochberg corrected p-value < 0.05, DESeq2, n as indicated). Blue numbers represent the number of differentially expressed genes at each stage. **(O)** Expression of genes associated with Nodal signalling in the full screen. Sandard deviations are shown. Size of circle represents number of reads. *Benjamini-Hochberg corrected p-value < 0.05 indicate significant asymmetry (DESeq2). HT, heart tube; LHF, late head fold.

Figure S1 related to Fig. 2. Development of protocols for single cell RNA sequencing of heart progenitor patterning

(A) Experimental overview of planned single cellRNA sequencing by isolation of heart progenitors from of *Mesp1*$^{Cre/+}$; *Rosa26*$^{mTmG/+}$ embryos at stage E8.5d. The second heart field is highlighted in green. **(B)** Expression level of the top 15 most highly expressed extracellular matrix genes in the cardiogenic region of E8.5e-f wildtype embryos. **(C)** Dotplots of 3 pilot FACS experiments showing levels of the cell death marker DRAQ7 (in x) and the size of objects (in y) at different time points after euthanization of the mother. Embryos were pooled in experiments 1-2 and isolated in experiment 3. Stages are indicated in (E). Single and alive cells were selected for further. **(D)** Summary table of associated quantifications. **(E)** Dotplot of experiment 3 of the micro-dissected heart field from a single E8.5d *Mesp1*$^{Cre/+}$; *Rosa26*$^{mTmG/+}$ embryo. 4251 cells of interest were counted as mGFP^{+} mTomato^{-} (R7?) and alive (based on Draq7 levels in D). Rare cells are double positive for mGFP and mTomato (R4). **(F)** Control of the micro-dissection of the left and right heart fields. Schema of the isolation of the left (light blue) and right (light red) heart fields in mouse embryos. **(G)** Summary of RT-qPCR validation of the indicated markers at sequential stages of heart looping. Colors indicate level of expression. HT, heart tube

Marks start of the publication

The following figures are designed for a publication in preparation. The provisional title of the publication is

Identification of Notch3 as a novel asymmetric factor in heart morphogenesis

Author list

Tobias Holm Bønnelykke[1,2], Emeline Perthame[3], Marie-Amandine Chabry[1], Mélanie Parisot[4], Audrey Desgrange[1]# and Sigolène Meilhac[1]#*

co-senior authors

* corresponding author

Affiliations

[1] *Université Paris Cité, Imagine - Institut Pasteur, Unit of Heart Morphogenesis, INSERM UMR1163, F-75015, Paris, France*

[2] *Sorbonne Université, Collège doctoral, F-75005 Paris, France*

[3] *Institut Pasteur, Université Paris Cité, Bioinformatics and Biostatistics Hub, F-75015 Paris, France*

[4] *Genomics Core Facility, Institut Imagine-Structure Fédérative de Recherche Necker, INSERM U1163 et INSERM US24/CNRS UAR3633, Université Paris Cité, Paris, France*

Contributions of authors (beyond T. Bønnelykke)

E. Perthame performed bioinformatic analyses of RNA sequencing and helped with visualization, M. A. Chabry collected and analyzed data for the *Nodal; Notch3* genetic interaction experiment as well as helped to perform mouse dissections, *in situ* hybridizations and RNAscope experiments, M. Parisot performed the RNA library building and -sequencing. A. Desgrange contributed to E9.5 heart shape analysis, carried out P0 phenotyping, embryo culture and *Nodal* mutant collection. A. Desgrange and S. Meilhac supervised the work, were

involved in experimental design and publication writing. See also *Acknowledgements* for other contributions.

Notes before reading

Figures 3, 4 and 6 (along with their supplementary figures) are publication ready. Figure 5, 7 and 9 (related to functional data) are underway and scheduled to be completed before the end of 2022.

Bulk sequencing of paired left- and right heart fields identifies *Notch3* as a novel left-sided marker

In order to identify novel genes involved in the left-right patterning of the embryonic heart, we performed bulk RNA sequencing on micro-dissected left- and right heart field tissue at E8.5f (Fig 3A, Fig S2A), as this is the earliest stage when left-right asymmetric morphological difference can be detected in the heart tube (le Garrec et al., 2017). Because both heart looping and the kinetics of the *Nodal* pathway are very dynamic, we decided to collect single left- and right heart fields, to increase resolution compared to embryo pooling prone to stage biases. We performed paired analysis of left/right differential expression.

We first set a threshold of expression compared to background levels, using standard statistical criteria (see *Material and Methods*), as well as expression of negative control genes, not expressed in the micro-dissected tissues (*Dmp1*: osteocyte marker, *Oc90*: inner ear marker, *Neurod1*: neuronal marker), and a positive control of a gene lowly expressed gene in the heart field, *Mmp9* (Desgrange et al., 2020) (Fig S2B). We controlled microdissections with molecular markers. Anterior (*En2*, *Wnt8b*) and posterior (*Hoxa5*, *Hoxb6*) markers were not detected. However, some neural tube markers (*Rfx4*, *Tfap2b*) were still present (Fig S2C), indicating that back tissues had not been completely removed during micro-dissections. Similarly, markers of mature cardiomyocytes (*Myh7b, Myoz1, Tnnt1*) are not detected or lowly expressed, indicating that the heart had been properly removed during micro-dissections. Second heart field markers (*Isl1, Six2, Fgf8*) are highly expressed, showing that the micro-dissected tissue contains second heart field cells. Markers of the juxta-cardiac field (*Tbx5, Mab21l2*) are also detected, indicated that the isolated tissue also contains cells of the juxta-cardiac field (Tyser et al., 2021).

At E8.5f, *Nodal* is no longer expressed, as shown previously (Desgrange et al., 2020). However, Nodal direct targets *Lefty2* and *Pitx2* were found highly enriched in the left side (Fig S2D), validating tissue preparation. Additionally, the left-sided gene *Six2* (Zhou et al., 2017) was also found enriched as expected, whereas *Snai1* (Ocaña et al., 2017) was found symmetric. Overall, our analysis of control genes validates micro-dissection to extract differential gene expression in the left and right heart field of the same embryo and screen for novel asymmetric genes.

44 genes were highly significantly asymmetric, with a Benjamini-Hochberg adjusted p-value < 0.05, while 442 genes were significantly asymmetric with a p-value < 0.05 but a Benjamini-Hochberg adjusted p-value > 0.05. We performed a pathway analysis (Ingenuity) to extract most significant differential expression. This highlighted the Notch pathway as activated on the left side (Fig 3C). We looked in more detail at the individual expression of Notch pathway genes. Five genes were found to be asymmetrically expressed (Fig 3D). *Dtx4* was excluded on the basis of previously published single cell RNA sequencing data (Tyser et al., 2021), as it is not expressed in heart progenitors but in the surrounding ectoderm (Fig S2E). We focused on *Notch3* as it encodes a receptor that upon ligand activation becomes a transcription factor, and it is thus central to signaling. Furthermore, it is the most highly expressed gene of the asymmetric pathway. To validate *Notch3* as an asymmetric gene, we investigated its expression pattern. Using whole-mount RNAscope *in situ* hybridization imaged in 3D, we quantified *Notch3* asymmetry in the heart field (Fig S2F). *Notch3* was confirmed to be asymmetrically expressed on the left (Fig 3E). From transversal sections (Fig 3e2, Fig3e3) *Notch3* expression was detected in the lateral plate mesoderm, which contains heart precursors, and absent in cardiomyocytes of the heart tube. *Notch3* expression extends posteriorly throughout the left lateral plate mesoderm. We also found expression in the node, the left-right organizer (Fig 3F). *Notch3* was observed in left-sided crown cells of the node (Fig 3f1), the site where asymmetric Nodal signaling is initiated (Collignon et al., 1996).

Our previous analysis of Nodal signaling (Desgrange et al., 2020), has highlighted a short time-window of expression and activity in heart precursors. We thus decided to investigate the dynamics of *Notch3*. We quantified *Notch3* asymmetry in heart progenitors at sequential stages (Fig 3G, Fig S2F), and found that *Notch3* asymmetry peaks at stage E8.5d, when it is ~ 4.5-fold more expressed on the left side. Expression becomes lower at E8.5f, when asymmetric heart morphogenesis begins (Le Garrec et al., 2017). As the pattern and transient

kinetics of *Notch3* asymmetric expression are similar to *Nodal*, we analyzed the overlap between the two genes. *Notch3* and *Nodal w*ere found co-expressed in the left lateral plate mesoderm (Fig 3H, Movie S1). Using published RNA sequencing in single heart progenitors at the same stages (Tyser et al., 2021), we found that *Notch3* was expressed in 75% (234/309) of *Nodal*-positive cells, thus showing that *Nodal* and *Notch3* are largely co-expressed in left heart progenitors (Fig S2G). Some *Nodal* only positive cells (ie *Notch3*-negative) were also observed by ISH (Fig S2H) and localized more laterally, compared to *Nodal* and *Notch3* co-expression which was more medial. Thus *Nodal* is expressed throughout the left splanchnic mesoderm, whereas *Notch3* is upregulated more medially (Fig S2H). This indicates a lateral regionalization of the lateral plate mesoderm.

Altogether, our bulk RNA sequencing strategy has identified a novel asymmetric gene, not a component of the Nodal pathway: *Notch3*. We have validated its dynamic asymmetric expression in the left lateral plate mesoderm containing heart precursors and found that it is co-expressed with *Nodal*. We next wondered about the relationship between *Nodal* and *Notch3* expression.

Figure 3. Left-sided enrichment of *Notch3* expression at E8.5.
(A) Outline of the left (light blue) and right (light red) heart field micro-dissected in the mouse embryo for RNA-sequencing. **(B)** MA plot representing relative gene expression between paired left and right heart field at E8.5f. Non-significant differential expression is represented in red, differential expression in green (p-value < 0.05), and blue (Benjamini-Hochberg (BH) corrected p-value < 0.05, Voom, n=4) **(C)** Ingenuity Pathway Analysis ordered according to significance and colour-coded for the activation state (z-score: blue, active pathway on the left; red, active pathway on the right). **(D)** Normalised read counts of genes involved in the Notch pathway in the left (blue) and right (red) heart field. The dotted line indicates the threshold of background expression. Whisker plots show the median, 25^{th}- and 75^{th} quartiles (boxes), and the extreme data points (whiskers). *p-value < 0.05, ** Benjamini-Hochberg corrected p-value < 0.05 (Voom, n=4). **(E-F)** Expression of *Notch3* (white) detected by whole mount RNAscope ISH at E8.5d, shown in frontal views (E1, cranial side of the embryo, F1, caudal side of the embryo) and transverse sections (E2-E3, F2, at the levels indicated in E1-F1) (n=6). **(G)** Quantification of normalized Notch3 asymmetric (left over right) expression in the heart field at sequential stages. The means are shown on a red dotted line and standard deviations are in blue (n=3 at E8.5c, 6 at E8.5d, 6 at E8.5e, 3 at E8.5f). **(H)** *Notch3* (white) and *Nodal* (magenta) co-expression detected by double whole mount RNAscope ISH at E8.5d, and shown in a frontal view (H1) and traverse section (H2) (n=5). The midline is indicated by a yellow dotted line. HT, heart tube; L, left; LPM, lateral plate mesoderm (green dotted outline); Myo, myocardium (red dotted outline); No, node ; R, right. See also Video S1 of *Notch3* (white) and *Nodal* (red) double RNAscope labelled embryo at stage E8.5d. Note video is inverted

Figure 3

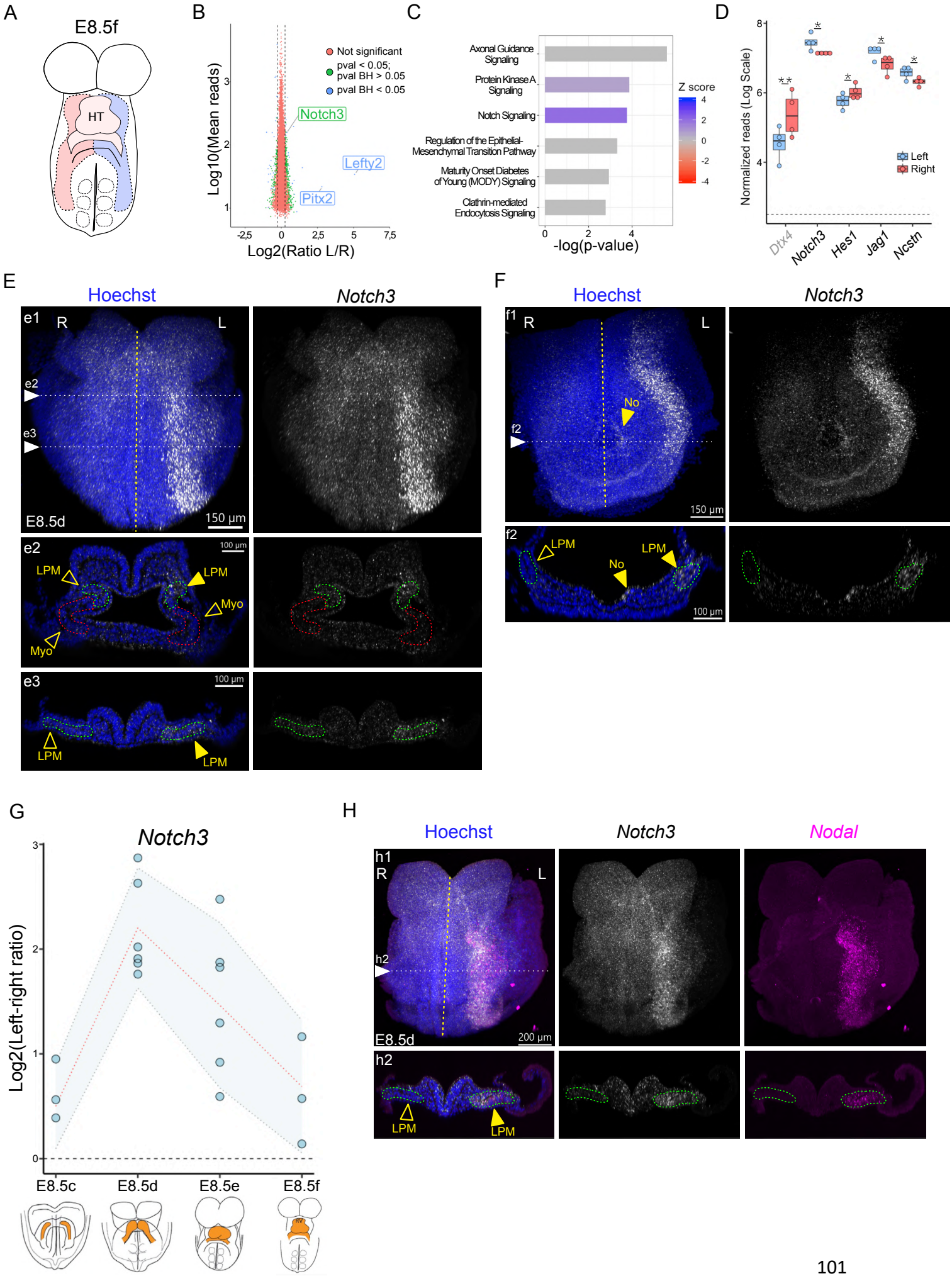
A
E8.5f
HT
B
Log10(Mean reads)
Log2(Ratio L/R)
Not significant
pval < 0.05;
pval BH > 0.05
pval BH < 0.05
Notch3
Lefty2
Pitx2
C
Axonal Guidance Signaling
Protein Kinase A Signaling
Notch Signaling
Regulation of the Epithelial-Mesenchymal Transition Pathway
Maturity Onset Diabetes of Young (MODY) Signaling
Clathrin-mediated Endocytosis Signaling
Z score
-log(p-value)
D
Normalized reads (Log Scale)
Left
Right
Dtx4
Notch3
Hes1
Jag1
Ncstn
E
Hoechst
Notch3
e1
e2
e3
E8.5d
150 µm
100 µm
LPM
Myo
F
Hoechst
Notch3
f1
f2
No
LPM
150 µm
100 µm
G
Notch3
Log2(Left-right ratio)
E8.5c
E8.5d
E8.5e
E8.5f
H
Hoechst
Notch3
Nodal
h1
h2
E8.5d
200 µm
LPM

Supplementary figure 2 related to Figure 3

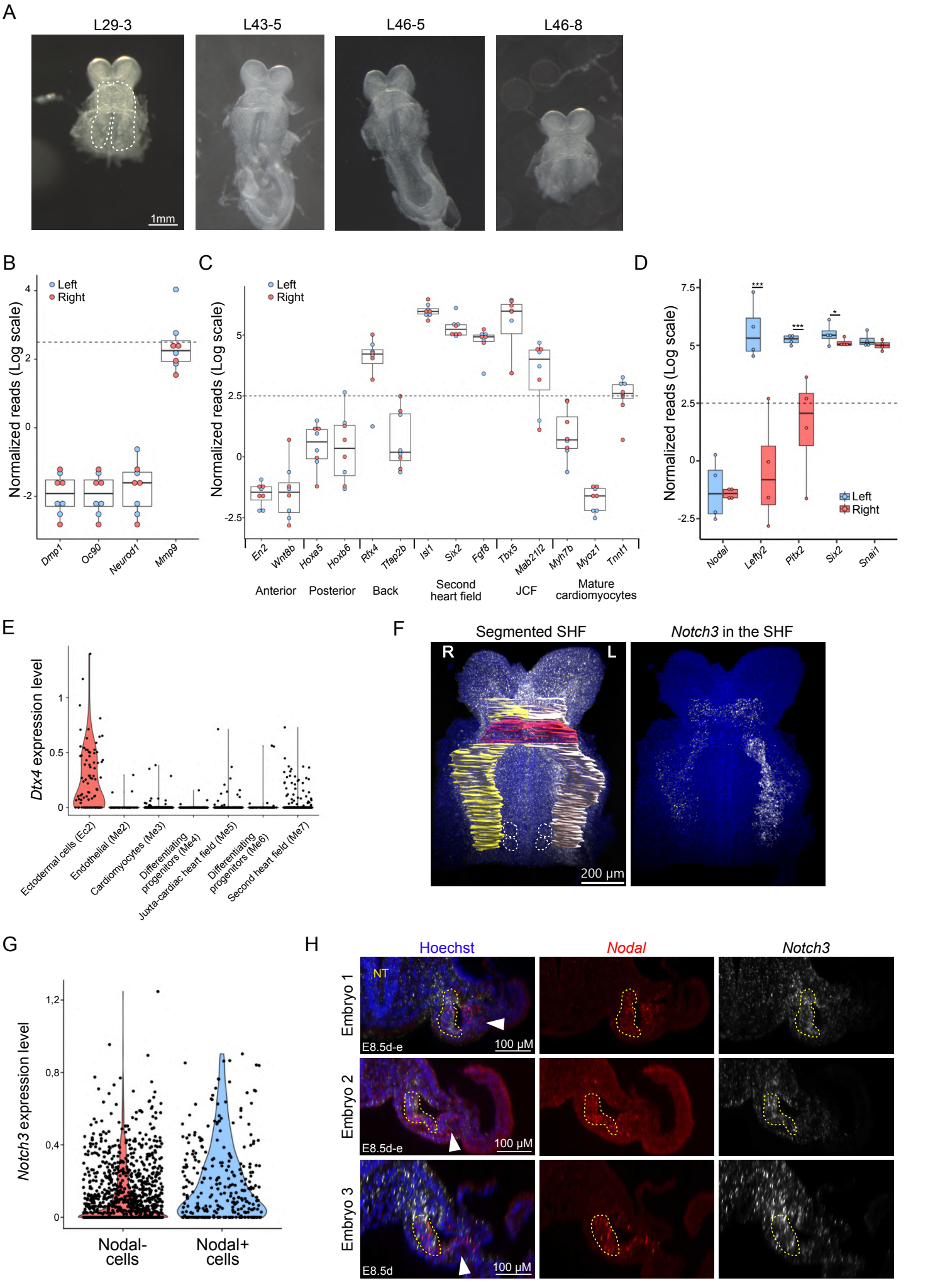

Figure S2 related to Fig. 3. Additional transcriptomic analyses.
(A) Brightfield images of embryos used for RNA sequencing at E8.5f. In the left panel, an outline of the dissected areas is shown. The identification number of embryos is given. **(B)** Normalized read counts of genes used to validate the threshold of expression in the transcriptomic analysis. The osteocyte gene *Dmp1*, inner ear marker *Oc90*, neuronal marker *Neurod1* are used as negative controls and *Mmp9* as a positive control, lowly expressed in left heart progenitors. Whisker plots show the median, 25th- and 75th quartiles (boxes), and the extreme data points (whiskers). **(C)** Normalized read counts of genes used as markers to control sample micro-dissection. *En2, Wnt8b* are anterior markers, *Hoxa5, Hoxb6* posterior markers, *Rfx4*, *Tfap2b* back markers, *Isl1, Six2, Fgf8* second heart field markers, *Tbx5, Mab21l2* juxta-cardiac field (JCF) markers and *Myh7b, Myoz1, Tnnt1* cardiomyocyte markers. The dotted line indicates the threshold of background expression. Whisker plots show the median, 25th- and 75th quartiles (boxes), and the extreme data points (whiskers). **(D)** Normalized read counts of genes used as markers to validate the left-right profile of samples. Nodal targets *Lefty2* and *Pitx2,* as well as *Six2* label the left side. *Snai1*, which was reported as a right marker, was not found asymmetric. *p-value between the left and right sides < 0.05, *** Benjamini-Hochberg corrected p-value < 0.00001 (Voom, n=4). Whisker plots show the median, 25th- and 75th quartiles (boxes), and the extreme data points (whiskers). **(E)** Violin plot of *Dtx4* expression in single cells from a published transcriptomic dataset at early E8.5, clustered as annotated (n= 89 Ec2, 59 Me2, 713 Me3, 221 Me4, 355 Me5, 65 Me6, 514 Me7). Dots are normalized reads per cell. (**F)** Segmentation of the cardiac region in 3D images, to quantify gene expression in the heart tube (red), left (white) or right (yellow) heart field. Somites are outlined by white dotted lines. Expression of *Notch3* within the segmented second heart field is extracted in the right panel. **(G)** Violin plot of *Notch3* expression in Nodal-negative (n=1559) and Nodal-positive (n=309) cells in the cardiac clusters (Me3-7) of the single cell transcriptomic dataset at early E8.5 (stages 1 to LHT). **(H)** Transversal section of the left LPM in three embryos, labelled by double wholemount RNAscope ISH of *Nodal* and *Notch3*. The region of *Notch3* and *Nodal* co-expression is outlined in yellow. Lateral cells positive for *Nodal* without high *Notch3* expression are indicated by a white arrowhead. L, left; SHF, second heart field; R, right.

Nodal is required in the lateral plate mesoderm to amplify *Notch3* asymmetric expression

Nodal and *Notch3* are co-expressed in the lateral plate mesoderm, yet Nodal asymmetry peaks from E8.5c (Desgrange et al., 2020), i.e. one stage before *Notch3* and the Nodal target *Lefty2* at E8.5d. We thus hypothesized that *Notch3* asymmetric expression could be downstream of Nodal signaling. To investigate this, we assessed *Notch3* expression in *Nodal* mutants, using a conditional mutant line, in which *Nodal* is inactivated in the mesoderm, but not in the node (Desgrange et al., 2020). 3D quantifications indicate that *Notch3* asymmetry is significantly reduced in *Nodal* mutants compared to littermate controls at E8.5d-e (Fig 4a-b). However, *Notch3* asymmetric expression is not completely abrogated in *Nodal* mutants. This is in

keeping with our previous finding that *Nodal* is required to amplify left-right asymmetries (Desgrange et al., 2020) and provides the first molecular evidence of this. In reverse, Notch signaling has been shown to directly activate *Nodal* in the left-right organizer (Raya et al., 2003). We thus analyzed *Nodal* expression in *Notch3*$^{-/-}$ mutants (Krebs et al., 2003). *Nodal* expression was found restricted to the left side of the lateral plate mesoderm (Fig S3A-B) and higher in the left crown of the node (Fig S3B) in *Notch3* mutants at E8.5c, as reported in wild-type embryos (Collignon et al., 1996) In addition, *Pitx2* expression at E8.5e was also unaffected (see Fig.8B). These experiments show that *Notch3* is downstream of Nodal signaling in cardiac progenitors, and therefore a candidate for regulating asymmetric heart morphogenesis.

Figure 4

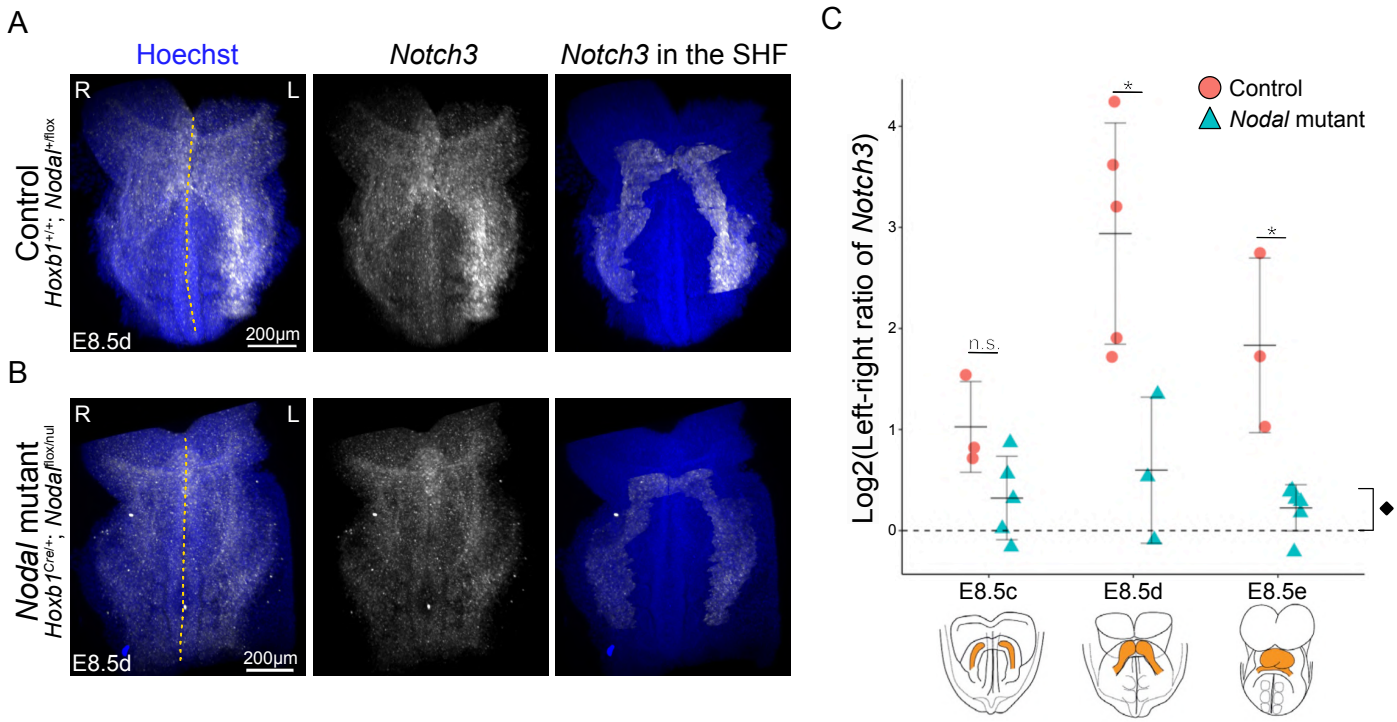

Figure 4. Decreased *Notch3* asymmetric expression in *Nodal* mutants.
(A-B) Whole mount RNAscope ISH of *Notch3* in control (A) and *Nodal* mutants (B) at E8.5d. Expression of *Notch3* within the segmented heart field is extracted in right panels. **(C)** Corresponding quantification of normalized *Notch3* asymmetric (left over right) expression in the heart field at sequential stages in controls (n= 3 at E8.5c, 5 at E8.5d, 3 at E8.5e) and *Nodal* mutants (n= 5 at E8.5c, 3 at E8.5d, 6 at E8.5e). Means and standard deviations are shown. *p-value < 0.05 (Mann-Whitney U test between controls and mutants). ♦p-value < 0.05 (Wilcoxon signed rank test to compare mutant levels with a symmetry hypothesis). The midline is indicated by a yellow dotted line. L, left; R, right.

Supplementary figure 3 related to figure 4

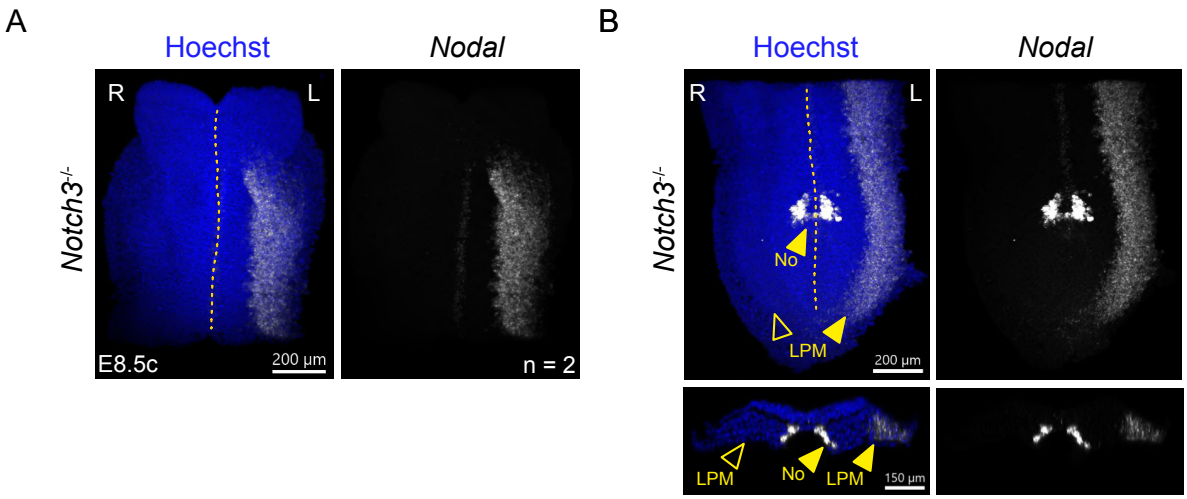

Figure S3 related to Fig. 4. *Nodal* expression in *Notch3* mutants.
(A-B) Whole mount RNAscope ISH of *Nodal* in *Notch3*$^{-/-}$ mutant embryos at E8.5c in anterior (A) and posterior (B) front views. The midline is indicated by a yellow dotted line. L, left; LPM, lateral plate mesoderm; No, node; R, right.

Notch3 mutants display mild heart looping defects with partial penetrance

We next examined the role of *Notch3* in asymmetric heart morphogenesis. *Notch3* mutants were recovered at the expected Mendelian ratio (Fig 5A-B), and were viable and fertile, as reported previously (Krebs et al., 2003).

We analysed in more detail heart morphogenesis in *Notch3* mutants at the end of the looping process. 80% of *Notch3*$^{-/-}$ embryonic hearts at E9.5 (Fig 5d1) were indistinguishable from wild-type littermates (Fig 5C), with normal heart looping and normal positions of the ventricles. In 20% of cases (see also Fig. 9B), the position of the ventricles appeared slightly affected with the right ventricle being posteriorly (Fig 5d2), anteriorly (Fig 5d4) positioned relative to the left ventricle, or with a more medial left ventricle (Fig 5d3). Hearts with an anterior right ventricle resemble to *Nodal* class 4 mutants (Desgrange et al., 2020). To quantify morphological defects, we performed High Resolution Episcopic Microscopy (HREM) on a first series of *Notch3*$^{-/-}$ mutants in 3D and segmented the heart tube (Fig 5E). Since these embryos were produced from *Notch3*$^{-/-}$ parents, no control littermate was available and we used controls from our previous analysis of *Nodal* mutants (Desgrange 2020). In this first series of mutants, some showed a normal positioning of the ventricles (Fig 5e2), while 2/9 displayed an anterior right ventricle (Fig 5e3). Heart tube length was not significantly different in *Notch3*

mutants and controls (Fig 5F), however, the orientation of the ventricles was significantly affected in *Notch3* mutants compared to controls (Fig 5G). To confirm these observations and look for other potential defects, we have designed a second batch in which we will compare control littermates with *Notch3*$^{-/-}$ mutants. As the defects are partially penetrant, we aim to quantify ~10 wild-types and ~20 mutants.

The anterior right ventricle phenotype is similar to *Nodal* class 4 mutants. We have previously shown that this mild phenotype is associated with congenital heart defects at birth (Desgrange et al., 2020). This prompted us to investigate if *Notch3* mutants have malformed hearts at birth. We collected a batch of *Notch3* homozygote and heterozygote mutants. We first imaged whole mount neonates by micro-CT imaging, and found none displaying an heterotaxy syndrome or laterality defects, as seen in *Nodal* mutants (data not shown). To obtain higher resolution of the heart structure, we subjected isolated hearts to HREM imaging (Fig 5H). 4/12 homozygote *Notch3* mutant hearts were normal (Fig 5h1-3), while 1/12 showed peri-membranous ventricular septal defect (Fig 5h4), 4/12 muscular ventricular septal defect (Fig 5h5-6), and 3/12 had a thinning of the RV, often associated with septal defects (Fig 5h5). Furthermore, we detected one heart with a dilated septal coronary artery (Fig 5h7), which is in keeping with the published role of Notch3 in coronary artery smooth muscle cell development (Volz et al., 2015) or the role of Notch3 in CADASIL syndrome (Joutel et al., 1996; Monet et al., 2007). 1/4 heterozygote *Notch3* mutants showed peri-membranous ventricular septal defect, and 2/4 thinning of the right ventricle.

In conclusion we show that *Notch3* mutants display cardiac phenotypes with partial penetrance, both at E9.5 with abnormal heart loops and at birth with structural heart defects, predominantly ventricular septal defects and a thinner right ventricle. Given the mild phenotype of *Notch3* mutant hearts, we wondered whether the absence of *Notch3* could be compensated by paralogue genes.

Figure 5

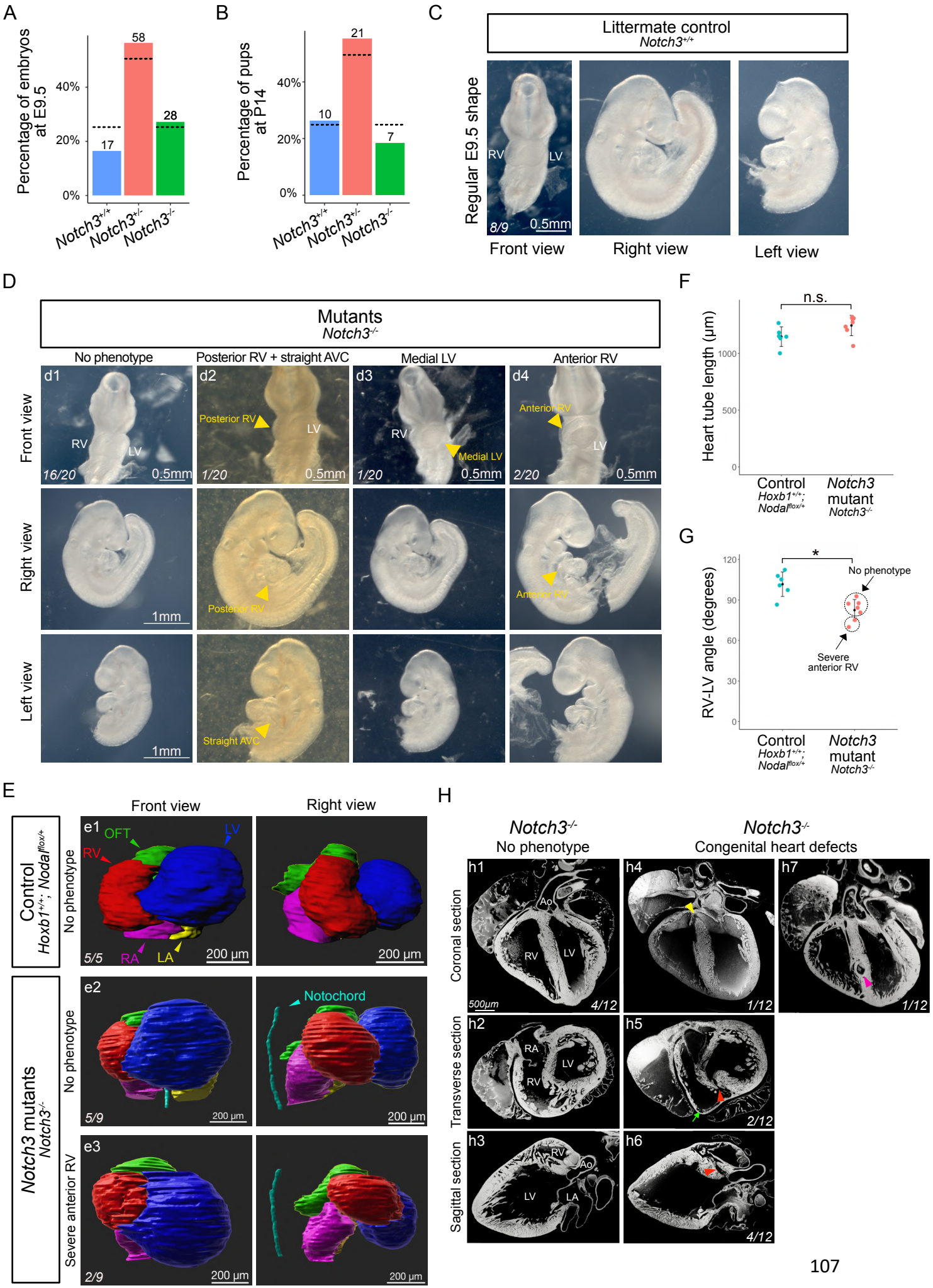
A
Percentage of embryos at E9.5
40%
20%
0%
58
17
28
Notch3+/+
Notch3+/-
Notch3-/-
B
Percentage of pups at P14
40%
20%
0%
21
10
7
Notch3+/+
Notch3+/-
Notch3-/-
C
Littermate control
Notch3+/+
Regular E9.5 shape
RV
LV
8/9
0.5mm
Front view
Right view
Left view
D
Mutants
Notch3-/-
No phenotype
Posterior RV + straight AVC
Medial LV
Anterior RV
Front view
Right view
Left view
d1
RV
LV
16/20
0.5mm
d2
Posterior RV
LV
1/20
0.5mm
d3
RV
Medial LV
1/20
0.5mm
d4
Anterior RV
LV
2/20
0.5mm
1mm
Posterior RV
Anterior RV
Straight AVC
F
n.s.
Heart tube length (µm)
1000
500
0
Control
Hoxb1+/+; Nodalflox/+
Notch3 mutant
Notch3-/-
G
*
RV-LV angle (degrees)
120
90
60
30
0
No phenotype
Severe anterior RV
Control
Hoxb1+/+; Nodalflox/+
Notch3 mutant
Notch3-/-
E
Front view
Right view
Control
Hoxb1+/+; Nodalflox/+
No phenotype
e1
OFT
LV
RV
5/5
RA
LA
200 µm
200 µm
Notch3 mutants
Notch3-/-
No phenotype
e2
5/9
200 µm
Notochord
200 µm
Severe anterior RV
e3
2/9
200 µm
200 µm
H
Notch3-/-
No phenotype
Notch3-/-
Congenital heart defects
Coronal section
h1
Ao
RV
LV
500µm
4/12
h4
1/12
h7
1/12
Transverse section
h2
RA
LV
RV
h5
2/12
Sagittal section
h3
RV
Ao
LV
LA
h6
4/12

Figure 5. Heart looping defects in *Notch3*$^{-/-}$ mutants.
(A-B) Histogram showing the percentage of genotypes recovered at the indicated stages, from litters of *Notch3*$^{+/-}$ x *Notch3*$^{+/-}$ crosses. The observed frequency is not significantly different from the expected Mendelian ratio (dotted lines) (p-value = 0.14 (E9.5), 0.64 (P14), chi-square tests, n as indicated). **(C-D)** Examples of brightfield images of a control littermate (B) and *Notch3*$^{-/-}$ mutant embryos (C) at E9.5. Phenotype variations are shown: no obvious defect (d1), posterior RV and straighter AVC (d2), medial LV (d3), anterior RV (d4). Embryos are shown in a front, right or left-sided view as indicated. Numbers in the bottom left corner report the observed frequency. **(E)** 3D-segmented heart tubes in control (e1) and *Notch3*$^{-/-}$ mutant embryos (e2-e3), shown in a front (left panel) and right-sided view (right panel). Numbers in the bottom left corner report the observed frequency. **(F)** Quantifications of the heart tube length in controls (n = 6) and *Notch3*$^{-/-}$ embryos (n = 7) at E9.5, which are not significantly different (two sided t-test). Means and standard deviations are shown. **(G)** Quantifications of ventricle orientation relative to the notochord in the same embryos. *p < 0.05 (two sided t-test). Means and standard deviations are shown. **(H)** Sections of *Notch3*$^{-/-}$ mutant hearts at P0, imaged by HREM. Defects include peri-membranous VSD (yellow arrowhead), muscular VSD (red arrowheads), dilatation of the septal coronary artery (pink arrowhead) and thin RV (green arrow). Numbers in the bottom right corner report the observed penetrance. AVC, atrioventricular canal; Ao, aorta; LA, left atrium; LV, left ventricle; ns, non-significant; RA, right atrium; RV, right ventricle; VSD, ventricular septal defect

Notch3 is the main Notch receptor in the lateral plate mesoderm and is the only asymmetric Notch receptor

The mouse has four Notch receptor paralogues, which have been reported to have both overlapping and specific functions (Hosseini-Alghaderi & Baron, 2020). We compared expression of *Notch1-4* at the stages when *Notch3* is asymmetrically expressed. In our RNA bulk sequencing, *Notch3* was the only gene asymmetrically expressed, and *Notch4* was expressed at very low levels (Fig 6A) and thus was not selected for further analysis. We then compared the expression profiles of *Notch* paralogues. *Notch1* was detected in the endocardium and dorsal aortas, as well as the posterior presomitic mesoderm, thus not overlapping with *Notch3* (Fig 6B). *Notch2* was more highly expressed in the floor plate of the neural tube and the notochord (Fig 6C) and laterally in a domain that we confirmed as the juxta-cardiac field by co-labelling with *Mab21l2* (Tyser et al., 2021) (Fig S4A). Thus, *Notch2* had a specific expression profile compared to other Notch, but was also detected more broadly at low levels, in particular in the domain of *Notch3* expression (Fig 6C). Using published single cell datasets (Tyser et al., 2021), we confirmed that *Notch1* and *Notch4* are specifically expressed in endothelial cells, *Notch2* and *Notch3* are both expressed in myocardial progenitors, with *Notch2* enriched in the juxta cardiac-field and first lineage trajectory (Me4-

5) and *Notch3* enriched in the second heart field and second lineage trajectory (Me6-7) (Fig S4B-C).

To further investigate where Notch signaling was active, we collected embryos from the Notch reporter mouse line CBF:H2B-Venus (Nowotschin et al., 2013). The reporter was detected in the dorsal aortas, endocardium and yolk sac (Fig S4D), which indicates that this line only reports Notch1 signaling. We performed wholemount immunofluorescent labelling of Notch1 intracellular domain (N1ICD), and found expression in the endocardium, dorsal aortas, and presomitic mesoderm, a very similar pattern to *Notch1* expression but sharper (Fig S4E). Unfortunately, no antibody for Notch2 and Notch3 intracellular domains are available, nor specific mouse reporter lines.

As both *Notch2* and *Notch3* are co-expressed in the second heart field, we quantified their respective asymmetry. *Notch2* asymmetry (Fold change: 1.17 towards the right) was negligible compared to that of *Notch3* (Fold change: 6.9 towards the left) (Fig 6D), showing that *Notch3* is the main asymmetric *Notch* receptor in the second heart field during heart looping.

To assess more directly whether Notch paralogues may compensate the absence of *Notch3*, we analyzed their expression in micro-dissected heart fields by RT-qPCR (Fig 6E). As a control, *Notch3* expression was confirmed downregulated in *Notch3* mutants compared to wildtype embryos. Primers within the deleted region (exons 8-9, Fig S4F) showed a 100% reduction, whereas primers outside showed a 75% reduction. *Notch1* and *Notch2* were found upregulated in mutants, while control genes, *Tbx1* (second heart field marker) and *Rfx4* (neural tube marker), were not significantly changed. This analysis suggests that increased expression levels of *Notch1/2* may compensate the absence of *Notch3*. We further mapped the expression profile of Notch2 and found no obvious change in *Notch3* mutants (Fig 6F). We quantified no asymmetry of *Notch2* expression in the second heart field of *Notch3* mutants (Fig 6G), thus indicating that *Notch2* upregulation in *Notch3* mutants is likely general.

Altogether, our data show that *Notch3* is the only asymmetric Notch receptor during heart looping, and that in the absence of *Notch3*, *Notch1* and *Notch2* are upregulated. Following this, we then questioned which genes and pathways that *Notch3* is regulating in the heartfield.

Figure 6

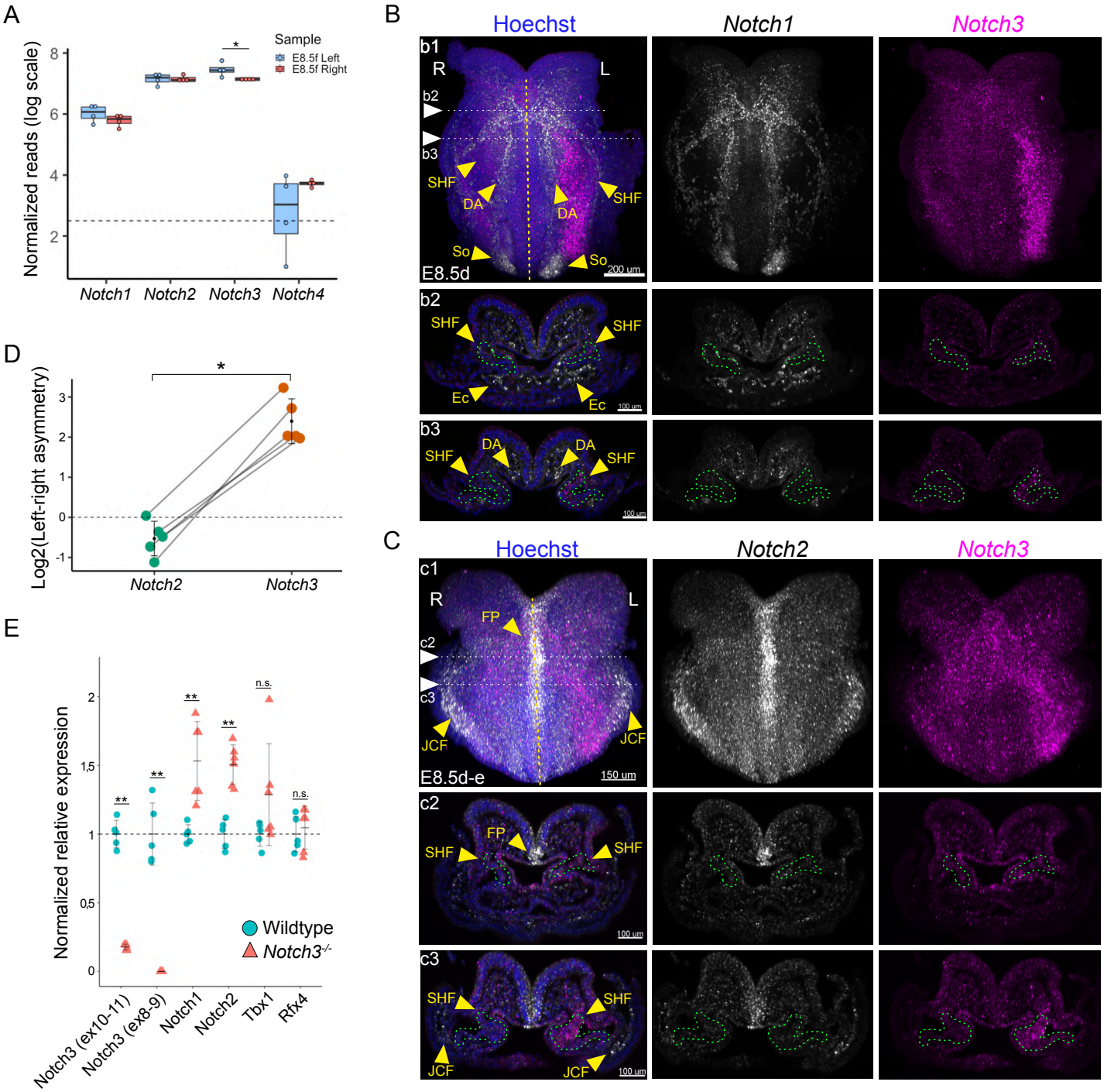
A
Normalized reads (log scale)
Sample
E8.5f Left
E8.5f Right
Notch1 Notch2 Notch3 Notch4
B
Hoechst
Notch1
Notch3
b1
R
L
b2
b3
SHF
DA
So
E8.5d
200 um
C
Hoechst
Notch2
Notch3
c1
FP
JCF
E8.5d-e
150 um
c2
c3
D
Log2(Left-right asymmetry)
Notch2
Notch3
E
Normalized relative expression
Wildtype
Notch3-/-
Notch3 (ex10-11)
Notch3 (ex8-9)
Notch1
Notch2
Tbx1
Rfx4
F
Hoechst
Notch2
Notch3-/-
f1
f2
G
E8.5.d
E8.5.e
E8.5.f
Log2(Left-right asymmetry)
Notch2 expression in the SHF of Notch3-/- mutants

Supplementary figure 4 related to figure 6

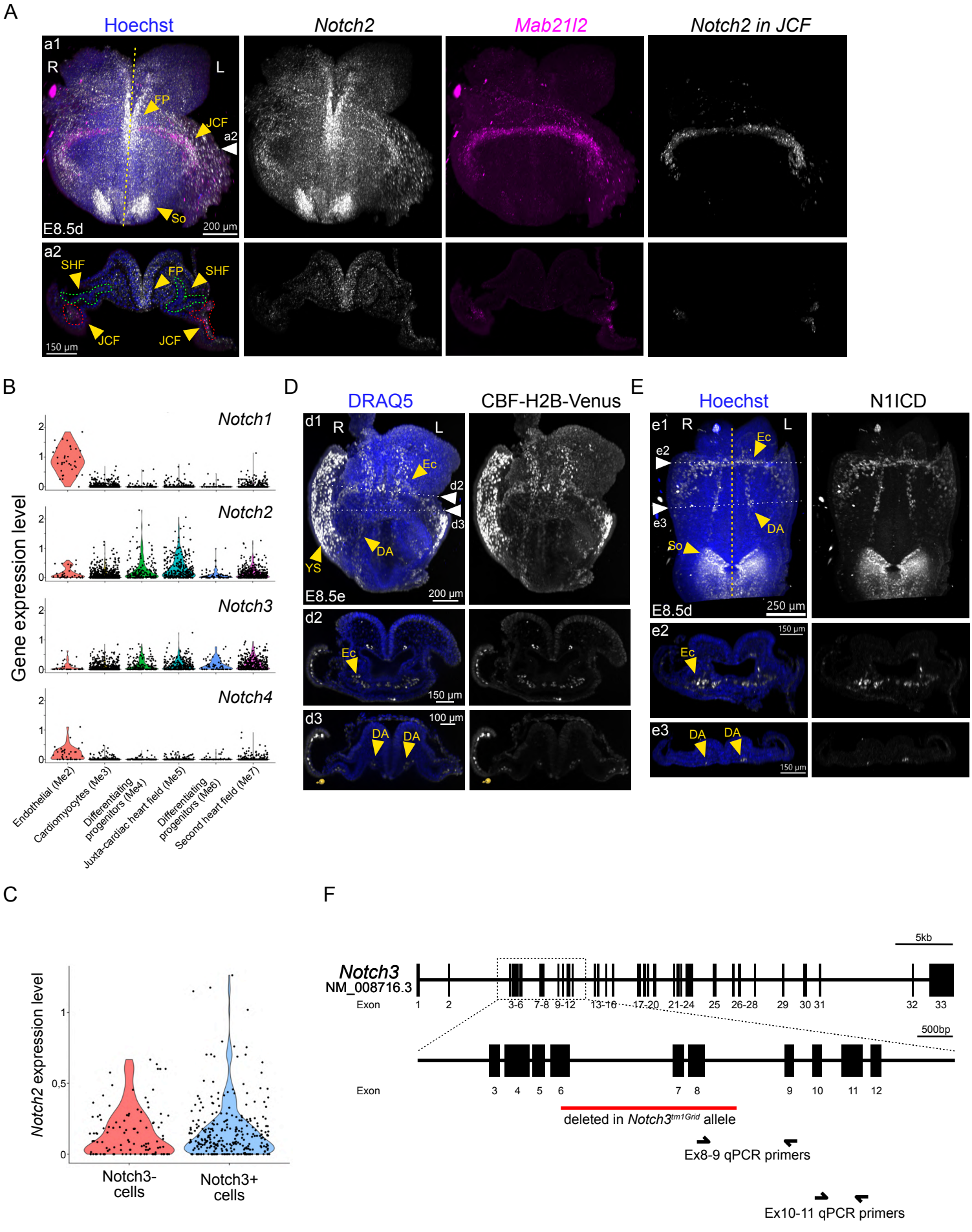

Figure 6. Notch receptor gene expression profile in control and *Notch3* mutants.
(A) Normalized read counts of Notch receptor genes in the left (blue) and right (red) heart field at E8.5f. The dotted line indicates the threshold of background expression. *p-value < 0.05 (Voom, n=4). Whisker plots show the median, 25th- and 75th quartiles (boxes), and the extreme data points (whiskers). **(B)** Relative *Notch1* (white) and *Notch3* (magenta) expression detected by double whole-mount RNAscope ISH at E8.5d, and shown in a front view (b1), and transverse sections (b2-b3), at the levels indicated in b1) (n=4). **(C)** Relative *Notch2* (white) and *Notch3* (magenta) expression detected by double whole-mount RNAscope ISH at E8.5d-e and shown in a front view (c1), and transverse sections (c2-c3 – at the levels indicated in c1) (n=5). **(D)** Corresponding quantifications of normalized *Notch2* and *Notch3* asymmetric (left over right) expression in the second heart field at E8.5d-e. *p-value < 0.01 (Two sided Mann-Whitney test to compare expression levels with a symmetry hypothesis, n = 5). **(E)** Relative expression of the indicated *Notch* genes and quantified by RT-qPCR in micro-dissected heart fields of wild-type (n=6) and Notch3$^{-/-}$ (n=5) embryos at stage E8.5d-e, and normalized to controls. *Tbx1* and *Rfx4* are used as control markers of the heart field and neural tube respectively. **p-value < 0.01 (two sided Mann-Whitney test). *Notch3* has been detected with primers outside (ex9-10) and inside (ex8-9) the region deleted in mutants (See Fig S4F). **(F)** *Notch2* (white) expression detected by whole-mount RNAscope ISH in *Notch3*$^{-/-}$ mutant embryos at stage E8.5d-e. The SHF is outlined in green. **(G)** Corresponding quantification of *Notch2* asymmetric (left over right) expression in the second heart field of Notch3$^{-/-}$ embryo between E8.5d-f. The asymmetry is non-significant (one sample Mann Whitney test). Means and standard deviations are shown. DA, dorsal aorta; Ec, endocardium; FP, floor plate; ISH, in situ hybridization; JCF, juxta-cardiac field; L, left; ns, non-significant; R, right; SHF, second heart field; So, somite.

Figure S4 related to Fig. 6. Additional profiling of Notch paralogues.
(A) Co-expression of *Notch2* (white) and the juxta-cardiac field marker *Mab21l2* (magenta) detected by double whole mount RNAscope ISH at stage E8.5d, and shown in a front view (a1) and transverse section (a2, at the level indicated in a1). Expression of *Notch2* within the segmented JCF domain is extracted in the right panel. The midline is indicated by a yellow dotted line (n=8). **(B)** Violin plots of *Notch1-4* expression in single cells from a published transcriptomic dataset at early E8.5 (Tyser et al, 2021), clustered as annotated (n= 35 Me2, n=627 Me3, n=169 Me4, n=287 Me5, n=63 Me6, n=386 Me7). **(C)** Violin plot of *Notch2* and *Notch3* expression in single cells of the second heart field cluster (Me7) at early E8.5 (stages 1 to late heart tube, dataset as in B). 84% of *Notch3*-positive cells (n=277) are lowly positive for *Notch2,* and *Notch2* is also detected in 73% of *Notch3*-negative cells (n=109). **(D)** Whole-mount fluorescent signal of a Notch reporter in a transgenic CBF-H2B-Venus embryo at E8.5e, shown in a front view (c1), and transverse sections (c2-c3, at the levels indicated in c1) (n=7). **(E)** Whole-mount immunofluorescence of cleaved Notch1 intracellular domain (N1ICD) at E8.5d, shown in a front view (d1), and transverse sections (d2-d3, at the levels indicated in d1) (n=11). **(F)** Schema of the *Notch3* locus mapping the deleted region in the knock-out allele, as well as qPCR primers used in Fig. 6E. DA, dorsal aorta ; Ec, endocardium ; FP, floor plate ; JCF, juxta-cardiac field (red dotted outline); L, left; R, right ; SHF, second heart field (green dotted outline) ; So, somites ; YS, yolk sac.

Marks end of figures specific for publication

Hey1 is left-sided in heart progenitors, downstream of *Nodal* rather than *Notch3*

To better understand Notch signaling in heart progenitors, we investigated Notch canonical ligands and targets. Of the five canonical Notch ligands, *Jag1* is the most highly expressed in the heart field and asymmetrically enriched on the left at E8.5f (Fig 7A). By immunostaining, Jag1 was detected in all cardiogenic populations, but more highly detected in differentiating cardiomyocytes, at the transition zone between the heart field and heart tube, as well as in the second heart field. This pattern overlapping with that of *Notch3*, makes Jag1 a good candidate to act as a ligand of Notch3 in the cardiogenic region.

We decided to investigate the expression of the classical Notch target gene *Hey1*, as *Hey1* has been shown to be a specific target of Notch3 in both regenerating retinal Müller glial cells (Sahu et al., 2021) and neural stem cells (Than-Trong et al., 2018). Furthermore, *Hey1* has been shown to be enriched in *Pitx2*$^{+}$ cells compared to *Pitx2*$^{-}$ cells of the second heart field cells (de Soysa et al., 2019), suggestive of asymmetry. By double *in situ* hybridization and quantification, we found that *Hey1* is asymmetrically expressed in the second heart field at a similar stage as *Notch3* (E8.5d). *Hey1* asymmetry is restricted to the heart field compared to the broader expression of *Notch3* throughout the lateral plate mesoderm (Fig 7C, G). The region of overlap between *Hey1* and *Notch3* is also positive for Jag1, suggesting active signaling of a ligand/receptor pair on a target gene. However, in *Notch3* mutants, *Hey1* was still expressed asymmetrically in the second heart field (Fig 7D, G), indicating that *Notch3* does not promote *Hey1* asymmetric expression. Beyond the second heart field, *Hey1* was also found expressed in the dorsal aortas, sinus venosus and endocardium. This expression pattern is reminiscent of that of *Notch1* and Notch reporters (Fig. 6B, S4C-D), suggesting that Notch1 could regulate *Hey1* in these tissues. Moreover, by exploring the kinetics of *Hey1* and *Notch3* expression in our full left-right bulk RNA sequencing screen (see Fig. 2), we found that *Hey1* becomes asymmetric at E8.5c, i.e. prior to *Notch3* and concomitant with *Nodal* (Fig 7H).

To directly test the regulation of *Hey1*, we examined its expression in *Nodal* conditional mutants and found that *Hey1* expression is unchanged in the sites of Notch1 activity (see Fig. 6B, S4C-D). However *Hey1* expression, and thus its asymmetry, are lost in the second heart field (Fig 7E-G). Our data thus support the conclusion that Nodal rather than Notch3 induce *Hey1* asymmetric expression in the second heart field. Thus, we had to perform a broader screen in order to identify Notch3 targets.

Figure 7

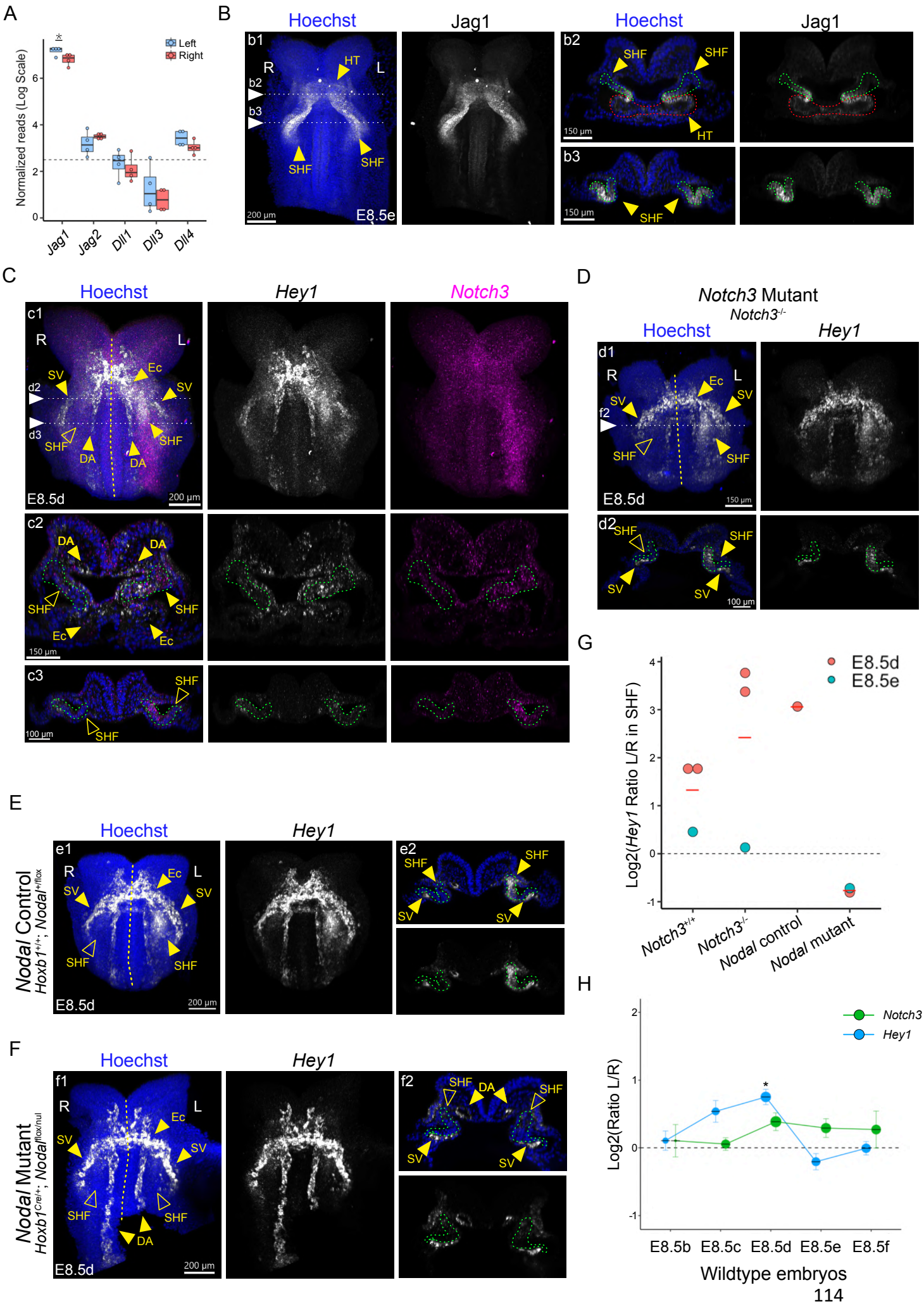
A
Left
Right
Normalized reads (Log Scale)
Jag1
Jag2
Dll1
Dll3
Dll4
B
Hoechst
Jag1
b1
R
L
HT
b2
b3
SHF
E8.5e
200 µm
150 µm
C
Hoechst
Hey1
Notch3
c1
SV
Ec
d2
d3
DA
E8.5d
c2
c3
D
Notch3 Mutant
Notch3-/-
d1
f2
d2
100 µm
E
Nodal Control
Hoxb1+/+; Nodalflox/+
e1
e2
F
Nodal Mutant
Hoxb1Cre/+; Nodaflox/nul
f1
f2
G
Log2(Hey1 Ratio L/R in SHF)
E8.5d
E8.5e
Notch3+/+
Notch3-/-
Nodal control
Nodal mutant
H
Log2(Ratio L/R)
Notch3
Hey1
E8.5b
E8.5c
E8.5d
E8.5e
E8.5f
Wildtype embryos

Figure 7. Expression of Notch ligand *Jag1* and Notch canonical target *Hey1*.
(A) Normalized read counts of Notch ligand genes in the left (blue) and right (red) wild-type heart field at E8.5f. The dotted line indicates the threshold of background expression. *p-value < 0.05 (Voom, n=4). Whisker plots show the median, 25th- and 75th quartiles (boxes), and the extreme data points (whiskers). **(B)** Jag1 whole-mount immunofluorescence in a wild-type embryo at E8.5e, shown in a frontal view (b1) and transverse sections (b2-b3) at the levels indicated in b1 (n=8). **(C)** Relative *Hey1* (white) and *Notch3* (magenta) expression detected by double whole mount RNAscope ISH at E8.5d-e, and shown in a front view (c1), and transverse sections (c2-c3), at the levels indicated in c1. Open arrowheads indicate absence of *Hey1* expression. **(D)** Whole-mount RNAscope ISH of *Hey1* in *Notch3* mutants at E8.5c-d, and shown in a front view (d1), and transverse section (d2), at the level indicated in d1 (n=4). Open arrowheads indicate absence of *Hey1* expression. **(E-F)** Expression of *Hey1* in control (G) and *Nodal* mutants (H) at E8.5d, and shown in front views (e1-f1) and transverse sections (e2-f2) at the levels indicated in e1-f1 (n= [1, 2]). Open arrowheads indicate absence of *Hey1* expression. **(G)** Associated quantifications of normalized *Hey1* asymmetric (left over right) expression in the second heart field at E8.5d-e in *Notch3*$^{+/+}$ (n=3), *Notch3*$^{-/-}$ (n=3), *Nodal* control (*Hoxb1*$^{+/+}$; *Nodal*$^{flox/+}$, n=1) and mutant (*Hoxb1*$^{Cre/+}$; *Nodal*$^{flox/nul}$, n=2) embryos. Means are shown. **(H)** Asymmetric expression of *Hey1* and *Notch3* detected by RNA sequencing at sequential stages in wild-type heart fields (see Fig. 2H-O). * Benjamini-Hochberg corrected p-value < 0.05 (DESeq2). Standard deviation are shown. Size of circle indicate number of reads. DA, dorsal aorta; Ec, endocardium; L, left; ns, non-significant ; R, right ; SHF, second heart field (green dotted outline) ; SV, sinus venosus.

Screening of potential Notch3 target genes in cardiac cells

In the absence of reporters for Notch3 signaling, we screened for potential Notch3 target genes in the single cell transcriptomic dataset (Tyser et al., 2021). We first analysed gene expression correlation with *Notch3* in all cardiac cells (Me3-Me7) and stages -1 to LHF (corresponding to our nomenclature of early headfold (EHF) to E8.5f, Le Garrec et al., 2017).

We identified 177 genes significantly positively correlated with *Notch3* and 79 genes significantly negatively correlated. Of the canonical Notch targets, *Hes* and *Hey* genes, only *Hey1* was significantly correlated (positively). Among the significantly correlated genes, we selected candidates which are expressed and became asymmetric at the time or after *Notch3* asymmetry in our bulk RNA sequencing of the heart field at 7 stages (see Fig 2) and based on previous literature of association with Notch signaling or the heart : 4 positively (*Hey1*, *Emilin1*, *Bcar3* and *Pald1*) and 7 negatively (*Crip2*, *Cap2*, *Dok4*, *Nebl*, *Nexn*, *Acta2* and *Actc1*) correlated genes. Crip2, encoding a transcription factor, has been found to interact with Notch3 in cancer cells (J. G. Jung et al., 2014) and knockdown of *crip2* in zebrafish leads to heart looping defects (Kim et al., 2014). In keeping with the enrichment of *Notch3* in cardiac precursors, and its published role in cell differentiation in other tissues (Bodas et al., 2021; Domenga et al., 2004),

we selected cardiac differentiation markers (Acta2 and *Actc1*). In addition, we probed classical Notch targets (*Hey1/2*, *Hes1), Atp1a1* as a published *Notch3* target (Than-Trong et al., 2018), as well as *Pitx2* because it has been shown to be negatively regulated by Notch signaling in Xenopus lateral plate mesoderm (Sakano et al., 2010). Erbb2 is associated with Notch3 in cancer (Pradeep et al., 2012).

We examined expression of these candidate genes by RT-qPCR in the heart field of control and *Notch3* mutants at E8.5e, the stage after *Notch3* asymmetry peaks (Fig 8B). A subset of targets was also tested at a later time point (E8.5g), with the idea that the lack of *Notch3* asymmetry may need more time to have an effect on gene expression (Fig 8C). The Notch targets *Hey1*, *Hey2, Atp1a1* and the genes negatively correlated with *Notch3*, *Crip2*, *Nexn* and *Actc10* were deregulated in *Notch3* mutants at E8.5e. However, several of these genes (*Hey1/2, Crip2, Nexn, Actc1*) behaved opposite to expectations from Spearman correlation, i.e., genes negatively correlated with *Notch3* were downregulated in *Notch3* mutants. Expression of most other candidate genes and at E8.5g were found not to be affected in *Notch3* mutants (*Emilin1*, *Pald1*, *Cap2*, *Dok4*, *Nebl*, *Acta2* and *Actc1*). By RNAscope ISH, we did not find any change in *Hey1* expression patterns in *Notch3* mutants compared to controls (Fig. 7D). Due to the fact that RNAscope staining is not a quantitative approach to compare gene expression levels in between embryos, this *Hey1* upregulation is likely an upregulation in tissues already expressing *Hey1*. Furthermore, given the compensatory expression of *Notch1/2* in *Notch3* mutants, the exacerbated expression of *Hey1/2, Crip2, Nexn, Actc1 at E8.5e* or the similar tendency of *Dok4* and *Nebl* at E8.5g (with p-values of 0.056 and 0.058 respectively), may reflect an overall increase in Notch signaling.

Given that bioinformatic predictions were not well validated by RT-qPCR, we revisited our Spearman correlation analysis. We sharpened the analysis to the clusters where *Notch3* is significantly expressed (Fig. S4B) and compared the specificity of candidates genes correlated with distinct Notch paralogues. For *Notch1* in endothelial cells (Me2), 13 positively and 31 negatively significantly correlated genes were predicted (Fig 8D), while for *Notch2* in the first lineage trajectory (Me4-5), 574 positively and 294 negatively significantly correlated genes were predicted (Fig 8E). For *Notch3* in heart progenitors and differentiating cell populations (Me4-7), only a single significantly correlated gene was predicted (Fig 8F). The poor prediction with *Notch3* may stem from the lower and broader expression of *Notch3* compared to *Notch1/2* (See Fig S4B). In our initial analysis of genes correlated with Notch3, 19/79 genes

negatively correlated with *Notch3* were associated with cardiac function and development (using the bioinformatic tool *Panther* from *Gene Ontology* - data not shown), thus reflecting a bias from the inclusion of cardiomyocyte cells rather than a role of *Notch3* in cardiac differentiation.

In conclusion, we have not yet identified convincing targets of Notch3, and further work will be required to understand its role of in the second heart field. In the remaining part of the results, we will describe alternative approaches we have used for exploring the role of Notch3 in heart morphogenesis.

Figure 8. Bioinformatic predictions of potential Notch targets in cardiac cells

(A) Volcano plot for co-expression analysis with *Notch3* expression levels. Spearman correlation between genes of the Tyser et al., 2021 dataset and *Notch3* expression levels in single embryonic cardiac cells (clusters Me3-7) is represented against its significance (n=1868 cells, adjusted p-value < 0.05 in red and blue, > 0.05 in green). Anti-correlated and correlated candidate genes are colored in red and blue respectively. Highlighted genes were selected for RT-qPCR analysis. **(B-C)** RT-qPCR analysis of gene expression in heart field micro-dissected as schematised at E8.5e (B) and E8.5g (C). Relative expression of selected genes in wild-type (n=6 at E8.5e, 4 at E8.5g) and Notch3$^{-/-}$ (n=5 at E8.5e, 3 at E8.5g) embryos and normalized to controls. *p-value < 0.05, **p-value < 0.01 (two sided Mann Whitney test). Standard deviations and means are shown. **(D-F)** Volcano plot for co-expression analysis with *Notch1* (D, n = 59 cells), *Notch2* (E, n = 556 cels) and *Notch3* (F, n = 1135 cells) expression levels in the indicated cell clusters of the dataset used in A. Adjusted p-value < 0.05 in red and blue, > 0.05 in green). Anti-correlated and correlated candidate genes are colored in red and blue respectively. HT, heart tube; n.s., not significant.

Figure 8

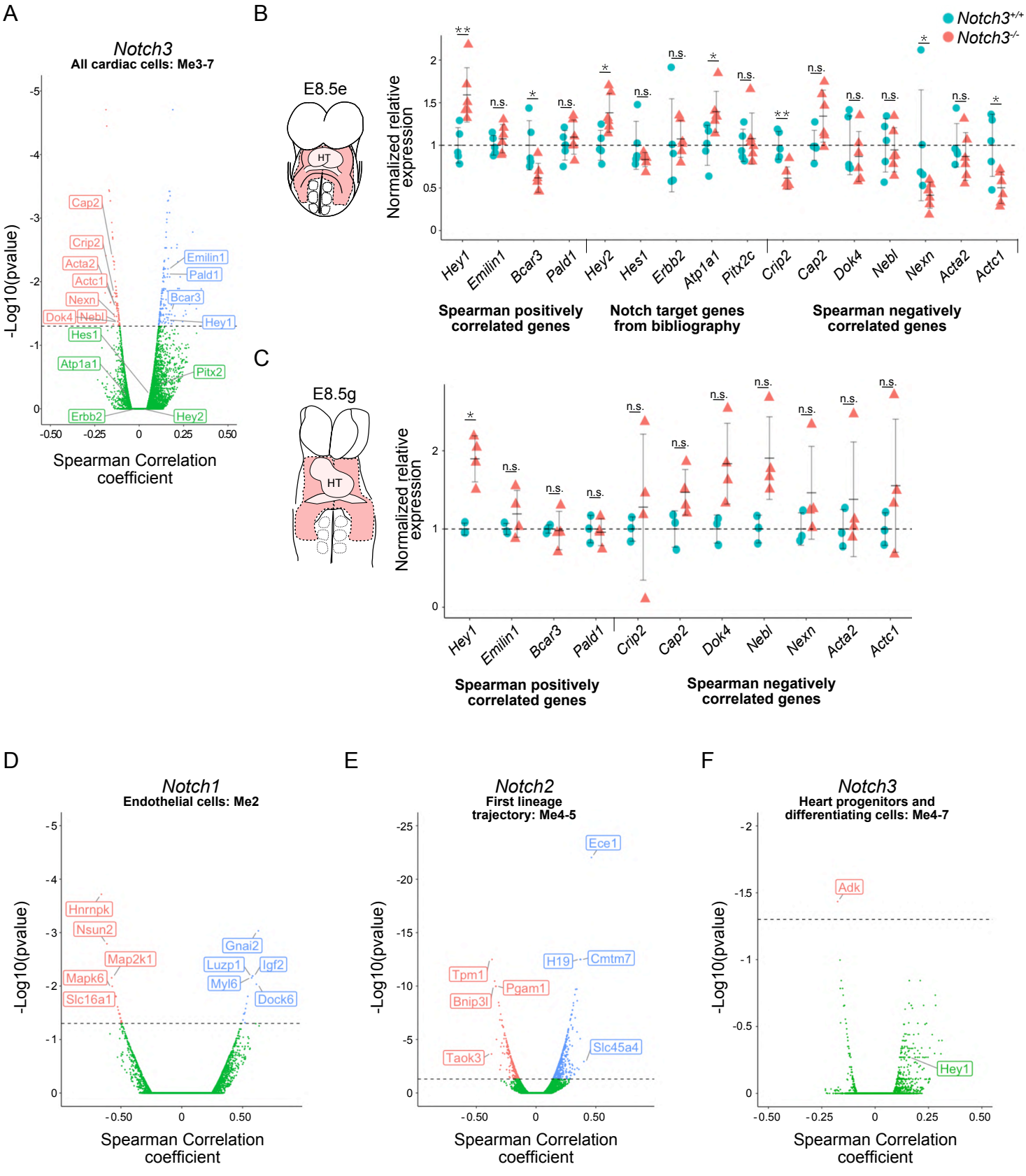
A
Notch3
All cardiac cells: Me3-7
-Log10(pvalue)
Spearman Correlation coefficient
Cap2
Crip2
Acta2
Actc1
Nexn
Dok4
Nebl
Hes1
Atp1a1
Erbb2
Emilin1
Pald1
Bcar3
Hey1
Pitx2
Hey2
B
E8.5e
HT
Notch3+/+
Notch3-/-
Normalized relative expression
Hey1
Emilin1
Bcar3
Pald1
Hey2
Hes1
Erbb2
Atp1a1
Pitx2c
Crip2
Cap2
Dok4
Nebl
Nexn
Acta2
Actc1
Spearman positively correlated genes
Notch target genes from bibliography
Spearman negatively correlated genes
C
E8.5g
HT
Normalized relative expression
Hey1
Emilin1
Bcar3
Pald1
Crip2
Cap2
Dok4
Nebl
Nexn
Acta2
Actc1
Spearman positively correlated genes
Spearman negatively correlated genes
D
Notch1
Endothelial cells: Me2
-Log10(pvalue)
Spearman Correlation coefficient
Hnrnpk
Nsun2
Map2k1
Mapk6
Slc16a1
Gnai2
Luzp1
Igf2
Myl6
Dock6
E
Notch2
First lineage trajectory: Me4-5
-Log10(pvalue)
Spearman Correlation coefficient
Ece1
H19
Cmtm7
Tpm1
Pgam1
Bnip3l
Taok3
Slc45a4
F
Notch3
Heart progenitors and differentiating cells: Me4-7
-Log10(pvalue)
Spearman Correlation coefficient
Adk
Hey1

Notch3 haploinsufficiency

We have identified in *Notch3* heterozygotes mild heart looping phenotypes at E9.5 with a 35% penetrance (n=37, Fig. 9B), structural heart defects at P0 with a 75% penetrance (n=4, see above), indicating that *Notch3* shows haploinsufficiency, as reported for *Notch1* (Koenig et al., 2017). The proportion of the more severe phenotype, anterior right ventricle, is lower in *Notch3* heterozygote mutants (0-4% depending on the cross) compared to *Notch3* homozygote mutants (10%).

To further investigate *Notch3* haploinsufficiency, we looked at *Notch3* transcription levels comparatively in wild-type, heterozygote and homozygote *Notch3* mutants. In the case of *Notch2*^{tm1Grid} mutants, alternative splicing near the knocked out site has been detected (McCright et al., 2001), thus generating a *Notch2* hypomorph allele rather than a null allele. To assess *Notch3*, we thus designed three different sets of qPCR primers : one set within the region depleted in the mutant allele (Ex8-9), one set next to it (Ex10-11) and one located multiple exons from it (Ex25-26) (See Fig. S4F). We compared transcript levels at stage E8.5e, right after the peak of asymmetric *Notch3* expression and at E8.5g, after *Notch3* asymmetry has ended (Fig S5A-B). We obtained similar results for all qPCR primer sets and at both stages : *Notch3* heterozygotes display on average 67.9% (± 5.94%) of transcript levels compared to wildtype, whereas *Notch3* homozygotes display 0% of ex8-9 and an average of 21.7% (± 7.52%) of other exons. Thus, our results show that *Notch3* heterozygotes have significantly decreased *Notch3* expression and also suggest no compensatory alternative splicing.

We then wondered if decreased *Notch3* levels could compromise *Notch3* asymmetry in *Notch3*$^{+/-}$ heterozygote embryos. Thus, we performed RNAscope in situ hybridization and quantified left-right asymmetry in the second heart field (Fig S5C-E). We found no significant difference between littermate controls and *Notch3*$^{+/-}$ heterozygote embryos (Fig S5E). As we have shown that *Notch1/2* are like compensation in *Notch3*$^{-/-}$ (Fig 6E), we investigated if these compensation were also occurring in *Notch3*$^{+/-}$, as this would suggest a compensation mechanism like for instance transcriptional adaption (El-Brolosy et al., 2019). We looked at the transcriptional levels of *Notch1/2* as well as *Hey1* and *Crip2* (which we had found to be differentially expressed between wildtype and *Notch3*$^{-/-}$) in wild-type, heterozygote and homozygote *Notch3* mutants and we found for all four genes that they were expressed at similar levels between *Notch3*$^{+/-}$ and *Notch3*$^{-/-}$. As such the *Notch3* heterozygous display gene

expression like the *Notch3* homozygous mutant, indicating that compensation is occurring also in the *Notch3*$^{+/-}$.

That *Notch3*$^{+/-}$ display cardiac phenotypes and that there is potentially compensation ongoing in the *Notch3*$^{+/-}$, indicates that Notch signaling is compromised in the *Notch3* heterozygous. To potentially reveal a stronger phenotype, we next aimed to understand in there was a genetic interaction between *Notch3* and *Nodal*.

Investigating genetic interaction between *Notch3* and *Nodal*

As we have shown that *Nodal* is required for amplifying *Notch3* asymmetric expression in the lateral plate mesoderm, we aimed to investigate if they also genetically interact. We generated new crosses to analyze *Nodal; Notch3* double heterozygotes (Fig 9A), compared to littermate single heterozygotes at E9.5. The frequency of phenotypes is summarized in Fig 9B. 35% Notch3 heterozygotes (*Notch3*$^{+/-}$; *Hoxb1*$^{+/+}$; *Nodal*$^{flox/+}$) showed mild looping phenotypes with medial left ventricle or malposed right ventricle (anterior or posterior) (Fig9a2 and a3). In double heterozygotes (*Notch3*$^{+/-}$; *Hoxb1*$^{Cre/+}$; *Nodal*$^{flox/+}$), we observed 40% of looping anomalies with medial left ventricle (Fig 9a4), isolated straight atrioventricular canal (Fig 9a5), and malposed right ventricle and a single embryo with anterior right ventricle. Furthermore, we also re-investigated previously collected *Nodal* heterozygotes (*Hoxb1*$^{Cre/+}$; *Nodal*$^{flox/+}$) and found posterior right ventricles in 2/10 cases (Fig 9a1). There is no obvious change in the distribution of phenotypes between *Notch3* single heterozygotes, *Nodal* single heterozygotes and *Notch3; Nodal* double heterozygotes. Thus, there is no evidence of genetic interaction between *Notch3* and *Nodal*.

An issue with the brightfield whole mount analysis is that it groups samples qualitatively into discrete groups. Therefore, we are now processing samples for 3D quantitative analysis of heart shape similarly to Desgrange et al., 2020. Embryos will be labelled by *in situ* hybridization with *Wnt11* and *Bmp2*, which mark the outflow tract and the atrioventricular canal, respectively. This labelling will guide the 3D segmentation of cardiac chambers after HREM imaging. Several parameters will be quantified, such as heart looping and cardiac chamber size, to conclude on differences between single and double heterozygotes.

As redundancy and compensation have been argued to mask the role of Notch3 (Hosseini-Alghaderi & Baron, 2020), we next aimed to develop an experimental system that would allow us to potentially circumvent Notch compensation.

Figure 9

A

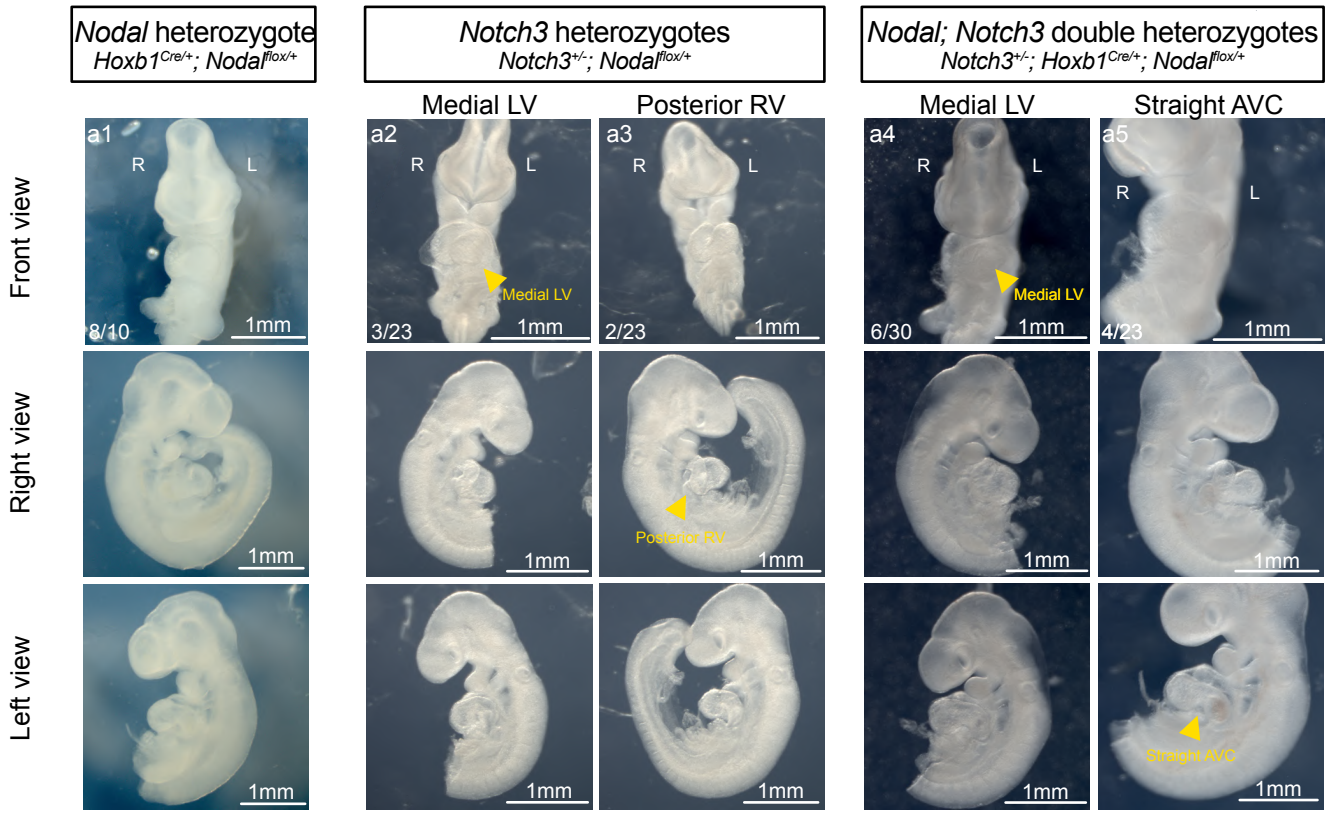

B

Phenotype

	Wildtype	*Nodal* heterozygote	*Notch3* heterozygote		*Notch3; Nodal* double heterozygote	*Notch3* homozygote
	Notch3$^{+/+}$; *Hoxb1*$^{+/+}$; *Nodal*$^{+/+}$	*Hoxb1*$^{cre/+}$; *Nodal*$^{flox/+}$	*Notch3*$^{+/-}$	*Notch3*$^{+/-}$; *Hoxb1*$^{+/+}$ *Nodal*$^{flox/+}$	*Notch3*$^{+/-}$; *Hoxb1*$^{Cre/+}$; *Nodal*$^{flox/+}$	*Notch3*$^{-/-}$
Regular shape	8 (89%)	8 (80%)	24 (65%)	15 (65%)	18 (60%)	16 (80%)
Straight AVC	0 (0%)	0 (0%)	0 (0%)	1 (4%)	4 (13%)	0 (0%)
Posterior RV	0 (0%)	2 (20%)	3 (8%)	2 (9%)	1 (3%)	0 (0%)
Posterior RV + straight AVC	0 (0%)	0 (0%)	0 (0%)	0 (0%)	0 (0%)	1 (5%)
Medial LV	0 (0%)	0 (0%)	7 (19%)	3 (13%)	6 (20%)	1 (5%)
Medial LV + Straight AVC	1 (11%)	0 (0%)	3 (8%)	1 (4%)	0 (0%)	0 (0%)
Anterior RV	0 (0%)	0 (0%)	0 (0%)	1 (4%)	1 (3%)	2 (10%)
Total embryos	9	10	37	23	30	20

Figure 9. Phenotype of *Notch3 ; Nodal* double heterozygotes.
(A) Brightfield images of E9.5 single or double heterozygote embryos for *Nodal* and *Notch3* knock-out. Embryos are shown in a front, right or left-sided view as indicated. Phenotype variations are illustrated: medial left ventricle (a2, a4), posterior right ventricle (a3) and straight AVC (a5). Numbers in the bottom left corner report the observed frequency. **(B)** Table summarizing the occurrence of phenotypes (lines) for the indicated genotypes (columns). AVC, atrioventricular canal; L, left; LV, left ventricle; R, right; RV, right ventricle

Supplementary figure 5 related to figure 9

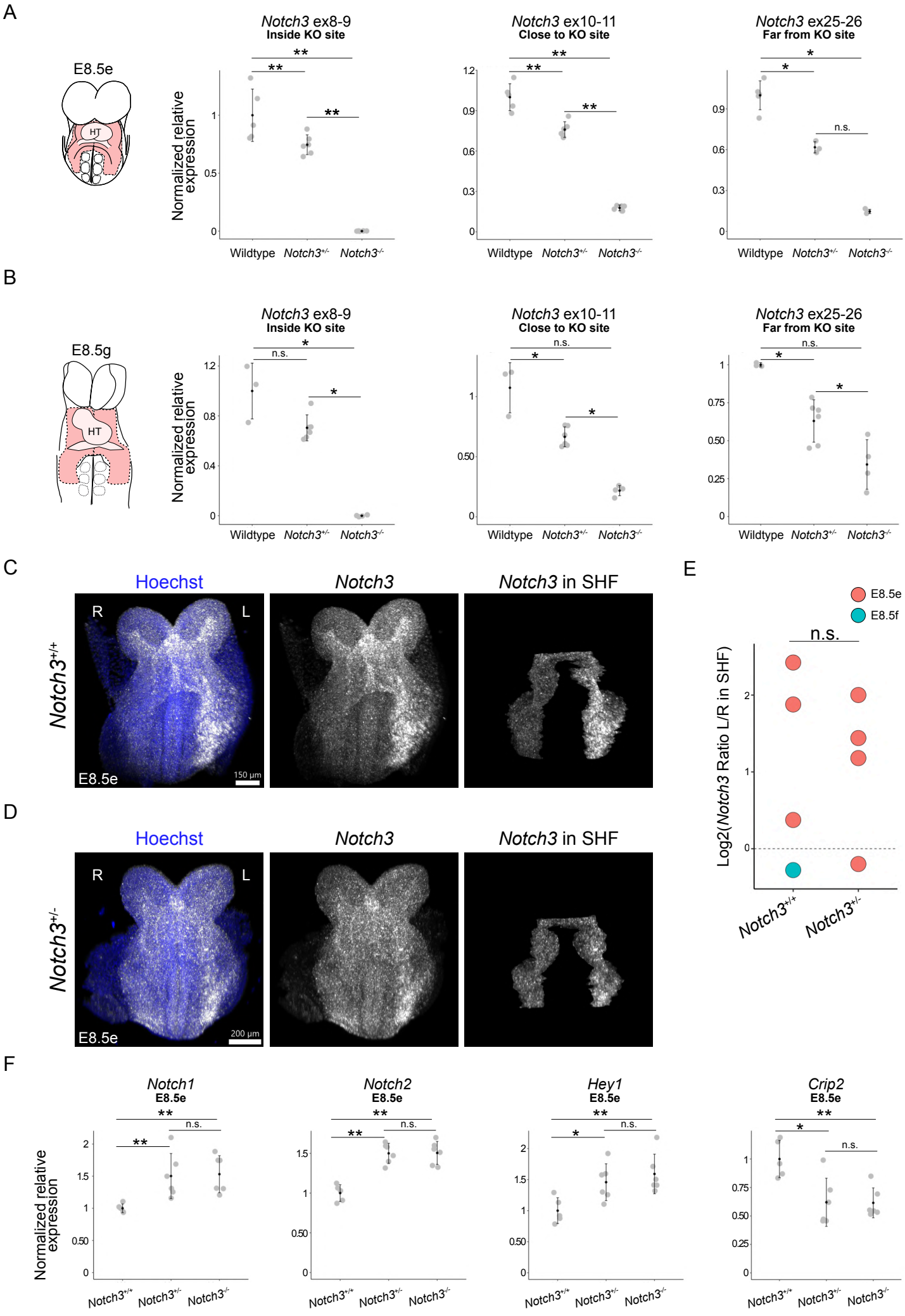

Figure S5 related to Fig. 9. Additional profiling of Notch3 heterozygote.
(A-B) Relative expression of *Notch3* in micro-dissected heart fields of wild-type (n=6 at E8.5e, 3 at E8.5g), *Notch3*$^{+/-}$ (n=6 except for E8.5 *ex25-26* n=3) and *Notch3*$^{-/-}$ (n=5 for *ex8-9* and *ex10-11* at E8.5e, n=3 for *ex25-26* at E8.5e, n=4 at E8.5g) embryos at stage E8.5e (A) and E8.5g (B), quantified by RT-qPCR using different primer pairs and normalized to wt. *p-value < 0.05, **p-value < 0.01 (two sided Mann Whitney test). Schema outline micro-dissected area and stage. Standard deviations and means are shown. **(C-D)** Whole-mount RNAscope ISH of *Notch3* in control (C) and *Notch3*$^{+/-}$ heterozygote (D) littermates at E8.5e. Expression of *Notch3* within the segmented heart field is extracted in right panels. **(E)** Corresponding quantification of *Notch3* left-right asymmetry in the second heart field (Wilcoxon two-sided test, n= [4, 4]). **(F)** Relative expression of *Notch1*, *Notch2*, *Hey1* and *Crip2* in micro-dissected heart fields of wild-type (n=6), *Notch3*$^{+/-}$ (n=5) and *Notch3*$^{-/-}$ (n=6) at stage E8.5e. *p-value < 0.05, **p-value < 0.01 (two sided Mann Whitney test). HT, heart tube; n.s., not significant.

Setting up conditions for lowering overall Notch signaling in *Notch3*$^{+/-}$ mutants to circumvent Notch compensation

As described earlier, the penetrance of heart looping defects is partial in *Notch3* mutants, and the phenotype is mild. Our analysis of Notch paralogue expression suggests that other Notch receptors may compensate for the absence of *Notch3*. To test this hypothesis and potentially reveal a stronger phenotype, we opted for a strategy validated in the zebrafish brain. *Notch3* heterozygote embryos were treated with a sub-phenotypic dose of Notch inhibition by γ-secretase inhibitors (Alunni et al., 2013). We first investigated the sub-phenotypic dosage of drugs in wild-type embryos using two different γ-secretase inhibitors (Olsauskas-Kuprys et al., 2013). In mouse embryo cultures, either DAPT or LY411575 was applied during the time window of *Notch3* asymmetric expression (E8.5c to g) and compared to controls treated with a corresponding volume of the adjuvant (DMSO). Embryos were then rinsed and grown in fresh media until 24h of overall culture (Fig 10A). DMSO controls showed varying degrees of development with various degrees of looping advancement (Fig 10B) The delay correlated with the stage at the start of the culture and with DMSO concentration, indicating potential toxicity of the adjuvant and delayed development in culture conditions.

At 25µM of DAPT and 1µM of LY411575, embryos looked similar to controls (Fig 10C). However, at 50µM of DAPT or at 5 and 10µM of LY411575, embryos had a striking phenotype of straight heart tubes, which is similar to *Mib1*$^{-/-}$ embryos (Barsi et al., 2005), a ubiquitin ligase necessary for the function of canonical Notch ligands. A summary of the results is reported in Fig 10D.

Thus, a sub-phenotypic dose has been identified in wildtype embryos for both DAPT and LY411575. We are now testing sub-phenotypic doses in *Notch3* heterozygote embryos to identify whether this will trigger heart looping defects.

Figure 10

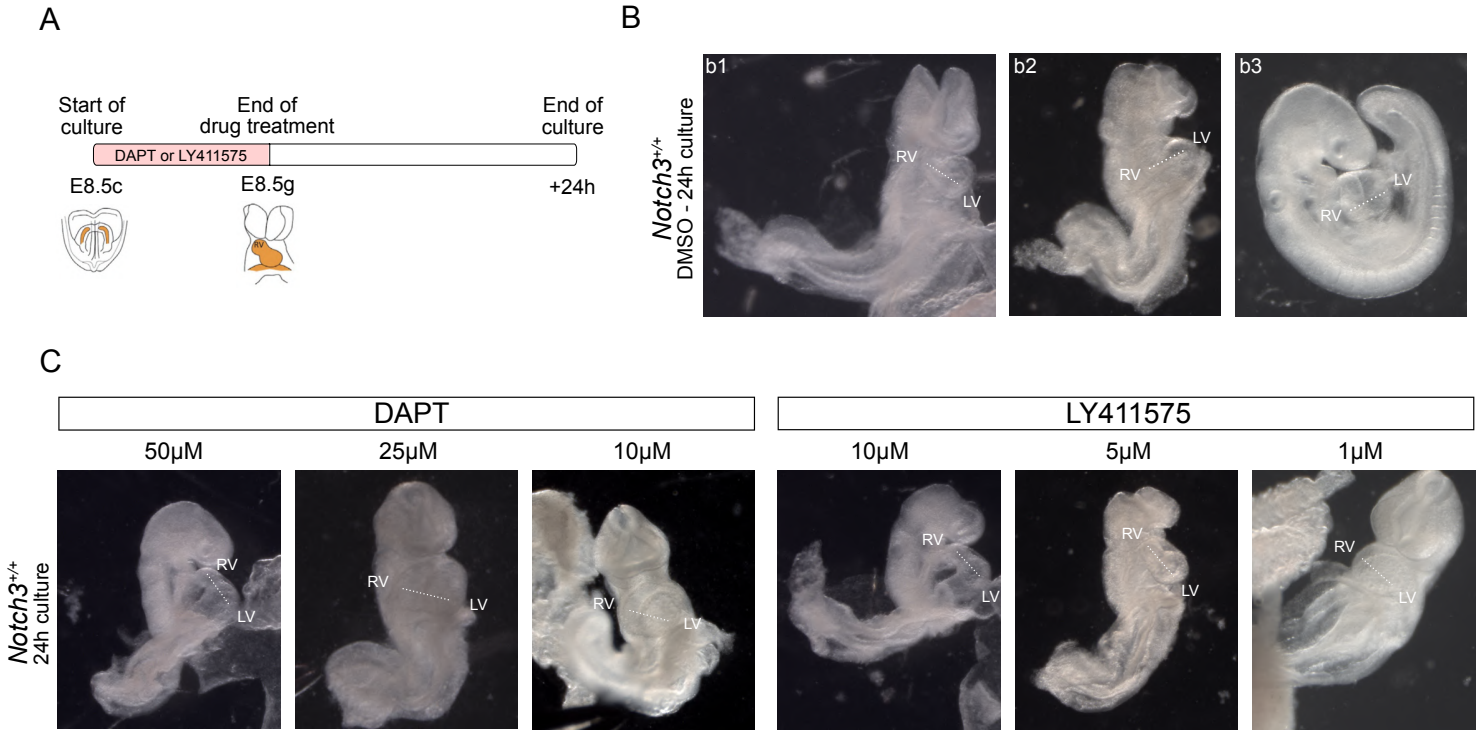

D

Drug	Concentration	Normal heart looping	Abnormal or straight tube
DMSO		6 (100%)	0 (0%)
DAPT	50μM	0 (0%)	3 (100%)
	25μM	4 (100%)	0 (0%)
	10μM	4 (80%)	1 (20%)
LY411575	10μM	1 (50%)	1 (50%)
	5μM	0 (0%)	3 (100%)
	1μM	2 (100%)	0 (0%)

Figure 10. Establishing a sub-phenotypic dosage of gamma-secretase inhibition in embryo culture.

(A) Experimental schema for dampening overall Notch signaling by treatment with γ-secretase inhibitors in embryo cultures, during the stages of *Notch3* asymmetry. **(B)** Brightfield images of three (b1-b3) control wild-type embryos treated with the adjuvant (DMSO), shown after 24h of culture. **(C)** Brightfield images of wild-type embryos treated with either DAPT or LY411575 at the indicated concentrations. **(D)** Table summarizing the phenotypes observed after 24h of culture. LV, left ventricle; RV, right ventricle.

Discussion

During the work of this PhD thesis, we developed new tools to identify novel asymmetrically expressed genes and to quantify their kinetics. We performed a bulk-RNA sequencing of left- and right heart progenitors at seven different stages morphological stages within the same day, and we developed imaging- and analyzing pipelines to validate candidates from this screen. From newly identified asymmetrically expressed genes, *Notch3* was validated and characterized in details. We show that *Notch3* is widely expressed at low levels, but transiently enriched in the left lateral plate mesoderm, including the second heart field, prior to heart looping. This upregulation is controlled by *Nodal*, as in the absence of *Nodal* in the lateral plate mesoderm, *Notch3* asymmetry is strongly reduced. This provides the first direct molecular evidence of Nodal as an amplifier of asymmetry. To look further into this, we explored if *Nodal* and *Notch3* are genetically interacting by generating *Nodal*; *Notch3* double heterozygotes, however we did not detect a change or increase in phenotypes.

We have observed that a target gene shown in the fish brain to be downstream of Notch3, *Hey1*, is asymmetrically expressed and overlaps with *Notch3* in left cardiac progenitors. Yet, its asymmetric expression in the second heart field is controlled by *Nodal* rather than *Notch3*.

Analyses of *Notch3*$^{-/-}$ mutant mice indicate that Notch3 is required for heart morphogenesis. The absence of *Notch3* affects heart looping at E9.5, as well as heart septation, myocardium and coronary size at birth. The right ventricle is more often impacted at both stages. We have found that *Notch3* heterozygotes, which have a 32% reduction in *Notch3* levels, may also display heart defects indicating haploinsufficiency. The mild mutant phenotypes of *Notch3* mutants and their partial penetrance raise the question of whether there is compensation by other Notch paralogue receptors in the absence of *Notch3*. In regards to this, we have found that *Notch1* and *Notch2* are more highly expressed in different cardiac tissues compared to *Notch3*, however *Notch2* is also expressed at low levels in the lateral plate mesoderm, thus overlapping with *Notch3*. Furthermore we show that *Notch3* is the only asymmetric Notch receptor. In *Notch3*$^{-/-}$ mutants, *Notch1* and *Notch2,* along with classical Notch target genes *Hey1* and *Hey2* as well as the Notch3 target from the fish brain *Atp1a1* are upregulated, indicating compensatory expression. However, the expression pattern of *Notch1/2* does not

change in *Notch3*$^{-/-}$ mutants and in particular remains symmetric. Finally, we have established conditions to overcome compensation by paralogue Notch receptors and will assess if this worsens heart looping defects.

There have been two main lines during the PhD: (1) the establishment of transcriptomics screens to identify left-right differences in heart progenitors and (2) the characterization of Notch3 as a novel asymmetric factor involved in heart morphogenesis. In this discussion, both lines will be considered and put into perspectives.

Advantages, limitations and perspective of the left-right RNA bulk sequencing approach

The identification of *Notch3* as a novel asymmetric gene has validated our screening strategy, which is based on paired analysis of micro-dissected and morphologically staged single embryos in combination with RNA sequencing technology optimized for small samples.

There have been previous reports of left-right transcriptomics screens which have investigated left-right transcriptional asymmetries in the developing mouse embryos. For instance, *Ablim1* was detected as a left-sided signal in such a screen (Stevens et al., 2010). However, in the micro-array transcriptomic analysis performed by Stevens et al., they identified only 18 left-sided and 14 right-sided differentially expressed genes, which is less compared to what we found (e.g. at stage E8.5d, the stage with the most differentially expressed genes, we identified 79 left-sided and 132 right-sided genes). Similarly, one of the other successful left-right asymmetry gene expression screens have also been done through using stage matched embryos in combination with precise dissections to explore left-right differences in the dorsal mesentery of the gut in the chick (Welsh et al., 2013, 2015).

Using RNA sequencing is a great approach to identify novel pathways asymmetrically expressed, as it is genome-wide and does not need the sequences of the targets *a priori*. However, it does not show the full picture. For instance, Rago et al., have shown that there are asymmetrically expressed miRNA in the heart progenitors, and these would not be detected through RNA sequencing approaches targeting mRNA (Rago et al., 2019).

Additionally, proteins in the extracellular matrix, which have been shown to regulate both heart- and gut looping, can be regulated on several levels. This is for instance illustrated by the glycosaminoglycan hyaluronan. Hyaluronan has been shown to be involved in the rotation of the gut, where it expands on the right side of the dorsal mesentery driving looping. However, it is not the hyaluronan gene that is upregulated on the right, rather it is its modifier *Tsg6*, which then drives hyaluronan expansion (Sivakumar et al., 2018). This shows that it is not only mRNA that can be asymmetric, but also small RNAs and posttranslational modification.

A way to systematically investigate changes in extracellular matrix composition between the left and right heart progenitors at different stages of heart looping would be to perform a screen of the proteomic composition through e.g. a mass spectrometry approach in a similar manner as we performed the left-right bulk RNA sequencing screen. Even though the tissue is small, recent advances are allowing mass spectrometry to identify the protein composition of single cells, thus it should be possible to perform a screen with enough resolution to identify left-right differences (Budnik et al., 2018).

One caveat of a screen looking at left-right asymmetries is that they assume that mRNA and proteins must be asymmetrically distributed to drive asymmetric morphogenesis, however this is not always the case. As shown in the fly, myosin proteins can drive rotations of organs in direction just through being chiral (Lebreton et al., 2018), and as such they do not need to be asymmetrically expressed. This might also be relevant in the heart tube. Although 3D modeling has shown that the sequential opposite asymmetries at the two poles of the tube along with buckling is sufficient to generate the rightwards helix (le Garrec et al., 2017), some evidence points towards the fact that the heart tube has an intrinsic capacity to curve, i.e. that not all asymmetry is driven by differences between the left- and right heart field. Isolated heart tubes grown in cultures will form a C-shape, which may be linked to an intrinsic cell chirality (Ray et al., 2018). If this is relevant for heart looping *in vivo* is not understood yet.

Albeit the above text describes the limitations of the left-right screen and the transcriptomics approach, it is still important to point out that the screen performed during this thesis work has identified many new asymmetrically expressed genes, which will lead to many new projects within the lab and likely in the end provide a better understanding of left-right asymmetric heart morphogenesis. A particularly interesting analysis to perform will be to

identify clusters of genes showing similar asymmetry kinetics (in a manner similar to what was done in (Soldatov et al., 2019) for developmental trajectories). And there are many interesting questions, e.g.: will genes within these clusters have common gene regulatory elements? Which pathways will they belong to? Will they display similar characteristics?

As a final note, a similar left-right bulk sequencing screen could be performed in the *Nodal* mutant. From this it would be possible to filter genes whose asymmetry is dependent or not on *Nodal*. Furthermore, it would help us understand Nodal biases the random generators of asymmetry, i.e. the buckling mechanism in the heart.

An expected challenge of this is that we expect these random generators to have random orientation in the absence of Nodal signaling. I.e., in some samples these genes would be asymmetrically expressed on the left, while in some other samples they would be asymmetrically expressed towards the right, and as such we would require a high number of observations. Furthermore, there are two independent asymmetries occurring at each end of the pole, and we expect that Nodal signaling will affect the arterial pole progenitors independently of the venous pole progenitors.

In my opinion, a better approach for studying the effects of missing *Nodal* in different heart progenitor populations would be to perform single cell RNA sequencing of heart progenitors in *Nodal* controls versus -mutants. This would allow to assess the effect that the absence of Nodal has on anterior and posterior progenitors (similarly to what was done for *Hand2* in heart progenitors of mutants versus controls in (de Soysa et al., 2019)).

This can be complicated by the lower sequencing quality of single cell RNA sequencing. From published single cell RNA sequencing of heart progenitors (de Soysa et al., 2019; Pijuan-Sala et al., 2019), it was not possible in our hands to extract information on left-right asymmetry or to go further into the patterning of the heart precursors. On a technical note, we need to overcluster heart progenitors before they separated into anterior- and posterior second heart field, and no matter how strongly we clustered the heart progenitors, we were never able to separate into left and right (which are marked by *Nodal*, *Lefty2* and *Pitx2*). Thus, our left-right RNA bulk sequencing approach with higher sequencing coverage and -depth was stronger in identifying novel left-right asymmetry genes. However, in the case of how single genes and signaling (like *Nodal*) affects one population, single cell RNA sequencing would be more appropriate.

Mesp1-Cre is an appropriate driver to explore single cell heterogeneity in second heart field progenitors

Although we ended up prioritizing the bulk RNA sequencing approach, conditions for performing single cell RNA sequencing were established during the thesis work. During the establishment of conditions, we also characterized cre-drivers to be used for FACS prior to single cell RNA sequencing. As shown in *Results – Fig. 1*, $Mesp1^{Cre}$; $R26^{mTmG}$ labels ~ 99 % of cells in the second heart field.

The characterization of *Mesp1* as a driver for cre-recombination prior to single cell RNA sequencing of heart progenitors is important, because it has been used in several single cell RNA sequencing papers (Lescroart et al., 2018; Zhang et al., 2021). This is in contrast to e.g. (de Soysa et al., 2019; Tyser et al., 2021), who did not use FACS prior to single cell RNA sequencing to avoid losing for cells of interest. This is particularly important, as using *Mesp1* as a driver comes with a risk. At adult stages, only 70% of heart cells are derived from *Mesp1*-expressing cells (Ragni et al., 2017), which leads to the possibility that some cell types are not including in this approach. However, Ragni et al. shows that the structures derived from the second heart field (such as the right ventricle and the atria) show very few non-labelled cells. This, in combination with the data presented in this thesis, suggests that *Mesp1-Cre* labels most second heart field cells, and is as such an appropriate marker for exploring heterogeneity in this population during early heart development.

The role of asymmetric *Notch3* in heart looping

From our analysis of the 3D heart structure in $Notch3^{-/-}$ mutants, we have found that 58.3% (7/12) displayed heart defects. 5/7 had ventricular septal defects, which are associated with defects in laterality (A. E. Lin et al., 2014), however ventricular septal defects can also arise without laterality defects, for instance through improper development of the septum (Lamers & Moorman, 2002). We also observed one instance of an enlarged coronary artery, which is fitting with the fact that Notch3 has been shown to regulate the formation of these arteries (Volz et al., 2015), which is in agreement with the role of Notch in vascularization in among other the brain (Domenga et al., 2004) and the retina (Liu et al., 2010).

Furthermore, several of the defects we identify in *Notch3*$^{-/-}$ are related to the right ventricle, for instance the mal-positioning at E9.5 and the thinning of the myocardium at P0. Fitting with that Notch3 could regulate proper formation of the right ventricle, we also found that one marker of cardiomyocyte formation (*Actc1*) was downregulated in the heart fields of *Notch3* mutants. It will be interesting to examine proliferation rate and the localization of markers of cardiomyocyte differentiation in *Notch3*$^{-/-}$ to investigate if they have defects.

At E9.5 20% of *Notch3*$^{-/-}$ embryos display an abnormal heart looping shape, showing that there is partial penetrance of heart defects in *Notch3* mutants at several stages in development. However, we are not able to draw conclusions on whether heart looping defects are the cause of ventricular septal defects, as it would require determining the phenotype of the *Notch3*$^{-/-}$ at E9.5 in the uterus and correlate it with cardiac defects observed at late gestational stages. The host lab has developed an imaging pipeline for phenotyping laterality defects at E9.5 and correlating this with heart defects at E18.5 (Desgrange et al., 2019), however with the subtle defects of *Notch3*$^{-/-}$ mutants at E9.5, an analysis like this is not possible, by lack of resolution of ultrasound imaging.

That the penetrance is partial reflects what has been shown for other Notch pathway mutants. For instance in *Hes1*$^{-/-}$ mutants, 38% display dextraposed aortas at E15.5 (with 75% of these showing ventricular septal defects) (Rochais et al., 2009), while in *Hey1*$^{-/-}$; *Heyl*$^{-/-}$ double mutants, between 21-82% of newborns showed ventricular septal defects (depending on the degree of inbreeding) (Fischer et al., 2007). All *Hey2*$^{-/-}$ have cardiac defects, albeit they vary from ventricular septal defects, Tetralogy of Fallot to enlarged heart (Donovan et al., 2002; Gessler et al., 2002). Similarly, inactivation of Notch signaling in all *Is1l*-derived cells also leads to cardiac defects (including ventricular septal defects) in all pups (High et al., 2009). Although the penetrance varies, it is interesting to note they all display ventricular septal defects similar to *Notch3* mutants.

Some Notch pathway mutants, like the *Heyl* and *Hey1* single mutants, do not display cardiac defects, while the *Hey1*; *Heyl* double mutants do, which shows that there is redundancy. Furthermore, because there is a difference in which types of phenotypes that arise (ranging from septal defects in *Hes1* mutants to enlarged hearts in *Hey2* mutants), it shows that there are potentially several mechanisms for how Notch signaling mutants can develop heart defects, and we are currently exploring how Notch3 is regulating this.

We have found that in the heart fields of *Notch3*$^{-/-}$, several Notch pathway genes and classical targets were upregulated (*Notch1, Notch2, Hey1, Hey2* and *Atp1a1*). Furthermore, we found that *Crip2, Nexn* and *Actc1* were downregulated. It is initially surprising to see increased expression of classical targets in a Notch pathway mutant, however it is likely due to compensation stemming from *Notch1* and *Notch2* upregulation (Potential mechanisms of compensation is discussed in *Discussion – Transcriptional adaptation as a potential compensation mechanisms*).

Due to the partial penetrance as well as potential compensation, understanding the roles of *Notch3* in heart progenitors is not trivial. This is further complicated by the lack of knowledge of specific targets of *Notch3* in cardiac cells, and the lack of tool to monitor *Notch3* signaling, such as N3ICD antibody or a specific reporter line. Additionally, *Notch3* has been shown to be able to both promote differentiation and promote stemness and quiescence (see *Introduction – Notch3*). One observation points against *Notch3* as a promoter of stemness in heart progenitors: *Hey1* is not positively regulated by *Notch3*, which is unlike known systems in which Notch3 promotes stemness (Sahu et al., 2021; Than-Trong et al., 2018). In contrast, gain-of-function of Notch3 by overexpression of *Notch3 intracellular domain* in cell cultures of airway epithelial ductal cells, in which Notch3 acts as a promoter of differentiation, leads to lowered expression of *Crip2* and *Nexn*, i.e. the contrary to what would be predicted from our loss-of-function observations (Bodas et al., 2021). Bodas et al., also observe that *Hey1*, *Hey2* and *Heyl* are all upregulated upon overexpression of *Notch3 intracellular domain*. This differences pinpoints that we need to study the role of *Notch3* in the heart progenitors in a cell specific context

To better understand how the absence of *Notch3* can lead to congenital heart defects (and to relate this to left-right asymmetry), there is a need to explore the cellular effects of *Notch3* in heart progenitors. As redundancy with Notch paralogues might obscure effects in *Notch3*$^{-/-}$ mutants, another strategy is to study overexpression of *Notch3* instead, or better; activation of Notch3 activity. Overexpression is less likely to be camouflaged by redundancy. For instance, an inducible *Notch3-intracellular domain* line was generated in (Lafkas et al., 2013), and using this, it was shown that activation of Notch3 signaling induces a quiescent stage in

mammary gland cells. However, it is believed that the expression of truncated *Notch intracellular domains* at non-physiological relevant high levels might circumvent the endogenous specificity of the respective Notch paralogues intracellular domains (Alunni et al., 2013). This, in combination with the fact that there are multiple Notch receptors present in the cardiogenic tissue at E8.5, could lead to observation of non-specific roles of Notch signaling in heart progenitors.

A way to circumvent this would be to generate a mouse line, where the levels of Notch3 activity is controllable. One possibility would be to have the expression of the *Notch3 intracellular domain* under the control of the doxycycline-inducible Tet-On promoter, where the levels of *Notch3 intracellular domain* is dependent on the dose of added doxycycline (Das et al., 2016). In such a context, changes in gene regulation could be studied at different levels of induction, and furthermore, it would help to investigate how specific the Notch3 intracellular domain is. It would be particularly interesting to explore if there is a difference between the targets regulated at high or low levels of *Notch3 intracellular domain*, and to identify targets that are dose-responsive.

However, such a project would take considerable time to perform, particularly if planned to do *in vivo*. A less complicated way to explore the role of Notch3 in heart progenitors would be to use a cardioid system, where organoids grown in 3D cell culture as clusters of cells are differentiated from pluripotent stage to cardiomyocytes (Hofbauer et al., 2021). Cardioids have been shown to form epicardium, myocardium and endocardium as well as self-organize into layers. Using a system like this to explore the effects of *Notch3* up- or downregulation during the cardiac progenitor stage of the protocol would be particularly useful to explore the role of *Notch3*. For instance, looking at which genes depend on Notch3 and examining if there will be the changes to the organoids would be key experiments to gain insight into the role of *Notch3*.

Beyond the left heart progenitors, we have found that *Notch3* is asymmetrically expressed throughout the whole left lateral plate mesoderm as well as in the node crown cells (see *Results – Fig. 3*). We have not formally shown that *Notch3* asymmetric expression amplified by *Nodal* in the node crown cells (as our *Nodal* mutant is conditional and only lacks *Nodal* in the lateral plate mesoderm).

There have been reports of asymmetric Notch pathway expression (*Dll1* and *Lfng*) in the Hensen's node of the chicken, but here it was argued that these were upstream of *Nodal* asymmetry in the crown cells (Raya et al., 2004), similarly to how Notch has been shown to be upstream of Nodal in the mouse (Przemeck et al., 2003). Furthermore, the pattern of *Dll1* and *Lfng* asymmetric expression in the Hensen's node of the chick is different compared to *Nodal* and *Notch3*, where the shape of *Dll1* and *Lfng* asymmetric expression is due to they extend further anteriorly on the left than on the right (See *Introduction - Fig 20*). This expression pattern could be related to the counter clockwise cell movements in Hensen's node (Gros et al., 2009), and it shows that finding Notch3 asymmetry in the node is a novel discovery.

But what about other Notch pathway components? We have found that *Hey1* asymmetry in the lateral plate mesoderm is regulated by *Nodal* in a *Notch3* independent manner, and it will be interesting to explore if *Hey1* is also asymmetrically expressed in the crown cells of the node and if this is dependent on *Notch*- or *Nodal* signaling.

It was surprising to us that *Hey1* asymmetry is independent of *Notch3*, as *Hey1* was reported as a target of *Notch3* in other tissues (Bodas et al., 2021; Sahu et al., 2021). Rather *Hey1* is upregulated in *Notch3*$^{-/-}$ mutants. This can be an indirect effect of compensatory *Notch1/2* upregulation and thus does not infer that *Hey1* is directly negatively regulated by *Notch3*. *Hes*- and *Hey* genes are classical targets of the Notch signaling pathway, however it has been found in cancer cell culture that TGF-β signaling through P-Smad2 (which is the same signal transducer used by *Nodal*) can directly induce *Hey1* in a Notch independent manner (Zavadil et al., 2004).

How *Nodal* then restricts *Hey1* expression to heart progenitors (in contrast to *Lefty2, Pitx2* and *Notch3*, which are expressed throughout the lateral plate mesoderm) is unknown, and it means that other factors beyond Nodal regulated *Hey1* expression. And although *Hey1*$^{-/-}$ mutants are viable (Fischer et al., 2004b), *Hey1* has been shown to inhibit myogenesis through forming heterodimers with the myogenic transcriptional factor MyoD (Buas et al., 2010). If *Hey1* has a similar role in heart progenitors as a repressor of cardiomyocyte formation is not known, however *Nodal* has been shown to regulate cardiomyocyte differentiation (Desgrange et al., 2020), and it remains to be tested if this regulation is dependent on *Hey1*. Additionally, *Hey1* has been explored in the context of the heart, where it is important for patterning the chambers (reviewed in MacGrogan et al., 2018). This is among others due to mutual

repression of *Bmp2*. Bmp signaling has been reported to be right-sided during heart development (Ocaña et al., 2017; Rago et al., 2019), and it remains to be tested if this right-sided Bmp signaling is dependent on *Hey1* e.g. through *Hey1* repression Bmp on the left side.

In Rago et al. it was shown that Bmp signaling is regulated by *Nodal* through miRNA (Rago et al., 2019). This might be relevant, as neither *Hey1* nor *Notch3* are predicted to have an ASE binding site near their promoter according to the bioinformatic analysis performed in (Desgrange et al., 2020). Furthermore, *Notch3* has been shown to be regulated by miRNA from the miR-106a-363 supercluster in the context of heart injury (J. H. Jung et al., 2021). In particular, *miR363* is interesting, as it was bioinformatically predicted by Rago et al., to be a candidate for asymmetric regulation of gene expression (Rago et al., 2019).

How *Nodal* regulates *Notch3* is relevant, as we find that initiation of *Notch3* asymmetry is not dependent on *Nodal* (in the lateral plate mesoderm). Rather *Nodal* is important for amplifying *Notch3* in the left lateral plate mesoderm, providing molecular evidence of *Nodal* as an amplifier of asymmetry on a molecular level. However, it is possible that *Notch3* is still dependent on symmetry breaking in the node to become left-sided. As mentioned, the conditional *Nodal* mutant we employ (*Hoxb1*^{Cre}; *Nodal*$^{flox/nul}$), still have a functioning left-right organizer, and it remains to be tested if Notch3 is still left-sided in e.g. the *Dnah11*^{iv} mouse mutant, which have a non-functioning node due to immotile cilia (McGrath et al., 2003). For instance, *Ablim1* has been reported to be still left-sided or absent in mutants without *Nodal* in the lateral plate mesoderm, while its expression is randomized in the *Dnah11*^{iv} mouse mutant (Stevens et al., 2010). It will be interesting to explore if Notch3 display a similar pattern.

Is the *Notch3*^{tm1Grid} allele a true null allele?

It was initially surprising that when we tried to predict genes regulated by *Notch3* (through our bioinformatical correlation analysis in combination with literature review. See *Results – Fig. 7+8*), we have not been able to validate many of these. Furthermore, the genes which we validated to be differentially expressed in heart progenitors of *Notch3*$^{+/+}$ versus *Notch3*$^{-/-}$ were behaving contrary to expected (i.e. the classical Notch pathway targets *Hey1, Hey2* and *Atp1a1* were upregulated instead of downregulated, and genes anti-correlated with *Notch3* - *Crip2*,

Nexn and *Actc1* - were downregulated instead of upregulated). This made us wonder if the *Notch3*^{tm1Grid} was a true null allele.

As described in the introduction, *Notch3* has 33 exons. In the *Notch3*^{tm1Grid} mouse mutant, exon 6-8 are removed (See *Results – Fig S4F*) (Krebs et al., 2003). These encode EGF-like repeats 10-13, and it is argued that since EGF-like repeat 11-12 are essential for the function of *Notch* in the fly and *Notch1* in human (Rebay et al., 1991), this should also be the case for *Notch3* (which is not necessarily true and should be tested). Krebs et al. validated their knockout using southern-, northern- and a western blot (using an antibody against Notch3 intracellular domain), however antibodies against Notch3 are notoriously complicated to use, which made us question if the *Notch3*^{tm1Grid} is a true null allele for *Notch3*. In particular this question was raised as it had previously been shown for *Notch2* that a hypomorph allele (*Notch2*^{tm1Grid}) was generated instead of true null allele, because of alternative splicing around the knockout site (McCright et al., 2001). Additionally, we found that in *Notch3*$^{-/-}$, there was still 21.7% transcript left, leaving the option that these might generate some functional Notch3 protein. This is relevant, as for instance the Notch intracellular domain is derived from a portion of the transcript.

Beyond the *Notch3*^{tm1Grid} mouse mutant, there are also two other reported null alleles; the *Notch3*^{tm1Khan} (Kitamoto et al., 2005) and the *Notch3*$^{tm1.1(KOMP)Vlcg}$ (Dickinson et al., 2016) (as described in *Introduction – Notch3*). Several evidence suggest that they are all true null alleles. First, for all of the alleles, antibodies against Notch3 intracellular domain are not able to detect any signal in homozygote mutants. Secondly, homozygote mutants for all three alleles are viable and fertile and have a healthy appearance (similarly to what we have found). (Canalis et al., 2021; Kitamoto et al., 2005; Krebs, Xue, et al., 2003). Thirdly, Notch reporter line and phenotypes related to arterial defects in *Notch3*^{tm1Grid} mouse mutant can be rescued by human *NOTCH3* (and even by human *NOTCH3* with CADASIL mutations, as CADASIL mutations are not functional knockouts) (Monet et al., 2007). Fourthly, the Notch3 mutants alleles have been shown to have phenotypes in a range of tissues - the *Notch3*^{tm1Grid}: differentiation defects in the arteries of the tail and brain (Domenga et al., 2004), the arteries of the retina (Liu et al., 2010), the kidney (Boulos et al., 2011) and coronary arteries (Volz et al., 2015) as well as in the airway epithelium (Li et al., 2009; Morimoto et al., 2012) and the spinal chord (Rusanescu & Mao, 2014); the *Notch3*^{tm1Khan}: quiescence in muscles (Kitamoto & Hanaoka, 2010) and the brain (Kawai et al., 2017); and the *Notch3*$^{tm1.1(KOMP)Vlcg}$: inhibition of

osteogenesis (Canalis et al., 2021). Unfortunately, the different alleles have not been investigated for the same phenotype, however given overall similar properties, it suggests that the *Notch3*^{tm1Grid} is a true null allele.

Summary of potential Notch pathway compensation in the heart fields of *Notch3*$^{-/-}$ mutants

From the studies conducted in this thesis, *Notch3* was found to be the only asymmetric Notch receptor in the heart progenitors at E8.5. *Notch4* is not expressed at this stage, while *Notch1* and *Notch2* are present in the cardiac progenitors, albeit their expression is left-right symmetric. *Notch2* and *Notch3* are widely expressed, while *Notch1* is restricted to the endocardium, the dorsal aortas and the sinus venosus (see *Results – Figure 6* and *Supplementary Figure 4*).

Because the heart defects observed at E9.5 and P0 are not fully penetrant in *Notch3*$^{-/-}$ mice, we hypothesized that this can either occur from two possibilities: 1) In the absence of *Notch3*, there is compensation by other Notch receptors which mitigates the effects of lacking *Notch3* or 2) the role of *Notch3* in heart progenitors is rather involved in a fine-tuning mechanism, meaning that the lack of *Notch3* would potentially only lead to mild defects without full penetrance.

In concordance with option 1, we found by qPCR that in the heart fields of *Notch3*$^{-/-}$, *Notch1/2* are upregulated at stage E8.5e (the stage after *Notch3* asymmetry peak), indicating potential compensation. However, when we examined the expression of *Notch1* and *Notch2* in *Notch3*$^{-/-}$ embryos at E8.5 using RNAscope staining and 3D imaging at E8.5d-f, neither *Notch1* nor *Notch2* had different expression patterns compared to wild-type mice, meaning that *Notch1* was still not expressed in the second heart field and *Notch2* expression in the second heart field was still symmetric.

This challenges the idea of compensation, because for compensation to occur, the compensating Notch receptors must be present where the missing Notch3 receptors are absent. However, RNAscope measures RNA transcript, and thus is not a readout of activity, but since we are unfortunately not able to measure the activity of Notch2 due to lack of appropriate tools, it is currently not possible to examine if Notch2 signaling becomes asymmetric in the *Notch3*$^{-/-}$.

Notch3 haploinsufficiency

We have found that *Notch3* heterozygotes display heart phenotypes with partial penetrance at both E9.5 and at P0 (3 out of 4 examined *Notch3*$^{+/-}$ hearts showed defects), which was unexpected given the low partial of heart defects in *Notch3*$^{-/-}$ mutants (20% at E9.5, 58.3% at P0) under the assumption that there is compensation in *Notch3*$^{-/-}$. At E9.5, 35% of *Notch3*$^{+/-}$ were shown to have an abnormal shape, but compared to the *Notch3*$^{-/-}$ mutants, the *Notch3*$^{+/}$ displayed a lower number of the most severe phenotype, the anterior right ventricle. Furthermore, we show that in the heart fields of *Notch3*$^{+/-}$ that *Notch1* and *Notch2* are upregulated compared to wildtype to similar levels of expression as observed in *Notch3*$^{-/-}$. Similarly, *Hey1* and *Crip2* show intermediate values between the wild-type and homozygote mutants, confirming that also on gene regulatory level, *Notch3*$^{+/-}$ are affected. Together, these data indicate that *Notch3* heterozygotes display intermediate phenotypes between wild-type and homozygous *Notch3* mutants.

That *Notch3* displays haploinsufficiency is reminiscent of the historic context, as the *Notch* gene name refers to the haploinsufficient phenotype observed in *Drosophila* (as homozygous Notch mutant is embryonic lethal) (Dexter, 1914; Morgan, 1917). Similarly, when looking at the mode of function of the Notch pathway (see *Introduction – Notch signaling*), there is no secondary messenger or signal amplification between the receptor and the Notch transcriptional complex, which means that the pathway will be sensitive to changes in dosage (Guruharsha et al., 2012).

Notch pathway components have been shown to display haploinsufficiency in the mouse and human. The most severe is the ligand *Dll4*, where heterozygous Dll4 mouse embryos display embryonic lethality (Krebs et al., 2004). In humans, heterozygosity of either *NOTCH2* or *JAG1* can lead to Alagille syndrome (L. Li et al., 1997; Mcdaniell et al., 2006), and *Jag1*$^{+/-}$ heterozygous mice have been shown to display some of the characteristics of the disease along with other phenotypes, such as a reduced number of cells division in neuronal progenitor cells (Blackwood et al., 2020).

Regarding *Notch3* role in vascularization, it has been reported that the retinal vasculature is similar between wildtype and *Notch3*$^{+/-}$ heterozygotes (whereas the branching is strongly reduced in *Notch3*$^{-/-}$ mutants) (H. Liu et al., 2010). However, when the *Notch3*$^{+/-}$ heterozygote has been examined for gene expression or Notch pathway activity in the retina or the cerebral

vasculature, it has been found that the *Notch3*$^{+/-}$ heterozygotes display intermediate expression levels between wildtype and *Notch3*$^{-/-}$ mutants (H. Liu et al., 2018; Monet et al., 2007). And it seems that *Notch3*$^{+/-}$ heterozygotes are sensitized, as for instance in mouse models of diabetes (diabetes is associated with retinopathy/loss of sight), the absence of one *Notch3* allele leads to more severe defects in the vasculature of the retina (H. Liu et al., 2018).

That the lack of Notch pathway components can lead to a higher sensitivity in diseases fits with the role of the Notch pathway in tissue regulation and homeostasis. This has also been explored in the heart, where haploinsufficiency of *Notch1* has been shown to increase the penetrance and severity of cardiac defects in for instance disease models of ascending aorta aneurysms and in mice with endothelial defects (Koenig et al., 2016, 2017). Koenig et al. also reported that *Notch1*$^{+/-}$ heterozygotes mice will develop aortic root dilation (which is related to ascending aorta aneurysm) at around 9 months if they are in the 129S6 background, indicating that the sensitivity to Notch component dosages is dependent on other genetic factors.

Returning to the observations of this thesis, it is still surprising that *Notch3* shows haploinsufficiency given that the penetrance of the *Notch3*$^{-/-}$ homozygous mutant is low (although it could be due to the targets of Notch3 are sensitive to reduction of dosage). Our data suggest compensation expression of Notch*1* and *Notch2*, however if the expression of these also lead to compensation mechanisms is not yet understood. However, if compensation mechanisms are present and they can rescue 80% of *Notch3*$^{-/-}$ at E9.5, how come they are not able to fully rescue defects in *Notch3*$^{+/-}$, where we find that there is still 67.9% of *Notch3* transcript remaining? This can be related to how compensation mechanisms function.

Transcriptional adaptation as a potential compensation mechanism

Our data indicate that there is compensation expression ongoing due to that in both *Notch3*$^{+/-}$ and in *Notch3*$^{-/-}$, there is an upregulation of *Notch1* and *Notch2* at stage E8.5e (the stage after *Notch3* asymmetry peak) as well as increased Notch activity (measured by *Hey1*, *Hey2* and *Atp1a1* expression increase), and these could potentially lead to a compensation mechanism.

Work in the lab of Didier Stainier has explored how organisms can compensate for genetic perturbations, and they have described a mechanism with they call transcriptional adaptation,

where mutations leading to mRNA degradation will induce the transcription of genes with similar sequences (termed adaptor genes) which will then be able to compensate (Sztal & Stainier, 2020). It was initially described in zebrafish, where morpholino knockdown have sometimes been found to have a more severe defect than knockout of the gene. This has been initially attributed to the fact that morpholinos can have off-target effects, however when Rossi et al. investigated the gene *egfl7*, they found that only *egfl7*$^{-/-}$ mutants (and not morpholino knockdown of *egfl7*) had increased expressed on genes with similar sequences (Rossi et al., 2015). These findings were later extended to mouse cells, and it was also found that alleles that undergo mRNA degradation show a higher degree of transcriptional adaptation (El-Brolosy et al., 2019). Although several mechanisms for transcriptional adaptation have been described, it is argued that mRNA degradation (through e.g. mechanism like non-mediated decay) is required for transcriptional adaptation (Sztal & Stainier, 2020).

We have found that *Notch3* expression levels are decreased in *Notch3* mutants which indicates no transcription or degradation. Furthermore, our data suggests that it is mRNA from the *Notch3* mutant allele that specifically not present in the cells, as qPCR experiments in *Notch3*$^{+/-}$ heterozygotes show similar expression levels for primers targeting both inside- and outside the deleted region (meaning that remaining mRNA in *Notch3*$^{+/-}$ is predominantly from the *Notch3* wildtype allele). This is in line with our findings that compensation is induced in both *Notch3* heterozygous and -homozygous mutants.

We were not able to detect any change of expression pattern of *Notch1* and *Notch2* in *Notch3*$^{-/-}$ mutants (for instance, *Notch2* remained symmetrically expressed in the second heart field in the absence of *Notch3*). No change for *Notch1/2/4* in *Notch3* mutants has been reported before (Kitamoto et al., 2005), and furthermore *Notch3* is widely expressed, so we would expect most cells to undergo transcriptional adaptation.

If the reason why *Notch3*$^{-/-}$ display a partial penetrance of defects is due to transcriptional adaptation mechanisms, understanding the role of *Notch3* in heart looping in *Notch3*$^{-/-}$ mutants will be complicated (as the roles of *Notch3* are obscured). For this reason, we have selected to perform the gamma-secretase inhibition in *Notch3*$^{+/-}$ to potentially reveal a stronger phenotype.

Already from the experiments to establish the conditions of drug treatment in embryo culture (See *Results – Fig. 10*), we have found one interesting observation. Wildtype embryos

treated with a high dosage of gamma-secretase inhibitor will display a straight heart tube (or in some cases, an abnormal heart tube) along with a shorter tail. These embryos phenocopy *Mib1*$^{-/-}$ and *Rbpj*$^{-/-}$ mutants (Barsi et al., 2005; Oka, Nakano, Wakeham, de la Pompa, et al., 1995; Souilhol, Cormier, Tanigaki, et al., 2006), where the defects in heart looping have been attributed to prior defects in the left-right organizer leading to laterality defects (Raya et al., 2003). At the stage where we begin our embryo culture (E8.5c), *Nodal* is already left-sided (Desgrange et al., 2020) and as such not dependent on a functional left-right organizer anymore (Nonaka et al., 2002). This indicates that Notch signaling (beyond the left-right organizer) can lead to severe heart looping defects.

Contributions of the thesis work to the molecular understanding of what drives heart looping

During this PhD thesis, two screens of left-right asymmetric genes in the heart field across multiple stages were performed, which lead to the identifications of many new potential asymmetric genes. From these screens, *Notch3* was selected for future validation and its expression was mapped in time and space. Furthermore, its left-right asymmetry dynamics were quantified and shown to be dependent on *Nodal*. A classic Notch pathway target, *Hey1*, was also found to be asymmetrically expressed at similar stages, however its asymmetry is dependent on *Nodal* rather than *Notch3*, and its asymmetry is only in the anterior lateral plate mesoderm (Figure 1A).

Both asymmetries are present at stage E8.5d and absent by E8.5f, which is the stage where the arterial pole rotation of the heart tube occurs, one of the first major morphological asymmetries of the embryo, indicating that *Notch3* and *Hey1* could play roles in directing heart looping prior to onset of looping. In accordance with this, 20% of *Notch3*$^{-/-}$ develop heart looping defects at E9.5 and 58% display cardiac defects at P0. These are the main findings of the PhD work, and they have been summarized in Figure 1A. However, the mechanism of how *Notch3* in the heart progenitors regulates proper cardiogenesis is still not understood and will be the subject of future studies.

Beyond *Notch3*, *Hey1* and the Nodal signaling pathway, other genes and signaling pathways have also been shown to be asymmetric in the heart progenitors. The expression pattern of some of these are shown in Figure 1B. Some of these, like *Six2*, are well studied – the

populations they contribute to has been mapped and experiments have been performed to understand their cellular effects (Zhou et al., 2017). Others, like *Ablim1*, are less characterized (Stevens et al., 2010).

In the left-right bulk sequencing screen, 447 different genes were identified to be candidates of asymmetric expression (the term *candidate* is used, as they should be validated using methods like what has been performed in this thesis). At the stage with the highest number of asymmetric candidates (E8.5d), more than 200 genes were identified. It remains to be explored how all these genes, which belong to many different pathways and have a very diverse range of function, are directing the complicated 3D process of heart looping.

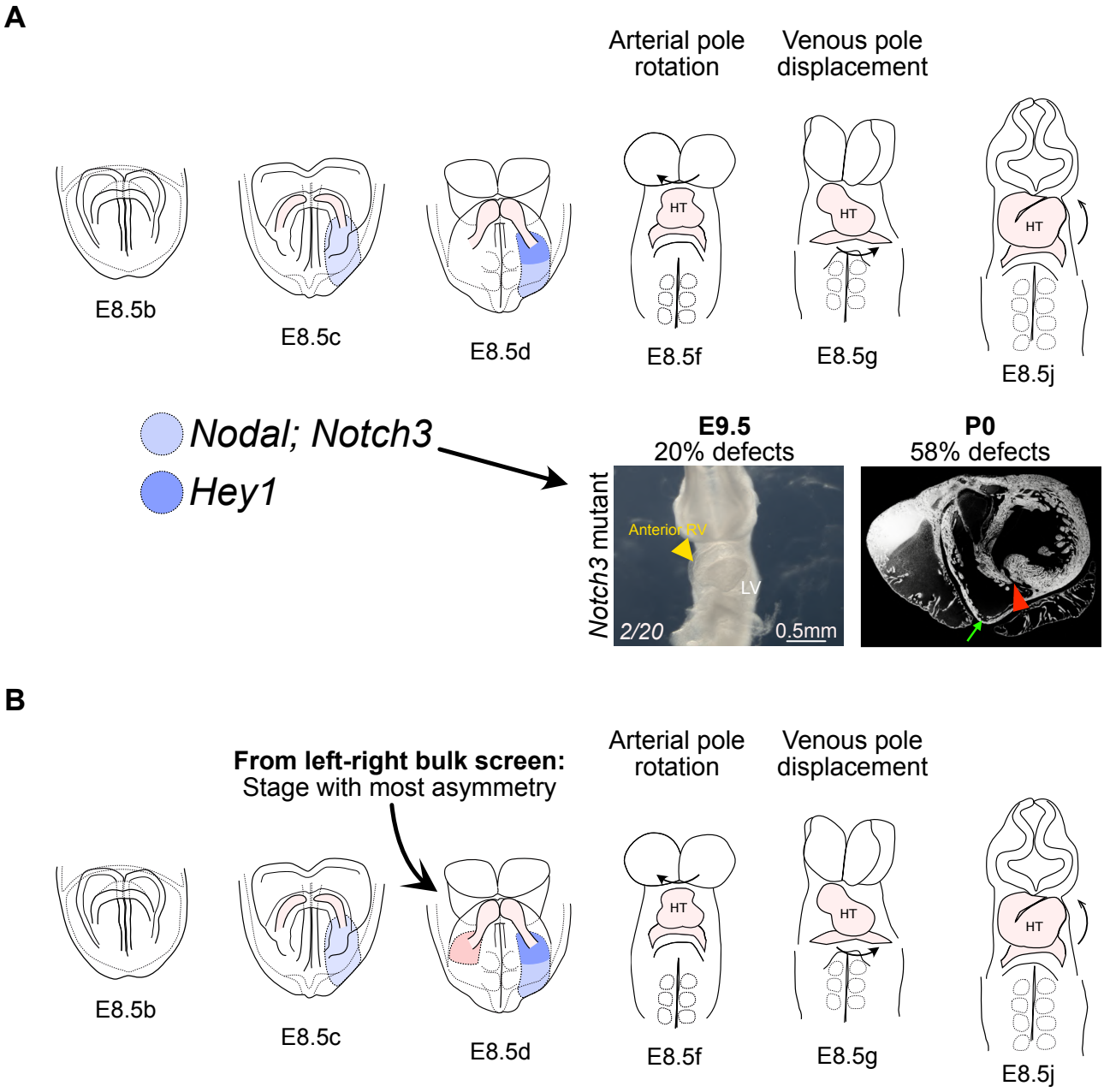

Figure 1. Summary of asymmetric signal during heart looping. (A) Main contributions of the thesis work to our understanding of heart looping. *Notch3* and *Hey1* were found the left-sided asymmetric at heart looping stages just prior to the arterial pole rotation, with Notch3 being asymmetric in the full lateral plate mesoderm, while *Hey1* asymmetry is restricted to the anterior lateral plate mesoderm. From investigations of the Notch3 mutant, 20% heart looping defects were found at E9.5, while at P0, 58% of mutants display congenital heart defects. **(B)** Expression pattern of some of the asymmetric genes and signals which have been identified in the litterature. Some genes, like *Pitx2*, *Six2* and *Mmp9* are also asymmetric at later stages, however this has not been indicated on the figure.

Conclusions and Perspectives

The underlying idea which drove the four years of work presented in this thesis was to identify novel genes and pathways, which could drive asymmetric heart morphogenesis, as we had recognized that many of these were not yet explored. We tackled this through a transcriptomics screen that we designed in a manner to be able to carefully explore the kinetics of left-right asymmetry in the heart progenitors during heart looping.

This screen was successful, as we identified novel asymmetrically expressed candidate genes, and the last two years of the thesis were spent of characterizing one of these candidates, the Notch receptor *Notch3*. We explored its spatiotemporal expression, its relationship to the left determinant Nodal and if the absence of *Notch3* could lead to heart defects. From these experiments we show that *Notch3* is asymmetrically expressed on the left, that its asymmetry in enhanced by Nodal (but that *Notch3* is still asymmetric in the absence of *Noda*l, providing the first molecular evidence of Nodal as an amplifier of asymmetry) and that in the absence of *Notch3*, cardiac defects arise with partial penetrance at embryonic and neonatal stages.

Moving beyond this, we are now exploring how the absence of *Notch3* can lead to cardiac defects. Is the partial penetrance due to compensation by other Notch receptors? What are the cellular roles of Notch3? How can Notch signaling drive asymmetric organogenesis, and is this also related to lateralized organs other than the heart?

Returning to the transcriptomics screen, we have generated a valuable tool to explore left-right asymmetry in the early formation of the heart, which will lead to several new studies. Similarly, to what has been done for Notch3, there will be other asymmetric genes to characterize. Furthermore, it will be interesting to explore genes with similar kinetics. Are these genes, which do not necessarily need to belong to the same pathway, responsible for driving specific aspects of heart looping? As asymmetric heart morphogenesis is related to cardiac defects, these questions are of great interest.

Bibliography

Aburjania, Z., Jang, S., Whitt, J., Jaskula-Stzul, R., Chen, H., & Rose, J. B. (2018). The Role of Notch3 in Cancer . *The Oncologist*, *23*(8), 900–911. https://doi.org/10.1634/theoncologist.2017-0677

Adachi, H., Saijoh, Y., Mochida, K., Ohishi, S., Hashiguchi, H., Hirao, A., & Hamada, H. (1999). *Determination of left/right asymmetric expression of nodal by a left side-specific enhancer with sequence similarity to a lefty-2 enhancer*. www.genesdev.org

Alunni, A., Krecsmarik, M., Bosco, A., Galant, S., Pan, L., Moens, C. B., & Bally-Cuif, L. (2013). Notch3 signaling gates cell cycle entry and limits neural stem cell amplification in the adult pallium. *Development (Cambridge)*, *140*(16), 3335–3347. https://doi.org/10.1242/dev.095018

Andersen, P., Uosaki, H., Shenje, L. T., & Kwon, C. (2012). Non-canonical Notch signaling: Emerging role and mechanism. In *Trends in Cell Biology* (Vol. 22, Issue 5, pp. 257–265). https://doi.org/10.1016/j.tcb.2012.02.003

Andersson, E. R., Sandberg, R., & Lendahl, U. (2011). Notch signaling: Simplicity in design, versatility in function. In *Development* (Vol. 138, Issue 17, pp. 3593–3612). https://doi.org/10.1242/dev.063610

Baeten, J. T., & Lilly, B. (2015). Differential regulation of NOTCH2 and NOTCH3 contribute to their unique functions in vascular smooth muscle cells. *Journal of Biological Chemistry*, *290*(26), 16226–16237. https://doi.org/10.1074/jbc.M115.655548

Bardot, E., Calderon, D., Santoriello, F., Han, S., Cheung, K., Jadhav, B., Burtscher, I., Artap, S., Jain, R., Epstein, J., Lickert, H., Gouon-Evans, V., Sharp, A. J., & Dubois, N. C. (2017). Foxa2 identifies a cardiac progenitor population with ventricular differentiation potential. *Nature Communications*, *8*. https://doi.org/10.1038/ncomms14428

Barsi, J. C., Rajendra, R., Wu, J. I., & Artzt, K. (2005). Mind bomb1 is a ubiquitin ligase essential for mouse embryonic development and Notch signaling. *Mechanisms of Development*, *122*(10), 1106–1117. https://doi.org/10.1016/j.mod.2005.06.005

Belo, J. A., Marques, S., & Inácio, J. M. (2017). The role of cerl2 in the establishment of left-right asymmetries during axis formation and heart development. In *Journal of Cardiovascular Development and Disease* (Vol. 4, Issue 4). MDPI. https://doi.org/10.3390/jcdd4040023

Bertrand, N., Roux, M., Ryckebüsch, L., Niederreither, K., Dollé, P., Moon, A., Capecchi, M., & Zaffran, S. (2011). Hox genes define distinct progenitor sub-domains within the second heart field. *Developmental Biology*, *353*(2), 266–274. https://doi.org/10.1016/j.ydbio.2011.02.029

Bessodes, N., Haillot, E., Duboc, V., Röttinger, E., Lahaye, F., & Lepage, T. (2012). Reciprocal Signaling between the Ectoderm and a Mesendodermal Left-Right Organizer Directs Left-Right Determination in the Sea Urchin Embryo. *PLoS Genetics*, *8*(12). https://doi.org/10.1371/journal.pgen.1003121

Blackwood, C. A., Bailetti, A., Nandi, S., Gridley, T., & Hébert, J. M. (2020). Notch Dosage: Jagged1 Haploinsufficiency Is Associated With Reduced Neuronal Division and Disruption of Periglomerular Interneurons in Mice. *Frontiers in Cell and Developmental Biology*, *8*. https://doi.org/10.3389/fcell.2020.00113

Blum, M., & Ott, T. (2018). Animal left–right asymmetry. *Current Biology*, *28*(7), R301–R304. https://doi.org/10.1016/j.cub.2018.02.073

Bodas, M., Subramaniyan, B., Moore, A. R., Metcalf, J. P., Ocañas, S. R., Freeman, W. M., Georgescu, C., Wren, J. D., & Walters, M. S. (2021). The notch3 downstream target heyl is required for efficient human airway basal cell differentiation. *Cells*, *10*(11). https://doi.org/10.3390/cells10113215

Bone, R. A., Bailey, C. S. L., Wiedermann, G., Ferjentsik, Z., Appleton, P. L., Murray, P. J., Maroto, M., & Kim Dale, J. (2014). Spatiotemporal oscillations of notch1, Dll1 and NICD are coordinated across the mouse PSM. *Development (Cambridge)*, *141*(24), 4806–4816. https://doi.org/10.1242/dev.115535

Boskovski, M. T., Yuan, S., Pedersen, N. B., Goth, C. K., Makova, S., Clausen, H., Brueckner, M., & Khokha, M. K. (2013). The heterotaxy gene GALNT11 glycosylates Notch to orchestrate cilia type and laterality. *Nature*, *504*(7480), 456–459. https://doi.org/10.1038/nature12723

Boulos, N., Helle, F., Dussaule, J. C., Placier, S., Milliez, P., Djudjaj, S., Guerrot, D., Joutel, A., Ronco, P., Boffa, J. J., & Chatziantoniou, C. (2011). Notch3 is essential for regulation of the renal vascular tone. *Hypertension*, *57*(6), 1176–1182. https://doi.org/10.1161/HYPERTENSIONAHA.111.170746

Bourane, S., Méchaly, I., Venteo, S., Garces, A., Fichard, A., Valmier, J., & Carroll, P. (2007). A SAGE-based screen for genes expressed in sub-populations of neurons in the mouse dorsal root ganglion. *BMC Neuroscience*, *8*. https://doi.org/10.1186/1471-2202-8-97

Bray, S. J. (2006). Notch signalling: A simple pathway becomes complex. In *Nature Reviews Molecular Cell Biology* (Vol. 7, Issue 9, pp. 678–689). https://doi.org/10.1038/nrm2009

Bray, S. J. (2016). Notch signalling in context. *Nature Reviews Molecular Cell Biology*, *17*(11), 722–735. https://doi.org/10.1038/nrm.2016.94

Brennan, J., Norris, D. P., & Robertson, E. J. (2002). Nodal activity in the node governs left-right asymmetry. *Genes and Development*, *16*(18), 2339–2344. https://doi.org/10.1101/gad.1016202

Brown, N. A., & Wolpert, L. (1990). The development of handedness in left/right asymmetry. *Development*, *109*, 1–9.

Buas, M. F., Kabak, S., & Kadesch, T. (2010). The notch effector Hey1 associates with myogenic target genes to repress myogenesis. *Journal of Biological Chemistry*, *285*(2), 1249–1258. https://doi.org/10.1074/jbc.M109.046441

Buckingham, M., Meilhac, S., & Zaffran, S. (2005). Building the mammalian heart from two sources of myocardial cells. In *Nature Reviews Genetics* (Vol. 6, Issue 11, pp. 826–835). https://doi.org/10.1038/nrg1710

Budnik, B., Levy, E., Harmange, G., & Slavov, N. (2018). SCoPE-MS: mass spectrometry of single mammalian cells quantifies proteome heterogeneity during cell differentiation. *Genome Biology*, *19*(1). https://doi.org/10.1186/s13059-018-1547-5

Cai, C. L., Liang, X., Shi, Y., Chu, P. H., Pfaff, S. L., Chen, J., & Evans, S. (2003). Isl1 identifies a cardiac progenitor population that proliferates prior to differentiation and contributes a majority of cells to the heart. *Developmental Cell*, *5*(6), 877–889. https://doi.org/10.1016/S1534-5807(03)00363-0

Canalis, E., Zanotti, S., Schilling, L., Eller, T., & Yu, J. (2021). Activation of Notch3 in osteoblasts/osteocytes causes compartment-specific changes in bone remodeling. *Journal of Biological Chemistry*, *296*. https://doi.org/10.1016/j.jbc.2021.100583

Carraro, G., Mulay, A., Yao, C., Mizuno, T., Konda, B., Petrov, M., Lafkas, D., Arron, J. R., Hogaboam, C. M., Chen, P., Jiang, D., Noble, P. W., Randell, S. H., McQualter, J. L., & Stripp, B. R. (2020). Single-cell reconstruction of human basal cell diversity in normal and idiopathic pulmonary fibrosis lungs. *American Journal of Respiratory and Critical Care Medicine*, *202*(11), 1540–1550. https://doi.org/10.1164/rccm.201904-0792OC

Castel, D., Mourikis, P., Bartels, S. J. J., Brinkman, A. B., Tajbakhsh, S., & Stunnenberg, H. G. (2013). Dynamic binding of RBPJ is determined by notch signaling status. *Genes and Development*, *27*(9), 1059–1071. https://doi.org/10.1101/gad.211912.112

Cheng, S. K., Olale, F., Brivanlou, A. H., & Schier, A. F. (2004). Lefty blocks a subset of TGFβ signals by antagonizing EGF-CFC coreceptors. *PLoS Biology*, *2*(2). https://doi.org/10.1371/journal.pbio.0020030

Cinquin, O. (2007). Understanding the somitogenesis clock: What's missing? In *Mechanisms of Development* (Vol. 124, Issues 7–8, pp. 501–517). https://doi.org/10.1016/j.mod.2007.06.004

Collignon, J., Varlet, I., & Robertson, E. J. (1996). Relationship between asymmetric nodal expression and the direction of embryonic turning. *Nature*, *381*, 155–158.

Collins, M. M., Maischein, H.-M., Dufourcq, P., Charpentier, M., Blader, P., & Stainier, Y. R. (2018). Pitx2c orchestrates embryonic axis extension via mesendodermal cell migration. *ELife*. https://doi.org/10.7554/eLife.34880.001

Coumailleau, F., Fürthauer, M., Knoblich, J. A., & González-Gaitán, M. (2009). Directional Delta and Notch trafficking in Sara endosomes during asymmetric cell division. *Nature*, *458*(7241), 1051–1055. https://doi.org/10.1038/nature07854

Coutelis, J.-B., Gonzalez-Morales, N., Geminard, C., & Noselli, S. (2014). Diversity and convergence in the mechanisms establishing L/R asymmetry in metazoa. *EMBO Reports*, *15*(9), 926–937. https://doi.org/10.15252/embr.201438972

Cui, C., Little, C. D., & Rongish, B. J. (2009). Rotation of organizer tissue contributes to left-right asymmetry. *Anatomical Record*, *292*(4), 557–561. https://doi.org/10.1002/ar.20872

D'Amato, G., Luxán, G., del Monte-Nieto, G., Martínez-Poveda, B., Torroja, C., Walter, W., Bochter, M. S., Benedito, R., Cole, S., Martinez, F., Hadjantonakis, A. K., Uemura, A., Jiménez-Borreguero, L. J., & de La Pompa, J. L. (2016). Sequential Notch activation regulates ventricular chamber development. *Nature Cell Biology*, *18*(1), 7–20. https://doi.org/10.1038/ncb3280

Das, A. T., Tenenbaum, L., & Berkhout, B. (2016). Tet-On Systems For Doxycycline-inducible Gene Expression. *Current Gene Therapy*, *16*, 156–167.

Davis, N. M., Kurpios, N. A., Sun, X., Gros, J., Martin, J. F., & Tabin, C. J. (2008). The Chirality of Gut Rotation Derives from Left-Right Asymmetric Changes in the Architecture of the Dorsal Mesentery. *Developmental Cell*, *15*(1), 134–145. https://doi.org/10.1016/j.devcel.2008.05.001

de Bellaing, A. M., Bonnet, D., & Houyel, L. (2021). Abnormal origin of the left pulmonary artery from the descending aorta and heterotaxy syndrome: An undescribed phenotypic association. *Cardiology in the Young*, *31*(7), 1193–1196. https://doi.org/10.1017/S1047951121002183

de Bono, C., Thellier, C., Bertrand, N., Sturny, R., Jullian, E., Cortes, C., Stefanovic, S., Zaffran, S., Théveniau-Ruissy, M., & Kelly, R. G. (2018). T-box genes and retinoic acid signaling regulate the segregation of arterial and venous pole progenitor cells in the murine second heart field. *Human Molecular Genetics*, *27*(21), 3747–3760. https://doi.org/10.1093/hmg/ddy266

de Chaumont, F., Dallongeville, S., Chenouard, N., Hervé, N., Pop, S., Provoost, T., Meas-Yedid, V., Pankajakshan, P., Lecomte, T., le Montagner, Y., Lagache, T., Dufour, A., & Olivo-Marin, J. C. (2012). Icy: An open bioimage informatics platform for extended reproducible research. In *Nature Methods* (Vol. 9, Issue 7, pp. 690–696). https://doi.org/10.1038/nmeth.2075

de Soysa, T. Y., Ranade, S. S., Okawa, S., Ravichandran, S., Huang, Y., Salunga, H. T., Schricker, A., del Sol, A., Gifford, C. A., & Srivastava, D. (2019). Single-cell analysis of cardiogenesis reveals basis for organ-level developmental defects. *Nature*, *572*(7767), 120–124. https://doi.org/10.1038/s41586-019-1414-x

de Zoysa, P., Liu, J., Toubat, O., Choi, J., Moon, A., Gill, P. S., Duarte, A., Sucov, H. M., & Kumar, S. R. (2020). Delta-like ligand 4-mediated Notch signaling controls proliferation of second heart field progenitor cells by regulating Fgf8 expression. *Development (Cambridge)*, *147*(17). https://doi.org/10.1242/dev.185249

Desgrange, A., le Garrec, J. F., Bernheim, S., Bønnelykke, T. H., & Meilhac, S. M. (2020). Transient Nodal Signaling in Left Precursors Coordinates Opposed Asymmetries Shaping the Heart Loop. *Developmental Cell*, *55*(4), 413-431.e6. https://doi.org/10.1016/j.devcel.2020.10.008

Desgrange, A., le Garrec, J.-F., & Meilhac, S. M. (2018). Left-right asymmetry in heart development and disease: forming the right loop. *Development*, *145*(22), dev162776. https://doi.org/10.1242/dev.162776

Desgrange, A., Lokmer, J., Marchiol, C., Houyel, L., & Meilhac, S. M. (2019). Standardised imaging pipeline for phenotyping mouse laterality defects and associated heart malformations, at multiple scales and multiple stages. *DMM Disease Models and Mechanisms*, *12*(7). https://doi.org/10.1242/dmm.038356

Dexter, J. S. (1914). The Analysis of a Case of Continuous Variation in Drosophila by a Study of its Linkage Relations. *The American Naturalist*, *48*(712–758), 712.

Dickinson, M. E., Flenniken, A. M., Ji, X., Teboul, L., Wong, M. D., White, J. K., Meehan, T. F., Weninger, W. J., Westerberg, H., Adissu, H., Baker, C. N., Bower, L., Brown, J. M., Brianna Caddle, L., Chiani, F., Clary, D., Cleak, J., Daly, M. J., Denegre, J. M., … Murakami, A. (2016). High-throughput discovery of novel developmental phenotypes. *Nature*, *537*(7621), 508–514. https://doi.org/10.1038/nature19356

Djenoune, L., Berg, K., Brueckner, M., & Yuan, S. (2022). A change of heart: new roles for cilia in cardiac development and disease. In *Nature Reviews Cardiology* (Vol. 19, Issue 4, pp. 211–227). Nature Research. https://doi.org/10.1038/s41569-021-00635-z

Dodou, E., Verzi, M. P., Anderson, J. P., Xu, S. M., & Black, B. L. (2004). Mef2c is a direct transcriptional target of ISL1 and GATA factors in the anterior heart field during mouse embryonic development. *Development*, *131*(16), 3931–3942. https://doi.org/10.1242/dev.01256

Dolk, H., Loane, M., & Garne, E. (2011). Congenital heart defects in Europe: Prevalence and perinatal mortality, 2000 to 2005. *Circulation*, *123*(8), 841–849. https://doi.org/10.1161/CIRCULATIONAHA.110.958405

Domenga, V., Fardoux, P., Lacombe, P., Monet, M., Maciazek, J., Krebs, L. T., Klonjkowski, B., Berrou, E., Mericskay, M., Li, Z., Tournier-Lasserve, E., Gridley, T., & Joutel, A. (2004). Notch3 is required for arterial identity and maturation of vascular smooth muscle cells. *Genes and Development*, *18*(22), 2730–2735. https://doi.org/10.1101/gad.308904

Domínguez, J. N., Meilhac, S. M., Bland, Y. S., Buckingham, M. E., & Brown, N. A. (2012). Asymmetric fate of the posterior part of the second heart field results in unexpected left/right contributions to both poles of the heart. *Circulation Research*, *111*(10), 1323–1335. https://doi.org/10.1161/CIRCRESAHA.112.271247

Donovan, J., Kordylewska, A., Jan, Y. N., & Utset, M. F. (2002). Tetralogy of Fallot and Other Congenital Heart Defects in Hey2 Mutant Mice. In *Current Biology* (Vol. 12).

Downs, K. M., & Davies, T. (1993). Staging of gastrulating mouse embryos by morphological landmarks in the dissecting microscope. *Development*, *118*, 1255–1666.

Duarte, A., Hirashima, M., Benedito, R., Trindade, A., Diniz, P., Bekman, E., Costa, L., Henrique, D., & Rossant, J. (2004). Dosage-sensitive requirement for mouse Dll4 in artery development. *Genes and Development*, *18*(20), 2474–2478. https://doi.org/10.1101/gad.1239004

El-Brolosy, M. A., Kontarakis, Z., Rossi, A., Kuenne, C., Günther, S., Fukuda, N., Kikhi, K., Boezio, G. L. M., Takacs, C. M., Lai, S. L., Fukuda, R., Gerri, C., Giraldez, A. J., & Stainier, D. Y. R. (2019). Genetic compensation triggered by mutant mRNA degradation. *Nature*, *568*(7751), 193–197. https://doi.org/10.1038/s41586-019-1064-z

Esteban, I., Schmidt, P., Desgrange, A., Raiola, M., Temiño, S., Meilhac, S. M., Kobbelt, L., & Torres, M. (2022). Pseudodynamic analysis of heart tube formation in the mouse reveals strong regional variability and early left–right asymmetry. *Nature Cardiovascular Research*, *1*(5), 504–517. https://doi.org/10.1038/s44161-022-00065-1

Fischer, A., & Gessler, M. (2007). Delta-Notch-and then? Protein interactions and proposed modes of repression by Hes and Hey bHLH factors. In *Nucleic Acids Research* (Vol. 35, Issue 14, pp. 4583–4596). Oxford University Press. https://doi.org/10.1093/nar/gkm477

Fischer, A., Schumacher, N., Maier, M., Sendtner, M., & Gessler, M. (2004). The Notch target genes Hey1 and Hey2 are required for embryonic vascular development. *Genes and Development*, *18*(8), 901–911. https://doi.org/10.1101/gad.291004

Fischer, A., Steidl, C., Wagner, T. U., Lang, E., Jakob, P. M., Friedl, P., Knobeloch, K. P., & Gessler, M. (2007). Combined loss of Hey1 and HeyL causes congenital heart defects because of impaired epithelial to mesenchymal transition. *Circulation Research*, *100*(6), 856–863. https://doi.org/10.1161/01.RES.0000260913.95642.3b

Franco Del Amo, F., Smith, D. E., Swiatek, P. J., Gendron-Maguire, M., Greenspan, R. J., McMahon, A. P., & Gridley, T. (1992). Expression pattern of Motch, a mouse homolog of Drosophila Notch, suggests an important role in early postimplantation mouse development. *Development*, *115*, 737–744.

Gabriel, G. C., & Lo, C. W. (2020). Left–right patterning in congenital heart disease beyond heterotaxy. *American Journal of Medical Genetics, Part C: Seminars in Medical Genetics*, *184*(1), 90–96. https://doi.org/10.1002/ajmg.c.31768

Gama-Norton, L., Ferrando, E., Ruiz-Herguido, C., Liu, Z., Guiu, J., Islam, A. B. M. M. K., Lee, S. U., Yan, M., Guidos, C. J., López-Bigas, N., Maeda, T., Espinosa, L., Kopan, R., & Bigas, A. (2015). Notch signal strength controls cell fate in the haemogenic endothelium. *Nature Communications*, *6*. https://doi.org/10.1038/ncomms9510

Garg, V., Muth, A. N., Ransom, J. F., Schluterman, M. K., Barnes, R., King, I. N., Grossfeld, P. D., & Srivastava, D. (2005). Mutations in NOTCH1 cause aortic valve disease. *Nature*, *437*(7056), 270–274. https://doi.org/10.1038/nature03940

George, R. M., Maldonado-Velez, G., & Firulli, A. B. (2020). The heart of the neural crest: Cardiac neural crest cells in development and regeneration. *Development*, *147*(20), 1–13. https://doi.org/10.1242/dev.188706

Gessler, M., Knobeloch, K.-P., Helisch, A., Amann, K., Schumacher, N., Rohde, E., Fischer, A., & Leimeister, C. (2002). Mouse gridlock: no aortic coarctation or deficiency, but fatal cardiac defects in Hey2 -/- mice. *Current Biology*, *12*, 1601–1604.

Grego-Bessa, J., Luna-Zurita, L., del Monte, G., Bolós, V., Melgar, P., Arandilla, A., Garratt, A. N., Zang, H., Mukouyama, Y. suke, Chen, H., Shou, W., Ballestar, E., Esteller, M., Rojas, A., Pérez-Pomares, J. M., & de la Pompa, J. L. (2007). Notch Signaling Is Essential for Ventricular Chamber Development. *Developmental Cell*, *12*(3), 415–429. https://doi.org/10.1016/j.devcel.2006.12.011

Gros, J., Feistel, K., Viebahn, C., Blum, M., & Tabin, J. C. (2009). Cell movements at Hensen's Node establish left/right asymmetric gene expression in the chick. *Science*, *324*(5929), 941–944. https://doi.org/10.1126/science.1172478

Guimier, A., Gabriel, G. C., Bajolle, F., Tsang, M., Liu, H., Noll, A., Schwartz, M., el Malti, R., Smith, L. D., Klena, N. T., Jimenez, G., Miller, N. A., Oufadem, M., de Bellaing, A. M., Yagi, H., Saunders, C. J., Baker, C. N., di Filippo, S., Peterson, K. A., … Gordon, C. T. (2015). MMP21 is mutated in human heterotaxy and is required for normal left-right asymmetry in vertebrates. *Nature Genetics*, *47*(11), 1260–1263. https://doi.org/10.1038/ng.3376

Guruharsha, K. G., Kankel, M. W., & Artavanis-Tsakonas, S. (2012). The Notch signalling system: Recent insights into the complexity of a conserved pathway. In *Nature Reviews Genetics* (Vol. 13, Issue 9, pp. 654–666). https://doi.org/10.1038/nrg3272

Hamada, H. (2020). Molecular and cellular basis of left-right asymmetry in vertebrates. In *Proceedings of the Japan Academy Series B: Physical and Biological Sciences* (Vol. 96, Issue 7, pp. 273–296). Japan Academy. https://doi.org/10.2183/PJAB.96.021

Hamada, Y., Kadokawa, Y., Okabe, M., Ikawa, M., Coleman, J. R., & Tsujimoto, Y. (1996). Mutation in ankyrin repeats of the mouse Notch2gene induces earlyembryonic lethalit. *Development*, *126*, 3415–3424.

Harvey, R. P. (2002). Patterning the vertebrate heart. *Nature Reviews Genetics*, *3*(7), 544–556. https://doi.org/10.1038/nrg843

Hermann, G. J., Leung, B., & Priess, J. R. (2000). Notch signaling and organ left-right asymmetry a LIN-12/Notch signaling pathway. *Development*, *127*, 3429–3440.

High, F. A., Jain, R., Stoller, J. Z., Antonucci, N. B., Min, M. L., Loomes, K. M., Kaestner, K. H., Pear, W. S., & Epstein, J. A. (2009). Murine Jagged1/Notch signaling in the second heart field orchestrates Fgf8 expression and tissue-tissue interactions during outflow tract development. *Journal of Clinical Investigation*, *119*(7), 1986–1996. https://doi.org/10.1172/jci38922

Hilton, E. N., Manson, F. D. C., Urquhart, J. E., Johnston, J. J., Slavotinek, A. M., Hedera, P., Stattin, E. L., Nordgren, A., Biesecker, L. G., & Black, G. C. M. (2007). Left-sided embryonic expression of the BCL-6 corepressor, BCOR, is required for vertebrate laterality determination. *Human Molecular Genetics*, *16*(14), 1773–1782. https://doi.org/10.1093/hmg/ddm125

Hofbauer, P., Jahnel, S. M., Papai, N., Giesshammer, M., Deyett, A., Schmidt, C., Penc, M., Tavernini, K., Grdseloff, N., Meledeth, C., Ginistrelli, L. C., Ctortecka, C., Salic, S., Novatchkova, M., & Mendjan, S. (2021). Cardioids reveal self-organizing principles of human cardiogenesis. *Cell*, *184*, 3299–3317.

Hori, K., Sen, A., & Artavanis-Tsakonas, S. (2013). Notch signaling at a glance. *Journal of Cell Science*, *126*(10), 2135–2140. https://doi.org/10.1242/jcs.127308

Hosseini-Alghaderi, S., & Baron, M. (2020). Notch3 in development, health and disease. In *Biomolecules* (Vol. 10, Issue 3). MDPI AG. https://doi.org/10.3390/biom10030485

Ishibashi, M., Ang, S.-L., Shiota, K., Nakanishi, S., Kageyama, R., & Guillemot, F. (1995). Targeted disruption of mammalian hairy and Enhancer of split homolog-1 (HES-1) of neural leads to up-regulation hehx-loop-.hellx factors, premature neurogenesls, and severe neural tube defects. *Genes & Development*, *9*, 3136–3148.

Ivanovitch, K., Temiño, S., & Torres, M. (2017). Live imaging of heart tube development in mouse reveals alternating phases of cardiac differentiation and morphogenesis. *ELife*, *6*, 1–30. https://doi.org/10.7554/elife.30668

Jaitin, D. A., Kenigsberg, E., Keren-Shaul, H., Elefant, N., Paul, F., Zaretsky, I., Mildner, A., Cohen, N., Jung, S., Tanay, A., & Amit, I. (2014). Massively Parallel Single-Cell RNA-Seq for Marker-Free Decomposition of Tissues into Cell Types. *Science*, *343*(6172), 776–779. https://doi.org/10.1126/science.1242747

Jia, G., Preussner, J., Chen, X., Guenther, S., Yuan, X., Yekelchyk, M., Kuenne, C., Looso, M., Zhou, Y., Teichmann, S., & Braun, T. (2018). Single cell RNA-seq and ATAC-seq analysis of cardiac progenitor cell transition states and lineage settlement. *Nature Communications*, *9*(1). https://doi.org/10.1038/s41467-018-07307-6

Jiang, X., Rowitch, D. H., Soriano, P., McMahon, A. P., & Sucov, H. M. (2000). Fate of the mammalian cardiac neural crest. *Development*, *127*, 1607–1616.

Joutel, A., Corpechot, C., Ducros, A., Vahedi, K., Chabriat, H., Mouton, P., Alamowitch, S., Domenga, V., Cécillion, M., Maréchal, E., Maciazek, J., Vayssiere, C., Cruaud, C., Cabanis, E.-A., Madeleine Ruchoux, M., Weissenbach, J., Bach, J. F., Germaine Bousser, M., & Tournier-Lasserve, E. (1996). Notch3 mutations in CADASIL, a hereditary adult-onset condition causing stroke and dementia. *Nature*, *383*, 707–710. http://www.nature.

Jung, J. G., Stoeck, A., Guan, B., Wu, R. C., Zhu, H., Blackshaw, S., Shih, I. M., & Wang, T. L. (2014). Notch3 Interactome Analysis Identified WWP2 as a Negative Regulator of Notch3 Signaling in Ovarian Cancer. *PLoS Genetics*, *10*(10). https://doi.org/10.1371/journal.pgen.1004751

Jung, J. H., Ikeda, G., Tada, Y., von Bornstädt, D., Santoso, M. R., Wahlquist, C., Rhee, S., Jeon, Y. J., Yu, A. C., O'brien, C. G., Red-Horse, K., Appel, E. A., Mercola, M., Woo, J., & Yang, P. C. (2021). miR-106a–363 cluster in extracellular vesicles promotes endogenous myocardial repair via Notch3 pathway in ischemic heart injury. *Basic Research in Cardiology*, *116*(1). https://doi.org/10.1007/s00395-021-00858-8

Jurand, A. (1974). Some aspects of the development of the notochord in mouse embryos. In *Embryol. exp. Morph* (Vol. 32).

Kajikawa, E., Horo, U., Ide, T., Mizuno, K., Minegishi, K., Hara, Y., Ikawa, Y., Nishimura, H., Uchikawa, M., Kiyonari, H., Kuraku, S., & Hamada, H. (2020). Nodal paralogues underlie distinct mechanisms for visceral left–right asymmetry in reptiles and mammals. *Nature Ecology and Evolution*, *4*(2), 261–269. https://doi.org/10.1038/s41559-019-1072-2

Katoh, M., & Katoh, M. (2007). Notch signaling in gastrointestinal tract. *International Journal of Oncology*, *30*, 247–251.

Katoh, T. A., Omori, T., Mizuno, K., Sai, X., Ikawa, Y., Nishimura, H., Itabashi, T., Kajikawa, E., Iwane, A. H., Ishikawa, T., Okada, Y., Nishizaka, T., & Hamada, H. (2022). Immotile cilia of the mouse node sense a fluid flow-induced mechanical force for left-right symmetry breaking. *BioRxiv*. https://doi.org/10.1101/2022.04.11.487968

Kaufman, M. H., & Navaratnam, V. (1981). Early differentiation of the heart in mouse embryos. *J. Anat*, *133*(2), 235–246.

Kawai, H., Kawaguchi, D., Kuebrich, B. D., Kitamoto, T., Yamaguchi, M., Gotoh, Y., & Furutachi, S. (2017). Area-specific regulation of quiescent neural stem cells by Notch3 in the adult mouse subependymal zone. *Journal of Neuroscience*, *37*(49), 11867–11880. https://doi.org/10.1523/JNEUROSCI.0001-17.2017

Kelly, R. G., Brown, N. A., & Buckingham, M. E. (2001). The Arterial Pole of the Mouse Heart Forms from Fgf10-Expressing Cells in Pharyngeal Mesoderm. *Developmental Cell*, *1*, 435–440.

Kelly, R. G., Buckingham, M. E., & Moorman, A. F. (2014). Heart fields and cardiac morphogenesis. *Cold Spring Harbor Perspectives in Medicine*, *4*(10), 1–10. https://doi.org/10.1101/cshperspect.a015750

Khoshnood, B., Lelong, N., Houyel, L., Thieulin, A. C., Jouannic, J. M., Magnier, S., Delezoide, A. L., Magny, J. F., Rambaud, C., Bonnet, D., & Goffinet, F. (2012). Prevalence, timing of diagnosis and mortality of newborns with congenital heart defects: A population-based study. *Heart*, *98*(22), 1667–1673. https://doi.org/10.1136/heartjnl-2012-302543

Kim, J. D., Kim, H. J., Koun, S., Ham, H. J., Kim, M. J., Rhee, M., & Huh, T. L. (2014). Zebrafish crip2 plays a critical role in atrioventricular valve development by downregulating the expression of ECM genes in the endocardial cushion. *Molecules and Cells*, *37*(5), 406–411. https://doi.org/10.14348/molcells.2014.0072

Kinder, S. J., Tsang, T. E., Quinlan, G. A., Hadjantonakis, A.-K., Nagy, A., & Tam, P. P. L. (1999). The orderly allocation of mesodermal cells to the extraembryonic structures and the anteroposterior axis during gastrulation of the mouse embryo. *Development*, *126*, 4691–4701.

Kisanuki, Y. Y., Hammer, R. E., Miyazaki, J. ichi, Williams, S. C., Richardson, J. A., & Yanagisawa, M. (2001). Tie2-Cre transgenic mice: A new model for endothelial cell-lineage analysis in vivo. *Developmental Biology*, *230*(2), 230–242. https://doi.org/10.1006/dbio.2000.0106

Kitagawa, M., Oyama, T., Kawashima, T., Yedvobnick, B., Kumar, A., Matsuno, K., & Harigaya, K. (2001). A Human Protein with Sequence Similarity to Drosophila Mastermind Coordinates the Nuclear Form of Notch and a CSL Protein To Build a Transcriptional Activator Complex on Target Promoters . *Molecular and Cellular Biology*, *21*(13), 4337–4346. https://doi.org/10.1128/mcb.21.13.4337-4346.2001

Kitajima, K., Oki, S., Ohkawa, Y., Sumi, T., & Meno, C. (2013). Wnt signaling regulates left-right axis formation in the node of mouse embryos. *Developmental Biology*, *380*(2), 222–232. https://doi.org/10.1016/j.ydbio.2013.05.011

Kitamoto, T., & Hanaoka, K. (2010). Notch3 null mutation in mice causes muscle hyperplasia by repetitive muscle regeneration. *Stem Cells*, *28*(12), 2205–2216. https://doi.org/10.1002/stem.547

Kitamoto, T., Takahashi, K., Takimoto, H., Tomizuka, K., Hayasaka, M., Tabira, T., & Hanaoka, K. (2005). Functional redundancy of the Notch gene family during mouse embryogenesis: Analysis of Notch gene expression in Notch3-deficient mice. *Biochemical and Biophysical Research Communications*, *331*(4), 1154–1162. https://doi.org/10.1016/j.bbrc.2005.03.241

Kitamura, K., Miura, H., Miyagawa-Tomita, S., Yanazawa, M., Katoh-Fukui, Y., Suzuki, R., Ohuchi, H., Suehiro, A., Motegi, Y., Nakahara, Y., Kondo, S., & Yokoyama, M. (1999). Mouse Pitx2 deficiency leads to anomalies of the ventral body wall, heart, extra- and periocular mesoderm and right pulmonary isomerism. *Development*, *126*, 5749–5758.

Klaus, A., Müller, M., Schulz, H., Saga, Y., Martin, J. F., & Birchmeier, W. (2012). Wnt/β-catenin and Bmp signals control distinct sets of transcription factors in cardiac progenitor cells. *Proceedings of the National Academy of Sciences of the United States of America*, *109*(27), 10921–10926. https://doi.org/10.1073/pnas.1121236109

Koenig, S. N., Bosse, K., Majumdar, U., Bonachea, E. M., Radtke, F., & Garg, V. (2016). Endothelial notch1 is required for proper development of the semilunar valves and cardiac outflow tract. *Journal of the American Heart Association*, *5*(4). https://doi.org/10.1161/JAHA.115.003075

Koenig, S. N., LaHaye, S., Feller, J. D., Rowland, P., Hor, K. N., Trask, A. J., Janssen, P. M. L., Radtke, F., Lilly, B., & Garg, V. (2017). Notch1 haploinsufficiency causes ascending aortic aneurysms in mice. *JCI Insight*, *2*(21). https://doi.org/10.1172/jci.insight.91353

Kokubo, H., Miyagawa-Tomita, S., Nakazawa, M., Saga, Y., & Johnson, R. L. (2005). Mouse hesr1 and hesr2 genes are redundantly required to mediate Notch signaling in the developing cardiovascular system. *Developmental Biology*, *278*(2), 301–309. https://doi.org/10.1016/j.ydbio.2004.10.025

Kokubo, H., Miyagawa-Tomita, S., Tomimatsu, H., Nakashima, Y., Nakazawa, M., Saga, Y., & Johnson, R. L. (2004). Targeted disruption of hesr2 results in atrioventricular valve anomalies that lead to heart dysfunction. *Circulation Research*, *95*(5), 540–547. https://doi.org/10.1161/01.RES.0000141136.85194.f0

Krebs, L. T., Iwai, N., Nonaka, S., Welsh, I. C., Lan, Y., Jiang, R., Saijoh, Y., O'Brien, T. P., Hamada, H., & Gridley, T. (2003). Notch signaling regulates left-right asymmetry determination by inducing Nodal expression. *Genes and Development*, *17*(10), 1207–1212. https://doi.org/10.1101/gad.1084703

Krebs, L. T., Shutter, J. R., Tanigaki, K., Honjo, T., Stark, K. L., & Gridley, T. (2004). Haploinsufficient lethality and formation of arteriovenous malformations in Notch pathway mutants. *Genes and Development*, *18*(20), 2469–2473. https://doi.org/10.1101/gad.1239204

Krebs, L. T., Xue, Y., Norton, C. R., Shutter, J. R., Maguire, M., Sundberg, J. P., Gallahan, D., Closson, V., Kitajewski, J., Callahan, R., Smith, G. H., Stark, K. L., & Gridley, T. (2000). Notch signaling is essential for vascular morphogenesis in mice. *Genes and Development*, *14*, 1343–1352. www.genesdev.org

Krebs, L. T., Xue, Y., Norton, C. R., Sundberg, J. P., Beatus, P., Lendahl, U., Joutel, A., & Gridley, T. (2003). Characterization of Notch3-Deficient Mice: Normal Embryonic Development and Absence of Genetic Interactions with a Notch1 Mutation. *Genesis*, *37*(3), 139–143. https://doi.org/10.1002/gene.10241

Kurpios, N. A., Ibañes, M., Davis, N. M., Lui, W., Katz, T., Martin, J. F., Carlos Izpisúa Belmonte, J., & Tabin, C. J. (2007). *The direction of gut looping is established by changes in the extracellular matrix and in cell:cell adhesion*. www.pnas.org/cgi/content/full/

Kwon, C., Qian, L., Cheng, P., Nigam, V., Arnold, J., & Srivastava, D. (2009). A regulatory pathway involving Notch1/β-catenin/Isl1 determines cardiac progenitor cell fate. *Nature Cell Biology*, *11*(8), 951–957. https://doi.org/10.1038/ncb1906

Lafkas, D., Rodilla, V., Huyghe, M., Mourao, L., Kiaris, H., & Fre, S. (2013). Notch3 marks clonogenic mammary luminal progenitor cells in vivo. *Journal of Cell Biology*, *203*(1), 47–56. https://doi.org/10.1083/jcb.201307046

Lamers, W. H., & Moorman, A. F. M. (2002). Cardiac septation: A late contribution of the embryonic primary myocardium to heart morphogenesis. In *Circulation Research* (Vol. 91, Issue 2, pp. 93–103). https://doi.org/10.1161/01.RES.0000027135.63141.89

le Garrec, J.-F., Domínguez, J. N., Desgrange, A., Ivanovitch, K. D., Raphaël, E., Bangham, J. A., Torres, M., Coen, E., Mohun, T. J., & Meilhac, S. M. (2017). A predictive model of asymmetric morphogenesis from 3D reconstructions of mouse heart looping dynamics. *ELife*, *6*, 1–35. https://doi.org/10.7554/elife.28951

Lebreton, G., Géminard, C., Lapraz, F., Pyrpassopoulos, S., Spéder, P., Cerezo, D., Ostap, E. M., & Noselli, S. (2018). Molecular to organismal chirality is induced by the conserved myosin 1D. *Science*, *362*(6417), 949–952. https://doi.org/10.1126/science.aat8642

Lee, J. D., & Anderson, K. v. (2008). Morphogenesis of the node and notochord: The cellular basis for the establishment and maintenance of left-right asymmetry in the mouse. In *Developmental Dynamics* (Vol. 237, Issue 12, pp. 3464–3476). https://doi.org/10.1002/dvdy.21598

Lescroart, F., Chabab, S., Lin, X., Rulands, S., Paulissen, C., Rodolosse, A., Auer, H., Achouri, Y., Dubois, C., Bondue, A., Simons, B. D., & Blanpain, C. (2014). Early lineage restriction in temporally distinct populations of Mesp1 progenitors during mammalian heart development. *Nature Cell Biology*, *16*(9), 829–840. https://doi.org/10.1038/ncb3024

Lescroart, F., Wang, X., Lin, X., Swedlund, B., Gargouri, S., Sànchez-Dànes, A., Moignard, V., Dubois, C., Paulissen, C., Kinston, S., Göttgens, B., & Blanpain, C. (2018). Defining the earliest step of cardiovascular lineage segregation by single-cell RNA-seq. *Science*, *359*, 1177–1181. http://science.sciencemag.org/

Li, L., Krantz, I. D., Deng, Y., Genin, A., Banta, A. B., Collins, C. C., Qi, M., Trask, B. J., Lin Kuo, W., Cochran, J., Costa, T., Ella Pierpont, M. M., Rand, E. B., Piccoli, D. A., Hood, L., & Spinner, N. B. (1997). *Alagille syndrome is caused by mutations in human Jagged1, which encodes a ligand for Notch1*. http://www.nature.com/naturegenetics

Li, X., Zhang, X., Leathers, R., Makino, A., Huang, C., Parsa, P., Maclas, J., Yuan, J. X. J., Jamieson, S. W., & Thistlethwaite, P. A. (2009). Notch3 signaling promotes the development of pulmonary arterial hypertension. *Nature Medicine*, *15*(11), 1289–1297. https://doi.org/10.1038/nm.2021

Liang, X., Wang, G., Lin, L., Lowe, J., Zhang, Q., Bu, L., Chen, Y., Chen, J., Sun, Y., & Evans, S. M. (2013). HCN4 dynamically marks the first heart field and conduction system precursors. *Circulation Research*, *113*(4), 399–407. https://doi.org/10.1161/CIRCRESAHA.113.301588

Limbourg, F. P., Takeshita, K., Radtke, F., Bronson, R. T., Chin, M. T., & Liao, J. K. (2005). Essential role of endothelial Notch1 in angiogenesis. *Circulation*, *111*(14), 1826–1832. https://doi.org/10.1161/01.CIR.0000160870.93058.DD

Lin, A. E., Krikov, S., Riehle-Colarusso, T., Frías, J. L., Belmont, J., Anderka, M., Geva, T., Getz, K. D., & Botto, L. D. (2014). Laterality defects in the national birth defects prevention study (1998-2007): Birth prevalence and descriptive epidemiology. *American Journal of Medical Genetics, Part A*, *164*(10), 2581–2591. https://doi.org/10.1002/ajmg.a.36695

Lin, A., Peiris, N. J., Dhaliwal, H., Hakim, M., Li, W., Ganesh, S., Ramaswamy, Y., Patel, S., & Misra, A. (2021). Mural cells: Potential therapeutic targets to bridge cardiovascular disease and

neurodegeneration. In *Cells* (Vol. 10, Issue 3, pp. 1–25). MDPI. https://doi.org/10.3390/cells10030593

Lin, J., & Nicastro, D. (2018). Asymmetric distribution and spatial switching of dynein activity generates ciliary motility. *Science*, *360*(6387). https://doi.org/10.1126/science.aar1968

Linask, K. K., Han, M., Cai, D. H., Brauer, P. R., & Maisastry, S. M. (2005). Cardiac morphogenesis: Matrix metalloproteinase coordination of cellular mechanisms underlying heart tube formation and directionality of looping. *Developmental Dynamics*, *233*(3), 739–753. https://doi.org/10.1002/dvdy.20377

Liu, H., Kennard, S., & Lilly, B. (2009). NOTCH3 expression is induced in mural cells through an autoregulatory loop that requires Endothelial-expressed JAGGED1. *Circulation Research*, *104*(4), 466–475. https://doi.org/10.1161/CIRCRESAHA.108.184846

Liu, H., Zhang, W., Kennard, S., Caldwell, R. B., & Lilly, B. (2010). Notch3 is critical for proper angiogenesis and mural cell investment. *Circulation Research*, *107*(7), 860–870. https://doi.org/10.1161/CIRCRESAHA.110.218271

Liu, H., Zhang, W., & Lilly, B. (2018). Evaluation of Notch3 deficiency in diabetes-induced pericyte loss in the Retina. *Journal of Vascular Research*, *55*(5), 308–318. https://doi.org/10.1159/000493151

Liu, L., Nemashkalo, A., Yoon Jung, J., Chhabra, S., Cecilia Guerra, M., Heemserk, I., & Warmflash, A. (2021). Nodal is a short-range morphogen with activity that spreads through a relay mechanism in human gastruloids. *BioRxiv*. https://doi.org/10.1101/2021.04.14.439902

Lopes, S. S., Lourenço, R., Pacheco, L., Moreno, N., Kreiling, J., & Saúde, L. (2010). Notch signalling regulates left-right asymmetry through ciliary length control. *Development*, *137*(21), 3625–3632. https://doi.org/10.1242/dev.054452

Lu, C. C., & Robertson, E. J. (2004). Multiple roles for Nodal in the epiblast of the mouse embryo in the establishment of anterior-posterior patterning. *Developmental Biology*, *273*(1), 149–159. https://doi.org/10.1016/j.ydbio.2004.06.004

Lu, M.-F., Pressman, C., Dyer, R., Johnson, R. L., & Martin, J. F. (1999). Function of Rieger syndrome gene in left-right asymmetry and craniofacial development. *Nature*, *401*, 276–278.

Lun, A. T. L., Bach, K., & Marioni, J. C. (2016). Pooling across cells to normalize single-cell RNA sequencing data with many zero counts. *Genome Biology*, *17*(1). https://doi.org/10.1186/s13059-016-0947-7

Luna-Zurita, L., Prados, B., Grego-Bessa, J., Luxán, G., del Monte, G., Benguría, A., Adams, R. H., Pérez-Pomares, J. M., & de La Pompa, J. L. (2010). Integration of a Notch-dependent mesenchymal gene program and Bmp2-driven cell invasiveness regulates murine cardiac valve formation. *Journal of Clinical Investigation*, *120*(10), 3493–3507. https://doi.org/10.1172/JCI42666

Luxán, G., Casanova, J. C., Martínez-Poveda, B., Prados, B., D'Amato, G., MacGrogan, D., Gonzalez-Rajal, A., Dobarro, D., Torroja, C., Martinez, F., Izquierdo-García, J. L., Fernández-Friera, L., Sabater-Molina, M., Kong, Y. Y., Pizarro, G., Ibañez, B., Medrano, C., García-Pavía, P., Gimeno, J. R., … de La Pompa, J. L. (2013). Mutations in the NOTCH pathway regulator MIB1 cause left ventricular noncompaction cardiomyopathy. *Nature Medicine*, *19*(2), 193–201. https://doi.org/10.1038/nm.3046

Luxán, G., D'Amato, G., MacGrogan, D., & de La Pompa, J. L. (2016). Endocardial Notch Signaling in Cardiac Development and Disease. In *Circulation Research* (Vol. 118, Issue 1, pp. e1–e18). Lippincott Williams and Wilkins. https://doi.org/10.1161/CIRCRESAHA.115.305350

MacGrogan, D., Münch, J., & de la Pompa, J. L. (2018). Notch and interacting signalling pathways in cardiac development, disease, and regeneration. *Nature Reviews Cardiology*, *15*(11), 685–704. https://doi.org/10.1038/s41569-018-0100-2

Madisen, L., Zwingman, T. A., Sunkin, S. M., Oh, S. W., Zariwala, H. A., Gu, H., Ng, L. L., Palmiter, R. D., Hawrylycz, M. J., Jones, A. R., Lein, E. S., & Zeng, H. (2010). A robust and high-throughput Cre reporting and characterization system for the whole mouse brain. *Nature Neuroscience*, *13*(1), 133–140. https://doi.org/10.1038/nn.2467

Maerker, M., Getwan, M., Dowdle, M. E., McSheene, J. C., Gonzalez, V., Pelliccia, J. L., Hamilton, D. S., Yartseva, V., Vejnar, C., Tingler, M., Minegishi, K., Vick, P., Giraldez, A. J., Hamada, H., Burdine, R. D., Sheets, M. D., Blum, M., & Schweickert, A. (2021). Bicc1 and Dicer regulate left-right patterning

through post-transcriptional control of the Nodal inhibitor Dand5. *Nature Communications*, *12*(1). https://doi.org/10.1038/s41467-021-25464-z

Mahadevan, A., Welsh, I. C., Sivakumar, A., Gludish, D. W., Shilvock, A. R., Noden, D. M., Huss, D., Lansford, R., & Kurpios, N. A. (2014). The left-right Pitx2 pathway drives organ-specific arterial and lymphatic development in the intestine. *Developmental Cell*, *31*(6), 690–706. https://doi.org/10.1016/j.devcel.2014.11.002

Männer, J. (2004). On Rotation, Torsion, Lateralization, and Handedness of the Embryonic Heart Loop: New Insights from a Simulation Model for the Heart Loop of Chick Embryos. *Anatomical Record - Part A Discoveries in Molecular, Cellular, and Evolutionary Biology*, *278*(1), 481–492. https://doi.org/10.1002/ar.a.20036

Marques, S., Borges, A. C., Silva, A. C., Freitas, S., Cordenonsi, M., & Belo, J. A. (2004). The activity of the Nodal antagonist Cerl-2 in the mouse node is required for correct L/R body axis. *Genes and Development*, *18*(19), 2342–2347. https://doi.org/10.1101/gad.306504

McCright, B., Gao, X., Shen, L., Lozier, J., Lan, Y., Maguire, M., Herzlinger, D., Weinmaster, G., Jiang, R., & Gridley, T. (2001). Defects in development of the kidney, heart and eye vasculature in mice homozygous for a hypomorphic Notch2 mutation. *Development*, *128*, 491–502.

Mcdaniell, R., Warthen, D. M., Sanchez-Lara, P. A., Pai, A., Krantz, I. D., Piccoli, D. A., & Spinner, N. B. (2006). NOTCH2 Mutations Cause Alagille Syndrome, a Heterogeneous Disorder of the Notch Signaling Pathway. *The American Journal of Human Genetics*, *79*, 169–173. www.ajhg.org

McFarlane, L., Truong, V., Palmer, J. S., & Wilhelm, D. (2013). Novel PCR assay for determining the genetic sex of mice. *Sexual Development*, *7*(4), 207–211. https://doi.org/10.1159/000348677

McGrath, J., Somlo, S., Makova, S., Tian, X., & Brueckner, M. (2003). Two Populations of Node Monocilia Initiate Left-Right Asymmetry in the Mouse. *Cell*, *114*, 61–73.

Meester, J. A. N., Verstraeten, A., Alaerts, M., Schepers, D., van Laer, L., & Loeys, B. L. (2019). Overlapping but distinct roles for NOTCH receptors in human cardiovascular disease. In *Clinical Genetics* (Vol. 95, Issue 1, pp. 85–94). Blackwell Publishing Ltd. https://doi.org/10.1111/cge.13382

Meilhac, S. M., & Buckingham, M. E. (2018). The deployment of cell lineages that form the mammalian heart. *Nature Reviews Cardiology*, *15*(11), 705–724. https://doi.org/10.1038/s41569-018-0086-9

Meilhac, S. M., Esner, M., Kelly, R. G., Nicolas, J. F., & Buckingham, M. E. (2004). The clonal origin of myocardial cells in different regions of the embryonic mouse heart. *Developmental Cell*, *6*(5), 685–698. https://doi.org/10.1016/S1534-5807(04)00133-9

Melby, A. E., Warga, R. M., & Kimmel, C. B. (1996). Specification of cell fates at the dorsal margin of the zebrafish gastrula. *Development*, *122*, 2225–2237.

Meno, C., Saijoh, Y., Fujii, H., Ikeda, M., Yokoyama, T., Toyoda, Y., & Hamada, H. (1996). Left-right asymmetric expression of the TGFP-family member lefty in mouse embryos. *Nature*, *381*, 151–155.

Meno, C., Takeuchi, J., Sakuma, R., Koshiba-Takeuchi Kazuko, Oshishi, S., Saijoh, Y., Miyazaki, J., ten Dijke, P., Ogura, T., & Hamada, H. (2001). Diffusion of Nodal Signaling Activity in the Absence of the Feedback Inhibitor Lefty2. *Developmental Cell*, *1*, 127–138.

Minegishi, K., Rothé, B., Komatsu, K. R., Ono, H., Ikawa, Y., Nishimura, H., Katoh, T. A., Kajikawa, E., Sai, X., Miyashita, E., Takaoka, K., Bando, K., Kiyonari, H., Yamamoto, T., Saito, H., Constam, D. B., & Hamada, H. (2021). Fluid flow-induced left-right asymmetric decay of Dand5 mRNA in the mouse embryo requires a Bicc1-Ccr4 RNA degradation complex. *Nature Communications*, *12*(1). https://doi.org/10.1038/s41467-021-24295-2

Miyamoto, M., Andersen, P., Sulistio, E., Liu, X., Murphy, S., Kannan, S., Nam, L., Miyamoto, W., Tampakakis, E., Hibino, N., Uosaki, H., & Kwon, C. (2021). Noncanonical Notch signals have opposing roles during cardiac development. *BioRxiv*. https://doi.org/10.1101/2021.08.09.455692

Monet, M., Domenga, V., Lemaire, B., Souilhol, C., Langa, F., Babinet, C., Gridley, T., Tournier-Lasserve, E., Cohen-Tannoudji, M., & Joutel, A. (2007). The archetypal R90C CADASIL-NOTCH3 mutation retains NOTCH3 function in vivo. *Human Molecular Genetics*, *16*(8), 982–992. https://doi.org/10.1093/hmg/ddm042

Montague, T. G., Gagnon, J. A., & Schier, A. F. (2018). Conserved regulation of nodal-mediated left-right patterning in zebrafish and mouse. *Development (Cambridge)*, *145*(24). https://doi.org/10.1242/dev.171090

Morgan, T. H. (1917). The Theory of the Gene. *The American Naturalist*, *51*(609), 513–544.

Morimoto, M., Nishinakamura, R., Saga, Y., & Kopan, R. (2012). Different assemblies of Notch receptors coordinate the distribution of the major bronchial Clara, ciliated and neuroendocrine cells. *Development (Cambridge)*, *139*(23), 4365–4373. https://doi.org/10.1242/dev.083840

Motoyuki, I., Cheol-Hee, K., Gregory, P., Takaya, O., Yun-Jin, J., Donovan, M., Sang-Yeob, Y., Kevin, L., Gavin, J. W., Linda, A.-M., Allan, M. W., Julian, L., Settara, C. C., & Ajay, B. C. (2003). Mind Bomb Is a Ubiquitin Ligase that Is Essential for Efficient Activation of Notch Signaling by Delta. *Developmental Cell*, *4*, 67–82.

Muzumdar, M. D., Tasic, B., Miyamichi, K., Li, L., & Luo, L. (2007). A Global Double-Fluorescent Cre Reporter Mouse. *Genesis (New York, N.Y. : 2000)*, *45*(6), 418–426. https://doi.org/10.1002/dvg

Nemir, M., Croquelois, A., Pedrazzini, T., & Radtke, F. (2006). Induction of cardiogenesis in embryonic stem cells via downregulation of Notch1 signaling. *Circulation Research*, *98*(12), 1471–1478. https://doi.org/10.1161/01.RES.0000226497.52052.2a

Noël, E. S., Verhoeven, M., Lagendijk, A. K., Tessadori, F., Smith, K., Choorapoikayil, S., den Hertog, J., & Bakkers, J. (2013). A Nodal-independent and tissue-intrinsic mechanism controls heart-looping chirality. *Nature Communications*, *4*(1). https://doi.org/10.1038/ncomms3754

Nonaka, S., Shiratori, H., Saijoh, Y., & Hamada, H. (2002). Determination of left–right patterning of the mouse embryo by artificial nodal flow. *Nature*, *418*(6893), 96–99. https://doi.org/10.1038/nature00835

Nonaka, S., Tanaka, Y., Okada, Y., Takeda, S., Harada, A., Kanai, Y., Kido, M., & Hirokawa, N. (1998). Randomization of Left-Right Asymmetry due to Loss of Nodal Cilia Generating Leftward Flow of Extraembryonic Fluid in Mice Lacking KIF3B Motor Protein. *Cell*, *95*, 829–837. www.cell.com/cgi/content/full/95/6/829/DC1

Nonaka, S., Yoshiba, S., Watanabe, D., Ikeuchi, S., Goto, T., Marshall, W. F., & Hamada, H. (2005). De novo formation of left-right asymmetry by posterior tilt of nodal cilia. *PLoS Biology*, *3*(8). https://doi.org/10.1371/journal.pbio.0030268

Norris, D. P., Brennan, J., Bikoff, E. K., & Robertson, E. J. (2002). The Foxh1-dependent autoregulatory enhancer controls the level of Nodal signals in the mouse embryo. *Development (Cambridge, England)*, *129*(14), 3455–3468. http://www.ncbi.nlm.nih.gov/pubmed/12091315

Norris, D. P., & Robertson, E. J. (1999). Asymmetric and node-specific nodal expression patterns are controlled by two distinct cis-acting regulatory elements. *Genes and Development*, *13*(12), 1575–1588. https://doi.org/10.1101/gad.13.12.1575

Nowotschin, S., Liao, J., Gage, P. J., Epstein, J. A., Campione, M., & Morrow, B. E. (2006). Tbx1 affects asymmetric cardiac morphogenesis by regulating Pitx2 in the secondary heart field. *Development*, *133*(8), 1565–1573. https://doi.org/10.1242/dev.02309

Nowotschin, S., Xenopoulos, P., Schrode, N., & Hadjantonakis, A. K. (2013). A bright single-cell resolution live imaging reporter of Notch signaling in the mouse. *BMC Developmental Biology*, *13*(1). https://doi.org/10.1186/1471-213X-13-15

Ocaña, O. H., Coskun, H., Minguillón, C., Murawala, P., Tanaka, E. M., Galcerán, J., Muñoz-Chápuli, R., & Nieto, M. A. (2017). A right-handed signalling pathway drives heart looping in vertebrates. *Nature*, *549*(7670), 86–90. https://doi.org/10.1038/nature23454

Oka, C., Nakano, T., Wakeham, A., de la Pompa, J. L., Mori, C., Sakai, T., Okazaki, S., Kawaichi, M., Shiota, K., Mak, T. W., & Honjo, T. (1995). Disruption of the mouse RBP-Jκgene results in early embryonic death. *Development*, *121*, 3291–3301.

Oki, S., Hashimoto, R., Okui, Y., Shen, M. M., Mekada, E., Otani, H., Saijoh, Y., & Hamada, H. (2007). Sulfated glycosaminoglycans are necessary for Nodal signal transmission from the node to the left lateral plate in the mouse embryo. *Development*, *134*(21), 3893–3904. https://doi.org/10.1242/dev.009464

Oki, S., Kitajima, K., Marques, S., Belo, J. A., Yokoyama, T., Hamada, H., & Meno, C. (2009). Reversal of left-right asymmetry induced by aberrant Nodal signaling in the node of mouse embryos. *Development*, *136*(23), 3917–3925. https://doi.org/10.1242/dev.039305

Olsauskas-Kuprys, R., Zlobin, A., & Osipo, C. (2013). Gamma secretase inhibitors of Notch signaling. In *OncoTargets and Therapy* (Vol. 6, pp. 943–955). https://doi.org/10.2147/OTT.S33766

Onuma, T. A., Hayashi, M., Gyoja, F., Kishi, K., Wang, K., Nishida, H., & de Robertis, E. M. (2020). A chordate species lacking Nodal utilizes calcium oscillation and Bmp for left-right patterning. *PNAS*, *117*(8), 4188–4198. https://doi.org/10.1073/pnas.1916858117/-/DCSupplemental

O'Rahilly, R., & Müller, F. (2003). Somites, spinal ganglia, and centra: Enumeration and interrelationships in staged human embryos, and implications for neural tube defects. *Cells Tissues Organs*, *173*(2), 75–92. https://doi.org/10.1159/000068948

Panin, V. M., Papayannopoulos, V., Wilson, R., & Irvine, K. D. (1997). Fringe modulates Notch–ligand interactions. *Nature*, *387*, 908–912.

Patten, B. M. (1922). The Formation of the Cardiac Loop in the Chick. *The American Journal of Anatomy*, *30*(3), 373–397.

Piedra, M. E., Icardo, J. M., Albajar, M., Rodriguez-Rey, J. C., & Ros, M. A. (1998). Pitx2 Participates in the Late Phase of the Pathway Controlling Left-Right Asymmetry. *Cell*, *94*, 319–324.

Pijuan-Sala, B., Griffiths, J. A., Guibentif, C., Hiscock, T. W., Jawaid, W., Calero-Nieto, F. J., Mulas, C., Ibarra-Soria, X., Tyser, R. C. V., Ho, D. L. L., Reik, W., Srinivas, S., Simons, B. D., Nichols, J., Marioni, J. C., & Göttgens, B. (2019). A single-cell molecular map of mouse gastrulation and early organogenesis. *Nature*, *566*(7745), 490–495. https://doi.org/10.1038/s41586-019-0933-9

Pradeep, C. R., Köstler, W. J., Lauriola, M., Granit, R. Z., Zhang, F., Jacob-Hirsch, J., Rechavi, G., Nair, H. B., Hennessy, B. T., Gonzalez-Angulo, A. M., Tekmal, R. R., Ben-Porath, I., Mills, G. B., Domany, E., & Yarden, Y. (2012). Modeling ductal carcinoma in situ: A HER2-Notch3 collaboration enables luminal filling. *Oncogene*, *31*(7), 907–917. https://doi.org/10.1038/onc.2011.279

Prall, O. W. J., Menon, M. K., Solloway, M. J., Watanabe, Y., Zaffran, S., Bajolle, F., Biben, C., McBride, J. J., Robertson, B. R., Chaulet, H., Stennard, F. A., Wise, N., Schaft, D., Wolstein, O., Furtado, M. B., Shiratori, H., Chien, K. R., Hamada, H., Black, B. L., … Harvey, R. P. (2007). An Nkx2-5/Bmp2/Smad1 Negative Feedback Loop Controls Heart Progenitor Specification and Proliferation. *Cell*, *128*(5), 947–959. https://doi.org/10.1016/j.cell.2007.01.042

Przemeck, G. K. H., Heinzmann, U., Beckers, J., & de Angelis, M. H. (2003). Node and midline defects are associated with left-right development in Delta1 mutant embryos. In *Development* (Vol. 130, Issue 1, pp. 3–13). https://doi.org/10.1242/dev.00176

Ragni, C. v., Diguet, N., le Garrec, J.-F., Novotova, M., Resende, T. P., Pop, S., Charon, N., Guillemot, L., Kitasato, L., Badouel, C., Dufour, A., Olivo-Marin, J.-C., Trouvé, A., McNeill, H., & Meilhac, S. M. (2017). Amotl1 mediates sequestration of the Hippo effector Yap1 downstream of Fat4 to restrict heart growth. *Nature Communications*, *8*(May 2016), 14582. https://doi.org/10.1038/ncomms14582

Rago, L., Castroviejo, N., Fazilaty, H., Garcia-Asencio, F., Ocaña, O. H., Galcerán, J., & Nieto, M. A. (2019). MicroRNAs Establish the Right-Handed Dominance of the Heart Laterality Pathway in Vertebrates. *Developmental Cell*, *51*(4), 446-459.e5. https://doi.org/10.1016/j.devcel.2019.09.012

Ray, P., Chin, A. S., Worley, K. E., Fan, J., Kaur, G., Wu, M., & Wan, L. Q. (2018). Intrinsic cellular chirality regulates left–right symmetry breaking during cardiac looping. *Proceedings of the National Academy of Sciences of the United States of America*, *115*(50), E11568–E11577. https://doi.org/10.1073/pnas.1808052115

Raya, A., Kawakami, Y., Rodríguez-Esteban, C., Büscher, D., Koth, C. M., Itoh, T., Morita, M., Raya, R. M., Dubova, I., Bessa, J. G., de la Pompa, J. L., & Izpisúa Belmonte, J. C. (2003). Notch activity induces Nodal expression and mediates the establishment of left-right asymmetry in vertebrate embryos. *Genes and Development*, *17*(10), 1213–1218. https://doi.org/10.1101/gad.1084403

Raya, A., Kawakami, Y., Rodríguez-Esteban, C., Ibañ es, M., Rasskin-Gutman, D., Rodríguez-Leó, J., Bü scher, D., Feijó, J. A., & Carlos Izpisú Belmonte, J. (2004). *Notch activity acts as a sensor for extracellular calcium during vertebrate left-right determination*. www.nature.com/nature

Rebay, L., Fleming, R. J., Fehon, R. G., Cherbas, L., Cherbas, P., & Artavanis-Tsakonas', S. (1991). Specific EGF Repeats of Notch Mediate Interactions with Delta and Serrate: Implications for Notch as a Multifunctional Receptor. In *Cell* (Vol. 67).

Rentschler, S., Harris, B. S., Kuznekoff, L., Jain, R., Manderfield, L., Lu, M. M., Morley, G. E., Patel, V. v., & Epstein, J. A. (2011). Notch signaling regulates murine atrioventricular conduction and the formation of accessory pathways. *Journal of Clinical Investigation*, *121*(2), 525–533. https://doi.org/10.1172/JCI44470

Rochais, F., Dandonneau, M., Mesbah, K., Jarry, T., Mattei, M. G., & Kelly, R. G. (2009). Hes1 is expressed in the second heart field and is required for outflow tract development. *PLoS ONE*, *4*(7). https://doi.org/10.1371/journal.pone.0006267

Rogers, K. W., Lord, N. D., Gagnon, J. A., Pauli, A., Zimmerman, S., Aksel, D. C., Reyon, D., Tsai, S. Q., Joung, J. K., & Schier, A. F. (2017). Nodal patterning without lefty inhibitory feedback is functional but fragile. *ELife*, *6*. https://doi.org/10.7554/eLife.28785.001

Rones, M. S., McLaughlin, K. A., & Mercola, M. (2000). Serrate and Notch specify cell fates in the heart field by suppressing cardiomyogenesis. *Development*, *127*, 3865–3876.

Rossi, A., Kontarakis, Z., Gerri, C., Nolte, H., Hölper, S., Krüger, M., & Stainier, D. Y. R. (2015). Genetic compensation induced by deleterious mutations but not gene knockdowns. *Nature*, *524*(7564), 230–233. https://doi.org/10.1038/nature14580

Rusanescu, G., & Mao, J. (2014). Notch3 is necessary for neuronal differentiation and maturation in the adult spinal cord. *Journal of Cellular and Molecular Medicine*, *18*(10), 2103–2116. https://doi.org/10.1111/jcmm.12362

Ryan, A. K., Blumberg, B., Rodriguez-Esteban, C., Yonei-Tamura, S., Tamura, K., Tsukui, T., de la Peñ, J., Sabbagh, W., Greenwald, J., Choe, S., Norris, D. P., Robertson, E. J., Evans, R. M., Rosenfeld, M. G., & Carlos Izpisú Belmonte, J. (1998). Pitx2 determines left-right asymmetry of internal organs in vertebrates. *Nature*, *394*, 545–551.

Saga, Y., Kitajima, S., & Miyagawa-Tomita, S. (2000). Mesp1 expression is the earliest sign of cardiovascular development. *Trends in Cardiovascular Medicine*, *10*(8), 345–352. https://doi.org/10.1016/S1050-1738(01)00069-X

Saga, Y., Sachiko, M.-T., Atsuya, T., Satoshim Kitajima, Jun-ichi, M., & Tohru, I. (1999). MesP1 is expressed in the heart precursor cells and required for the formation of a single heart tube. *Development*, *126*, 3437–3447.

Sahu, A., Devi, S., Jui, J., & Goldman, D. (2021). Notch signaling via Hey1 and Id2b regulates Müller glia's regenerative response to retinal injury. *GLIA*, *69*(12), 2882–2898. https://doi.org/10.1002/glia.24075

Saijoh, Y., Adachi, H., Mochida, K., Ohishi, S., Hirao, A., & Hamada, H. (1999). *Distinct transcriptional regulatory mechanisms underlie left-right asymmetric expression of lefty-1 and lefty-2*. www.genesdev.org

Saijoh, Y., Oki, S., Ohishi, S., & Hamada, H. (2003). Left-right patterning of the mouse lateral plate requires Nodal produced in the node. *Developmental Biology*, *256*(1), 161–173. https://doi.org/10.1016/S0012-1606(02)00121-5

Sakano, D., Kato, A., Parikh, N., McKnight, K., Terry, D., Stefanovic, B., & Kato, Y. (2010). BCL6 Canalizes Notch-Dependent Transcription, Excluding Mastermind-like1 from Selected Target Genes during Left-Right Patterning. *Developmental Cell*, *18*(3), 450–462. https://doi.org/10.1016/j.devcel.2009.12.023

Salguero-Jiménez, A., Grego-Bessa, J., D'Amato, G., Jiménez-Borreguero, L. J., & de la Pompa, J. L. (2018). Myocardial notch1-rbpj deletion does not affect NOTCH signaling, heart development or function. *PLoS ONE*, *13*(12). https://doi.org/10.1371/journal.pone.0203100

Sampaio, P., Ferreira, R. R., Guerrero, A., Pintado, P., Tavares, B., Amaro, J., Smith, A. A., Montenegro-Johnson, T., Smith, D. J., & Lopes, S. S. (2014). Left-right organizer flow dynamics: How much cilia activity reliably yields laterality? *Developmental Cell*, *29*(6), 716–728. https://doi.org/10.1016/j.devcel.2014.04.030

Savin, T., Kurpios, N. A., Shyer, A. E., Florescu, P., Liang, H., Mahadevan, L., & Tabin, C. J. (2011). On the growth and form of the gut. *Nature*, *476*(7358), 57–63. https://doi.org/10.1038/nature10277

Schroeder, T., Fraser, S. T., Ogawa, M., Nishikawa, S., Oka, C., Bornkamm, G. W., Nishikawa, S.-I., Honjo, T., & Just, U. (2003). Recombination signal sequence-binding protein J alters mesodermal cell fate decisions by suppressing cardiomyogenesis. *PNAS*, *100*(7), 4018–4023. www.pnas.orgcgidoi10.1073pnas.0438008100

Sebé-Pedrós, A., Saudemont, B., Chomsky, E., Plessier, F., Mailhé, M. P., Renno, J., Loe-Mie, Y., Lifshitz, A., Mukamel, Z., Schmutz, S., Novault, S., Steinmetz, P. R. H., Spitz, F., Tanay, A., & Marlow, H. (2018). Cnidarian Cell Type Diversity and Regulation Revealed by Whole-Organism Single-Cell RNA-Seq. *Cell*, *173*(6), 1520-1534.e20. https://doi.org/10.1016/j.cell.2018.05.019

Shih, I. M., & Wang, T. L. (2007). Notch signaling, γ-secretase inhibitors, and cancer therapy. In *Cancer Research* (Vol. 67, Issue 5, pp. 1879–1882). https://doi.org/10.1158/0008-5472.CAN-06-3958

Shimizu, K., Chiba, S., Kumano, K., Hosoya, N., Takahashi, T., Kanda, Y., Hamada, Y., Yazaki, Y., & Hirai, H. (1999). *Mouse Jagged1 Physically Interacts with Notch2 and Other Notch Receptors ASSESSMENT BY QUANTITATIVE METHODS**. http://www.jbc.org

Shimizu, K., Chiba, S., Saito, T., Kumano, K., & Hirai, H. (2000). Physical interaction of Delta1, Jagged1, and Jagged2 with Notch1 and Notch3 receptors. *Biochemical and Biophysical Research Communications*, *276*(1), 385–389. https://doi.org/10.1006/bbrc.2000.3469

Shiratori, H., Sakuma, R., Watanabe, M., Hashiguchi, H., Mochida, K., Sakai, Y., Nishino, J., Saijoh, Y., Whitman, M., & Hamada, H. (2001). Two-Step Regulation of Left–Right Asymmetric Expression of Pitx2: Initiation by Nodal Signaling and Maintenance by Nkx2. *Molecular Cell*, *7*, 137–149.

Sivakumar, A., & Kurpios, N. A. (2018). Transcriptional regulation of cell shape during organ morphogenesis. In *Journal of Cell Biology* (Vol. 217, Issue 9, pp. 2987–3005). Rockefeller University Press. https://doi.org/10.1083/jcb.201612115

Sivakumar, A., Mahadevan, A., Lauer, M. E., Narvaez, R. J., Ramesh, S., Demler, C. M., Souchet, N. R., Hascall, V. C., Midura, R. J., Garantziotis, S., Frank, D. B., Kimata, K., & Kurpios, N. A. (2018). Midgut Laterality Is Driven by Hyaluronan on the Right. *Developmental Cell*, *46*(5), 533-551.e5. https://doi.org/10.1016/j.devcel.2018.08.002

Soldatov, R., Kaucka, M., Kastriti, M. E., Petersen, J., Chontorotzea, T., Englmaier, L., Akkuratova, N., Yang, Y., Häring, M., Dyachuk, V., Bock, C., Farlik, M., Piacentino, M. L., Boismoreau, F., Hilscher, M. M., Yokota, C., Qian, X., Nilsson, M., Bronner, M. E., … Adameyko, I. (2019). Spatiotemporal structure of cell fate decisions in murine neural crest. *Science*, *364*(6444). https://doi.org/10.1126/science.aas9536

Souilhol, C., Cormier, S., Monet, M., Vandormael-Pournin, S., Joutel, A., Babinet, C., & Cohen-Tannoudji, M. (2006). NAS transgenic mouse line allows visualization of notch pathway activity in vivo. *Genesis*, *44*(6), 277–286. https://doi.org/10.1002/dvg.20208

Souilhol, C., Cormier, S., Tanigaki, K., Babinet, C., & Cohen-Tannoudji, M. (2006). RBP-Jκ-Dependent Notch Signaling Is Dispensable for Mouse Early Embryonic Development. *Molecular and Cellular Biology*, *26*(13), 4769–4774. https://doi.org/10.1128/mcb.00319-06

Spéder, P., Ádám, G., & Noselli, S. (2006). Type ID unconventional myosin controls left-right asymmetry in Drosophila. *Nature*, *440*(7085), 803–807. https://doi.org/10.1038/nature04623

Srinivas, S., Watanabe, T., Lin, C.-S., William, C., Tanabe, Y., Jessell, T., & Costantini, F. (2001). Cre reporter strains produced by targeted insertion of EYFP and ECFP into the ROSA26 locus. *BMC Developmental Biology*, *1*(1), 4. https://doi.org/10.1186/1471-213X-1-4

Stevens, J., Ermakov, A., Braganca, J., Hilton, H., Underhill, P., Bhattacharya, S., Brown, N. A., & Norris, D. P. (2010). Analysis of the asymmetrically expressed Ablim1 locus reveals existence of a lateral plate Nodal-independent left sided signal and an early, left-right independent role for nodal flow. In *BMC Developmental Biology* (Vol. 10). http://www.biomedcentral.com/1471-213X/10/54

Stuart, T., Butler, A., Hoffman, P., Hafemeister, C., Papalexi, E., Mauck, W. M., Hao, Y., Stoeckius, M., Smibert, P., & Satija, R. (2019). Comprehensive Integration of Single-Cell Data. *Cell*, *177*(7), 1888-1902.e21. https://doi.org/10.1016/j.cell.2019.05.031

Sulik, K., Dehart, D. B., Inagaki, T., Carson, J. L., Vrablic, T., Gesteland, K., & Schoenwolf, G. C. (1994). Morphogenesis of the Murine Node and Notochordal Plate. *Developmental Dynamics*, *201*, 260–278.

Sun, Y., Liang, X., Najafi, N., Cass, M., Lin, L., Cai, C. L., Chen, J., & Evans, S. M. (2007). Islet 1 is expressed in distinct cardiovascular lineages, including pacemaker and coronary vascular cells. *Developmental Biology*, *304*(1), 286–296. https://doi.org/10.1016/j.ydbio.2006.12.048

Susaki, E. A., Tainaka, K., Perrin, D., Yukinaga, H., Kuno, A., & Ueda, H. R. (2015). Advanced CUBIC protocols for whole-brain and whole-body clearing and imaging. *Nature Protocols*, *10*(11), 1709–1727. https://doi.org/10.1038/nprot.2015.085

Szenker-Ravi, E., Ott, T., Khatoo, M., de Bellaing, A. M., Goh, W. X., Chong, Y. L., Beckers, A., Kannesan, D., Louvel, G., Anujan, P., Ravi, V., Bonnard, C., Moutton, S., Schoen, P., Fradin, M., Colin, E., Megarbane, A., Daou, L., Chehab, G., … Reversade, B. (2022). Discovery of a genetic module essential for assigning left–right asymmetry in humans and ancestral vertebrates. *Nature Genetics*, *54*(1), 62–72. https://doi.org/10.1038/s41588-021-00970-4

Sztal, T. E., & Stainier, Y. R. (2020). Transcriptional adaptation: A mechanism underlying genetic robustness. *Development (Cambridge)*, *147*(15). https://doi.org/10.1242/dev.186452

Takao, D., Nemoto, T., Abe, T., Kiyonari, H., Kajiura-Kobayashi, H., Shiratori, H., & Nonaka, S. (2013). Asymmetric distribution of dynamic calcium signals in the node of mouse embryo during left-right axis formation. *Developmental Biology*, *376*(1), 23–30. https://doi.org/10.1016/j.ydbio.2013.01.018

Takeuchi, J. K., Lickert, H., Bisgrove, B. W., Sun, X., Yamamoto, M., Chawengsaksophak, K., Hamada, H., Yost, H. J., Rossant, J., & Bruneau, B. G. (2007). Baf60c is a nuclear Notch signaling component required for the establishment of left-right asymmetry. *Proceedings of the National Academy of Sciences of the United States of America*, *104*(3), 846–851. https://doi.org/10.1073/pnas.0608118104

Tanaka, C., Sakuma, R., Nakamura, T., Hamada, H., & Saijoh, Y. (2007). Long-range action of Nodal requires interaction with GDF1. *Genes and Development*, *21*(24), 3272–3282. https://doi.org/10.1101/gad.1623907

Tanaka, K., Kato, A., Angelocci, C., Watanabe, M., & Kato, Y. (2014). A potential molecular pathogenesis of cardiac/laterality defects in Oculo-Facio-Cardio-Dental syndrome. *Developmental Biology*, *387*(1), 28–36. https://doi.org/10.1016/j.ydbio.2014.01.003

Tavares, B., Jacinto, R., Sampaio, P., Pestana, S., Pinto, A., Vaz, A., Nica Roxo-Rosa, M., Gardner, R., Lopes, T., Schilling, B., Henry, I., Saú De, L., & Santos Lopes, S. (2017). Notch/Her12 signalling modulates, motile/immotile cilia ratio downstream of Foxj1a in zebrafish left-right organizer. *ELife*. https://doi.org/10.7554/eLife.25165.001

Than-Trong, E., Ortica-Gatti, S., Mella, S., Nepal, C., Alunni, A., & Bally-Cuif, L. (2018). Neural stem cell quiescence and stemness are molecularly distinct outputs of the notch3 signalling cascade in the vertebrate adult brain. *Development (Cambridge)*, *145*(10). https://doi.org/10.1242/dev.161034

Timmerman, L. A., Grego-Bessa, J., Raya, A., Bertrán, E., Pérez-Pomares, J. M., Díez, J., Aranda, S., Palomo, S., McCormick, F., Izpisúa-Belmonte, J. C., & de La Pompa, J. L. (2004). Notch promotes epithelial-mesenchymal transition during cardiac development and oncogenic transformation. *Genes and Development*, *18*(1), 99–115. https://doi.org/10.1101/gad.276304

Tremblay, C., Loomba, R. S., Frommelt, P. C., Perrin, D., Spicer, D. E., Backer, C., & Anderson, R. H. (2017). Segregating bodily isomerism or heterotaxy: Potential echocardiographic correlations of morphological findings. *Cardiology in the Young*, *27*(8), 1470–1480. https://doi.org/10.1017/S104795111700049X

Tyser, R. C. V., Ibarra-Soria, X., McDole, K., Jayaram, S. A., Godwin, J., Brand, T. A. H. V. den, Miranda, A. M. A., Scialdone, A., Keller, P. J., Marioni, J. C., & Srinivas, S. (2021). Characterization of a common progenitor pool of the epicardium and myocardium. *Science*, *371*(6533), 1–18. https://doi.org/10.1126/science.abb2986

Tyser, R. C. V., & Srinivas, S. (2020). The first heartbeat—origin of cardiac contractile activity. *Cold Spring Harbor Perspectives in Biology*, *12*(7), 1–12. https://doi.org/10.1101/cshperspect.a037135

Tyser, R., Miranda, A., Chen, C.-M., Davidson, S. M., Srinivas, S., & Riley, P. R. (2016). Calcium handling precedes cardiac differentiation to initiate the first heartbeat. *ELife*. https://doi.org/10.7554/eLife.17113.001

Tzouanacou, E., Wegener, A., Wymeersch, F. J., Wilson, V., & Nicolas, J. F. (2009). Redefining the Progression of Lineage Segregations during Mammalian Embryogenesis by Clonal Analysis. *Developmental Cell*, *17*(3), 365–376. https://doi.org/10.1016/j.devcel.2009.08.002

Verzi, M. P., McCulley, D. J., de Val, S., Dodou, E., & Black, B. L. (2005). The right ventricle, outflow tract, and ventricular septum comprise a restricted expression domain within the secondary/anterior heart field. *Developmental Biology*, *287*(1), 134–145. https://doi.org/10.1016/j.ydbio.2005.08.041

Vincent, S. D., Norris, D. P., Ann Le Good, J., Constam, D. B., & Robertson, E. J. (2004). Asymmetric Nodal expression in the mouse is governed by the combinatorial activities of two distinct regulatory elements. *Mechanisms of Development*, *121*(11), 1403–1415. https://doi.org/10.1016/j.mod.2004.06.002

Vingerhoets, G., Gerrits, R., & Verhelst, H. (2021). Atypical brain asymmetry in human situs inversus: Gut feeling or real evidence? In *Symmetry* (Vol. 13, Issue 4). MDPI AG. https://doi.org/10.3390/sym13040695

Volz, K. S., Jacobs, A. H., Chen, H. I., Poduri, A., McKay, A. S., Riordan, D. P., Kofler, N., Kitajewski, J., Weissman, I., & Red-Horse, K. (2015). Pericytes are progenitors for coronary artery smooth muscle. *ELife*, *4*(OCTOBER2015). https://doi.org/10.7554/eLife.10036.001

Wang, Q., Zhao, N., Kennard, S., & Lilly, B. (2012). Notch2 and notch3 function together to regulate vascular smooth muscle development. *PLoS ONE*, *7*(5). https://doi.org/10.1371/journal.pone.0037365

Wang, Z., Gerstein, M., & Snyder, M. (2009). RNA-Seq: a revolutionary tool for transcriptomics. *Nature Reviews. Genetics*, *10*(1), 57–63.

Watanabe, Y., Kokubo, H., Miyagawa-Tomita, S., Endo, M., Igarashi, K., Aisaki, K. I., Kanno, J., & Saga, Y. (2006). Activation of Notch1 signaling in cardiogenic mesoderm induces abnormal heart morphogenesis in mouse. *Development*, *133*(9), 1625–1634. https://doi.org/10.1242/dev.02344

Welsh, I. C., Kwak, H., Chen, F. L., Werner, M., Shopland, L. S., Danko, C. G., Lis, J. T., Zhang, M., Martin, J. F., & Kurpios, N. A. (2015). Chromatin Architecture of the Pitx2 Locus Requires CTCF- and Pitx2-Dependent Asymmetry that Mirrors Embryonic Gut Laterality. *Cell Reports*, *13*(2), 337–349. https://doi.org/10.1016/j.celrep.2015.08.075

Welsh, I. C., Thomsen, M., Gludish, D. W., Alfonso-Parra, C., Bai, Y., Martin, J. F., & Kurpios, N. A. (2013). Integration of left-right Pitx2 transcription and Wnt signaling drives asymmetric gut morphogenesis via Daam2. *Developmental Cell*, *26*(6), 629–644. https://doi.org/10.1016/j.devcel.2013.07.019

Whiteman, P., de Madrid, B. H., Taylor, P., Li, D., Heslop, R., Viticheep, N., Tan, J. Z., Shimizu, H., Callaghan, J., Masiero, M., Li, J. L., Banham, A. H., Harris, A. L., Lea, S. M., Redfield, C., Baron, M., & Handford, P. A. (2013). Molecular basis for jagged-1/serrate ligand recognition by the notch receptor. *Journal of Biological Chemistry*, *288*(10), 7305–7312. https://doi.org/10.1074/jbc.M112.428854

Williams, J. L., Paudyal, A., Awad, S., Nicholson, J., Grzesik, D., Botta, J., Meimaridou, E., Maharaj, A. v., Stewart, M., Tinker, A., Cox, R. D., & Metherell, L. A. (2020). Mylk3 null c57bl/6n mice develop cardiomyopathy, whereas nnt null c57bl/6j mice do not. *Life Science Alliance*, *3*(4). https://doi.org/10.26508/LSA.201900593

Xue, Y., Gao, X., Lindsell, C. E., Norton, C. R., Chang, B., Hicks, C., Gendron-Maguire, M., Rand, E. B., Weinmaster, G., & Gridley, T. (1999). Embryonic lethality and vascular defects in mice lacking the Notch ligand Jagged1. In *Human Molecular Genetics* (Vol. 8, Issue 5). https://academic.oup.com/hmg/article/8/5/723/661242

Yim, D., Nagata, H., Lam, C. Z., Grosse-Wortmann, L., Seed, M., Jaeggi, E., & Yoo, S. J. (2018). Disharmonious Patterns of Heterotaxy and Isomerism: How Often Are the Classic Patterns Breached? *Circulation: Cardiovascular Imaging*, *11*(2). https://doi.org/10.1161/CIRCIMAGING.117.006917

Zaffran, S., Kelly, R. G., Meilhac, S. M., Buckingham, M. E., & Brown, N. A. (2004). Right ventricular myocardium derives from the anterior heart field. *Circulation Research*, *95*(3), 261–268. https://doi.org/10.1161/01.RES.0000136815.73623.BE

Zavadil, J., Cermak, L., Soto-Nieves, N., & Böttinger, E. P. (2004). Integration of TGF-β/Smad and Jagged1/Notch signalling in epithelial-to-mesenchymal transition. *EMBO Journal*, *23*(5), 1155–1165. https://doi.org/10.1038/sj.emboj.7600069

Zhang, Q., Carlin, D., Zhu, F., Cattaneo, P., Ideker, T., Evans, S. M., Bloomekatz, J., & Chi, N. C. (2021). Unveiling Complexity and Multipotentiality of Early Heart Fields. *Circulation Research*, *129*(4), 474–487. https://doi.org/10.1161/CIRCRESAHA.121.318943

Zhang, R., Boareto, M., Engler, A., Louvi, A., Giachino, C., Iber, D., & Taylor, V. (2019). Id4 Downstream of Notch2 Maintains Neural Stem Cell Quiescence in the Adult Hippocampus. *Cell Reports*, *28*(6), 1485-1498.e6. https://doi.org/10.1016/j.celrep.2019.07.014

Zhou, Z., Wang, J., Guo, C., Chang, W., Zhuang, J., Zhu, P., & Li, X. (2017). Temporally Distinct Six2-Positive Second Heart Field Progenitors Regulate Mammalian Heart Development and Disease. *Cell Reports*, *18*(4), 1019–1032. https://doi.org/10.1016/j.celrep.2017.01.002

Zhu, L., Belmont, J. W., & Ware, S. M. (2006). Genetics of human heterotaxias. In *European Journal of Human Genetics* (Vol. 14, Issue 1, pp. 17–25). https://doi.org/10.1038/sj.ejhg.5201506

Zhu, X., Shi, C., Zhong, Y., Liu, X., Yan, Q., Wu, X., Wang, Y., & Li, G. (2020). Cilia-driven asymmetric Hedgehog signalling determines the amphioxus left-right axis by controlling Dand5 expression. *Development (Cambridge)*, *147*(1). https://doi.org/10.1242/dev.182469

Annex

To the publication in Annex #1 (Desgrange et al., 2020), I contributed with three sets of experiments as well as comments on the manuscript.

1) Nodal pathway qPCR (Fig 2A + Fig S4A)
2) Pitx2 isoform qPCR (Fig S4C)
3) Mapping and quantifications of *Nodal*^{LacZ} within the second heart field (Described in text)

Article

Developmental Cell

Transient Nodal Signaling in Left Precursors Coordinates Opposed Asymmetries Shaping the Heart Loop

Graphical Abstract

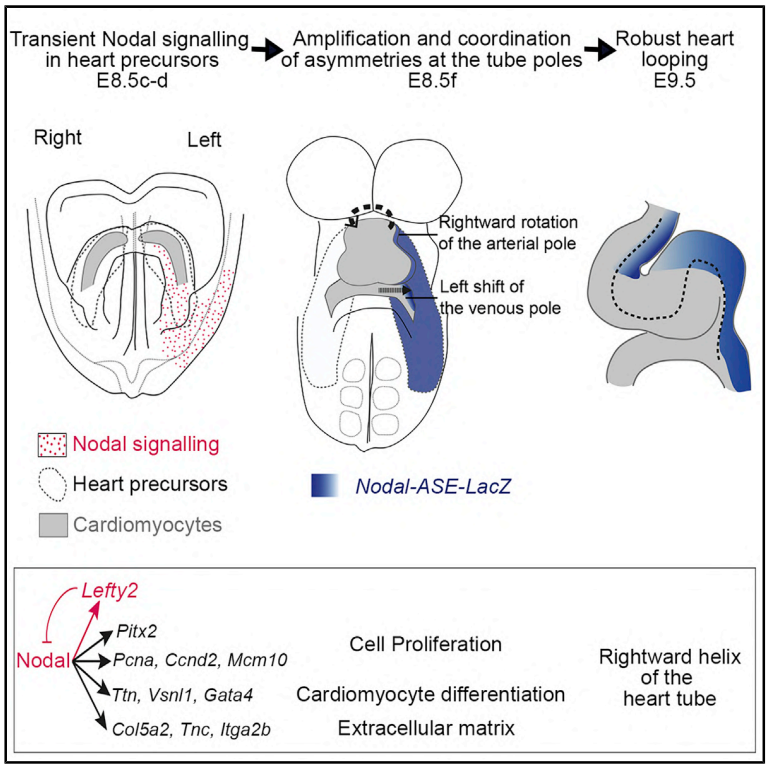

Highlights

- Nodal signaling is transient in left precursors of the embryonic heart tube
- Nodal is not required to initiate heart looping
- Nodal generates a helical shape by modulating asymmetries at the heart tube poles
- Nodal effectors are proliferation, differentiation, and extracellular matrix genes

Authors

Audrey Desgrange, Jean-François Le Garrec, Ségolène Bernheim, Tobias Holm Bønnelykke, Sigolène M. Meilhac

Correspondence

sigolene.meilhac@institutimagine.org

In Brief

Nodal is expressed on the left side of the embryo and associated with the heterotaxy syndrome. Desgrange et al. now demonstrate that Nodal is not required to initiate heart looping but instead regulates asymmetric morphogenesis of the heart by shaping the embryonic heart tube as a helix.

Desgrange et al., 2020, Developmental Cell *55*, 413–431
November 23, 2020
https://doi.org/10.1016/j.devcel.2020.10.008

CellPress

Developmental Cell

CellPress

Article

Transient Nodal Signaling in Left Precursors Coordinates Opposed Asymmetries Shaping the Heart Loop

Audrey Desgrange,[1] Jean-François Le Garrec,[1] Ségolène Bernheim,[1] Tobias Holm Bønnelykke,[1,2] and Sigolène M. Meilhac[1,3,*]

[1]Université de Paris, *Imagine* - Institut Pasteur, Unit of Heart Morphogenesis, INSERM UMR1163, 75015 Paris, France

[2]Sorbonne Université, Collège Doctoral, 75005 Paris, France

[3]Lead Contact

*Correspondence: sigolene.meilhac@institutimagine.org

https://doi.org/10.1016/j.devcel.2020.10.008

SUMMARY

The secreted factor Nodal, known as a major left determinant, is associated with severe heart defects. Yet, it has been unclear how it regulates asymmetric morphogenesis such as heart looping, which align cardiac chambers to establish the double blood circulation. Here, we report that Nodal is transiently active in precursors of the mouse heart tube poles, before looping. In conditional mutants, we show that Nodal is not required to initiate asymmetric morphogenesis. We provide evidence of a heart-specific random generator of asymmetry that is independent of Nodal. Using 3D quantifications and simulations, we demonstrate that Nodal functions as a bias of this mechanism: it is required to amplify and coordinate opposed left-right asymmetries at the heart tube poles, thus generating a robust helical shape. We identify downstream effectors of Nodal signaling, regulating asymmetries in cell proliferation, differentiation, and extracellular matrix composition. Our study uncovers how Nodal regulates asymmetric organogenesis.

INTRODUCTION

Left-right asymmetric organogenesis is essential for vertebrates. Impairment of left-right patterning leads to human diseases such as the heterotaxy syndrome, affecting the asymmetry or concordance of the positions of visceral organs (Van Praagh, 2006). Heterotaxy is associated with complex congenital heart defects, which determine the prognosis of patients (Lin et al., 2014). Asymmetric organogenesis has been theorized by Brown and Wolpert (1990) to occur in two sequential steps: (1) a symmetry-breaking event, transforming molecular chirality into a left-right bias, which coordinates laterality throughout the embryo; (2) organ-specific random generators of asymmetry, which generate asymmetric organ shapes and are modulated by the left-right bias. Studies of the left-right organizer support step 1, whereas random generators of asymmetry in step 2 are still poorly characterized.

How the bilateral symmetry is broken in the early embryo is now well established. This involves a left-right organizer, referred to as the node in the mouse, which forms as a pit of ciliated cells at embryonic day (E)7.5 (see Lee and Anderson, 2008; Shiratori and Hamada, 2006). The motility of cilia generates a leftward fluid flow (Nonaka et al., 1998), which is required between the 1 to 6 somite stages for the asymmetric expression of components of Nodal signaling. *Dand5*, encoding a Nodal antagonist, is the first gene asymmetrically expressed, on the right side of the perinodal region (Kawasumi et al., 2011; Marques et al., 2004). As a result, Nodal, a secreted factor of the TGF-β family, becomes active only on the left side of the perinodal region, as detected by the phosphorylation of the Smad2 transcription factor (Kawasumi et al., 2011). It stimulates its own asymmetric expression in the left perinodal region and the left lateral plate mesoderm (Brennan et al., 2002; Saijoh et al., 2003). *Nodal* expression is initiated lateral to the node, then propagates anteriorly and posteriorly in the left lateral plate mesoderm by autoactivation (Lowe et al., 1996; Vincent et al., 2004). Nodal also activates its own antagonists *Lefty1/2*, suggestive of a patterning mechanism by reaction-diffusion as shown in the fish blastula (Müller et al, 2012). The negative feedback loop ensures transient expression of *Nodal* in the lateral plate mesoderm, where heart precursors are localized, between the 3 and 6 somite stages. *Nodal* is not expressed within the heart tube (Collignon et al., 1996; Vincent et al., 2004). Deletion of the asymmetric enhancer (ASE) of *Nodal* dramatically reduces left-sided *Nodal* expression and impairs the formation of the heart and lungs (Norris et al., 2002). Similarly, the conditional inactivation of *Nodal* in the mesoderm impairs left-right asymmetry of the heart, lungs, spleen, and stomach (Kumar et al., 2008). Nodal is thus a major left determinant, required in the lateral plate mesoderm for asymmetric organogenesis. The phenotype of *Nodal* mutants is either symmetrical, i.e., right isomerism as seen in the lungs, spleen, and atria, or randomly lateralized, as seen in the stomach, gut, heart apex, or heart tube (Brennan et al., 2002; Kumar et al.,

2008; Lowe et al., 2001; Saijoh et al., 2003). Beyond its asymmetric expression in cell precursors of the lateral plate mesoderm, it has remained unclear by which mechanism Nodal regulates the morphogenesis of visceral organs.

The primordium of the heart is a tube, which grows by addition of precursor cells from the heart field to the arterial (cranial) and venous (caudal) poles (Domínguez et al., 2012; Kelly et al., 2001). The heart becomes asymmetrical during the process of heart looping, which transforms the tubular primordium into a helix. This process, which has been extensively studied in the chick embryo, is crucial to position the cardiac chambers relative to each other and thus establish the double blood circulation (see Desgrange et al., 2018). From 3D (dimensions) reconstructions in the mouse embryo at E8.5, we have previously characterized the spatiotemporal dynamics of heart looping and established specific staging criteria (Figure 1A). A model for a heart-specific random generator of asymmetry was proposed (Le Garrec et al., 2017). This is based on buckling, when the heart tube grows between fixed poles as a mechanism able to generate random deformations. We uncovered sequential and opposed asymmetries at the poles, which can bias the buckling to generate a helix: a rightward rotation of the arterial pole at E8.5f, followed by an asymmetric ingression of heart precursors at the venous pole at E8.5g. Finally, the progressive breakdown of the dorsal mesocardium provides an additional mechanical constraint that reinforces looping, as suggested also by inhibition of matrix metalloproteases in the chick (Linask et al, 2005). On these bases, we have generated a computer model, which can predict the shape of the heart loop, not only its direction, thus, providing an original framework to analyze asymmetric heart morphogenesis. However, the molecular mechanisms of the left-right asymmetries at the heart tube poles have remained unknown.

Nodal (Brennan et al., 2002; Kumar et al., 2008; Lowe et al., 2001; Saijoh et al., 2003) or components of Nodal signaling, such as the transcription factor Foxh1, the co-receptor Cfc1, or the protease Furin (von Both et al., 2004; Roebroek et al., 1998; Yan et al., 1999), have been shown to control the direction of the heart loop. These studies have focused on the binary looping direction, as a readout of the symmetry-breaking event, but have not addressed the specific shape of the heart helix, as a readout of the heart-specific generator of asymmetry. In addition to heart looping, left-right patterning of cardiac precursors is important for the left-right identity of atrial chambers and the morphogenesis of the outflow tract. Clonal analyses of myocardial cells have shown a differential origin of the pulmonary and aortic trunks from left and right precursors, respectively (Lescroart et al., 2010, 2012). In keeping with the spiraling of the great arteries in the mature heart, the outflow tract undergoes a rightward rotation (Bajolle et al., 2006), which follows that of the arterial pole during heart looping (Le Garrec et al., 2017). Regionalization of the outflow tract prefigures the separation of the great arteries, as marked by *Sema3c* (Théveniau-Ruissy et al., 2008). Outflow tract defects have been associated with *Nodal* mutations in mouse models (Kumar et al., 2008; Lowe et al., 2001; Saijoh et al., 2003) and in patients, including a higher occurrence of pulmonary atresia and transposition of the great arteries (Bouvagnet and de Bellaing, 2016; Mohapatra et al., 2009).

A pending question is the identification of the molecular effectors downstream of Nodal signaling, and how they control asymmetric cell behavior during organogenesis. Targets of the Nodal pathway have been mainly identified in the context of zebrafish gastrulation (Bennett et al., 2007), ES cell differentiation (Brown et al., 2011), or in cell cultures (Coda et al., 2017; Guzman-Ayala et al., 2009), but not in the context of left-right asymmetric organogenesis. A target gene of Nodal signaling in the left lateral plate mesoderm is the isoform *Pitx2c*, which is expressed asymmetrically in the heart tube, mainly in the inner curvature (Campione et al., 2001; Furtado et al., 2011), and regulates asymmetric cell proliferation and atrial cell identity (Galli et al, 2008). However, contrary to Nodal, *Pitx2* or its isoform *Pitx2c* are not required for the proper direction of heart looping (Liu et al., 2002; Lu et al., 1999), highlighting the existence of other Nodal target genes during this process.

Here, we address the specific role of Nodal for mouse heart looping with a high spatiotemporal resolution. We mapped the cardiac precursor cells expressing *Nodal* and determined the time window of Nodal activity. We generated conditional *Nodal* mutants, using *Hoxb1*^{Cre} to target the mesoderm. We combined quantifications of the heart shape in 3D and computer simulations to assess how Nodal controls the heart-specific generator of asymmetry. Our results show that the generator of asymmetry is independent of Nodal and that Nodal is required to amplify and bias pre-existing asymmetries at the tube poles. We show that *Pitx2c* is not required for mediating the biasing signal of Nodal. By transcriptomic analyses, we identify other targets of Nodal, involved in the regulation of asymmetric cell behavior at the heart tube poles. Overall, Nodal is essential for the robust rightward helical shape of the heart. This has functional impact for the blood circulation, given that heart looping underlies the alignment of cardiac chambers.

RESULTS

Nodal Is Expressed in Myocardial Precursors Contributing to a Quarter of the Heart Poles

Since *Nodal* is transiently expressed in the left lateral plate mesoderm and not within the heart tube, we investigated whether *Nodal*-expressing cells are genuine heart precursors. We took advantage of the *Nodal-ASE-lacZ* transgenic line, in which the β-galactosidase is produced under the control of the asymmetric enhancer of *Nodal*. The known perdurance of *lacZ* mRNA and/or β-galactosidase (Echelard et al., 1994) provides a pulse-chase readout of *Nodal* expression in the left lateral plate mesoderm. By 3D imaging of stained embryos at progressive stages of heart looping (Figure 1A), β-galactosidase-positive cells were found not only in the left second heart field but also in the inner curvature of the heart tube poles: in the left sinus venosus, the myocardium of the dorsal left atrium, of the superior atrio-ventricular canal and of the left outflow tract (Figures 1B–1G; Video S1). A sharp boundary was observed within the right ventricle and at the entrance of the left ventricle, such that the two ventricles at E9.5 were largely devoid of β-galactosidase staining (Figure 1H). In the outflow tract, the domain positive for *Sema3c*, a marker of the pulmonary trunk (Théveniau-Ruissy et al., 2008), is broader and includes that of *Nodal-ASE-lacZ* (Figures 1I and 1J). No staining was observed in the endocardium (Video S1). After segmentation of the heart tube myocardium, we measured that a fraction of 17% ± 5% (n = 16) is colonized by β-galactosidase-positive cells, at all stages

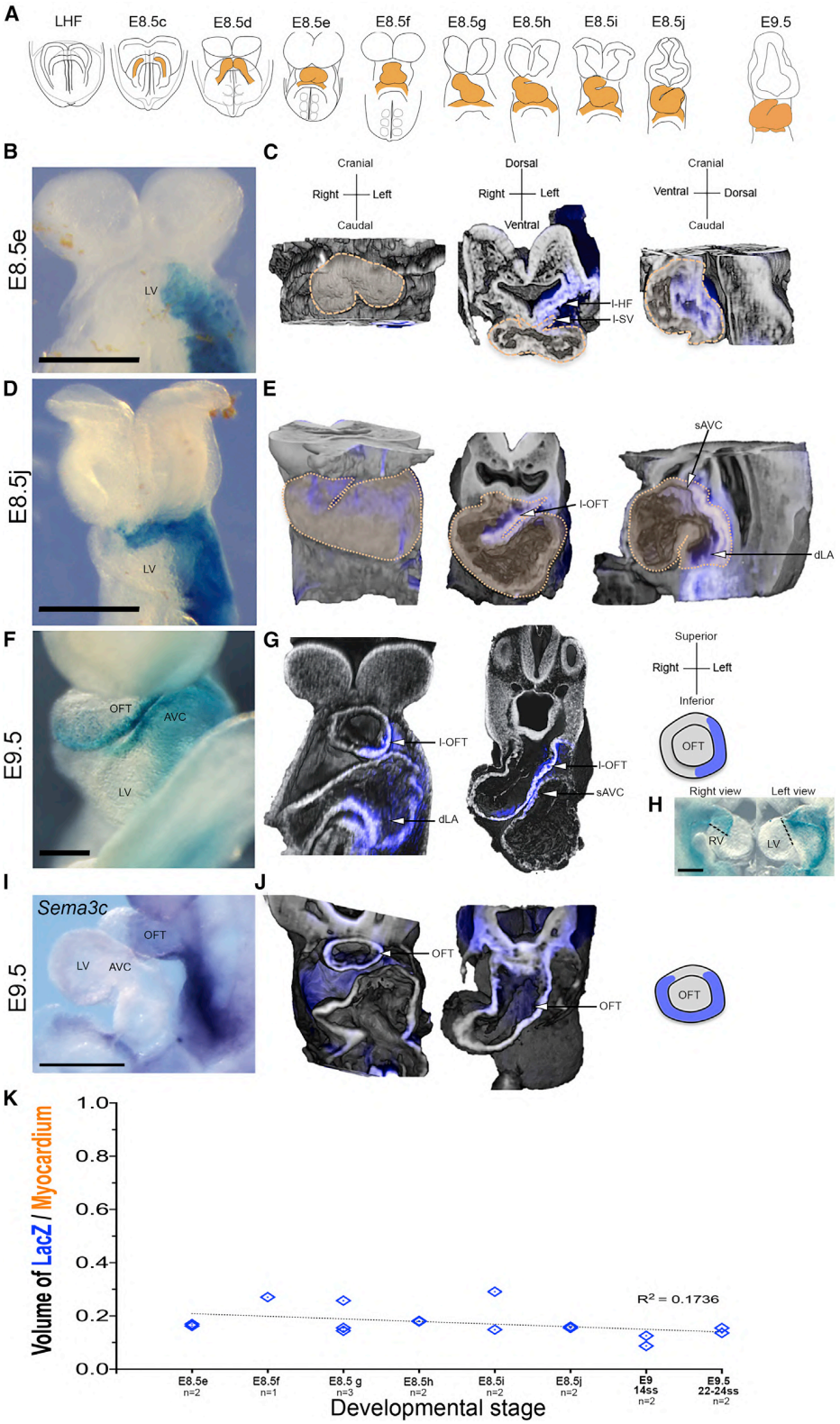

Figure 1. Tracing Cells that Have Expressed Nodal with the *Nodal-ASE-LacZ* Transgene

(A) Schematic representation of the stages of heart looping in the mouse. The cardiac crescent forms at E8.5c and bulges at E8.5d, while cardiomyocytes differentiate (orange). The cardiac tube forms at E8.5e and elongates, with the right ventricle visible from E8.5f and the outflow region from E8.5h. At E8.5g, the

(legend continued on next page)

between E8.5e and E9.5 (Figure 1K). If we consider only the heart regions colonized by β-galactosidase-positive cells, i.e., discarding the ventricles, the fraction increases to 26% ± 4% (n = 4 at E8.5j and E9.5). Thus, we show that left cardiac precursors, which contribute to the ventricles, barely express *Nodal*, whereas left cardiac precursors expressing *Nodal* contribute to a quarter of the cells in the heart tube poles.

Nodal Is Transiently Active before Heart Looping, at E8.5c–e

Nodal expression in the lateral plate mesoderm has been previously reported at 3–6 somite stages (Vincent et al., 2004). However, we found that somitogenesis is not synchronized with heart morphogenesis (Kaufman and Navaratnam, 1981; Le Garrec et al., 2017), so we re-analyzed *Nodal* expression within the context of heart looping stages. By qRT-PCR of the cardiac region, we found expression of *Nodal* at E8.5c–d (Figure 2A), which is compatible with the 3–6 somite window. We then assessed the time window when *Nodal* is active. First, we analyzed the expression of its target *Lefty2*, which we found expressed at E8.5c–e, peaking one stage after Nodal (Figure 2A). Because a mouse litter at E8.5 contains embryos within a range of different looping stages, we used drug treatment in embryo cultures to interfere with Nodal signaling at a specific stage. The SB505124 drug was shown previously to efficiently abrogate Alk signaling (DaCosta Byfield et al., 2004; Hagos and Dougan, 2007). This includes Nodal/activin receptors (Alk4/7), as well as Tgfβr1 receptors (Alk5) that have not been reported to play a role in left-right patterning. When applied to embryos at E8.5c over 8 h, i.e., until E8.5e, SB505124 repressed the expression of the Nodal-specific target genes *Pitx2* and *Lefty2*, whereas it only decreased it upon treatment at E8.5d and had no effect at E8.5e, compared with treatment with the adjuvant (Figures 2B–2E). Exposure over a shorter period of 4 h, i.e., until E8.5d, partially reduced *Pitx2* expression. Taken together, these observations indicate a transient time window of Nodal signaling, between E8.5c and E8.5e, thus, before heart looping.

Nodal Inactivation in the Mesoderm Leads to Four Classes of Looping Defects

To study in more detail looping anomalies, we generated *Nodal* conditional mutants, using *Hoxb1*$^{Cre/+}$ as a driver that is expressed from the onset of gastrulation in the mesoderm (Forlani et al., 2003), overlapping with *Nodal* asymmetric expression. This provides a model of mesoderm-specific *Nodal* inactivation, different from previous lines (Figure S1). We first collected mutants at birth and found a heterotaxy phenotype, including lung, colon, and heart defects (Table 1), but no anomaly in most abdominal organs (intestine, spleen, stomach, and liver) as reported in other types of *Nodal* mutant lines (Brennan et al., 2002; Kumar et al., 2008; Lowe et al., 2001; Saijoh et al., 2003). Then, we collected embryos at E9.5, when heart looping is complete in wild-type embryos, and analyzed the heart phenotype of *Nodal* mutants. In a collection of 56 mutants, we observed 4 classes of anomalies (Figure 3A), with an equal frequency (Figure 3B). The classes are defined by the position of the ventricles: inversely lateralized (class 1), both on the right side (class 2), both on the left side (class 3), or normally lateralized (class 4). To confirm the identity of the ventricles, and more generally assess whether heart segments were correctly patterned, we performed a double *in situ* hybridization (ISH), using *Wnt11* as a marker of the outflow tract (Zhou et al., 2007) and *Bmp2* as a marker of the atrio-ventricular canal (Ma et al., 2005) and ventral left atrium. In addition to the sulcus separating the ventricles, this was enough to identify all cardiac segments in a single labeling experiment (Figure 3C). Staining of *Nodal* mutants indicated normal patterning of the heart tube and confirmed the localization of the right and left ventricles in the different classes of mutants. To further assess whether mutant phenotypes represent a continuum or discrete classes, we performed a principal component analysis of the shape of the tube axis, which was extracted as a set of 33 parameters from 3D images by HREM (high-resolution episcopic microscopy) (Video S2). The independent clustering of each class of mutants rules out the hypothesis of a phenotypic continuum (Figures 3D and 3E). We conclude that *Nodal* inactivation in the lateral plate mesoderm impairs the positioning of the embryonic ventricles, leading to four possible configurations, with equal frequency. The full penetrance of heart defects at birth such as complete atrio-ventricular septal defect and malposition of the great arteries (Table 1) indicate that even the milder looping phenotype of class 4 mutants leads to congenital heart defects.

Nodal Inactivation in the Mesoderm Randomizes Heart Looping Direction

Nodal inactivation was previously reported to randomize the direction of heart looping (Brennan et al., 2002; Kumar et al., 2008; Lowe et al., 2001). However, the method used to assess the loop direction was not defined. Since the looped heart tube has a helical shape, we propose to define the direction of heart looping as the orientation of the tube axis helix, seen cranially at E9.5 (as schematized in Figure 4B). 3D reconstructions of the heart loop were color coded for cardiac segments (Figure 4A; Videos S2, S3, S4, S5, and S6); the 3D shape of the tube axis was extracted and averaged for at least 5 embryos (Figure 4B). This shows that heart looping is rightward in class 2 and 4 *Nodal*

tube appears tilted on the right side, so that the right ventricle is progressively repositioned (E8.5i) to the right side of the left ventricle (E8.5j). At E9.5 the outflow tract is bent, and the arterial/venous poles are closer.

(B–H) Brightfield images (B, D, F, and H) and 3D images by HREM (C, E, and G) of *Nodal-ASE-lacZ* embryos at E8.5e, n = 2 (B and C), E8.5j, n = 2 (D and E) and E9.5, n = 2 (F and H). Ventral views (left panels), transversal (third panel), and sagittal (right panel) sections are shown, with β-galactosidase staining in blue. The orange dotted line outlines the heart tube. Regionalization of the staining in the outflow tract is schematized on the right (G). The black dotted lines in (H) highlight sharp boundaries between β-galactosidase-positive and -negative regions.

(I and J) Brightfield image (I) and 3D images by HREM (J) of *Sema3c* ISH (in blue), n = 2.

(K) Quantification of the β-galactosidase-positive myocardium volume at the indicated stages of heart looping. The low correlation coefficient (R^2) indicates a constant fraction at the different stages. Scale bars: 200 μm. dLA, dorsal left atrium; LHF, late headfold stage; l-HF, left heart field; (l-)OFT, (left) outflow tract; l-SV, left sinus venousus; LV, left ventricle; n, number of observations; RV, right ventricle; sAVC, superior atrio-ventricular canal; ss, somite stage. See also Video S1.

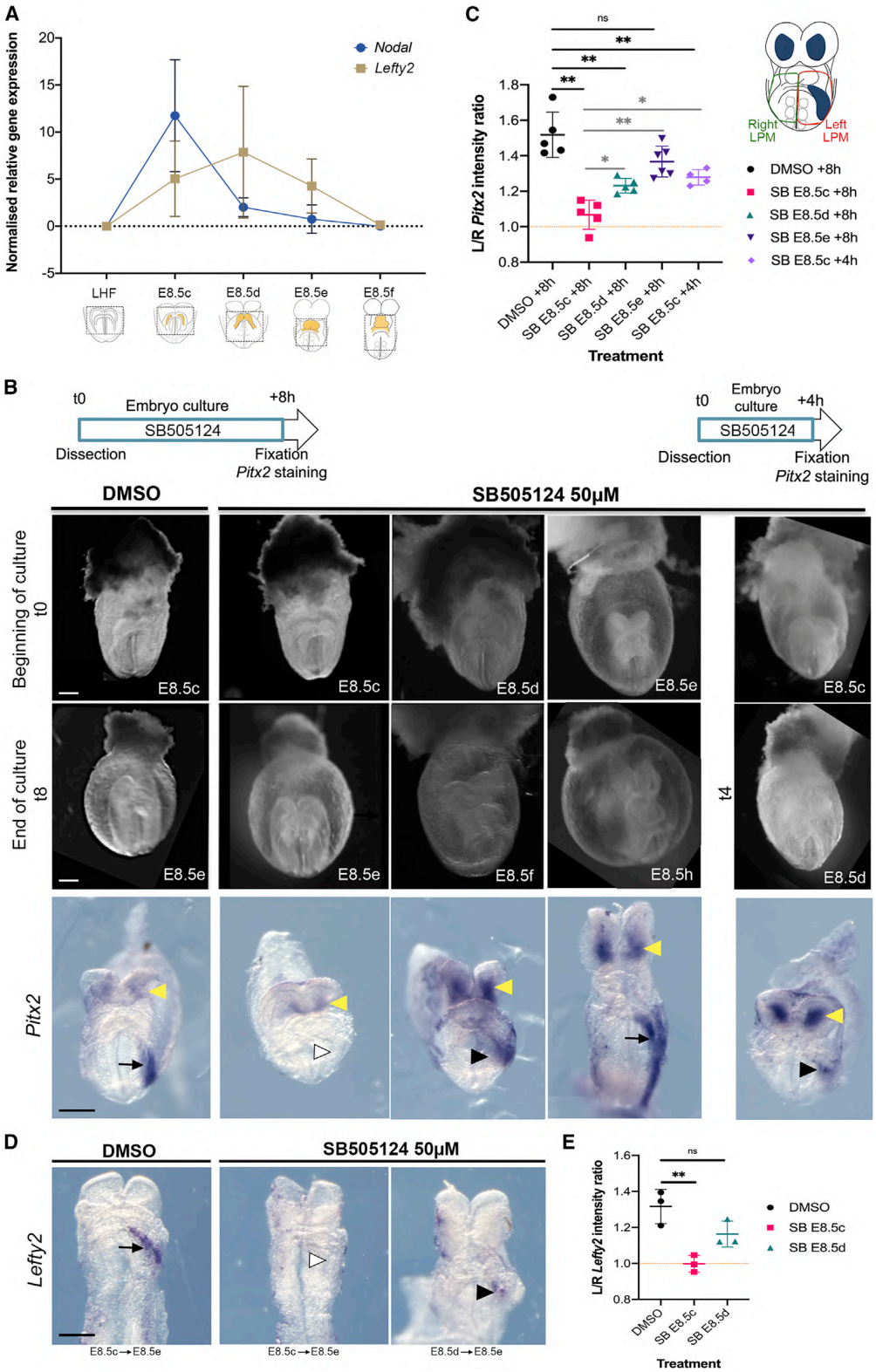

(legend on next page)

mutants, as in control littermates, whereas it is leftward in class 1 and 3 mutants. Given the equal frequency of the mutant classes, we conclude that the direction of heart looping is indeed randomized, when *Nodal* is inactivated in the mesoderm. However, the description of the loop direction is not sufficient to characterize heart defects, since mutant classes 2 and 4 or classes 1 and 3 have distinct shapes.

Existence of a Random Generator of Asymmetry Independent of Nodal

Within the framework of the model of heart looping that we have proposed previously (Le Garrec et al., 2017), we analyzed whether the associated parameters are affected. Heart looping depends on the buckling of the heart tube, growing between fixed poles. In any class of $Nodal^{flox/null}$;$Hoxb1^{Cre/+}$ mutants, we found no significant difference in growth compared with control littermates (Figures S2A–S2F). The distance between the mutant heart poles did not significantly differ from controls (Figure S2G). Finally, the breakdown of the dorsal mesocardium, which modulates the degree of buckling, occurred normally in the mutant samples (Figure S2H). Thus, *Nodal* inactivation affects neither the growth nor the buckling of the heart tube.

In contrast to *Foxh1* mutants, in which ventral loops with no obvious left-right asymmetry were observed (von Both et al., 2004), *Nodal* mutant hearts still have an asymmetric shape, though abnormal. We quantified the degree of heart looping in *Nodal* mutants, as evidenced by the progressive repositioning of the right ventricle, which, in control embryos, is cranial at E8.5e and right-sided at E8.5j relative to the left ventricle (Le Garrec et al., 2017). This measure provides a quantitative definition of the discrete classes of mutant hearts, taking into account that the angle is mirror imaged in classes 1 and 3 (Figure 4C). In none of the mutants has this orientation remained cranio-caudal, indicating an asymmetric deformation of the tube. However, the repositioning of the right ventricle was significantly reduced in *Nodal* mutant classes 1, 2, and 3. These observations point to the persistence of some degree of heart looping in *Nodal* mutants, supporting the idea that a heart-specific random generator of asymmetry remains functional in the absence of Nodal.

Nodal Inactivation Affects Left-Right Asymmetries at the Heart Tube Poles

Our previous computer simulations have shown that the buckling is biased by sequential and opposed left-right asymmetries at the arterial and venous poles. These are important to correctly shape the helix of the heart loop (Le Garrec et al., 2017). One manifestation of these asymmetries is the leftward displacement of the venous pole from E8.5g. This was absent or inverted in 3/5 *Nodal* mutants at E8.5h, when mutant classes cannot be determined (Figure S3D). At E9.5, the leftward displacement, which is accentuated in control embryos, was significantly reduced in class 2, 4 *Nodal* mutants and abrogated (midline location) in class 1, 3 mutants (Figure 4D). At the arterial pole, we observed anomalies in the curvature of the outflow tract at E9.5. From a cranial view, the outflow tract was significantly straighter in class 1, 3, 4 *Nodal* mutants compared with controls (Figures 4B and 4E), whereas in a lateral view, it was straighter in class 1, 2, 3 mutants (Figures 4F, S3A, and S3B). Earlier at E8.5f, we detected a reduced rotation of the arterial pole in 9 mutants analyzed, and 5 cases of reversed direction (Figure S3C).

When analyzing the expression patterns of *Wnt11* and *Bmp2* in 3D, we noticed that they are regionalized in wild-type heart tube poles at E9.5 and that this is not detectable in brightfield images. *Wnt11*, which is a known target of *Pitx2* (Zhou et al., 2007), was found asymmetrically expressed on the left side of the outflow tract at E9.5 (Figures 4G and 4H), in a similar domain to *Nodal-ASE-lacZ* (Figure 1F). *Bmp2* was detected in the left, but not right, ventral atrium (Figure 4I). This provides molecular markers of the left-right identities of the heart poles, where sequential and opposed asymmetries are important to shape the heart loop. In *Nodal* mutants, *Bmp2* expression was found correctly left-sided in classes 2 and 4, which loop rightward. In reverse, it was abnormal in classes 1 and 3, which loop leftward (Figure 4I). However, we observed distinct abnormal patterning of *Bmp2* in the atria: bilateral, partially penetrant, in class 1 mutants, and midline, fully penetrant, in class 3 mutants. Bilateral staining is reminiscent of atrial isomerism, as also detected at birth by the anatomy of atrial appendages (Table 1), whereas midline staining may reflect the position of the atrio-ventricular canal, which fails to be displaced laterally in class 3 mutants (Figures 4B and 4D). At the arterial pole of *Nodal* mutants, *Wnt11* expression was also correctly left-sided in classes 2 and 4, whereas it was incorrectly localized to the superior outflow tract in classes 1 and 3, with a partial penetrance in class 1 (Figures 4G–4H). This staining may reflect an abnormal rotation of the outflow tract, as also detected at birth by the malposition of the great arteries (Table 1). Our observations thus indicate that the left-right patterning of the heart poles correlates with the

Figure 2. Temporal Window of *Nodal* Expression and Signaling

(A) Quantification of *Nodal* and *Lefty2* expression by qRT-PCR in microdissected cardiac regions (dotted lines) at LHF (n = 3), E8.5c (n = 4), E8.5d (n = 5), E8.5e (n = 4), and E8.5f (n = 4 and 3, respectively). The dotted line indicates the threshold of expression, based on primer efficiency in a reference sample. Means and standard deviations are shown.

(B) The experimental design of embryo cultures is schematized, for a drug exposure of 8 h (left) or 4 h (right). Examples of embryos are shown at the beginning (top panels) and end (middle panels) of the cultures, treated with the inhibitor of Nodal signaling (SB505124) or with the adjuvant (DMSO). ISH of *Pitx2* at the end of the culture is in the lower panels, indicating strong (arrows), reduced (black arrowheads) or absent (white arrowhead) expression in the left lateral plate mesoderm. Bilateral expression in the oral ectoderm (yellow arrowheads) provides a control.

(C) Corresponding quantification of *Pitx2* expression, as the ratio between the left and right lateral plate mesoderm (see schema). *p < 0.05, **p < 0.01 (one-way ANOVA with a Tukey Kramer post-hoc test compared with DMSO [black] or between treatments [gray], n = 5, 5, 5, 6, and 4). The orange dotted line indicates symmetric expression.

(D) ISH of *Lefty2* at the end of the culture, with the timing of drug treatment indicated below.

(E) Corresponding quantification of *Lefty2* expression. **p < 0.01 (one-way ANOVA with a Tukey Kramer post-hoc test compared with DMSO, n = 3 per condition). Scale bars: 200 μm. LHF, late headfold stage; LLPM, left lateral plate mesoderm; LV, left ventricle; n, number of observations; RLPM, right lateral plate mesoderm; RV, right ventricle.

Table 1. Situs of Visceral Organs and Congenital Heart Defects at Perinatal Stages (E18.5 and P0)

	Control (n = 10) *Nodal*$^{flox/+}$; *Hoxb1*$^{+/+}$	Mutant (n = 33) *Nodal*$^{flox/Nul}$; *Hoxb1*$^{Cre/+}$
Heart Apex Position		
Levocardia	100%	43%
Mesocardia	0%	21%
Dextrocardia	0%	36%
Heart Malformations		
Complete atrio-ventricular septal defect	0%	100%
Malposition of the great arteries	0%	100%
Right atrial isomerism	0%	70%
Bronchus Anatomy		
Situs solitus	100%	0%
Right isomerism	0%	100%
Colon Flexure		
Normal	100%	64%
Abnormal	0%	36%
Spleen Position		
Situs solitus	100%	100%
Liver Lobation		
Situs solitus	100%	100%
Stomach Position		
Situs solitus	100%	100%

10/31 *Nodal*$^{flox/Nul}$; *Hoxb1*$^{Cre/+}$ mutants were recovered at E18.5 and 23/150 at P0, indicating normal Mendelian ratios (p = 0.96, n = 181, chi-square test). Right atrial isomerism is defined by the symmetry of the right atrial appendages. See Desgrange et al. (2019) for the phenotyping nomenclature.

direction of the heart loop (abnormal in classes 1, 3), but *Wnt11*/*Bmp2* markers are not enough to predict a unique mutant class.

Taken together, our 3D analyses show that Nodal is required for the proper shape of the outflow tract, for the correct position of the venous pole and the right ventricle. In class 1 and 3 *Nodal* mutants, leftward looping is associated with more severe anomalies and defective regionalization of the arterial and venous poles.

Nodal Is Required to Amplify and Coordinate Left-Right Asymmetries

To understand the mechanism leading to the 4 classes of shapes generated in the absence of Nodal, we used our computer model of heart looping (Le Garrec et al., 2017). Based on our observations in *Nodal* mutants, we reasoned that the parameters of buckling itself were normal, whereas the left-right asymmetries at the poles were changed. Randomizing the laterality of two parameters (asymmetry at the arterial and venous poles) would be sufficient to generate 4 classes of shapes. However, we also noticed that the shape of control embryos was not observed in mutants. Class 4 mutants are closest to the control phenotype, yet significantly deviate from it (Figures 4D, 4E, 5A, and 5C), indicative of incomplete heart looping. In reverse, we also noticed that the leftward loops are not mirror images of the wild-type heart (Figures 4A, 5B, and 5C), again indicative of incomplete heart looping. Given the reduced asymmetries observed at the poles (Figures 4D, S3C, and S3D), we thus postulated that they not only had a variable laterality but also a reduced intensity. We simulated a 50% reduction of intensity, which is within the range of our observations. Computer simulations testing these hypotheses were sufficient to reproduce the 4 classes of mutant shapes, as defined by the position of the ventricles (Figures 5D compared with 3A). To further validate the simulations, we predicted the orientation of the right ventricle-left ventricle axis in all classes of shapes and observed a remarkable correlation with the biological values (Figure 5E). The model, including both a randomized laterality and a reduction of asymmetries at the poles, is thus able to recapitulate *Nodal* mutant shapes. Our work demonstrates that Nodal is required to amplify and coordinate opposed left-right asymmetries at the poles of the heart tube, thus, generating a robust helical shape.

Nodal Modulates Cell Proliferation, Differentiation and Extracellular Matrix Composition

To understand how Nodal could modulate left-right asymmetries at a molecular level, we first analyzed its main target, the transcription factor Pitx2. We quantified by qRT-PCR that *Pitx2c* is expressed as early as *Nodal* but maintained after E8.5e (Figures S4A and S4B). We then analyzed mutant embryos, in which the asymmetric enhancer of *Pitx2* is deleted (*Pitx2*$^{\Delta ASE/\Delta ASE}$), or the asymmetrically expressed isoform *Pitx2c* inactivated. We detected mild malformations of the heart loop at E9.5: abnormal patterning of the atria in *Pitx2*$^{\Delta ASE/\Delta ASE}$ hearts (*Bmp2* in Figure S4D), which is one aspect of *Nodal* mutants, and malposition of the atrio-ventricular canal in *Pitx2*$^{\Delta ASE/\Delta ASE}$ and *Pitx2c*$^{null/null}$ mutants (orange arrowheads Figures S4D and S4E), which was not observed in *Nodal* mutants. ISH with a probe detecting the three isoforms of *Pitx2*, and qRT-PCR of *Pitx2* isoforms suggest compensation by the *Pitx2a/b* isoforms in the absence of *Pitx2c* (Figures S4B and S4C). We then looked at *Pitx2* mutants, in which all three isoforms are inactivated. *Pitx2abc*$^{tm1Sac/tm1Sac}$ mutants displayed mild malpositions of the atrio-ventricular canal (Figure S4F). 6/12 *Pitx2abc*$^{tm1Jfm/tm1Jfm}$ mutants as well as all *Pitx2abc*$^{tm1Sac/tm1Sac}$ mutants resemble the mild phenotype of *Pitx2c*$^{null/null}$ mutants. 3/12 *Pitx2abc*$^{tm1Jfm/tm1Jfm}$ mutants had more severe looping anomalies, as judged by the more cranial position of the right ventricle and the more medial position of the left ventricle, whereas the most severe mutants (3/12) were very similar to class 2 *Nodal* mutants (Figures S4F compared with 3A). The leftward displacement of the venous pole was significantly decreased in *Pitx2abc*$^{tm1Jfm/tm1Jfm}$ mutants only (Figure S4G). Thus, *Pitx2* mutants do not phenocopy the full spectrum of heart looping defects in *Nodal* mutants.

To identify other targets of Nodal, we used a transcriptomic approach. The heart region (Figure 6A) was isolated at E8.5e–f, just after *Nodal* extinction (Figure 2A) and just before the morphological changes of heart looping. We compared the transcriptome in control and mutant samples. We first validated the dissection and genotype of samples, based on specific markers (Figures S5A and S5B). Then, we analyzed the GO terms of 481 differentially expressed genes (Table S1; Figure S5C), showing cell-cycle, collagen, chromatin, and muscle terms as

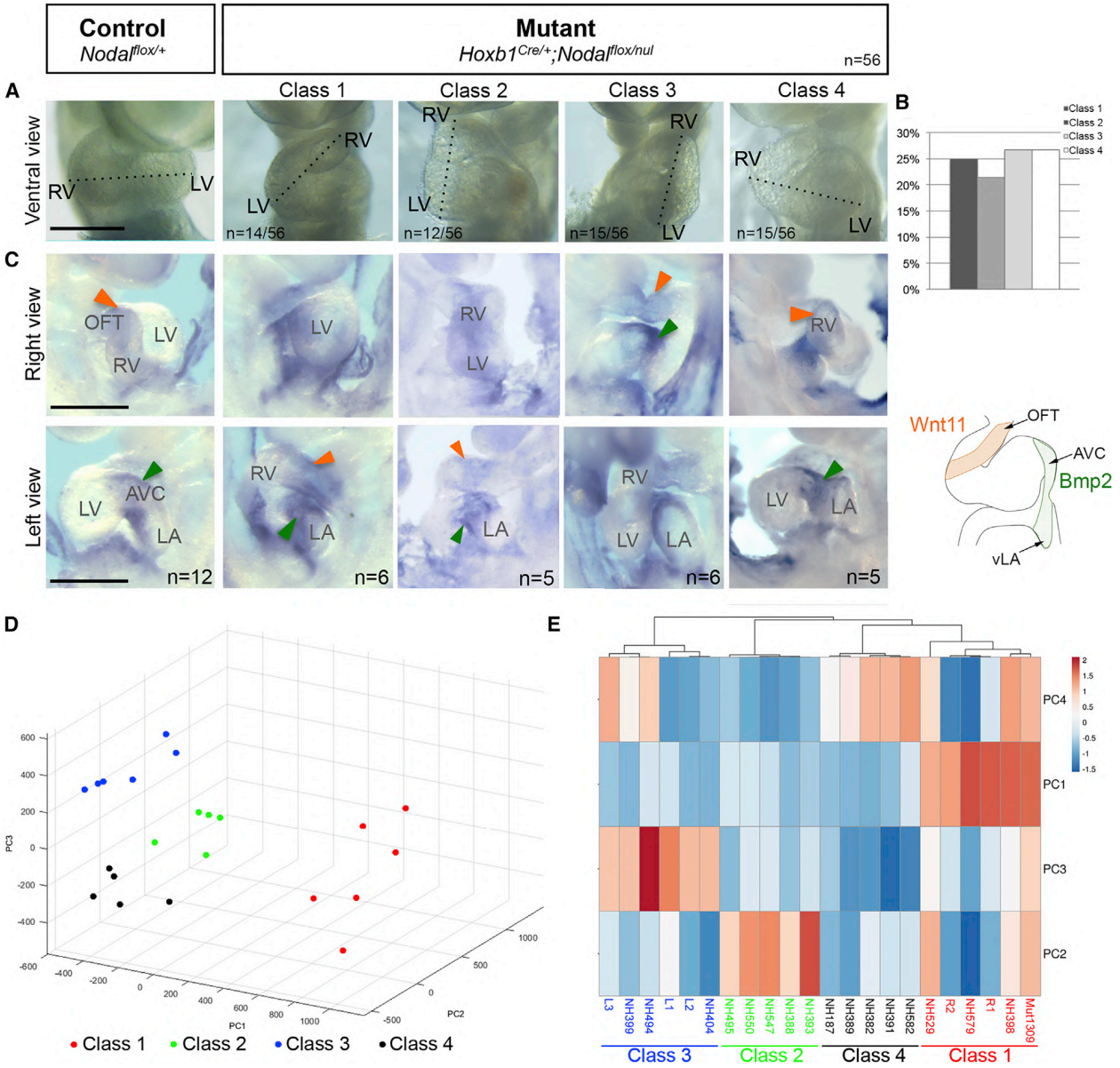

Figure 3. Classes of Looping Defects in *Nodal*$^{flox/nul}$;*Hoxb1*$^{Cre/+}$ Mutants

(A) Brightfield images of control and mutant embryos at E9.5. Four classes of looping defects are detected, based on the positions of the right and left ventricles.

(B) Equal frequency of the four classes of mutants (p value = 0.93, chi^2 test, n = 56 mutant embryos from 33 litters).

(C) Double ISH of *Wnt11* (orange arrowheads), labeling the outflow tract and the right ventricle, and *Bmp2* (green arrowheads) labeling the superior atrio-ventricular canal and the ventral left atrium. See also Videos S2, S3, S4, S5, and S6 and Figure S1.

(D) Principal component (PC) analysis of 33 parameters characterizing the loop shape in the different classes of mutants.

(E) Clustering of individual mutants based on the four principal components, the values of which is color coded from blue to orange. Scale bars: 400 μm. AVC, atrio-ventricular canal; LA, left atrium; LV, left ventricle; n, number of observations; OFT, outflow tract; RV, right ventricle; vLA, ventral left atrium. See also Figure S1; Videos S2, S3, S4, S5, and S6.

significantly enriched gene sets. The cell-cycle genes *Ccnd2*, *Ccne1*, *Cdc25a*, *Cdc6*, *Cdt1*, *Mcm3/5/10*, and *Pcna* were significantly upregulated in *Nodal* mutants, whereas the cell-cycle exit gene *Cdkn1b* was significantly downregulated (Figure 6B). To confirm an effect on cell proliferation, we labeled embryos with the mitotic marker phosphorylated histone H3 at different stages of heart looping (Figure 6C). Since *Nodal* is expressed in the left heart field, we quantified mitotic cells as a ratio between the right and left heart fields. In control embryos, we observed asymmetric proliferation, with significantly more mitotic cells on the right side from E8.5f onward (Figure 6D). In contrast, in *Nodal* mutants, no significant asymmetry was observed at E8.5e–i. Thus, molecular and cellular analyses support a role for Nodal in controlling the asymmetric proliferation of heart precursors.

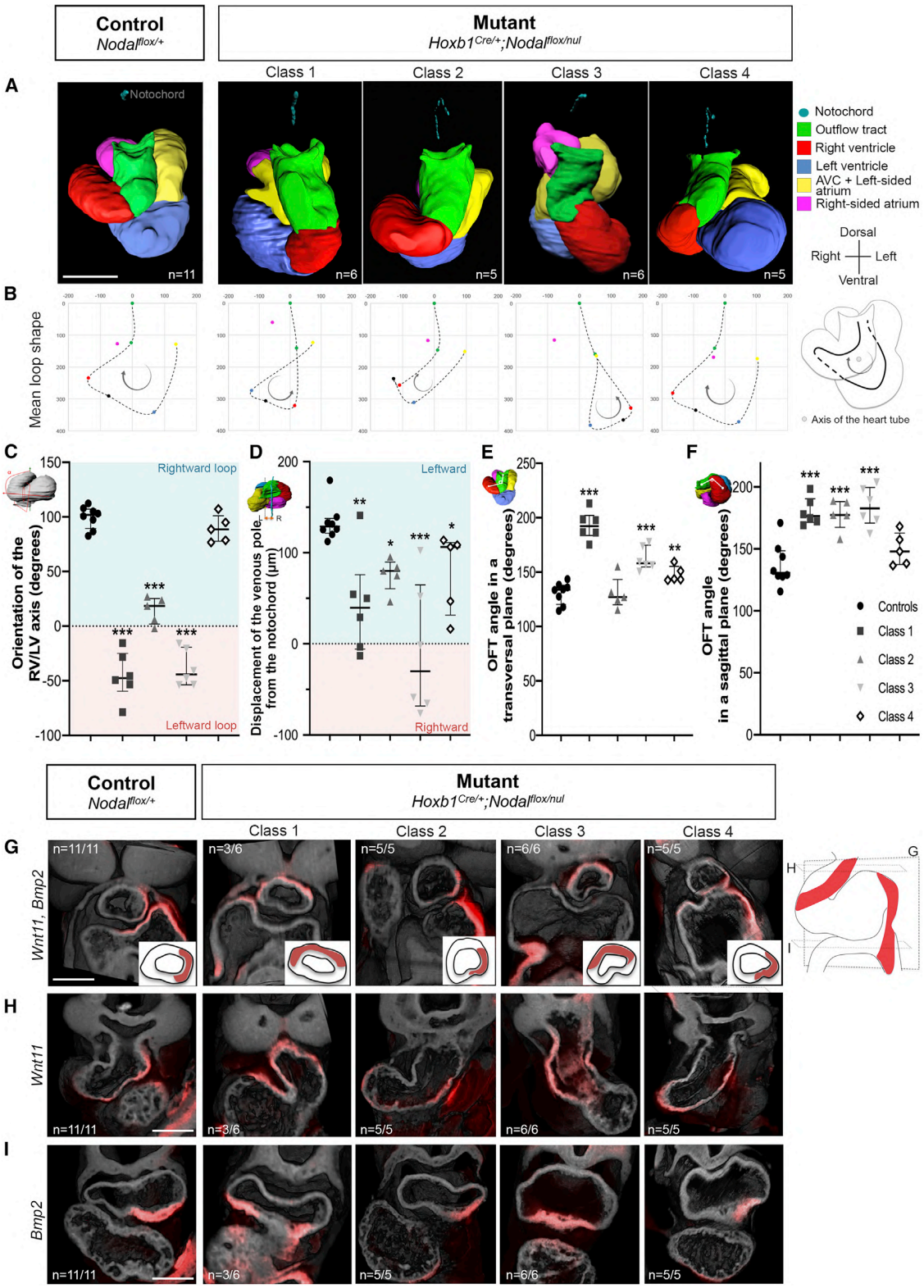

Figure 4. Quantification of Looping Defects in *Nodal*$^{flox/null}$;*Hoxb1*$^{Cre/+}$ Mutants

(A) Cranial views of the 3D-segmented heart tube in control and mutants at E9.5, with regions color coded based on *Bmp2/Wnt11* expression and histology. The samples are aligned with the notochord vertical. See also Videos S2, S3, S4, S5, and S6.

(legend continued on next page)

Differentially expressed genes also include genes involved in cardiomyocyte differentiation, such as *Ttn*, *Tnnt1*, and *Vsnl1* (Figure 6E), which are significantly downregulated in *Nodal* mutants. More generally, in a list of 112 cardiomyocyte differentiation genes (Table S2), the vast majority is slightly downregulated (Figures 6E and 6F). With a statistical bootstrap approach, we conclude that there is a collective significant effect of *Nodal* inactivation on cardiomyocyte differentiation. As a validation, we imaged in 3D the expression pattern of *Tnnt1* and *Vsnl1*, encoding a subunit of the slow skeletal troponin and a calcium-binding protein, respectively (Figures 6G and 6H). Expression was detected at the arterial (*Tnnt1*) and venous poles (*Tnnt1* and *Vsnl1*). *Tnnt1* was regionalized similarly to *Nodal-ASE-lacZ* (see Figure 1F) in the left outflow tract and left atrium. Expression of *Tnnt1* was decreased in all *Nodal* mutant classes and bilateralized in the atria of classes 1 and 2. Expression of *Vsnl1* was decreased at the venous pole (atria and proepicardium) of class 1, 2, and 3 mutants.

Other GO terms characterizing genes differentially expressed in controls and *Nodal* mutants relate to collagen and the extracellular matrix (Figure S5C). Several genes encoding extracellular matrix proteins, such as Col1a1/2, Col3a1, Col5a1/2, Col9a3, Reln, Tnc, the extracellular matrix receptor Itga2b, or the matrix metallopeptidase Mmp9, were significantly downregulated in *Nodal* mutants (Figure 7A). This was validated by 3D imaging of expression patterns. *Tnc* expression, which was detected in the heart precursors and arterial pole (Figure 7B), as previously reported (Stennard et al., 2005), was reduced in the arterial pole of *Nodal* mutants. We found higher expression of *Mmp9* (Figures 7C and 7D) and *Col5a2* (Figures 7E and 7F) on the left in control embryos. Expression of *Mmp9* in the outflow tract overlaps with that of *Pitx2*, indicative of Nodal signaling domain (Figure 7G). These asymmetries were lost in *Nodal* mutants (Figures 7C–7E).

To gain insight into genes directly regulated by Nodal signaling we performed bioinformatics analyses of the presence of asymmetric enhancers (ASE) in the vicinity of differentially expressed genes, corresponding to a pair of FoxH1-binding sites, as shown previously in the bona fide Nodal direct target genes *Nodal*, *Pitx2*, and *Lefty2* (Saijoh et al., 1999; Shiratori et al., 2001). 40% of the genes differentially expressed in *Nodal* mutants, including extracellular matrix genes (*Tnc*, *Col5a1/2*, *Col3a1*, *Col1a2*, *Itga2b, Reln*), and 50% of the cardiomyocyte differentiation genes, such as *Vsnl1*, *Gata4, Ttn, Mef2c, Tbx5, Actc1*, and *Cacna1d* contained an ASE signature, which is a significant enrichment compared with the total gene list (chi^2 test p = 0.036 n = 481, 16,954; p = 0.0007 n = 112, 16,954) (Table S3). All together these results indicate that Nodal signaling controls, in part directly, the asymmetric expression of genes involved in cardiomyocyte differentiation and extracellular matrix composition, whereas it controls indirectly, potentially via Pitx2, genes involved in cell proliferation.

Thus, our molecular analyses identify effectors of Nodal signaling, further supporting its role in amplifying left-right asymmetries at the poles of the heart tube.

DISCUSSION

We have mapped in 3D the asymmetric contribution of *Nodal*-expressing precursor cells to the heart tube poles and determined the time window of Nodal signaling, just before heart looping. Our quantitative analyses in conditional mutants further demonstrate that Nodal does not initiate asymmetric morphogenesis, but rather functions as a biasing signal, to coordinate and amplify opposed left-right asymmetries at the heart tube poles, and thus generate a robust helical shape. We have identified genes downstream of Nodal, which are involved in regulating asymmetries in cell proliferation, differentiation or in the composition of the extracellular matrix.

Nodal signaling has been initially identified as the first pathway restricted to the left side of the embryo (Collignon et al., 1996; Levin et al., 1995; Lowe et al., 1996). Nodal is not only required in the node (Brennan et al., 2002) but also in the lateral plate mesoderm (Kumar et al., 2008; Saijoh et al., 2003). Our conditional mutant line indicates a requirement of Nodal in the lateral plate mesoderm for the asymmetric morphogenesis of the heart, lungs, and colon, but not for that of the spleen, stomach, and gut affected in other *Nodal* mutants (Brennan et al., 2002; Kumar et al., 2008; Lowe et al., 1996; Norris et al., 2002; Saijoh et al., 2003). Using 3D reconstructions and more resolutive staging criteria, we now provide a higher spatiotemporal resolution of Nodal signaling in myocardial precursor cells, before heart looping. *Pitx2*, a known target of Nodal, was shown to be dispensable for the proper direction of heart looping (Ammirabile et al., 2012; Liu et al., 2002; Lu et al., 1999), thus, ruling out a role for mediating the biasing function of Nodal. Our mutant analysis indicates that the ASE enhancer of *Pitx2* is required for the atrial situs, but not for heart looping. Although *Pitx2c* was previously reported as the only asymmetric isoform (Kitamura et al., 1999), we now provide evidence that *Pitx2a/b* isoforms are also expressed in the lateral plate mesoderm and are redundant with *Pitx2c* to modulate heart looping. Upon inactivation of the three *Pitx2* isoforms,

(B) The mean trace of the tube axis is represented by a dotted line showing the shape and direction of the heart loop in controls and mutants. The origin (position 0) represents the exit of the outflow tract, seen on a transversal projection (perpendicular to the notochord). Other colored points are the centers of gravity of the corresponding regions, with an additional point (black) at the interventricular sulcus. The arrow indicates the looping direction, from the venous to the arterial pole.
(C) Quantification of the orientation of the RV/LV axis relative to the notochord in controls and the different classes of mutants. Positive (blue) and negative (orange) numbers correspond to the right and left position of the RV, respectively.
(D) Quantification of the lateral displacement of the venous pole.
(E and F) Quantification of the curvature of the outflow tract in the transversal (E) and sagittal (F) planes. Means and standard deviations are shown. *p < 0.05, **p < 0.01, ***p < 0.001 (Kruskal-Wallis test compared with controls, n = 11 controls, n = 6, 5, 6, and 5 for classes 1, 2, 3, and 4, respectively). See also Figures S2 and S3.
(G–I) 3D images by HREM of control and mutant embryos. The expression of *Wnt11* and *Bmp2* is in red, the histology in gray. Section planes (G, frontal; H, transverse at the arterial pole; I, transverse at the venous pole) and the control *Wnt11/Bmp2* pattern are schematized on the right. Regionalization of the staining in the outflow tract is schematized in the bottom right corner of panels in G. AVC, atrio-ventricular canal; L, left; LV, left ventricle; n, number of observations; OFT, outflow tract; R, right; RV, right ventricle. Scale bars: 200 μm. See also Figures S2 and S3.

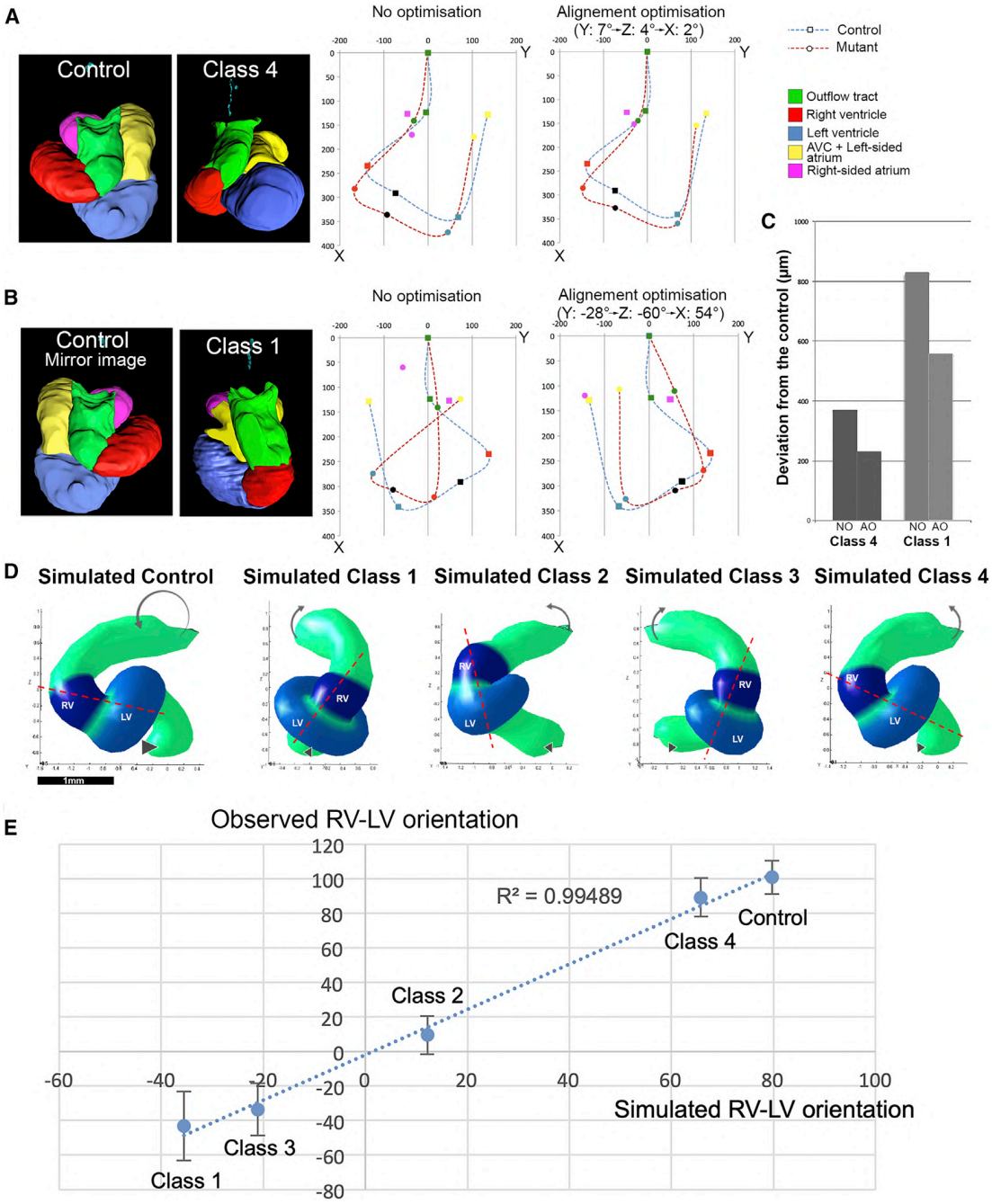

Figure 5. Simulations of Looping Defects in *Nodal* Mutants by Randomized Laterality and Reduced Asymmetry at the Heart Tube Poles

(A–C) Superimposition of the mean heart loop shape (see Figure 4B), seen in a transversal projection, of controls and class 4 *Nodal*$^{flox/null}$;*Hoxb1*$^{Cre/+}$ mutants (A), and of mirror imaged control hearts and class 1 mutants (B). The exit of the outflow tract is taken as a landmark for the alignment. The optimized alignment was obtained by sequential rotations around the three axes as indicated. (C) Quantification of the misalignment, as the total distance between the mutant and control landmark positions.

(D) Computer simulations of heart looping, with different input conditions. The control simulations are run with a 25° rotation of the arterial pole (arrow) and a 2.8-fold asymmetric growth at the venous pole (arrowhead). In mutant simulations, the parameters were reduced by half (see the reduced size of arrows and arrowheads). In simulated class 1, asymmetries at the arterial and venous poles were reversed, in simulated class 2 only the venous pole asymmetry was reversed, in simulated class 3 only the arterial pole asymmetry was reversed. The RV/LV axis is marked by a dotted red line, joining the centroids of the two regions.

(E) Correlation (R^2, Pearson coefficient) between the observed and simulated RV/LV axes (n = 11 controls, n = 6, 5, 6, and 5 for classes 1, 2, 3, and 4, respectively). Means and standard deviations of the observed values are plotted (see Figure 4C). LV, left ventricle; NO, no optimization; AO, alignment optimization; RV, right ventricle.

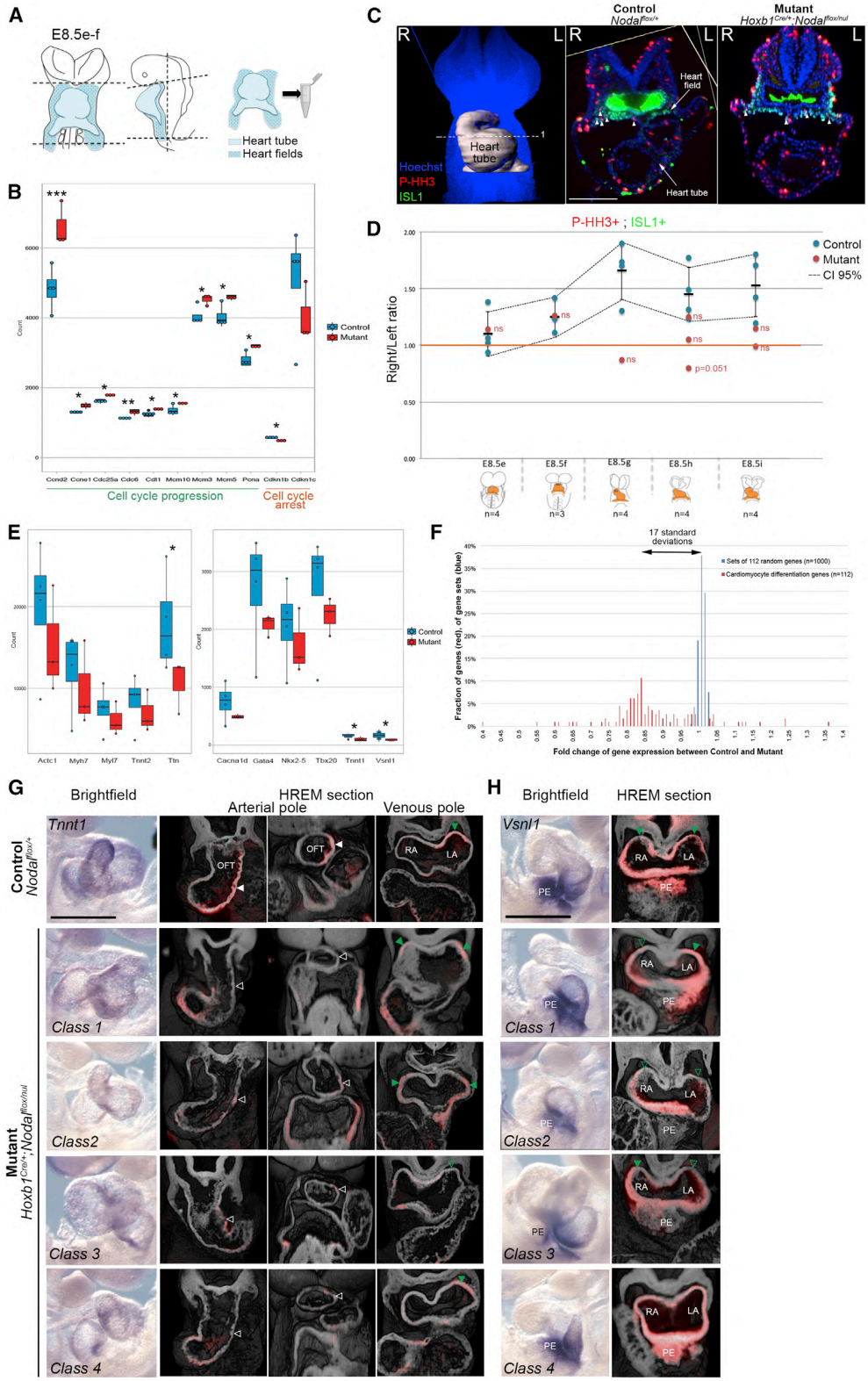

(legend on next page)

anomalies of ventricle position had been reported (Kitamura et al., 1999; Lin et al., 1999; Martin et al., 2010), which we find, in the most severe cases, similar to one class of *Nodal* mutants. *Pitx2* mutants also display specific anomalies, not detected in *Nodal* mutants, such as malposition of the atrio-ventricular canal, in agreement with previous reports (Kitamura et al., 1999; Lu et al., 1999). Thus, Pitx2 mediates aspects of Nodal signaling and has also independent roles. Our transcriptomic analysis identifies targets of Nodal signaling, modulating the proliferation, differentiation, and extracellular matrix composition of cardiac cells, providing a mechanism for how Nodal may generate or amplify molecular left-right asymmetries. Several of these targets (*Tnnt1*, *Vsnl1*, *Col5a2, Mmp9*, and *Tnc*) are expressed asymmetrically in the heart tube poles or heart field, in agreement with the contribution of *Nodal*-expressing cells. Our transcriptomic data highlight downregulation in *Nodal* mutants of many genes involved in myocardial differentiation, including some previously identified in the context of left-right asymmetry, such as *Acta1* (Noël et al., 2013) or *Hcn4* (Pai et al., 2017), whereas *Myh10* expression (Linask et al., 2003) was unchanged. Detection of an ASE enhancer suggests direct regulation by Nodal signaling of half of our gene list, which will have to be confirmed with biochemical approaches. Previous targets of Nodal signaling had been identified in ES cells or during fish gastrulation and mesendoderm specification (Bennett et al., 2007; Brown et al., 2011; Coda et al., 2017; Guzman-Ayala et al., 2009). We have detected little overlap with our gene list (Nodal pathway components, *Cyp26a1*), in keeping with distinct roles of Nodal in distinct tissues and at distinct stages. A common theme is a role of Nodal in cell differentiation, and potentially in cell proliferation and rearrangements, relevant also to Nodal re-expression during cancer progression and metastasis (see Quail et al., 2013).

The phenotype of asymmetry can be decomposed into several components: the initiation of the asymmetry, the fold difference between the left and right, and the laterality of the difference, i.e., whether a left determinant is localized on the anatomical right or left side. We show that Nodal is not required to initiate asymmetric heart looping. In the absence of *Nodal*, heart looping is not randomized in the sense that specific shapes are generated, rather than a continuum of random shapes. The observation of 4 classes of heart loop shapes with an equal frequency supports the model that independent left-right asymmetries at the two heart poles determine the loop shape. It is the laterality of these asymmetries, which is randomized in *Nodal* mutants, but not the process of asymmetry per se. Such a biasing role for Nodal has also been reported for the stomach (Kumar et al., 2008; Saijoh et al., 2003) or for the migration of the parapineal nucleus in the fish diencephalon (Concha et al., 2000). In other instances, Nodal is required to initiate asymmetry and its absence leads to symmetrical phenotypes or isomerism. This is the case for atrial identity, the formation of the mouse lungs and spleen (Brennan et al., 2002; Kumar et al., 2008; Lowe et al., 2001; Saijoh et al., 2003), or for the expression of *cxcr4b*, an early marker of the left habenular nucleus in the fish diencephalon (Roussigné et al., 2009). Our quantitative analyses of shape further show that *Nodal* mutant hearts are distinct from the control shape and from a mirror image. This demonstrates a previously uncharacterized role for Nodal in amplifying left-right asymmetries. Our transcriptomic analysis provides molecular candidates for mediating this amplification. The fact that the reversal of asymmetries does not generate a perfect mirror image of organs may explain why situs inversus totalis (incidence 3/100,000) is not always asymptomatic but can be associated with anomalies in the heart, spleen, and intestinal rotation (Lin et al., 2014).

Our study supports the two-step model of asymmetric organogenesis proposed by Brown and Wolpert (1990) and provides a demonstration of the concept of an organ-specific random generator of asymmetry. In the absence of *Nodal*, we show that some degree of asymmetric morphogenesis occurs, as reported also upon bilateral expression of *Nodal*, in *Snai1* mutants (Murray and Gridley, 2006). This is in agreement with the existence of a generator of asymmetry that is independent of the Nodal left-right bias. We had shown previously that heart looping can be reproduced by a buckling mechanism, when the heart tube grows between fixed poles (Le Garrec et al., 2017). Disruption of buckling, when heart tube growth is impaired, leads to straight tubes, as exemplified in *Tbx20* or *Nkx2-5* mutants (Lyons et al., 1995;

Figure 6. Nodal Targets Modulating Cell Proliferation and Differentiation

(A) Outline (blue) of the region isolated for RNA sequencing at E8.5e–f.

(B) Normalized sequence counts of genes associated with the cell cycle, differentially expressed fold change ≥ 1.2 or $p < 0.05$) in control (n = 4) and *Nodal* mutant (n = 3) samples. *$p < 0.05$, ***$p < 0.001$ (DESeq2). Whisker plots show the median, 25th, 75th quartiles (boxes), and the extreme data points (whiskers). See also Table S1.

(C) Whole-mount immunofluorescence of the heart field marker Isl1 and the mitotic marker phospho-histoneH3 (P-HH3) in controls and mutants. White arrowheads point to double positive cells. L, left; R, right. Scale bar: 200 μm.

(D) Quantification of cell proliferation in the right and left heart field in control (n = 4, 3, 4, 4, 4 at E8.5e, f, g, h, i, respectively) and mutant (n = 1, 1, 1, 3, 2 at E8.5e, f, g, h, i, respectively) embryos at the indicated stages of heart looping. Means, standard deviations, and confidence intervals (CIs) are shown for control samples. Proliferation ratios significantly deviate from 1 in control samples from the E8.5f stage, indicating proliferation asymmetry. Proliferation rates are not significantly different from a homogenous distribution between the left and right in any mutant sample (chi-square test of homogeneity).

(E) Normalized sequence counts of genes associated with cardiomyocyte differentiation, in control (n = 4) and mutant (n = 3) samples. *$p < 0.05$ (DESeq2).

(F) Bootstrap statistical analysis to compare the fold change in the expression of 112 cardiomyocyte genes (red), between controls and mutants, with that of 1,000 randomly sampled sets of 112 genes (blue). The mean fold change for cardiomyocyte genes (0.87) lies 17 standard deviations away from the mean of randomly sampled sets (1.01), indicating a globally significant downregulation of genes involved in cardiomyocyte differentiation. See also Table S2.

(G) Brightfield images (left column) and 3D images by HREM (right columns) of *Tnnt1* ISH in control (upper line) and mutant (lower lines) samples at E9.5. The mutant class is indicated in the bottom (n = 1, 3, 2, and 3 for classes 1, 2, 3, and 4, respectively). Filled and empty arrowheads point to high and low expression in the inner curvature of the outflow tract (white) and left atrium (green), respectively. Note that *Tnnt1* expression is bilateralized in the atria of class 2–3 *Nodal* mutants.

(H) *Vsnl1* ISH in control (upper line) and mutant (lower lines) samples at E9.5. Filled and empty arrowheads point to high and low expression in the atria (green), respectively. The mutant class is indicated in the bottom (n = 1, 2, 2, and 3 for classes 1, 2, 3, and 4, respectively) LA, left atrium; OFT, outflow tract; PE, proepicardium; RA, right atrium. Scale bars: 400 μm. See also Figures S4 and S5; Tables S1, S2, and S3.

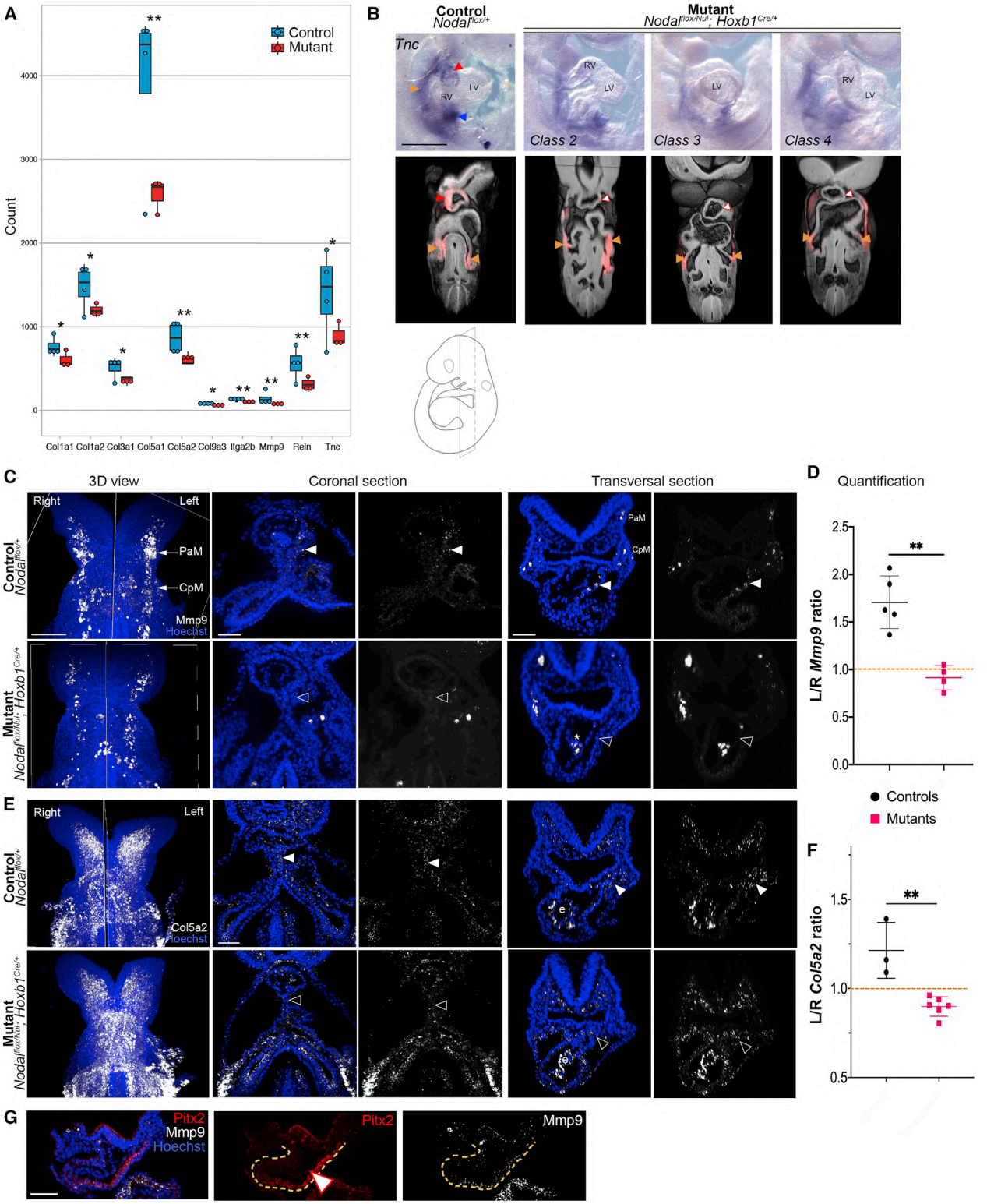

Figure 7. Nodal Targets Related to the Extracellular Matrix

(A) Normalized sequence counts of genes associated with the extracellular matrix, differentially expressed (fold change ≥1.2 or $p < 0.05$) in control (n = 4) and mutant (n = 3) samples. *$p < 0.05$, **$p < 0.01$ (DESeq2). Whisker plots show the median, 25th, 75th quartiles (boxes) and the extreme data points (whiskers).

(legend continued on next page)

Stennard et al., 2005). Computer simulations show that the buckling mechanism in isolation generates random deformations, whereas small left-right asymmetries at the tube poles are sufficient to bias them. Our work points to the existence of left-right asymmetries at the heart tube poles, independent of Nodal, which orient the buckling of the heart tube. The nature of these asymmetries remains to be uncovered, whether they are stochastic, trivial differences or whether they are genetically controlled asymmetries. The facts that the mutant heart loops are not a continuous spectrum of random shapes and that pole asymmetries are clearly detectable in *Nodal* mutants would support the latter hypothesis. However, the underlying molecular mechanism remains unknown. For the arterial pole rotation, the asymmetric cell proliferation that we have observed in the heart field from E8.5g depends on Nodal signaling and thus would not fit as a mechanism. More promising would be actomyosin, which was shown to be important for the later phase of heart looping in the fish, independently of Nodal (Noël et al., 2013) or for the rotation of another tube, the fly hindgut (Chougule et al., 2020). Asymmetries preceding that of Nodal are evident in the brain, involving Fgf, Notch, or Wnt/β-catenin signaling (see Güntürkün and Ocklenburg, 2017), or in the frog embryo, involving ion channels or cytoskeletal rearrangements (Pai et al., 2017).

For the looping of a tube, such as the embryonic heart, intrinsic and extrinsic mechanisms can intervene, depending on whether the asymmetric determinant acts inside or outside the tube. We show that *Nodal* is transiently required in cardiac precursor cells between E8.5c–e. This supports the idea of an extrinsic role of Nodal for heart looping, i.e., in cells outside the heart tube. Whether there are additional intrinsic determinants of heart looping, e.g., regulating differential growth within the tube, remains to be demonstrated. *Nodal*-expressing cells contribute to the myocardium of the arterial and venous poles, but neither to the left ventricle nor to the majority of the right ventricle. This is reminiscent of the second myocardial lineage (Meilhac et al., 2004) and is consistent with fate mapping of the left second heart field (Domínguez et al., 2012). Our observations of largely negative ventricles would thus suggest that cells of the first lineage are not sensitive to left-right patterning. Indeed, they are defined first (Meilhac et al., 2004), ingress first in the primitive streak (Lescroart et al., 2014), differentiate earlier (Ivanovitch et al., 2017), and reach the heart region (cardiac crescent) before the node has become a left-right organizer at the late headfold (LHF) stage (Kawasumi et al., 2011) and before the heart field expresses *Nodal* at E8.5c. Thus, the second heart field, which provides cells for the elongation of the heart tube, as a pre-requisite of the buckling mechanism, and is patterned by Nodal signaling, appears as a driving force of heart looping.

Our quantification of the coverage of the *Nodal-ASE-lacZ* staining suggests a 25% contribution of *Nodal*-expressing cells to the heart poles at E9.5. Given the short time window of *Nodal* expression and the perdurance of β-galactosidase a day later, we expect that most of *Nodal*-expressing cells in the lateral plate mesoderm are labeled with the *Nodal-ASE-lacZ* transgene, compared with a hypothetical *Nodal-ASE-Cre* transgene, which would induce a delay in the initial activation of a reporter. *Nodal-ASE-lacZ* staining thus provides a 3D map of left derivatives in the looped heart tube. The percentage below 50% raises the questions of whether all left cells in the second heart field express *Nodal*, and/or whether left precursor cells contribute less to the heart tube compared with right cells. The higher proliferation of cells that we detect in the right second heart field, as well as the asymmetric contribution of right versus left grafts in the chick precardiac mesoderm (Stalsberg, 1969) would support the second hypothesis.

Our work provides insight into the left-right patterning of cardiac cells, showing that it is a spatiotemporal dynamic process rather than a single event. We have previously detected opposed and sequential left-right asymmetries at the arterial and venous poles (Le Garrec et al., 2017). We now report molecular left-right patterning of the outflow tract (*Wnt11*) and atria (*Bmp2*), which is defective in *Nodal* and *Pitx2*$^{\Delta ASE/\Delta ASE}$ mutants, consistent with malposition of the great arteries and atrial isomerism at birth. However, these molecular anomalies are not fully penetrant and not predictive of a class of abnormal heart looping. This indicates that left-right asymmetry is regulated independently in the different segments of the heart, for the situs of the atria, the position of the atrio-ventricular canal, the relative position of the ventricles, and the regionalization of the outflow tract. With more markers of the heart tube poles identified in our transcriptomic analysis, the molecular signature of the asymmetry of cardiac segments will be refined. Another cardiac asymmetry is the curvature of the outflow tract, arising between E8.5j and E9.5, under the control of Nodal. This curvature is not reproduced in our computer simulations, suggesting that it is not related to the buckling. It is also not correlated with proliferation differences (data not shown), leaving its origin unclear.

In the clinics, heterotaxy is a laterality defect associated with mutations affecting the formation or signaling of the left-right organizer (Guimier et al., 2015). The clinical picture is very variable, in terms of associations of left-right anomalies between different organs or between different heart segments (Desgrange et al., 2019; Lin et al., 2014). Even looking at a single structure such as the atria, the parameters of the anatomy of the appendages and of the connection of the inferior caval vein are not always concordant (Tremblay et al., 2017). This is the basis of

(B) Brightfield images (upper line) and 3D images by HREM (lower lines) of *Tnc* ISH in control (left column) and mutant (right columns) samples at E9.5 (n = 2 in each mutant class). Filled and empty arrowheads point to high and low expression, respectively, in the outflow tract (red), heart precursors (orange), and pro-epicardium (blue).
(C and E) *Mmp9* (C) and *Col5a2* (E) expression detected by whole-mount RNAscope ISH at E8.5g–h. Filled and empty white arrowheads point to high and low expression, respectively, in the heart field and myocardium. Asterisk, blood autofluorescence.
(D and F) Corresponding quantification of asymmetric expression in controls and mutants. **p < 0.01 (Student's t test compared with controls, n = 5 controls, 4 mutants for *Mmp9* and n = 3 controls, 6 mutants for *Col5a2*). The orange dotted line indicates symmetric expression. Signal in the endocardium (e) is not quantified.
(G) Co-expression of *Pitx2* and *Mmp9* in the left outflow tract (outline) by whole-mount RNAscope ISH at E9 (n = 1). CpM, cardiopharyngeal mesoderm; L, left; LV, left ventricle; PaM, paraxial mesoderm; R, right; RV, right ventricle. Scale bars: 400 (B) and 100 (C, E, and G) μm. See also Table S3.

debates in the nomenclature of heterotaxy, for the qualification of isomerism (Jacobs et al., 2007). Clinical variability may relate to the fact that left-right asymmetry is regulated independently at different levels and that Nodal regulates either the initiation or the laterality of asymmetry. The previous focus on the symmetry-breaking event as a binary decision (left, right) has masked the dynamics of left-right patterning. In the future, it will be important to correlate classes of abnormal heart loop shapes with specific congenital heart defects. Quantifications of the contribution of different factors to the fine shape of the heart loop, not just its direction, are expected to provide novel perspectives in understanding the origin of severe congenital heart defects associated with heterotaxy or other types of cardiac chamber misalignment.

SUPPORTING CITATIONS

The following references appear in the supplemental information: Bertrand et al. (2011); Constam and Robertson (2000); Muccielli et al. (1996); Schweickert et al. (2000).

STAR★METHODS

Detailed methods are provided in the online version of this paper and include the following:

- KEY RESOURCES TABLE
- RESOURCE AVAILABILITY
  - Lead Contact
  - Material Availability
  - Data and Code Availability
- EXPERIMENTAL MODEL AND SUBJECT DETAILS
- METHOD DETAILS
  - Embryo Culture
  - Wholemount β-galactosidase Staining and Immunofluorescence
  - RT-qPCR
  - RNA *In Situ* Hybridisation
  - HREM (High-Resolution Episcopic Microscopy)
  - RNA Sequencing
  - FEA Modeling of the Heart Tube
  - Phenotyping at Perinatal Stages
- QUANTIFICATION AND STATISTICAL ANALYSIS
  - Quantification of the Proportion of β-galactosidase Staining
  - Quantification of the ISH Signal
  - Quantification of Immunoflorescence and RNAscope ISH Signal
  - **3**D Rendering and Visualisation
  - Quantification of the Geometry of the Heart Loop
  - Principal Components Analysis and clustering
  - Bioinformatics Analyses of the RNA Sequences
  - Bioinformatics Analysis of ASE Elements
  - Bootstrap Inference on Transcriptomic Data
  - Statistical Analysis

SUPPLEMENTAL INFORMATION

Supplemental Information can be found online at https://doi.org/10.1016/j.devcel.2020.10.008.

ACKNOWLEDGMENTS

We thank V. Benhamo, L. Guillemot, L. Bombardelli, M. Bertrand, A. Murukutla, V. Nikovics, J.-P. Mulon, J. Lokmer, and C. Cimper for technical assistance, J.N. Domínguez for advice in embryo culture, J. Collignon for *Nodal-ASE-lacZ* embryos, H. Hamada and Y. Ikawa for *Pitx2*$^{\Delta ASE/\Delta ASE}$ embryos, B. Sanketi, T.T. Tran, N. Kurpios, and J. Martin for *Pitx2c*$^{null/null}$ mice and *Pitx2abc*$^{tm1Jfm/\ tm1Jfm}$ embryos, M. Campione for *Pitx2abc*$^{tm1Sac/tm1Sac}$ embryos, L. Robertson for *Nodal*$^{flox/flox}$ mice, S. Zaffran for *Hoxb1*$^{Cre/+}$ mice, the histology and imaging platforms of the SFR Necker, C. Bole-Feysot and O. Alibeu of the Genomics platform, N. Cagnard of the Bioinformatics platform, C. Dicu and the LEAT animal facility. This work was supported by core funding from the Institut Pasteur, state funding from the Agence Nationale de la Recherche under "Investissementsd'avenir" program (ANR-10-IAHU-01), a grant from the ANR (16-CE17-0006-01) to S.M.M. and the MSD-Avenir fund (Devo-Decode project). A.D., S.B., and T.B. have benefited from a fellowship of the Fondation Lefoulon Delalande, the Société Française de Pédiatrie, and the Pasteur - Paris University (PPU) International PhD Program respectively; S.M.M. is an INSERM research scientist.

AUTHOR CONTRIBUTIONS

Conceptualization, A.D., J.-F.L.G., S.M.M.; Methodology, A.D. and J.-F.L.G.; Software, J.-F.L.G.; Formal Analysis, J.-F.L.G. and A.D.; Investigation, A.D., J.-F.L.G., S.B., and T.B.; Writing – Original Draft, S.M.M.; Writing – Review & Editing, A.D., J.-F.L.G., and S.M.M.; Visualization, A.D., J.-F.L.G., and S.B.; Supervision, S.M.M. and A.D.; Project Administration, S.M.M.; Funding Acquisition, S.M.M. and A.D.

DECLARATION OF INTERESTS

The authors declare no competing interests.

Received: October 11, 2019
Revised: July 17, 2020
Accepted: October 9, 2020
Published: November 9, 2020

REFERENCES

Ammirabile, G., Tessari, A., Pignataro, V., Szumska, D., Sutera Sardo, F., Benes, J., Balistreri, M., Bhattacharya, S., Sedmera, D., and Campione, M. (2012). Pitx2 confers left morphological, molecular, and functional identity to the sinus venosus myocardium. Cardiovasc. Res. *93*, 291–301.

Arenkiel, B.R., Gaufo, G.O., and Capecchi, M.R. (2003). Hoxb1 neural crest preferentially form glia of the PNS. Dev. Dyn. *227*, 379–386.

Bajolle, F., Zaffran, S., Kelly, R.G., Hadchouel, J., Bonnet, D., Brown, N.A., and Buckingham, M.E. (2006). Rotation of the myocardial wall of the outflow tract is implicated in the normal positioning of the great arteries. Circ. Res. *98*, 421–428.

Bennett, J.T., Joubin, K., Cheng, S., Aanstad, P., Herwig, R., Clark, M., Lehrach, H., and Schier, A.F. (2007). Nodal signaling activates differentiation genes during zebrafish gastrulation. Dev. Biol. *304*, 525–540.

Bertrand, N., Roux, M., Ryckebusch, L., Niederreither, K., Dollé, P., Moon, A., Capecchi, M., and Zaffran, S. (2011). Hox genes define distinct progenitor subdomains within the second heart field. Dev. Biol. *353*, 266–274.

Bouvagnet, P., and de Bellaing, A.M. (2016). Human Genetics of d-transposition of the great arteries. In Congenital Heart Diseases: The Broken Heart, S. Rickert-Sperling, R. Kelly, and D. Driscoll, eds. (Springer), pp. 439–447.

Brennan, J., Norris, D.P., and Robertson, E.J. (2002). Nodal activity in the node governs left-right asymmetry. Genes Dev. *16*, 2339–2344.

Brown, N.A., and Wolpert, L. (1990). The development of handedness in left/right asymmetry. Development *109*, 1–9.

Brown, S., Teo, A., Pauklin, S., Hannan, N., Cho, C.H.H., Lim, B., Vardy, L., Dunn, N.R., Trotter, M., Pedersen, R., and Vallier, L. (2011). Activin/nodal signaling controls divergent transcriptional networks in human embryonic stem cells and in endoderm progenitors. Stem Cells *29*, 1176–1185.

Campione, M., Ros, M.A., Icardo, J.M., Piedra, E., Christoffels, V.M., Schweickert, A., Blum, M., Franco, D., and Moorman, A.F.M. (2001). Pitx2 expression defines a left cardiac lineage of cells: evidence for atrial and ventricular molecular isomerism in the iv/iv mice. Dev. Biol. *231*, 252–264.

Chougule, A., Lapraz, F., Földi, I., Cerezo, D., Mihály, J., and Noselli, S. (2020). The Drosophila actin nucleator DAAM is essential for left-right asymmetry. PLoS Genet. *16*, e1008758.

Coda, D.M., Gaarenstroom, T., East, P., Patel, H., Miller, D.S.J., Lobley, A., Matthews, N., Stewart, A., and Hill, C.S. (2017). Distinct modes of SMAD2 chromatin binding and remodeling shape the transcriptional response to NODAL/activin signaling. Elife *6*, e22474.

Collignon, J., Varlet, I., and Robertson, E.J. (1996). Relationship between asymmetric nodal expression and the direction of embryonic turning. Nature *381*, 155–158.

Concha, M.L., Burdine, R.D., Russell, C., Schier, A.F., and Wilson, S.W. (2000). A nodal signaling pathway regulates the laterality of neuroanatomical asymmetries in the zebrafish forebrain. Neuron *28*, 399–409.

Constam, D.B., and Robertson, E.J. (2000). SPC4/PACE4 regulates a TGFβ signaling network during axis formation. Genes Dev. *14*, 1146–1155.

DaCosta Byfield, S., Major, C., Laping, N.J., and Roberts, A.B. (2004). SB-505124 is a selective inhibitor of transforming growth factor-beta type I receptors ALK4, ALK5, and ALK7. Mol. Pharmacol. *65*, 744–752.

de Chaumont, F., Dallongeville, S., Chenouard, N., Hervé, N., Pop, S., Provoost, T., Meas-Yedid, V., Pankajakshan, P., Lecomte, T., Le Montagner, Y., et al. (2012). Icy: an open BioImage informatics platform for extended reproducible research. Nat. Methods *9*, 690–696.

de Soysa, T.Y., Ranade, S.S., Okawa, S., Ravichandran, S., Huang, Y., Salunga, H.T., Schricker, A., del Sol, A., Gifford, C.A., and Srivastava, D. (2019). Single-cell analysis of cardiogenesis reveals basis for organ-level developmental defects. Nature *572*, 120–124.

DeLaughter, D.M., Bick, A.G., Wakimoto, H., McKean, D., Gorham, J.M., Kathiriya, I.S., Hinson, J.T., Homsy, J., Gray, J., Pu, W., et al. (2016). Single-cell resolution of temporal gene expression during heart development. Dev. Cell *39*, 480–490.

Desgrange, A., Le Garrec, J.-F., and Meilhac, S.M. (2018). Left-right asymmetry in heart development and disease: forming the right loop. Development *145*, dev162776.

Desgrange, A., Lokmer, J., Marchiol, C., Houyel, L., and Meilhac, S.M. (2019). Standardised imaging pipeline for phenotyping mouse laterality defects and associated heart malformations, at multiple scales and multiple stages. Dis. Model Mech. *12*, dmm038356.

Domínguez, J.N., Meilhac, S.M., Bland, Y.S., Buckingham, M.E., and Brown, N.A. (2012). Asymmetric fate of the posterior part of the second heart field results in unexpected left/right contributions to both poles of the heart. Circ. Res. *111*, 1323–1335.

Downs, K.M., and Davies, T. (1993). Staging of gastrulating mouse embryos by morphological landmarks in the dissecting microscope. Development *118*, 1255–1266.

Echelard, Y., Vassileva, G., and McMahon, A.P. (1994). cis-acting regulatory sequences governing Wnt-1 expression in the developing mouse CNS. Development *120*, 2213–2224.

Feiner, L., Webber, A.L., Brown, C.B., Lu, M.M., Jia, L., Feinstein, P., Mombaerts, P., Epstein, J.A., and Raper, J.A. (2001). Targeted disruption of semaphorin 3C leads to persistent truncus arteriosus and aortic arch interruption. Development *128*, 3061–3070.

Forlani, S., Lawson, K.A., and Deschamps, J. (2003). Acquisition of Hox codes during gastrulation and axial elongation in the mouse embryo. Development *130*, 3807–3819.

Furtado, M.B., Biben, C., Shiratori, H., Hamada, H., and Harvey, R.P. (2011). Characterization of Pitx2c expression in the mouse heart using a reporter transgene. Dev. Dyn. *240*, 195–203.

Gage, P.J., Suh, H., and Camper, S.A. (1999). Dosage requirement of Pitx2 for development of multiple organs. Development *126*, 4643–4651.

Galli, D., Domínguez, J.N., Zaffran, S., Munk, A., Brown, N.A., and Buckingham, M.E. (2008). Atrial myocardium derives from the posterior region of the second heart field, which acquires left-right identity as Pitx2c is expressed. Development *135*, 1157–1167.

Guimier, A., Gabriel, G.C., Bajolle, F., Tsang, M., Liu, H., Noll, A., Schwartz, M., El Malti, R., Smith, L.D., Klena, N.T., et al. (2015). MMP21 is mutated in human heterotaxy and is required for normal left-right asymmetry in vertebrates. Nat. Genet. *47*, 1260–1263.

Güntürkün, O., and Ocklenburg, S. (2017). Ontogenesis of lateralization. Neuron *94*, 249–263.

Guzman-Ayala, M., Lee, K.L., Mavrakis, K.J., Goggolidou, P., Norris, D.P., and Episkopou, V. (2009). Graded Smad2/3 activation is converted directly into levels of target gene expression in embryonic stem cells. PLoS One *4*, e4268.

Hagos, E.G., and Dougan, S.T. (2007). Time-dependent patterning of the mesoderm and endoderm by Nodal signals in zebrafish. BMC Dev. Biol. *7*, 22.

Ivanovitch, K., Temiño, S., and Torres, M. (2017). Live imaging of heart tube development in mouse reveals alternating phases of cardiac differentiation and morphogenesis. Elife *6*, e30668.

Jacobs, J.P., Anderson, R.H., Weinberg, P.M., Walters, H.L., Tchervenkov, C.I., Del Duca, D., Franklin, R.C.G., Aiello, V.D., Béland, M.J., Colan, S.D., et al. (2007). The nomenclature, definition and classification of cardiac structures in the setting of heterotaxy. Cardiol. Young *17*, 1–28.

Kaufman, M.H., and Navaratnam, V. (1981). Early differentiation of the heart in mouse embryos. J. Anat. *133*, 235–246.

Kawasumi, A., Nakamura, T., Iwai, N., Yashiro, K., Saijoh, Y., Belo, J.A., Shiratori, H., and Hamada, H. (2011). Left–right asymmetry in the level of active Nodal protein produced in the node is translated into left–right asymmetry in the lateral plate of mouse embryos. Dev. Biol. *353*, 321–330.

Kelly, R.G., Brown, N.A., and Buckingham, M.E. (2001). The arterial pole of the mouse heart forms from FGF10-expressing cells in pharyngeal mesoderm. Dev. Cell *1*, 435–440.

Kennaway, R., Coen, E., Green, A., and Bangham, A. (2011). Generation of diverse biological forms through combinatorial interactions between tissue polarity and growth. PLoS Comput. Biol. *7*, e1002071.

Kitamura, K., Miura, H., Miyagawa-Tomita, S., Yanazawa, M., Katoh-Fukui, Y., Suzuki, R., Ohuchi, H., Suehiro, A., Motegi, Y., Nakahara, Y., et al. (1999). Mouse Pitx2 deficiency leads to anomalies of the ventral body wall, heart, extra- and periocular mesoderm and right pulmonary isomerism. Development *126*, 5749–5758.

Kumar, A., Lualdi, M., Lewandoski, M., and Kuehn, M.R. (2008). Broad mesodermal and endodermal deletion of Nodal at postgastrulation stages results solely in left/right axial defects. Dev. Dyn. *237*, 3591–3601.

Le Garrec, J.F., Domínguez, J.N., Desgrange, A., Ivanovitch, K.D., Raphaël, E., Bangham, J.A., Torres, M., Coen, E., Mohun, T.J., and Meilhac, S.M. (2017). A predictive model of asymmetric morphogenesis from 3D reconstructions of mouse heart looping dynamics. Elife *6*, e28951.

Lee, J.D., and Anderson, K.V. (2008). Morphogenesis of the node and notochord: the cellular basis for the establishment and maintenance of left-right asymmetry in the mouse. Dev. Dyn. *237*, 3464–3476.

Lescroart, F., Chabab, S., Lin, X., Rulands, S., Paulissen, C., Rodolosse, A., Auer, H., Achouri, Y., Dubois, C., Bondue, A., et al. (2014). Early lineage restriction in temporally distinct populations of Mesp1 progenitors during mammalian heart development. Nat. Cell Biol. *16*, 829–840.

Lescroart, F., Kelly, R.G., Le Garrec, J.F., Nicolas, J.F., Meilhac, S.M., and Buckingham, M. (2010). Clonal analysis reveals common lineage relationships between head muscles and second heart field derivatives in the mouse embryo. Development *137*, 3269–3279.

Lescroart, F., Mohun, T., Meilhac, S.M., Bennett, M., and Buckingham, M. (2012). Lineage tree for the venous pole of the heart: clonal analysis clarifies controversial genealogy based on genetic tracing. Circ. Res. *111*, 1313–1322.

Levin, M., Johnson, R.L., Stern, C.D., Kuehn, M.R., and Tabin, C.J. (1995). A molecular pathway determining left-right asymmetry in chick embryogenesis. Cell *82*, 803–814.

L'Honoré, A., Coulon, V., Marcil, A., Lebel, M., Lafrance-Vanasse, J., Gage, P., Camper, S., and Drouin, J. (2007). Sequential expression and redundancy of Pitx2 and Pitx3 genes during muscle development. Dev. Biol. *307*, 421–433.

Li, G., Xu, A., Sim, S., Priest, J.R., Tian, X., Khan, T., Quertermous, T., Zhou, B., Tsao, P.S., Quake, S.R., and Wu, S.M. (2016). Transcriptomic profiling maps anatomically patterned subpopulations among single embryonic cardiac cells. Dev. Cell *39*, 491–507.

Lin, A.E., Krikov, S., Riehle-Colarusso, T., Frías, J.L., Belmont, J., Anderka, M., Geva, T., Getz, K.D., and Botto, L.D.; National Birth Defects Prevention Study (2014). Laterality defects in the national birth defects prevention study (1998-2007): birth prevalence and descriptive epidemiology. Am. J. Med. Genet. A *164A*, 2581–2591.

Lin, C.R., Kioussi, C., O'Connell, S., Briata, P., Szeto, D., Liu, F., Izpisúa-Belmonte, J.C., and Rosenfeld, M.G. (1999). Pitx2 regulates lung asymmetry, cardiac positioning and pituitary and tooth morphogenesis. Nature *401*, 279–282.

Linask, K.K., Han, M., Cai, D.H., Brauer, P.R., and Maisastry, S.M. (2005). Cardiac morphogenesis: matrix metalloproteinase coordination of cellular mechanisms underlying heart tube formation and directionality of looping. Dev. Dyn. *233*, 739–753.

Linask, K.K., Han, M.D., Linask, K.L., Schlange, T., and Brand, T. (2003). Effects of antisense misexpression ofCFC on downstream flectin protein expression during heart looping. Dev. Dyn. *228*, 217–230.

Liu, C., Liu, W., Palie, J., Lu, M.F., Brown, N.A., and Martin, J.F. (2002). Pitx2c patterns anterior myocardium and aortic arch vessels and is required for local cell movement into atrioventricular cushions. Development *129*, 5081–5091.

Lowe, L.A., Supp, D.M., Sampath, K., Yokoyama, T., Wright, C.V., Potter, S.S., Overbeek, P., and Kuehn, M.R. (1996). Conserved left-right asymmetry of nodal expression and alterations in murine situs inversus. Nature *381*, 158–161.

Lowe, L.A., Yamada, S., and Kuehn, M.R. (2001). Genetic dissection of nodal function in patterning the mouse embryo. Development *128*, 1831–1843.

Lu, C.C., and Robertson, E.J. (2004). Multiple roles for Nodal in the epiblast of the mouse embryo in the establishment of anterior-posterior patterning. Dev. Biol. *273*, 149–159.

Lu, M.F., Pressman, C., Dyer, R., Johnson, R.L., and Martin, J.F. (1999). Function of Rieger syndrome gene in left-right asymmetry and craniofacial development. Nature *401*, 276–278.

Lyons, I., Parsons, L.M., Hartley, L., Li, R., Andrews, J.E., Robb, L., and Harvey, R.P. (1995). Myogenic and morphogenetic defects in the heart tubes of murine embryos lacking the homeo box gene Nkx2-5. Genes Dev *9*, 1654–1666.

Ma, L., Lu, M.F., Schwartz, R.J., and Martin, J.F. (2005). Bmp2 is essential for cardiac cushion epithelial-mesenchymal transition and myocardial patterning. Development *132*, 5601–5611.

Marques, S., Borges, A.C., Silva, A.C., Freitas, S., Cordenonsi, M., and Belo, J.A. (2004). The activity of the Nodal antagonist Cerl-2 in the mouse node is required for correct L/R body axis. Genes Dev *18*, 2342–2347.

Martin, J.F., Amendt, B.A., and Bronw, N. (2010). Pitx2 in cardiac left–right asymmetry and human disease. In Heart Development and Regeneration, N. Rosenthal and R.P. Harvey, eds. (Elsevier), pp. 307–322.

Meilhac, S.M., Esner, M., Kelly, R.G., Nicolas, J.F., and Buckingham, M.E. (2004). The clonal origin of myocardial cells in different regions of the embryonic mouse heart. Dev. Cell *6*, 685–698.

Metsalu, T., and Vilo, J. (2015). ClustVis: a web tool for visualizing clustering of multivariate data using principal component analysis and heatmap. Nucleic Acids Res *43*, W566–W570.

Mohapatra, B., Casey, B., Li, H., Ho-Dawson, T., Smith, L., Fernbach, S.D., Molinari, L., Niesh, S.R., Jefferies, J.L., Craigen, W.J., et al. (2009). Identification and functional characterization of NODAL rare variants in heterotaxy and isolated cardiovascular malformations. Hum. Mol. Genet. *18*, 861–871.

Muccielli, M.L., Martinez, S., Pattyn, A., Goridis, C., and Brunet, J.F. (1996). Otlx2, an Otx-related homeobox gene expressed in the pituitary gland and in a restricted pattern in the forebrain. Mol. Cell. Neurosci. *8*, 258–271.

Müller, P., Rogers, K.W., Jordan, B.M., Lee, J.S., Robson, D., Ramanathan, S., and Schier, A.F. (2012). Differential diffusivity of Nodal and Lefty underlies a reaction-diffusion patterning system. Science *336*, 721–724.

Murray, S.A., and Gridley, T. (2006). Snail family genes are required for left-right asymmetry determination, but not neural crest formation, in mice. Proc. Natl. Acad. Sci. USA *103*, 10300–10304.

Noël, E.S., Verhoeven, M., Lagendijk, A.K., Tessadori, F., Smith, K., Choorapoikayil, S., den Hertog, J., and Bakkers, J. (2013). A Nodal-independent and tissue-intrinsic mechanism controls heart-looping chirality. Nat. Commun. *4*, 2754.

Nonaka, S., Tanaka, Y., Okada, Y., Takeda, S., Harada, A., Kanai, Y., Kido, M., and Hirokawa, N. (1998). Randomization of left-right asymmetry due to loss of nodal cilia generating leftward flow of extraembryonic fluid in mice lacking KIF3B motor protein. Cell *95*, 829–837.

Norris, D.P., Brennan, J., Bikoff, E.K., and Robertson, E.J. (2002). The Foxh1-dependent autoregulatory enhancer controls the level of Nodal signals in the mouse embryo. Development *129*, 3455–3468.

Norris, D.P., and Robertson, E.J. (1999). Asymmetric and node-specific nodal expression patterns are controlled by two distinct cis-acting regulatory elements. Genes Dev. *13*, 1575–1588.

Ola, R., Lefebvre, S., Braunewell, K.H., Sainio, K., and Sariola, H. (2012). The expression of visinin-like 1 during mouse embryonic development. Gene Expr. Patterns *12*, 53–62.

Pai, V.P., Willocq, V., Pitcairn, E.J., Lemire, J.M., Paré, J.F., Shi, N.Q., McLaughlin, K.A., and Levin, M. (2017). HCN4 ion channel function is required for early events that regulate anatomical left-right patterning in a nodal and lefty asymmetric gene expression-independent manner. Biol. Open *6*, 1445–1457.

Quail, D.F., Siegers, G.M., Jewer, M., and Postovit, L.M. (2013). Nodal signalling in embryogenesis and tumourigenesis. Int. J. Biochem. Cell Biol. *45*, 885–898.

Roebroek, A.J., Umans, L., Pauli, I.G., Robertson, E.J., van Leuven, F., Van de Ven, W.J., and Constam, D.B. (1998). Failure of ventral closure and axial rotation in embryos lacking the proprotein convertase furin. Development *125*, 4863–4876.

Roussigné, M., Bianco, I.H., Wilson, S.W., and Blader, P. (2009). Nodal signalling imposes left-right asymmetry upon neurogenesis in the habenular nuclei. Development *136*, 1549–1557.

Saijoh, Y., Adachi, H., Mochida, K., Ohishi, S., Hirao, A., and Hamada, H. (1999). Distinct transcriptional regulatory mechanisms underlie left-right asymmetric expression of lefty-1 and lefty-2. Genes Dev. *13*, 259–269.

Saijoh, Y., Oki, S., Ohishi, S., and Hamada, H. (2003). Left–right patterning of the mouse lateral plate requires nodal produced in the node. Dev. Biol. *256*, 160–172.

Schindelin, J., Arganda-Carreras, I., Frise, E., Kaynig, V., Longair, M., Pietzsch, T., Preibisch, S., Rueden, C., Saalfeld, S., Schmid, B., et al. (2012). Fiji: an open-source platform for biological-image analysis. Nat. Methods *9*, 676–682.

Schweickert, A., Campione, M., Steinbeisser, H., and Blum, M. (2000). Pitx2 isoforms: involvement of Pitx2c but not Pitx2a or Pitx2b in vertebrate left–right asymmetry. Mech. Dev. *90*, 41–51.

Shiratori, H., and Hamada, H. (2006). The left-right axis in the mouse: from origin to morphology. Development *133*, 2095–2104.

Shiratori, H., Sakuma, R., Watanabe, M., Hashiguchi, H., Mochida, K., Sakai, Y., Nishino, J., Saijoh, Y., Whitman, M., and Hamada, H. (2001). Two-step regulation of left-right asymmetric expression of Pitx2: initiation by nodal signaling and maintenance by Nkx2. Mol. Cell *7*, 137–149.

Shiratori, H., Yashiro, K., Shen, M.M., and Hamada, H. (2006). Conserved regulation and role of Pitx2 in situs-specific morphogenesis of visceral organs. Development *133*, 3015–3025.

Stalsberg, H. (1969). The origin of heart asymmetry: right and left contributions to the early chick embryo heart. Dev. Biol. *19*, 109–127.

Stennard, F.A., Costa, M.W., Lai, D., Biben, C., Furtado, M.B., Solloway, M.J., McCulley, D.J., Leimena, C., Preis, J.I., Dunwoodie, S.L., et al. (2005). Murine T-box transcription factor Tbx20 acts as a repressor during heart development, and is essential for adult heart integrity, function and adaptation. Development *132*, 2451–2462.

Théveniau-Ruissy, M., Dandonneau, M., Mesbah, K., Ghez, O., Mattei, M.G., Miquerol, L., and Kelly, R.G. (2008). The del22q11.2 candidate gene Tbx1Controls regional outflow tract identity and coronary artery patterning. Circ. Res. *103*, 142–148.

Tremblay, C., Loomba, R.S., Frommelt, P.C., Perrin, D., Spicer, D.E., Backer, C., and Anderson, R.H. (2017). Segregating bodily isomerism or heterotaxy: potential echocardiographic correlations of morphological findings. Cardiol. Young *27*, 1470–1480.

Van Praagh, R. (1972). The segmental approach to diagnosis in congenital heart disease. Birth Defects Orig. Artic. Ser. *8*, 4–23.

Van Praagh, S. (2006). Cardiac malpositions and the heterotaxy syndromes. In Nadas' Pediatric Cardiology, J.F. Keane, J.E. Lock, and D.C. Fyler, eds. (Saunders Elsevier), pp. 589–608.

Verzi, M.P., McCulley, D.J., De Val, S., Dodou, E., and Black, B.L. (2005). The right ventricle, outflow tract, and ventricular septum comprise a restricted expression domain within the secondary/anterior heart field. Dev. Biol. *287*, 134–145.

Vincent, S.D., Norris, D.P., Le Good, J.A., Constam, D.B., and Robertson, E.J. (2004). Asymmetric Nodal expression in the mouse is governed by the combinatorial activities of two distinct regulatory elements. Mech. Dev. *121*, 1403–1415.

von Both, I., Silvestri, C., Erdemir, T., Lickert, H., Walls, J.R., Henkelman, R.M., Rossant, J., Harvey, R.P., Attisano, L., and Wrana, J.L. (2004). Foxh1 is essential for development of the anterior heart field. Dev. Cell *7*, 331–345.

Yan, Y.T., Gritsman, K., Ding, J., Burdine, R.D., Corrales, J.D., Price, S.M., Talbot, W.S., Schier, A.F., and Shen, M.M. (1999). Conserved requirement for EGF-CFC genes in vertebrate left-right axis formation. Genes Dev *13*, 2527–2537.

Zhou, W., Lin, L., Majumdar, A., Li, X., Zhang, X., Liu, W., Etheridge, L., Shi, Y., Martin, J., Van de Ven, W., et al. (2007). Modulation of morphogenesis by noncanonical Wnt signaling requires ATF/CREB family–mediated transcriptional activation of TGFβ2. Nat. Genet. *39*, 1225–1234.

STAR★METHODS

KEY RESOURCES TABLE

REAGENT or RESOURCE	SOURCE	IDENTIFIER
Antibodies		
Isl1 and Isl2 homeobox	DSHB	39.4D5; RRID: AB_2314683
Recombinant Anti-Histone H3 (phospho S10 + T11) antibody	Abcam	ab32107; RRID: AB_732930
Phospho-Smad2 (Ser465/467) Rabbit mAb	Cell Signaling	3101; RRID: AB_331673
Goat anti-rabbit Alexa Fluor 546 secondary antibody	Thermofischer scientific	A11035; RRID: AB_2534093
Goat anti-mouse IgG2b Alexa Fluor 488 secondary antibody	Thermofischer scientific	A21141; RRID: AB_2535778
Streptavidin Alexafluor conjugated 546	Invitrogen	S11225; RRID: AB_10626776
Hoechst 33342	Life Technologies	H3570
Chemicals, Peptides, and Recombinant Proteins		
SB 505124, ALK5 inhibitor	Abcam	ab144402
Critical Commercial Assays		
JB-4 embedding kit	Polysciences	00226-1
RNeasy micro kit	Qiagen	74004
Reverse transcription kit	Qiagen	205311
Universal Plus mRNA-seq kit	Nugen	0508-96
RNAscope multiplex fluorescent detection Kit	Biotechne (ACD)	323110
TSA cyanine 5 reagent pack	Akoya Biosciences	SAT704A001EA
Deposited Data		
GEO submission GSE148123	NCBI	GSE148123
Experimental Models: Organisms/Strains		
Mouse: Wild-type C57Bl6J	Jackson	MGI:3028467
Mouse: *Nodal*$^{flox/flox}$	Lu and Robertson, 2004	MGI:3056345
Mouse: Nodal-ASE-LacZ	Norris and Robertson, 1999	
Mouse: *Hoxb1*$^{Cre/+}$	Arenkiel et al., 2003	MGI:2668513
Mouse: *Pitx2*$^{\Delta ASE}$	Shiratori et al., 2006	MGI:3767234
Mouse: *Pitx2c*$^{null/null}$	Liu et al., 2002	MGI:2445428
Mouse: *Pitx2abc*$^{tm1Sac/tm1Sac}$	Gage et al., 1999	MGI:1857844
Mouse: *Pitx2abc*$^{tm1Jfm/tm1Jfm}$	Lu et al., 1999	MGI:2136268
Oligonucleotides		
Nodal reverse primer CCTGACTCAAAACCCAAGGC	This paper.	N/A
Nodal forward primer ATTCCAGCAGTTGAGGCAGA	This paper.	N/A
Nodal forward primer CCACCCAATTTCTAGCCCAG	This paper.	N/A
Mouse Tnnt1 antisense riboprobe generation Fwd: 5' to 3' GGTCAAGGCAGAACAGAAGC	This paper.	N/A
Mouse Tnnt1 antisense riboprobe generation Rev+T7: 5' to 3' TAATACGACTCACTATAGCTC CACACAGCAGGTCATGT	This paper.	N/A

(*Continued on next page*)

Continued

REAGENT or RESOURCE	SOURCE	IDENTIFIER
Mouse Tnc antisense riboprobe generation Fwd: 5' to 3' ctaccatcgccaccaagttt	This paper	N/A
Mouse Tnc antisense riboprobe generation Rev+SP6: 5' to 3' ATTTAGGTGAC ACTATAGattcttctctgcggtctcca	This paper	N/A
Mouse Nodal primer for RTqPCR Fwd: 5' to 3' GGCAACGCCGACATCATTTG	This paper.	N/A
Mouse Nodal primer for RTqPCR Rev: 5' to 3' CAGCAGGCTCTGGATGTAGG	This paper.	N/A
Mouse Pitx2c primer for RTqPCR Fwd: 5' to 3' GAGGTGCATACAATCTCCGATA	This paper.	N/A
Mouse Pitx2c primer for RTqPCR Rev: 5' to 3' TGCCGCTTCTTCTTGGAC	This paper.	N/A
Mouse Lefty2 primer for RTqPCR Rev : 5' to 3' CACAATTGCCTTGAGCTCCGTAGTC	This paper.	N/A
Mouse Lefty2 primer for RTqPCR Fwd : 5' to 3' ATCGACTCTAGGCTCGTGTCCATC	This paper.	N/A
Mouse Pitx2ab primer for RTqPCR Rev: 5' to 3' ACTTGGCACCCTCAAGATCC	This paper.	N/A
Mouse Pitx2ab primer for RTqPCR Fwd: 5' to 3' CTCCCATTCCCGGTTATCGGC	This paper.	N/A
RNAscope probe Mm-Col5a2-O1	Biotechne (ACD)	538021
RNAscope probe Mm-Mmp9	Biotechne (ACD)	315941
Recombinant DNA		
pBSSK-Bmp2		Gift from C. Vesque, Developmental Biology Laboratory, IBPS
pBSSK-Lefty2	Saijoh et al., 1999	Gift from J. Collignon, Institut Jacques Monod
pBSSK-Pitx2	L'Honoré et al., 2007	Gift from J. Drouin, IRCM
pBKCMV-Sema3c	Feiner et al., 2001	Gift from R. Kelly, IBDM
pYXASC-Vsnl1	Ola et al., 2012	Gift from H. Sariola, Developmental biology, University of Helsinky
pWnt11		Gift from S. Evans, UCSD
Software and Algorithms		
ImageJ/Fiji	Schindelin et al., 2012	RRID:SCR_002285
Imaris	Bitplane	RRID:SCR_007370
Icy	de Chaumont et al., 2012	RRID:SCR_010587
Gftbox algorithm Matlab Finite Element Analysis package simulating biological growth	Kennaway et al., 2011; Le Garrec et al., 2017	http://cmpdartsvr3.cmp.uea.ac.uk/wiki/BanghamLab/index.php/Software
ClustVis	Metsalu and Vilo, 2015	RRID : SCR_017133
Matlab	The Mathworks	RRID: SCR_001622
R	R Project for Statistical Computing	RRID: SCR_001905
Fuzznuc	EMBOSS-MS software	
Prism	Graphpad	RRID: SCR_002798

RESOURCE AVAILABILITY

Lead Contact

Further information and requests for resources and reagents should be directed to and will be fulfilled by the Lead Contact, Sigolène M. Meilhac (sigolene.meilhac@institutimagine.org)

Material Availability

This study did not generate new unique reagents.

All stable reagents generated in this study are avaible from commercial sources or the Lead Contact without restriction

Data and Code Availability

The RNAseq dataset generated during this study is available at the NCBI Gene Expression Omnibus (GEO) database with the accession number GEO: GSE148123.

The published article includes all codes generated or analysed during this study (see Data S1 and S2)

EXPERIMENTAL MODEL AND SUBJECT DETAILS

Wild-type mouse embryos were from a C57Bl6J genetic background. The *Nodal-ASE-lacZ* transgenic line (Norris and Robertson, 1999), *Nodal*$^{flox/flox}$ (Lu and Robertson, 2004), *Pitx2*$^{\Delta ASE/\Delta ASE}$ (Shiratori et al., 2006) and *Pitx2c*$^{null/null}$ (tm3.1Jfm allele) (Liu et al., 2002) were maintained in a mixed genetic background. The *Pitx2abc*$^{tm1Sac/tm1Sac}$ (Gage et al, 1999) line was maintained in C57Bl6/J; the *Pitx2abc*$^{tm1Jfm/\ tm1Jfm}$ (Lu et al, 1999) line was maintained in 129S4/SvJaeS (milder phenotypes) or C57Bl6/J (most severe phenotype) backgrounds. *Nodal*$^{null/+}$ mice were generated by crossing *Nodal*$^{flox/flox}$ males with *Mef2cAHFCre* transgenic females (Verzi et al., 2005) and then crossed to *Hoxb1*$^{Cre/+}$ (Arenkiel et al., 2003). *Nodal*$^{null/+}$;*Hoxb1*$^{Cre/+}$ males were maintained in a mixed genetic background and crossed to Nodal$^{flox/flox}$ females to generate *Nodal* conditional mutants. Both male and female embryos were collected and used randomly for experiments. Embryonic day (E) 0.5 was defined as noon on the day of vaginal plug detection. Heart looping stages from E8.5c to E8.5j were defined according to the previously published nomenclature (Le Garrec et al., 2017), whereas E8.5a and E8.5b are equivalent to EHF and LHF stages respectively (Downs and Davies, 1993). The number of somites was evaluated from the HREM images. All embryos were genotyped by PCR. For the genotyping of *Nodal* alleles, primers were designed to detect the wild-type (540b), floxed (590b) and deleted (1050b) alleles. Animals were housed in the Laboratory of Animal Experimentation and Transgenesis of the SFR Necker, Imagine Campus, Paris and in the animal facility of the Institut Pasteur. Animal procedures were approved by the ethical committees of the Institut Pasteur and Paris Descartes and the French Ministry of Research.

METHOD DETAILS

Embryo Culture

For drug treatment, wild-type E8.5 embryos were collected in Hank's solution. We tested a range of drug concentrations (20-50μM) to avoid toxicity on embryo development and promote efficient *Pitx2* downregulation. A working concentration of 50μM of SB505124 or an equivalent volume of the adjuvant (DMSO) were added to the 75% rat serum, 25% T6 medium, supplemented with 1X Penicillin/Streptomycin. Embryos were cultured with 5% CO_2, 5% O2, in rolling bottles in a precision incubator (BTC Engineering, Milton, Cambridge, UK). At the end of the treatment, embryos were rinsed in PBS and fixed in paraformaldehyde (PFA) 4%. Brightfield images were acquired at the beginning and the end of the culture with a Zeiss AxioCamICc5 Camera and a Zeiss StereoDiscovery V20 stereomicroscope with a Plan Apo 1.0X objective. Drug treatment over 8 hours did not affect overall embryo development, as quantified by the number of newly added somites (3.1±0.6 and 2.8±0.5 somites in DMSO (n=8) and SB505124 (n=29) treated embryos respectively, p=0.19, Wilcoxon test).

Wholemount β-galactosidase Staining and Immunofluorescence

Embryos were collected at E8.5 or E9.5. The heart was arrested in diastole with 250mM KCL (E9.5). *Nodal-ASE-LacZ* transgenic embryos were fixed in 4% PFA – 5mM EGTA – 2mM MgCl2 for 10min. Embryos where then permeabilized in 0.2% NP40 – 2mM MgCl2 – 0.1% sodium deoxycholate 30min and stained overnight in Xgal solution. Immunofluorescence on whole mount E8.5 embryos was performed after removal of the left headfold as a landmark, using CUBIC clearing as described in (Le Garrec et al., 2017), with Hoechst as a nuclear counterstain. Multi-channel 16-bit images were acquired with a Z.1 lightsheet microscope (Zeiss) and a 20X/1.0 objective. Automatic detection of mitotic cells was performed with the Spots plugin of Imaris and co-localisation with Isl1 staining was evaluated manually. Given morphological variations in mutant embryos, their stage of development was evaluated based on the length of the heart tube, using the quantifications of Le Garrec et al. (2017) as a reference. P-Smad2 staining was adapted from Kawasumi et al (2011). E8.5 embryos were fixed 2h in 4% PFA, and gradually dehydrated into methanol. We used 3% H_2O_2 for bleaching before rehydratation. Samples were blocked with the TSA Blocking Reagent (Perkin Elmer), incubated with the primary antibody Phospho-Smad2 (1/50) during 48h at 4°C and 4h with the Alexa Fluor conjugated secondary antibody (1/500). Embryos were then cleared in gradually concentrated glycerol before imaging with a fluorescent Stereomicroscope in 80% gycerol.

RT-qPCR

At earlier stages (LHF-E8.5d), cardiogenic regions were isolated as shown in Figure 2A. From E8.5e, the heart tube was removed. From E8.5c the heart field was bisected to keep the left half only. The posterior boundary is set at the level of the second somite, in agreement with fate maps (Domínguez et al., 2012). At E9.5, embryos were cut into three pieces: ''the head'' until the second branchial arch, the ''heart region'' until the proepicardium and depleted from the neural tube, the rest as ''the tail''. The tissue was flash frozen in liquid nitrogen. RNAs were extracted in TRIzol-Chloroform and purified using the RNeasy micro kit. Reverse transcription was carried out using the Quantitect Reverse Transcription kit. Quantitative PCR was carried out using a real-time PCR system (Bio-Rad), and primers as listed in the Key Resources Table. *Polr2b* was chosen from the RNA-seq dataset as a reference housekeeping gene, because of its expression in the range of Nodal pathway components (2000 counts), with no variability between samples, including controls and mutants. The mRNA expression levels were measured relatively to *Polr2b* and normalized with a reference cDNA sample (pool of 4 embryos at E8.5c, d, g, and j), using the standard ΔΔCt method.

RNA *In Situ* Hybridisation

ISH was performed on wholemount embryos after fixation in PFA 4% and dehydratation in methanol 100% following standard protocols. *Lefty2, Pitx2, Wnt11, Bmp2, Sema3c*, *Vsnl1* riboprobes were transcribed from plasmids. *Tnc* and *Tnnt1* probes were synthetized by PCR, using primers listed in the Key Resources Table. Hybridization signals were detected by alkaline phosphatase (AP)-conjugated anti-DIG antibodies (1/2500; Roche), which were revealed with NBT/BCIP (magenta) substrate (Roche). After staining, the samples were washed in PBS and post-fixed. Brightfield images were acquired with a Zeiss AxioCamICc5 Camera and a Zeiss StereoDiscovery V20 stereomicroscope with a Plan Apo 1.0X objective.

RNAscope ISH was performed with Mutliplex Fluorescent v2 Assay (Advanced Cell Diagnostic, cat. no.323110). E8.5 embryos were fixed 24h in PFA at 4% and dehydratated in methanol 100%. The protocol was adapted from (de Soysa et al., 2019). *mm-Col5a2-C1* (Cat No. 538021) and *mm-Mmp9-C1* (Cat No. 315941) probes were used, together with Hoechst as a nuclear counterstain. Amplification steps were performed using the TSA cyanine5 amplification kit (Akoya Bioscence). Samples were then transferred in R2 CUBIC clearing reagents. Multi-channel 16-bit images were acquired with a Z.1 lightsheet microscope (Zeiss) and a 20X/1.0 objective.

HREM (High-Resolution Episcopic Microscopy)

Embryos or hearts were collected and embedded in methacrylate resin (JB4) containing eosin and acridine orange as contrast agents (Le Garrec et al., 2017; Desgrange et al., 2019). One or two channel images of the surface of the resin block were acquired using the optical high-resolution episcopic microscope (Indigo Scientific) and a 1X Apo objective repeatedly after removal of 1.56-1.7 μm (embryos) and 2.34 μm (hearts) thick sections: the tissue architecture was imaged with a GFP filter and the staining of enzymatic precipitates with a RFP filter. The dataset comprises 500-1700 images of 0.96-1.85 μm resolution in x and y depending on the stage. Icy (de Chaumont et al., 2012) and Fiji (ImageJ) softwares were used to crop or scale the datasets. 3D reconstructions were performed with the Fiji plugin Volume Viewer or Imaris (Bitplane).

RNA Sequencing

Embryos were microdissected and the tissue was flash frozen in liquid nitrogen. RNA was extracted in TRIzol-Chloroform and purified using the RNeasy micro kit. RNA quality and quantity were assessed using RNA Screen Tape 6000 Pico LabChips with the Tape Station (Agilent Technologies). All RINs were higher than 9.0. The library was established using the Nugen Universal Plus mRNA-Seq kit, using 20 ng of total RNAs as recommended by the manufacturer. The oriented cDNAs produced from the poly-A+ fraction were PCR amplified (15-18 cycles). An equimolar pool of the final indexed RNA-Seq libraries was sequenced on an Illumina HiSeq2500, with paired-end reads of 130 bases and a mean sequencing depth of 58 millions per sample. The RNA-seq data are available in the NCBI Gene Expression Omnibus (GEO) database with the accession number GEO: GSE148123.

FEA Modeling of the Heart Tube

The model is based on the GFtbox finite element analysis software, using a cylindrical mesh, with fixed poles and a dorsal constraint simulating the progressive breakdown of the dorsal mesocardium (Le Garrec et al., 2017). At each successive step during a simulation, each element is deformed according to a growth tensor field specified from the hypotheses of the model.

The control model is based on the following input parameters, chosen to simulate the control shape (Le Garrec et al., 2017) : basic longitudinal growth (2.5%, with a peak value of 5% ventrally between steps 1-40), 25 degree rightward rotation at the arterial pole (1.1% circumferential growth per step, positive on the left side, negative on the right side), asymmetric longitudinal growth at the venous pole (peak value of 7% on the right, 2.5% on the left), circumferential growth in the ventricles (0.9% in the ventral right ventricle, 0.4% in the dorsal right ventricle, 1.4% in the left ventricle). Simulations were run for 100 steps. The MATLAB code containing the interaction function of the GFtbox model, and used to generate the control shape in Figure 6A, is provided in Data S1.

The simulations of the mutant shapes were obtained by a 50% reduction in the intensity of the asymmetries at both poles and by simulating the four possible combinations of lateralization at the arterial/venous poles: normal/normal, normal/inverted, inverted/normal and inverted/inverted. The MATLAB code containing the interaction function of the GFtbox model, and used to generate the mutant shapes in Figure 6A is provided in Data S2. This code is edited to run the inverted/inverted combination ("Class 1"), the alternative codes for each of the three other combinations being included as commented lines under the headings "Class 2-4".

Phenotyping at Perinatal Stages

The situs and anatomy of visceral organs were evaluated by micro-CT imaging (Quantum FX, perkin Elmer) after 72h of Lugol staining (Desgrange et al., 2019). The heart structure was phenotyped on 3D reconstruction of HREM images, based on the segmental approach (Van Praagh, 1972).

QUANTIFICATION AND STATISTICAL ANALYSIS

Quantification of the Proportion of β-galactosidase Staining

Hearts were segmented from HREM images using the IMARIS software (Bitplane). The contour of the myocardium was manually outlined at regular Z intervals of the GFP channel, and the Create Surface function was used to reconstruct the 3D surface. Signal of the β-galactosidase staining intersecting with the myocardium was obtained using the "mask selection" function to extract a new channel and create another 3D surface. The volume of each surface was extracted and the proportion of the stained myocardium was calculated.

Quantification of the ISH Signal

Brightfield images were transformed into 8 bit images and black and white were inverted. Two Regions of Interest (ROIs) were drawn, around the right and left lateral plate mesoderm, as schematized in Figure 2C. The average intensity signal of each ROI was used to calculate the left/right ratio.

Quantification of Immunoflorescence and RNAscope ISH Signal

The cardiac region was segmented in the 3D lightsheet images using the IMARIS software (Bitplane). The heart/myocardium and heart field were manually outlined at regular intervals of the Hoechst channel and the Create surface function was used to reconstruct the 3D surface. The headfolds and second somite were used as cranial and caudal boundaries of the heart field respectively. This surface was bisected, using the notochord as a midline reference for the heart field, to extract the P-HH3, Mmp9 or Col5a2 channels on the left and right sides. We used the Spot Detector tool to count the number of mitotic cells or RNA molecules and calculate the left/right ratio.

3D Rendering and Visualisation

We used Fiji Volume Viewer plugin to assess *in situ* labeling within the heart tube in 3D. In parallel we segmented the myocardium from HREM using the IMARIS software (Bitplane). This 3D surface was used to extract the RFP channel corresponding to *in situ* signal within the object. The extracted signal was used to automatically generate a corresponding 3D surface.

Quantification of the Geometry of the Heart Loop

From the 3D reconstruction of the myocardium contour, the axis of the cardiac tube was extracted, using eight landmarks along the length of the tube. Three of these landmarks were obtained with the IMARIS Oblique Slicer function intersecting the tube perpendicularly, and by computation of the centroid of the polygon (MATLAB geom3d library : function polygonCentroid3d) : one at the exit of the outflow tract, one at the sulcus between the two ventricles, and one at the bifurcation of the two atria. The five other landmarks were obtained by sub-division of the volume into the outflow tract (positive for *Wnt11*), the right ventricle (without cushions), the left ventricle, the atrio-ventricular canal and left atrium (positive for *Bmp2*) and the right atrium. The center of gravity of each of these volumes was computed, using IMARIS.

The 3D coordinates of the eight landmarks were used to draw the loop of the tube axis as shown in Figure 4. All the hearts were aligned so that the notochord coincides with the Z axis, and the dorsal-ventral axis with the X axis. This alignment was performed using two landmarks on the notochord and two landmarks defining the bisectrix of the neural groove, then applying two successive 3D rotations to the axis coordinates, using an in-house MATLAB code: first a rotation aligning the notochord with the Z axis, then a rotation aligning the dorsal-ventral axis with the X axis. All measurements shown in Figure 4 were done on these alignments and averaged for all analysed samples (n indicated in Figure 4A). The orientation of the RV/LV axis relative to the notochord, the distance of the venous pole (taken as the bifurcation of the tube) relative to the notochord, the distance between the poles and the tube length, the rotation of the tube at E8.5f were calculated as in Le Garrec et al., 2017. The OFT angles were directly measured on the aligned loops after projection on the indicated planes (transversal : XY; sagittal : XZ). E8.5f *Nodal* mutants in Figure S3C were classified as rightward or leftward depending on the number of asymmetric points in the arterial half of the heart tube (from 75μm after the bifurcation).

Superimposition of the loops shown in Figure 5 was obtained by optimization of composite 3D rotations (combining rotations around the three coordinate axes) of the mutant loops relative to the control loop. The 3 basic rotation matrices were each successively incremented by 1° and combined in alternative order (because of non-commutation) to explore the full space of 3D rotations around the exit of the outflow tract taken as a fixed point. Optimization was obtained by minimizing the sum of the euclidean distances between each of the seven mutant landmarks and the corresponding control landmarks. The computations were implemented in MATLAB.

Quantifications of the rotation of the arterial pole and the left displacement of the venous pole at E8.5 were performed as described in Le Garrec et al., 2017 from HREM and lightsheet images respectively.

Principal Components Analysis and clustering

A Principal Components Analysis was performed on 33 variables describing the heart loop in 22 *Nodal* conditional mutants. All segmented hearts were registered, using the exit of the outflow tract as origin, the notochord as Z-axis, and the dorsal-ventral axis as X-axis. The variables are the X, Y, and Z coordinates of 6 landmarks along the loop (outflow tract, right ventricle, inter-ventricular sulcus, left ventricle, atrio-ventricular canal/left atrium, right atrium -see Figure 4A), as well as the angles between the 5 segments defined by these landmarks and projected on the 3 planes perpendicular to the embryonic axes (dorsal-ventral, cranial-caudal, left-right). Variance scaling was applied by dividing the coordinate variables by the ratio between their average standard deviation and the average standard deviation of the angular variables. The covariance matrix and its diagonalization were then computed with Matlab. The 4 highest eigenvalues, cumulatively accounting for 85% of the total variance, were retained together with their eigenvectors for clustering, using the ClustVis R-package (Metsalu and Vilo, 2015), with correlation distance and average linkage.

Bioinformatics Analyses of the RNA Sequences

FASTQ files were mapped to the ENSEMBL [Mouse GRCm38] reference using Hisat2 and counted by featureCounts from the Subread R package. Read count normalisations and group comparisons were performed by three independent and complementary statistical methods: DESeq2, edgeR and LimmaVoom. Flags were computed from counts normalized to the mean coverage. All normalized counts <20 were considered as background (flag 0) and >=20 as signal (flag=1). P50 lists used for the statistical analysis regroup the genes showing flag=1 for at least half of the compared samples. Unsupervised cluster analysis was performed by hierarchical clustering using the Spearman correlation similarity measure and average linkage algorithm. The results of the three methods were filtered for differentially expressed genes between control and mutant samples, on the basis of a p-value lower than 0.05 and a fold change greater than 1.2. Functional analyses were carried out using the Gene Ontology database (PANTHER Overrepresentation test).

Bioinformatics Analysis of ASE Elements

The analysis was performed as described in Guzman-Ayala et al., 2009 on the Ensembl GRch38 mouse reference genome (48,526 genes). *Nodal, Lefty2* and *Pitx2* were used as positive controls.

Bootstrap Inference on Transcriptomic Data

In order to assess how significantly genes of cardiomyocyte differentiation deviate from the average gene expression fold change between control and mutant samples, a bootstrap method was applied. The analysis was restricted to the 9,375 genes with a minimum of 150 normalised counts (see Figure S5B). 112 were selected as cardiomyocyte differentiation (Table S2), because they encode sarcomere components, ion channels, transcription factors, adhesion proteins or signals required for cardiomyocyte differentiation, or on the basis of previous RNA-seq datasets (DeLaughter et al., 2016; Li et al., 2016). The 9,375 genes were resampled 1,000 times, with replacement, into sub-samples of 112 genes (MATLAB RandStream method using the Mersenne twister generator). The means and standard deviations of the fold change distribution between mutant and control embryos for these 1,000 bootstrap samples were assessed, and compared to the mean and standard deviation for the 112 genes of cardiomyocyte differentiation.

Statistical Analysis

Sample size was checked post-hoc, using the calculator powerandsamplesize.com, in order to ensure a power of at least 0.8, with a type I error probability of 0.05, with an effect size of 20%. The collection of full litters was used to randomise imaging experiments. Group allocation was based on PCR genotyping. 3 outliers were excluded from geometric analysis based on a lower number of somites (Figures 4 and S2). One mutant sample was discarded from the RNA-seq analysis because of a poor gene coverage. All sample numbers (n) indicated in the text refer to biological replicates, i.e. different embryos. Investigators were blinded to allocation during imaging and phenotypic analysis, but not during quantifications. Tests were performed with Excel and R. The correlation between two data series was quantified by the square of the Pearson coefficient R^2. The regression line was computed using the least square method. Comparisons of two centre-values were done on the average, or the geometrical mean when ratios were compared, using a Student two-tailed test. When more than two centre-values were compared, an ANOVA was calculated, with a Tukey Kramer post-hoc test, unless a normal distribution could not be assumed, in which case a Kruskal Wallis test was used. For comparing left and right angles at successive positions, a paired Student test was used. The 95% confidence intervals for the mean were calculated assuming a normal distribution of measurements. A chi^2 test was used to evaluate the randomisation of class frequency and the symmetry of proliferation rates between left and right heart precursors.

Developmental Cell, Volume *55*

Supplemental Information

Transient Nodal Signaling in Left Precursors Coordinates Opposed Asymmetries Shaping the Heart Loop

Audrey Desgrange, Jean-François Le Garrec, Ségolène Bernheim, Tobias Holm Bønnelykke, and Sigolène M. Meilhac

Supplemental Information

Supplemental figures

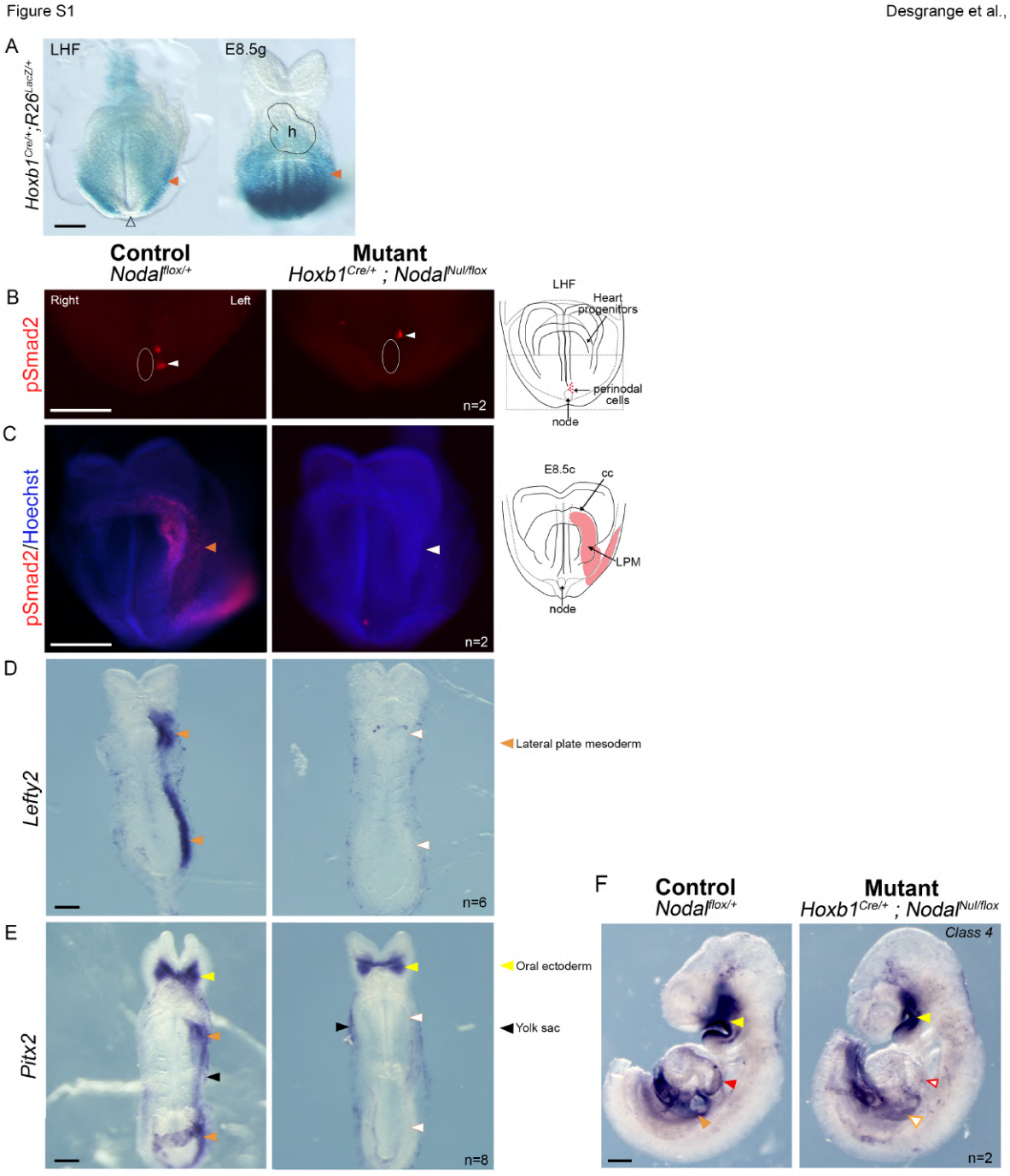

Fig. S1 related to Fig. 3. Disruption of Nodal signalling in *Nodal*$^{flox/null}$;*Hoxb1*$^{Cre/+}$ mutants.

(A) Brightfield images of *Hoxb1*$^{Cre/+}$;*R26*$^{LacZ/+}$ embryos showing β-galactosidase staining in the posterior mesoderm (orange arrowhead), but not the node (black arrowhead) at the indicated stages. The heart (h) is outlined in black. *Hoxb1*$^{Cre/+}$ targets heart precursors in the

posterior heart field (Bertrand et al., 2011). However, since Nodal signalling is initiated lateral to the node and propagates anteriorly by auto-activation (Lowe et al., 1996; Vincent et al., 2004), *Nodal*$^{flox/null}$;*Hoxb1*$^{Cre/+}$ conditional mutants are deprived of Nodal signalling throughout the lateral plate mesoderm. (B) Wholemount immunofluorescence of the Nodal effector Phospho-Smad2 showing active Nodal signalling in left perinodal cells (white arrowhead) in control and *Nodal* mutant samples at the late headfold (LHF) stage. The node is outlined in white. (C) At E8.5c Phospho-Smad2 is detected in the left lateral plate mesoderm (orange arrowhead) of control, but not mutant (white arrowhead) embryos. (D-E) ISH of the indicated *Nodal* targets, showing no expression in the left lateral plate mesoderm of mutant (white arrowheads) compared to control (orange arrowheads) embryos at E8.5d-h. The symmetrical expression of *Pitx2* in the oral ectoderm (yellow arrowheads) and yolk sac (black arrowheads) is maintained in *Nodal* mutants, in agreement with previous reports (Constam and Robertson, 2000; Mucchielli et al., 1996; Schweickert et al., 2000). From 23 mutant embryos stained (C-E) and 3 analysed by RNAseq (Fig. S5), we can calculate (by random sampling of 4 distinct populations) that there is a 0.5% probability to have missed a class of mutants (see Fig. 3), which is thus an unlikely event. (F) We have further analysed *Nodal* mutants with the mildest phenotype (Class 4) at E9.5 and found no cardiac *Pitx2* expression (red arrowheads). This supports complete disruption of Nodal signalling in all mutant classes, rather than a dose effect in each class. cc, cardiac crescent; LHF, late headfold stage; LPM, lateral plate mesoderm; n, number of observations. Scale bars: 200μm.

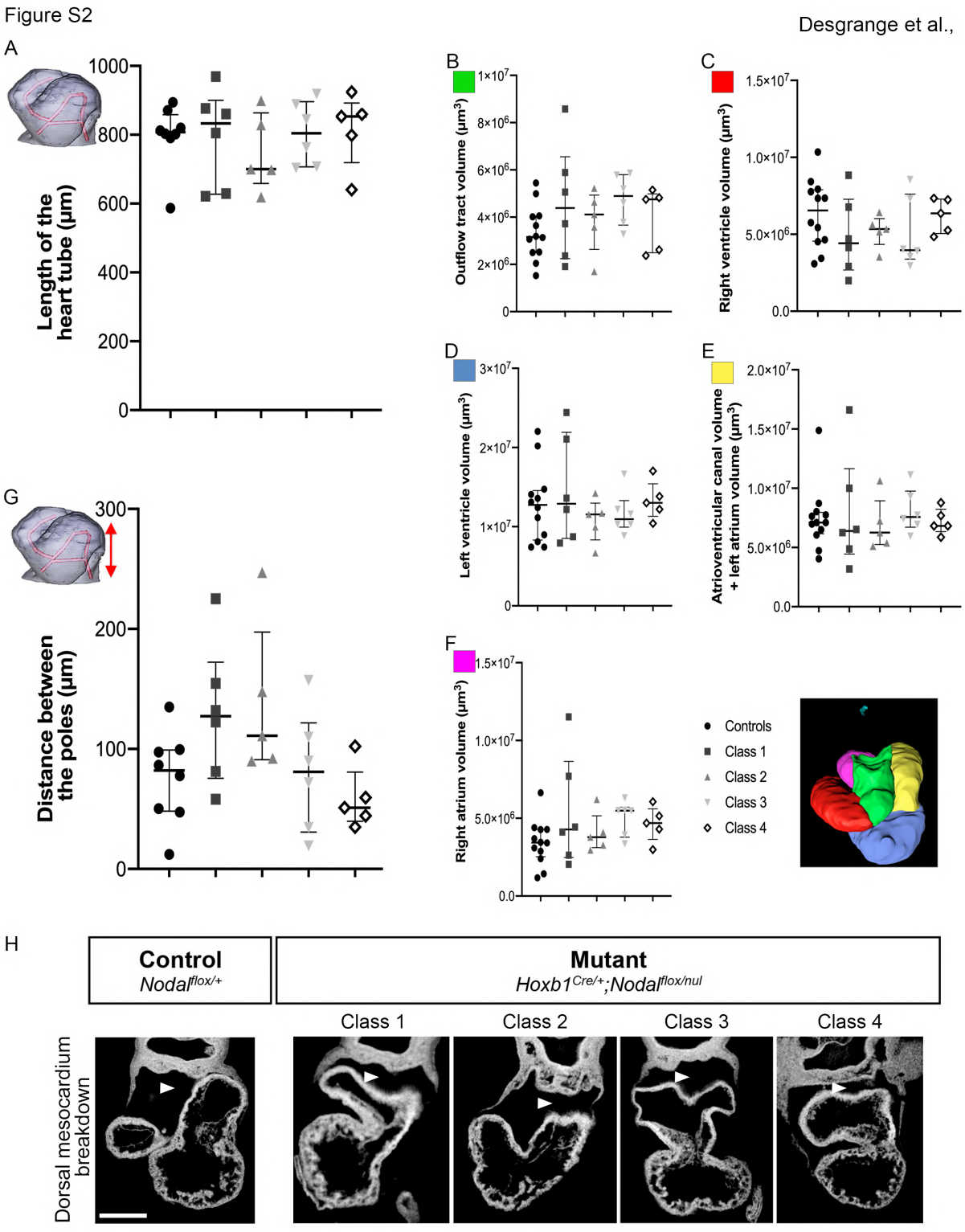

Fig. S2 related to Fig 4. Normal growth and buckling parameters in *Nodal*$^{flox/null}$;*Hoxb1*$^{Cre/+}$ mutant hearts.

Quantification of the length of the heart tube (A), of the volume of the outflow tract (B), the right (C) and left (D), ventricles, the atrio-ventricular canal/left atrium (E) and the right atrium

(F), of the distance between the heart tube poles (G) comparatively in control and the different classes of *Nodal* mutant hearts at E9.5. Means and standard deviations are shown in red, with no significant difference between controls and mutants (ANOVA, n=11 controls and n=6, 5, 6, 5 for classes 1, 2, 3, 4 respectively). (H) Transverse sections of HREM 3D images showing the absence of dorsal mesocardium (arrowhead) in control and mutants. Scale bar: 200μm.

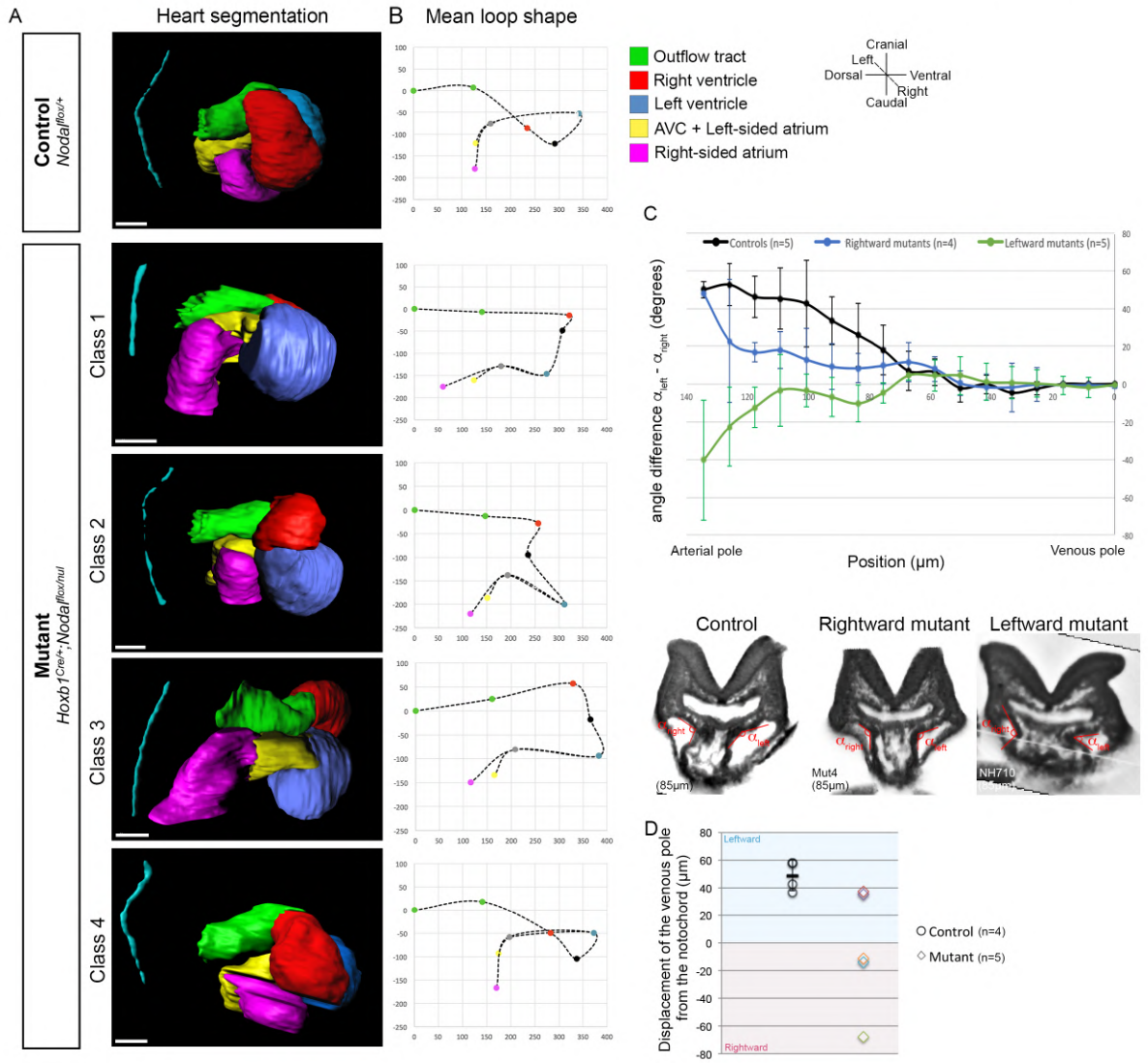

Fig. S3 related to Fig. 4. Rotation and curvature of the outflow tract in *Nodal*$^{flox/null}$;*Hoxb1*$^{Cre/+}$ mutants

(A) Sagittal views of the 3D segmented heart tube in control and mutants at E9.5, with regions colour-coded, based on *Bmp2/Wnt11* expression and histology (n=11 controls and n=6, 5, 6, 5 for classes 1, 2, 3, 4 respectively). (B) The mean trace of the tube axis for control and mutant hearts is indicated by a dotted line and shown on a sagittal projection relative to the notochord axis. The origin (position 0) represents the exit of the outflow tract. Other colored points are the centers of gravity of the corresponding regions, with additional points at the interventricular sulcus (black) and the bifurcation of the atria (grey). n as in Fig4A. (C) Quantification of the arterial pole rotation at E8.5f, as the left-right difference in the angle between the heart tube and the dorsal pericardial wall. The black line shows the mean and standard deviations of 5 littermate controls. Mutants are classified as rightward or leftward

depending on the angle difference observed from position 75μm. Examples of transverse embryo sections are shown below. The position, along the notochord, of sections is measured as the distance to the bifurcation between the two atrial regions (μm). (D) Quantification of the displacement of the venous pole in control and mutants at E8.5h. Mutants are plotted individually, because classes 1-4 of mutants cannot be determined at this stage. AVC, atrio-ventricular canal; n=number of observations. Scale bars: 100μm.

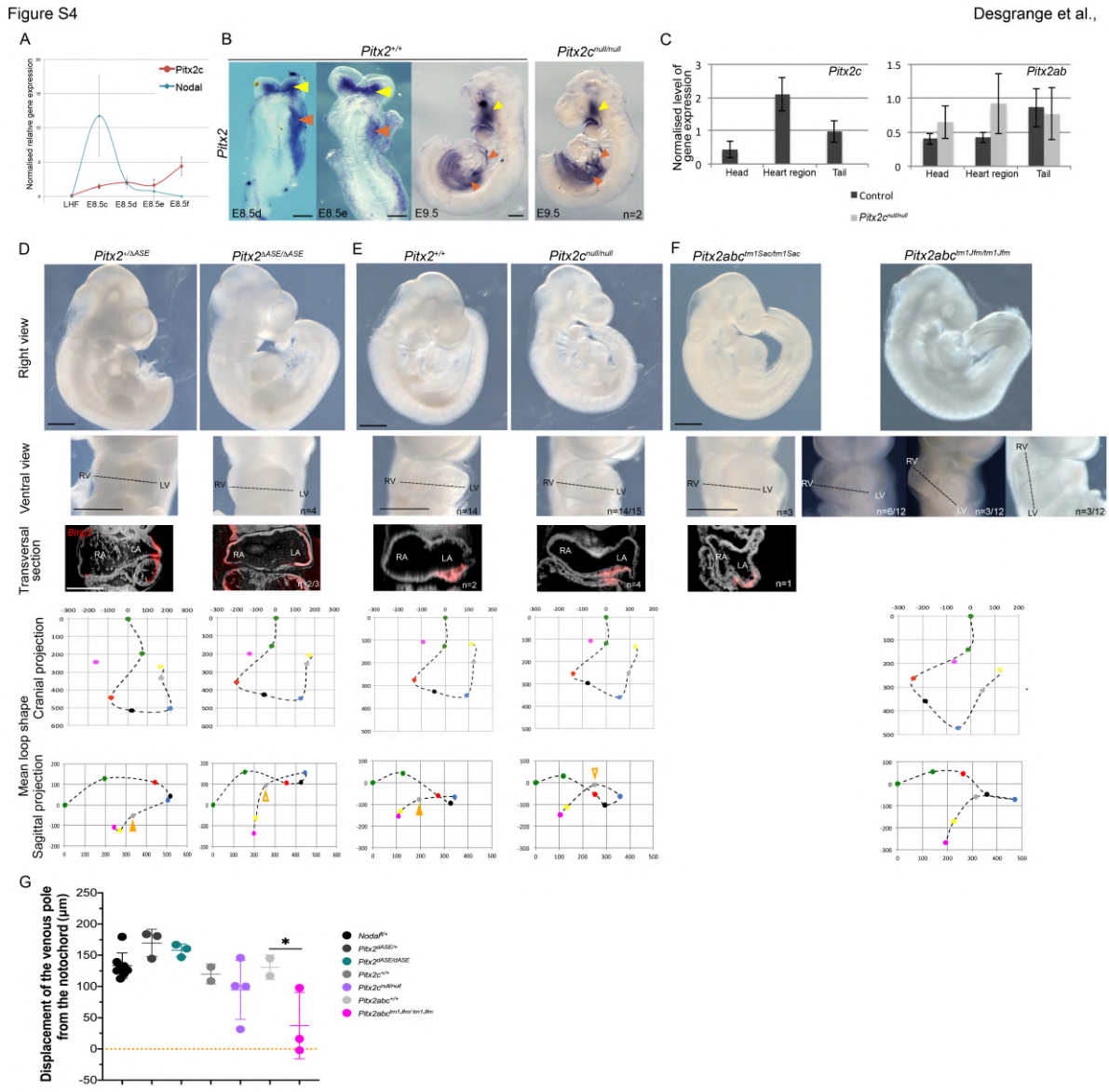

Fig. S4 related to Fig. 6. Expression and role of *Pitx2c* during heart looping

(A) *Pitx2c* was previously reported as the asymmetrically expressed isoform of *Pitx2* (Kitamura et al., 1999; Schweickert et al., 2000). Quantification of *Pitx2c* expression by RT-qPCR, relative to *Nodal* (see Fig. 2A, same n) in control embryos. Both expressions are initiated at E8.5c. Means and standard deviations are shown. (B) ISH of *Pitx2* (3 isoforms) at the indicated stages, showing asymmetric expression in the left lateral plate mesoderm (orange arrowheads) and bilateral expression in the oral ectoderm (yellow arrowheads) in control embryos, as well as in *Pitx2c* mutants. (C) Quantitative expression of *Pitx2* isoforms (a/b and c) by RT-qPCR in microdissected regions of control (n=4) and *Pitx2c* mutant embryos (n=4). (D-F) Phenotype of an allelic series of *Pitx2* mutant embryos at E9.5 (E-F) and E10 (D). Brightfield images of the embryo (first line) and heart loop (second line) are

shown. The dotted lines highlight the alignment of the ventricles. HREM images (third line) show *Bmp2* expression (red) in the atrial region, which is abnormally bilateral in *Pitx2*$^{\Delta ASE/\Delta ASE}$ mutants. The mean trace of the tube axis was reconstructed (bottom lines, n=3, 3 (D), n=2, 4 (E), n=2 of the intermediate phenotype (F)) with the same colour code as in Fig. 4B. The orange arrowhead points to the position of the atrio-ventricular canal (empty arrowhead, abnormal). (G) Quantification of the lateral displacement of the venous pole. *p-value<0.05 (one-way ANOVA with Tukey Kramer post-hoc test, n=8, 3, 3, 2, 4, 2, 3). HF, heart field; LA, left atrium; LV, left ventricle; RA, right atrium; RV, right ventricle. n, number of observations. Scale bars: 200µm (B, F for transversal section), 500µm (D, E, F for right and ventral views).

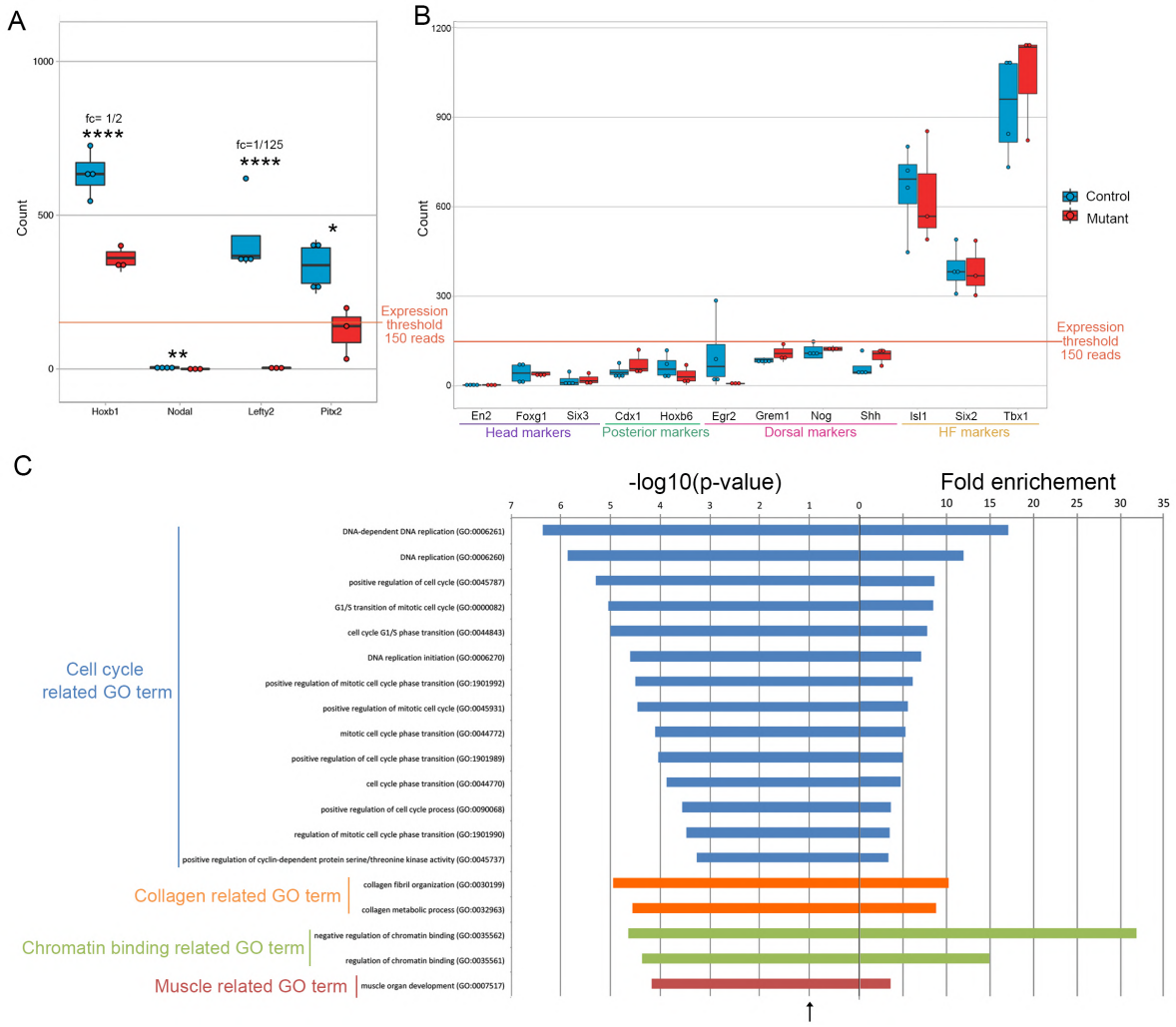

Fig. S5 related to Fig. 6. Transcriptomic analyses in control and *Nodal*$^{flox/null}$;*Hoxb1*$^{Cre/+}$ mutants.

(A) Normalised sequence counts of genes validating the genotypes of control (*Nodal*$^{flox/+}$;*Hoxb1*$^{+/+}$) *and* mutant (*Nodal*$^{flox/null}$;*Hoxb1*$^{Cre/+}$) embryos. The Nodal target *Lefty2* is the most downregulated gene of the dataset. fc, fold change. (B) Normalised sequence counts of genes validating the microdissection, by removal of head, posterior and dorsal markers and enrichment of heart field (HF) markers. *p-value<0.05, **p<0.01, ****p<0.0001; n=4 controls and 3 mutants (DESeq2). Whisker plots show the median, 25th, 75th quartiles (boxes) and the extreme datapoints (whiskers). (C) Gene Ontology (GO) analysis of enriched biological processes reflecting gene expression changes, ordered by p-value. The black arrow shows the threshold of significance.